OFDM and MC-CDMA
for Broadband Multi-user Communications, WLANs
and Broadcasting

by

L. Hanzo, M. Münster, B.J. Choi and T. Keller

*We dedicate this monograph to the numerous contributors of this field, many
of whom are listed in the Author Index*

Title Page - for Wiley to do

Copyright Page - for Wiley to do

About the Authors

Lajos Hanzo received his degree in electronics in 1976 and his doctorate in 1983. During his career in telecommunications he has held various research and academic posts in Hungary, Germany and the UK. Since 1986 he has been with the Department of Electronics and Computer Science, University of Southampton, UK, where he holds the chair in telecommunications. He has co-authored 10 books on mobile radio communications, published about 400 research papers, organised and chaired conference sessions, presented overview lectures and has been awarded a number of distinctions. Currently he heads an academic research team, working on a range of research projects in the field of wireless multimedia communications sponsored by industry, the Engineering and Physical Sciences Research Council (EPSRC) UK, the European IST Programme and the Mobile Virtual Centre of Excellence (VCE), UK. He is an enthusiastic supporter of industrial and academic liaison and he offers a range of industrial courses. He is also an IEEE Distinguished Lecturer. For further information on research in progress and associated publications please refer to http://www-mobile.ecs.soton.ac.uk

Dr. Byoung-Jo Choi received his BSc and MSc degrees in Electrical Engineering from KAIST, Korea, in 1990 and 1992, respectively. He has been working for LG Electronics, Korea, since Jan.,1992, where he was involved in developing the KoreaSat monitoring system, Digital DBS transmission system and W-CDMA based Wireless Local Loop (WLL) system. He was awarded the PhD degree in Mobile Communications at the University of Southampton, UK, where he was as a postdoctoral research assistant from Sep. 2001 to Aug. 2002. He is a recipient of the British Chevening Scholarship awarded by the British Council, UK. His current research interests are associated with mobile communication systems design with empasis on adaptive modulation aided OFDM, MC-CDMA and W-CDMA.

Thomas Keller studied Electrical Engineering at the University of Karlsruhe, Ecole Superieure d'Ingenieurs en Electronique et Electrotechnique, Paris, and the University of Southampton. He graduated with a Dipl.-Ing. degree in 1995. Between 1995 and 1999 he had been with the Wireless Multimedia Communications Group at the University of Southampton, where he completed his PhD in mobile communications. His areas of interest include adaptive OFDM transmission, wideband channel estimation, CDMA and error correction coding. He recently joined Ubinetics, Cambridge, UK, where he is involved in the research

and development of third-genertion wireless systems. Dr. Keller co-authored two monographs and about 30 various research papers.

Other Wiley and IEEE Press Books on Related Topics [1]

- R. Steele, L. Hanzo (Ed): Mobile Radio Communications: Second and Third Generation Cellular and WATM Systems, John Wiley-IEEE Press, 2nd edition, 1999, ISBN 07 273-1406-8, p 1064

- L. Hanzo, W. Webb, and T. Keller, *Single- and Multi-Carrier Quadrature Amplitude Modulation: Principles and Applications for Personal Communications, WLANs and Broadcasting*. IEEE Press, 2000.

- L. Hanzo, F.C.A. Somerville, J.P. Woodard: Voice Compression and Communications: Principles and Applications for Fixed and Wireless Channels; IEEE Press-John Wiley, 2001, p 642

- L. Hanzo, P. Cherriman, J. Streit: Wireless Video Communications: Second to Third Generation and Beyond, IEEE Press, 2001, p 1093

- L. Hanzo, T.H. Liew, B.L. Yeap: Turbo Coding, Turbo Equalisation and Space-Time Coding, John Wiley, 2002, p 751

- J.S. Blogh, L. Hanzo: Third-Generation Systems and Intelligent Wireless Networking: Smart Antennas and Adaptive Modulation, John Wiley, 2002, p408

- L. Hanzo, C.H. Wong, M.S. Yee: Adaptive wireless transceivers: Turbo-Coded, Turbo-Equalised and Space-Time Coded TDMA, CDMA and OFDM systems, John Wiley, 2002, p 737

---

[1]For detailed contents please refer to http://www-mobile.ecs.soton.ac.uk)

Contents

Acknowledgments

Lajos Hanzo, Matthias Münster, Buyong-Jo Choi and Thomas Keller
Department of Electronics and Computer Science
University of Southampton

Chapter 1

Prologue

1.1 Motivation of the Book

Whilst the concept of Orthogonal Frequency Division Multiplexing (OFDM) has been known since 1966 [1], it has only reached sufficient maturity for employment in standard systems during the 1990s. OFDM exhibits numerous advantages over the family of more conventional serial modem schemes [2], although it is only natural that it also imposes a number of disadvantages. The discussion of the associated design tradeoffs of OFDM and Multi-Carrier Code Division Multiple Access (MC-CDMA) systems constitute the topic of this monograph and in this context our discussions include the following fundamental issues:

1) A particularly attractive feature of OFDM systems is that they are capable of operating without a classic channel equaliser, when communicating over dispersive transmission media, such as wireless channels, while conveniently accommodating the time- and frequency-domain channel quality fluctuations of the wireless channel.

   Explicitly, the channel SNR variation versus both time and frequency of an indoor wireless channel is shown in a three-dimensional form in Figure 1.1 versus both time and frequency, which suggests that OFDM constitues convenient framework for accommodating the channel quality fluctuations of the wireless channel, as it will be briefly augmented below. This channel transfer function was recorded for the channel impulse response of Figure 1.2, by simply transforming the impulse response to the frequency domain at regular time intervals, while its taps fluctuated according to the Rayleigh distribution.

   These channel quality fluctuations may be readily accommodated with the aid of subband-adaptive modulation as follows. Such an adaptive OFDM (AOFDM) modem is characterized by Figure 1.3, portraying at the top a contour plot of the above-mentioned wireless channel's signal-to-noise ratio (SNR) fluctuation versus both time and frequency for each OFDM subcarrier. We note at this early stage that these channel quality fluctuations may be mitigated with the aid of frequency-domain channel equalisation, as it will be detailed throughout the book, but nonetheless, they cannot be
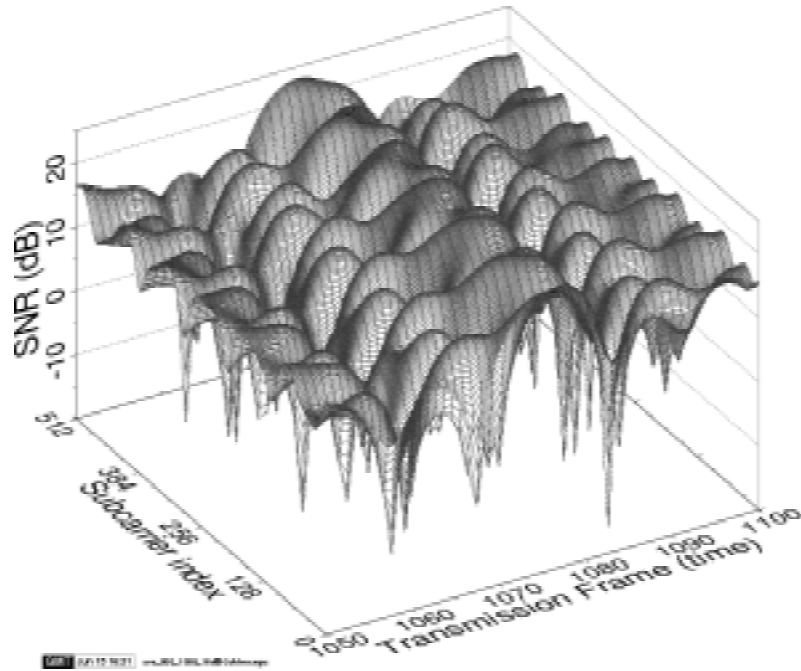
Figure 1.1: Instantaneous channel SNR for all 512 subcarriers versus time, for an average channel SNR of 16 dB over the channel characterized by the channel impulse response (CIR) of Figure 1.2.
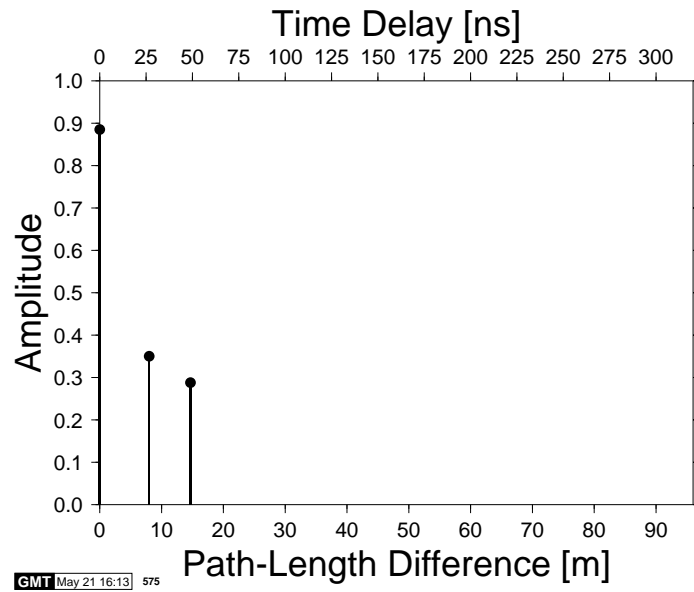
Figure 1.2: Indoor three-path WATM channel impulse response.

entirely erradicated.

More specifically, it can be seen in Figure 1.1 that when the channel is of high quality — as for example in the vicinity of the OFDM symbol index of 1080 — the subband-adaptive modem considered here for the sake illustration used the same modulation mode, as the identical-throughput conventional fixed-rate OFDM modem in all sub-carriers, which was 1 bit per symbol (BPS) in this example, as in conventional Binary Phase Shift Keying (BPSK). By contrast, when the channel is hostile — for example, around frame 1060 — the subband-adaptive modem transmitted zero bits per symbol in some subbands, corresponding to disabling transmissions in the low-quality subbands. In order to compensate for the loss of throughput in this subband, a higher-order modulation mode was used in the higher quality subbands.

In the centre and bottom subfigures of Figure 1.3 the modulation mode chosen for each 32-subcarrier subband is shown versus time for two different high-speed wireless modems communicating at either 3.4 or 7.0 Mbps, respectively, again, coresponding to an average throughput of either 1 or 2 BPS.

However, these adaptive transceiver principles are not limited to OFDM transmissions. In recent years the concept of intelligent multi-mode, multimedia transceivers (IMMT) has emerged in the context of a variety of wireless systems [2–7]. The range of various existing solutions that have found favour in already operational standard systems was summarised in the excellent overview by Nanda *et al.* [5]. *The aim of these adaptive transceivers is to provide mobile users with the best possible compromise amongst a number of contradicting design factors, such as the power consumption of the hand-held portable station (PS), robustness against transmission errors, spectral efficiency, teletraffic capacity, audio/video quality and so forth [4].*

2) Another design alternative applicable in the context of OFDM systems is that the channel quality fluctuations observed for example in Figure 1.1 are averaged out with the aid of frequency-domain spreading codes, which leads to the concept of Multi-Carrier Code Division Multiple Access (MC-CDMA). In this scenario typically only a few chips of the spreading code are obliterated by the frequency-selective fading and hence the chances are that the spreading code and its conveyed data may still be recoverable. The advantage of this approach is that in contrast to AOFDM based communications, in MC-CDMA no channel quality estimation and signalling is necessitated. Therefore OFDM and MC-CDMA will be comparatively studied in Part II of this monograph. Part III will also consider the employment of Walsh-Hadamard code based spreading of each subcarrier's signal across the entire OFDM bandwidth, which was found an efficient frequency-domain fading counter measure capable of operating without the employment of adaptive modulation.

3) A further techique capable of mitigating the channel quality fluctuations of wireless channels is constituted by space-time coding, which will be also considered as an attractive anti-fading design option capable of ataining a high diversity gain. Space-time coding employs several transmit and receive antennas for the sake of achieving diversity gain and hence an improved performance.

4) By contrast, in Part III of the book we employ multiple antennas at the base-station for a different reason, namely for the sake of supporting multiple users, rather than for
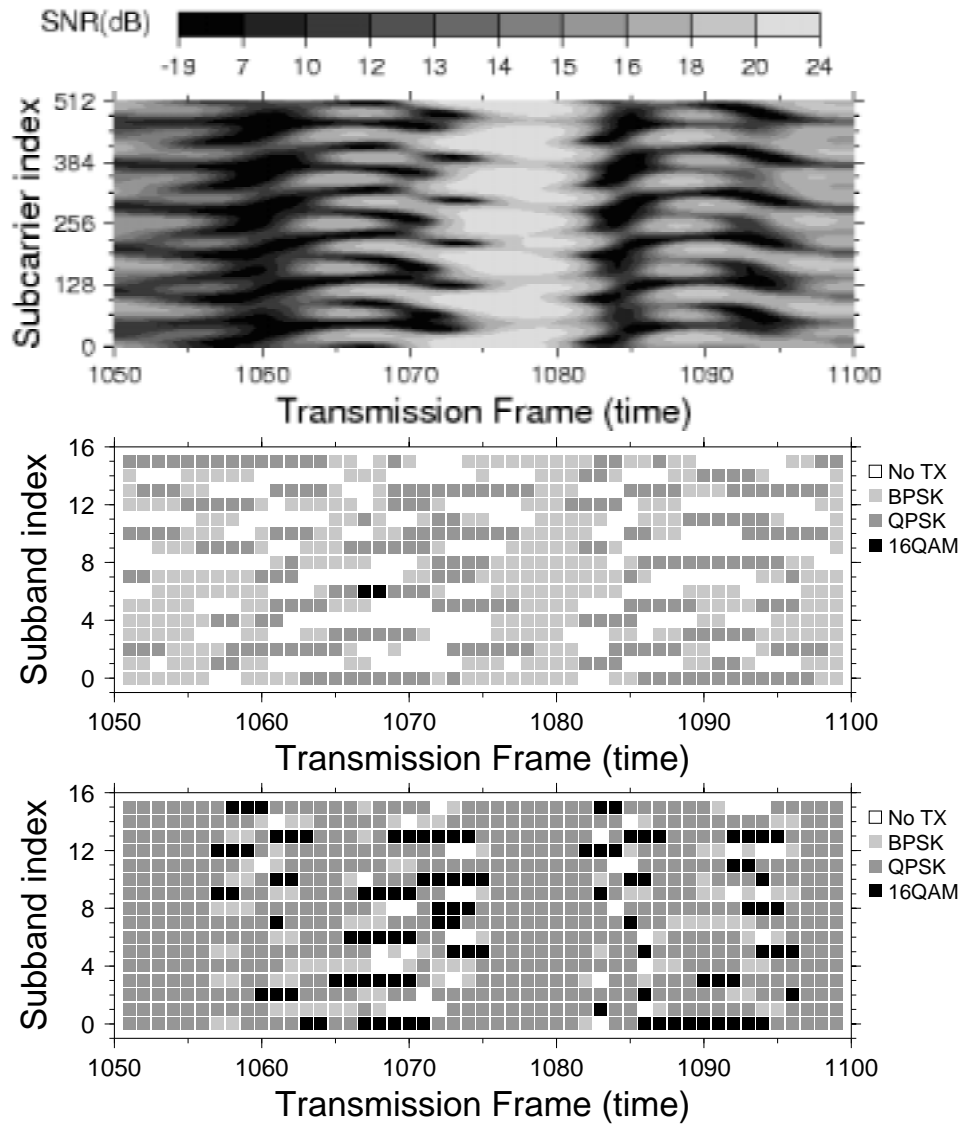
Figure 1.3: The micro-adaptive nature of the subband-adaptive OFDM modem. The top graph is a contour plot of the channel SNR for all 512 subcarriers versus time. The bottom two graphs show the modulation modes chosen for all 16 32-subcarrier subbands for the same period of time. The middle graph shows the performance of the 3.4 Mbps subband-adaptive modem, which operates at the same bit rate as a fixed BPSK modem. The bottom graph represents the 7.0 Mbps subband-adaptive modem, which operated at the same bit rate as a fixed QPSK modem. The average channel SNR was 16 dB.

achieving transmit diversity gain. This is possible, since the users' channel impulse responses (CIR) or channel transfer functions are accurately estimated and hence these channel transfer functions may be viewed as unique user signture sequences, which allow us to recognise and demultiplex the transmissions of the individual users, in a similar fashion to the unique user-specific spreading codes employed in CDMA systems. We note, however that this technique is only capable of reliably separating the users communicating within the same bandwidth, if their CIRs are sufficiently different. This assumption is typically valid for the uplink, although it may have a limited validity, when the base station receives from mobile stations in its immediate vicinity. By contrast, different techniques have to be invoked for downlink multiuser transmissions.

Our intention with the book is multifold:

1) Firstly, to pay tribute to all researchers, colleagues and valued friends, who contributed to the field. Hence this book is dedicated to them, since without their quest for better transmission solutions for wireless communications this monograph could not have been conceived. They are too numerous to name here, hence they appear in the author index of the book. Our hope is that the conception of this monograph on the topic will provide an adequate portrayal of the community's research and will further fuel this innovation process.

2) We expect to stimulate further research by exposing open research problems and by collating a range of practical problems and design issues for the practitioners. The coherent further efforts of the wireless research community is expected to lead to the solution of the range of outstanding problems, ultimately providing us with flexible wireless transceivers exhibiting a performance close to information theoretical limits.

1.2   Orthogonal Frequency Division Multiplexing History

1.2.1   Early Classic Contributions

The first OFDM scheme was proposed by Chang in 1966 [1] for dispersive fading channels. During the early years of the evolution of OFDM research the contributions due to the efforts of Weinstein, Peled, Ruiz, Hirosaki, Kolb, Cimini, Schüssler, Preuss, Rückriem, Kalet *et al.* [1, 8–20] have to be mentioned. As an unquestionable proof of its maturity, OFDM was standardised as the European digital audio broadcast (DAB) as well as digital video broadcast (DVB) scheme. It constituted also a credible proposal for the recent third-generation mobile radio standard competition in Europe. Finally, OFDM was recently selected as the high performance local area network's (HIPERLAN) transmission technique as well as becoming part of the IEEE 802.11 Wireless Local Area Network (WLAN) standard.

The system's operational principle is that the original bandwidth is divided in a high number of narrow sub-bands, in which the mobile channel can be considered non-dispersive. Hence no channel equaliser is required and instead of implementing a bank of sub-channel modems they can be conveniently implemented by the help of a single fast fourier Transformer (FFT). This scheme will be the topic of Chapters 18-23.

These OFDM systems - often also termed as frequency division multiplexing (FDM) or multi-tone systems - have been employed in military applications since the 1960s, for example by Bello [21], Zimmerman [8], Powers and Zimmerman [22], Chang and Gibby [23] and others. Saltzberg [24] studied a multi-carrier system employing orthogonal time–staggered quadrature amplitude modulation (O-QAM) of the carriers.

The employment of the discrete Fourier transform (DFT) to replace the banks of sinusoidal generators and the demodulators was suggested by Weinstein and Ebert [9] in 1971, which significantly reduces the implementation complexity of OFDM modems. In 1980, Hirosaki [20] suggested an equalisation algorithm in order to suppress both intersymbol and intersubcarrier interference caused by the channel impulse response or timing and frequency errors. Simplified OFDM modem implementations were studied by Peled [13] in 1980, while Hirosaki [14] introduced the DFT based implementation of Saltzberg's O-QAM OFDM system. From Erlangen University, Kolb [15], Schüßler [16], Preuss [17] and Rückriem [18] conducted further research into the application of OFDM. Cimini [10] and Kalet [19] published analytical and early seminal experimental results on the performance of OFDM modems in mobile communications channels.

More recent advances in OFDM transmission were presented in the impressive state-of-the-art collection of works edited by Fazel and Fettweis [25], including the research by Fettweis *et al.* at Dresden University, Rohling *et al.* at Braunschweig University, Vandendorp at Loeven University, Huber *et al.* at Erlangen University, Lindner *et al.* at Ulm University, Kammeyer *et al.* at Brehmen University and Meyr *et al.* [26, 27] at Aachen University, but the individual contributions are too numerous to mention. Important recent references are the books by van Nee and Prasad [28] as well as by Vandenameele, van der Perre and Engels [29].

While OFDM transmission over mobile communications channels can alleviate the problem of multipath propagation, recent research efforts have focused on solving a set of inherent difficulties regarding OFDM, namely the peak–to–mean power ratio, time and frequency synchronisation, and on mitigating the effects of the frequency selective fading channel. These issues are addressed below with reference to the literature, while their more in-depth treatment is given throughout the book.

1.2.2 Peak-to-mean power ratio

It is plausibe that the OFDM signal - which is the superposition of a high number of modulated sub-channel signals - may exhibit a high instantaneous signal peak with respect to the average signal level. Furthermore, large signal amplitude swings are encountered, when the time domain signal traverses from a low instantaneous power waveform to a high power waveform, which may results in a high out-of-band (OOB) harmonic distortion power, unless the transmitter's power amplifier exhibits an extremely high linearity across the entire signal level range. This then potentially contaminates the adjacent channels with adjacent channel interference. Practical amplifiers exhibit a finite amplitude range, in which they can be considered almost linear. In order to prevent severe clipping of the high OFDM signal peaks - which is the main source of OOB emissions - the power amplifier must not be driven into saturation and hence they are typically operated with a certain so-called back-off, creating a certain "head room" for the signal peaks, which reduces the risk of amplifier saturation and OOB emmission. Two different families of solutions have been suggested in the literature, in

order to mitigate these problems, either reducing the peak-to-mean power ratio, or improving the amplification stage of the transmitter.

More explicitly, Shepherd [30], Jones [31], and Wulich [32] suggested different coding techniques which aim to minimise the peak power of the OFDM signal by employing different data encoding schemes before modulation, with the philosophy of choosing block codes whose legitimate code words exhibit low so-called Crest factors or peak-to-mean power envelope fluctuation. Müller [33], Pauli [34], May [35] and Wulich [36] suggested different algorithms for post-processing the time domain OFDM signal prior to amplification, while Schmidt and Kammeyer [37] employed adaptive subcarrier allocation in order to reduce the crest factor. Dinis and Gusmão [38–40] researched the use of two-branch amplifiers, while the clustered OFDM technique introduced by Daneshrad, Cimini and Carloni [41] operates with a set of parallel partial FFT processors with associated transmitting chains. OFDM systems with increased robustness to non-linear distortion have been proposed by Okada, Nishijima and Komaki [42] as well as by Dinis and Gusmão [43]. These aspects of OFDM transmissions will be treated in substantial depth in Part II of the book.

1.2.3 Synchronisation

Time and frequency synchronisation between the transmitter and receiver are of crucial importance as regards to the performance of an OFDM link [44, 45]. A wide variety of techniques have been proposed for estimating and correcting both timing and carrier frequency offsets at the OFDM receiver. Rough timing and frequency acquisition algorithms relying on known pilot symbols or pilot tones embedded into the OFDM symbols have been suggested by Claßen [26], Warner [46], Sari [47], Moose [48], as well as Brüninghaus and Rohling [49]. Fine frequency and timing tracking algorithms exploiting the OFDM signal's cyclic extension were published by Moose [48], Daffara [50] and Sandell [51]. OFDM synchronisation issues are the topics of Chapter 5.

1.2.4 OFDM/CDMA

Combining multi-carrier OFDM transmissions with code division multiple access (CDMA) allows us to exploit the wideband channel's inherent frequency diversity by spreading each symbol across multiple subcarriers. This technique has been pioneered by Yee, Linnartz and Fettweis [52], by Chouly, Brajal and Jourdan [53], as well as by Fettweis, Bahai and Anvari [54]. Fazel and Papke [55] investigated convolutional coding in conjunction with OFDM/CDMA. Prasad and Hara [56] compared various methods of combining the two techniques, identifying three different structures, namely multi-carrier CDMA (MC-CDMA), multi-carrier direct sequence CDMA (MC-DS-CDMA) and multi-tone CDMA (MT-CDMA). Like non-spread OFDM transmission, OFDM/CDMA methods suffer from high peak-to-mean power ratios, which are dependent on the frequency domain spreading scheme, as investigated by Choi, Kuan and Hanzo [57]. Part II of the book considers the related design trade-offs.

Year	Author	Contribution
'91	Höher [58]	Cascaded 1D-FIR channel transfer factor interpolation was carried out in the frequency- and time-direction for frequency-domain PSAM.
'93	Chow, Cioffi and Bingham [59]	Subcarrier-by-subcarrier based LMS related channel transfer factor equalization techniques were employed.
'94	Wilson, Khayata and Cioffi [60]	Linear channel transfer factor filtering was invoked in the time-direction for DDCE.
'95	van de Beek, Edfors, Sandell, Wilson and Börjesson [61]	DFT-aided CIR-related domain Wiener-filter based noise-reduction was advocated for DDCE. The effects of leakage in the context of non-sample-spaced CIRs were analysed.
'96	Edfors, Sandell, van de Beek, Wilson and Börjesson [62]	SVD-aided CIR-related domain Wiener-filter based noise-reduction was introduced for DDCE.
	Frenger and Svensson [63]	MMSE-based frequency-domain channel transfer factor prediction was proposed for DDCE.
	Mignone and Morello [64]	FEC was invoked for improving the DDCE's remodulated reference.
'97	Tufvesson and Maseng [65]	An analysis of various pilot patterns employed in frequency-domain PSAM was provided in terms of the system's BER for different Doppler frequencies. Kalman filter-aided channel transfer factor estimation was used.
	Höher, Kaiser and Robertson [66, 67]	Cascaded 1D-FIR Wiener filter channel interpolation was utilized in the context of 2D-pilot pattern aided PSAM
'98	Li, Cimini and Sollenberger [68]	An SVD-aided CIR-related domain Wiener filter based noise-reduction was achieved by employing CIR-related tap estimation filtering in the time-direction.
	Edfors, Sandell, van de Beek, Wilson and Börjesson [69]	A detailed analysis of SVD-aided CIR-related domain Wiener-filter based noise-reduction was provided for DDCE, which expanded the results of [62].
	Tufvesson, Faulkner and Maseng [70]	Wiener filter-aided frequency-domain channel transfer factor prediction assisted pre-equalization was studied.
	Itami, Kuwabara, Yamashita, Ohta and Itoh [71]	Parametric finite-tap CIR model based channel estimation was employed for frequency-domain PSAM.

Table 1.1: Contributions on channel transfer factor estimation for single-transmit antenna assisted OFDM.

Year	Author	Contribution
'99	Al-Susa and Ormondroyd [72]	DFT-aided Burg-algorithm assisted adaptive CIR-related tap prediction filtering was employed for DDCE.
	Yang, Letaief, Cheng and Cao [73]	Parametric, ESPRIT-assisted channel estimation was employed for frequency-domain PSAM.
'00	Li [74]	Robust 2D frequency-domain Wiener filtering was suggested for employment in frequency-domain PSAM using 2D pilot patterns.
'01	Yang, Letaief, Cheng and Cao [75]	Detailed discussions of parametric, ESPRIT-assisted channel estimation were provided in the context of frequency-domain PSAM [73].
	Zhou and Giannakis [76]	Finite alphabet-based channel transfer factor estimation was proposed.
	Wang and Liu [77]	Polynomial frequency-domain channel transfer factor interpolation was contrived.
	Yang, Cao, and Letaief [78]	DFT-aided CIR-related domain one-tap Wiener-filter based noise-reduction was investigated, which is supported by variable frequency-domain Hanning windowing.
	Lu and Wang [79]	A Bayesian blind turbo receiver was contrived for coded OFDM systems.
	Li and Sollenberger [80]	Various transforms were suggested for CIR-related tap estimation filtering assisted DDCE.
	Morelli and Mengali [81]	LS- and MMSE based channel transfer factor estimators were compared in the context of frequency-domain PSAM.
'02	Chang and Su [82]	Parametric quadrature surface based frequency-domain channel transfer factor interpolation was studied for PSAM.
	Necker and Stüber [83]	Totally blind channel transfer factor estimation based on the finite alphabet property of PSK signals was investigated.

Table 1.2: Contributions on channel transfer factor estimation for single-transmit antenna assisted OFDM.

1.2.5   Decision-Directed Channel Estimation

In recent years numerous research contributions have appeared on the topic of channel transfer function estimation techniques designed for employment in single-user, single transmit antenna assisted OFDM scenarios, since the availability of an accurate channel transfer function estimate is one of the prerequisites for coherent symbol detection at an OFDM receiver. The techniques proposed in the literature can be classified as *pilot-assisted*, *decision-directed* (DD) and *blind* channel estimation (CE) methods.

In the context of pilot-assisted channel transfer function estimation a subset of the available subcarriers is dedicated to the transmission of specific pilot symbols known to the receiver, which are used for 'sampling' the desired channel transfer function. Based on these samples of the frequency domain transfer function, the well-known process of interpolation is used for generating a transfer function estimate for each subcarrier residing between the pilots. This is achieved at the cost of a reduction of the number of useful subcarriers available for data transmission. The family of *pilot-assisted* channel estimation techniques was investigated for example by Chang and Su [82], Höher [58, 66, 67], Itami *et al.* [71], Li [74], Tufvesson and Maseng [65], Wang and Liu [77], as well as Yang *et al.* [73, 78, 84].

By contrast, in the context of Decision-Directed Channel Estimation (DDCE) all the sliced and remodulated subcarrier data symbols are considered as pilots. In the absence of symbol errors and also depending on the rate of channel fluctuation, it was found that accurate channel transfer function estimates can be obtained, which are often of better quality in terms of the channel transfer function estimator's mean-square error (MSE), than the estimates offered by pilot-assisted schemes. This is because the latter arrangements usually invoke relatively sparse pilot patterns.

The family of *decision-directed* channel estimation techniques was investigated for example by van de Beek *et al.* [61], Edfors *et al.* [62, 69], Li *et al.* [68], Li [80], Mignone and Morello [64], Al-Susa and Ormondroyd [72], Frenger and Svensson [63], as well as Wilson *et al.* [60]. Furthermore, the family of *blind* channnel estimation techniques was studied by Lu and Wang [79], Necker *et al.* [83], as well as by Zhou and Giannakis [76]. The various contributions have been summarized in Tables 1.1 and 1.2.

In order to render the various DDCE techniques more amenable to employment in scenarios associated with a relatively high rate of channel variation expressed in terms of the OFDM symbol normalized Doppler frequency, linear prediction techniques well-known from the speech coding literature [85, 86] can be invoked. To elaborate a little further, we will substitute the CIR-related tap estimation filter - which is part of the two-dimensional channel transfer function estimator proposed in [68] - by a CIR-related tap prediction filter. The employment of this CIR-related tap prediction filter enables a more accurate estimation of the channel transfer function encountered during the forthcoming transmission timeslot and thus potentially enhances the performance of the channel estimator. We will be following the general concepts described by Duel-Hallen *et al.* [87] and the ideas presented by Frenger and Svensson [63], where frequency-domain prediction filter assisted DDCE was proposed. Furthermore, we should mention the contributions of Tufvesson *et al.* [70, 88], where a prediction filter assisted frequency domain pre-equalization scheme was discussed in the context of OFDM. In a further contribution by Al-Susa and Ormondroyd [72], adaptive prediction filter assisted DDCE designed for OFDM has been proposed upon invoking techniques known from speech-coding, such as the Levinson-Durbin algorithm or the Burg algorithm [85,89,90]

in order to determine the predictor coefficients.

In contrast to the above-mentioned single-user OFDM scenarios, in a multi-user OFDM scenario the signal received by each antenna is constituted by the superposition of the signal contributions associated with the different users- or transmit antennas. Note that in terms of the multiple-input multiple-output (MIMO) structure of the channel the multi-user single-transmit antenna scenario is equivalent for example to a single-user space-time coded (STC) scenario using multiple transmit antennas. For the latter a Least-Squares (LS) error channel estimator was proposed by Li *et al.* [91], which aims at recovering the different transmit antennas' channel transfer functions on the basis of the output signal of a specific reception antenna element and by also capitalizing on the remodulated received symbols associated with the different users. The performance of this estimator was found to be limited in terms of the mean-square estimation error in scenarios, where the product of the number of transmit antennas and the number of CIR taps to be estimated per transmit antenna approaches the total number of subcarriers hosted by an OFDM symbol. As a design alternative, in [92] a DDCE was proposed by Jeon *et al.* for a space-time coded OFDM scenario of two transmit antennas and two receive antennas.

Specifically, the channel transfer function[1] associated with each transmit-receive antenna pair was estimated on the basis of the output signal of the specific receive antenna upon *subtracting* the interfering signal contributions associated with the remaining transmit antennas. These interference contributions were estimated by capitalizing on the knowledge of the channel transfer functions of all interfering transmit antennas predicted during the $(n-1)$-th OFDM symbol period for the n-th OFDM symbol, also invoking the corresponding remodulated symbols associated with the n-th OFDM symbol. To elaborate further, the difference between the subtraction based channel transfer function estimator of [92] and the LS estimator proposed by Li *et al.* in [91] is that in the former the channel transfer functions predicted during the previous, i.e. the $(n-1)$-th OFDM symbol period for the current, i.e. the n-th OFDM symbol are employed for both symbol detection *as well as* for obtaining an updated channel estimate for employment during the $(n+1)$-th OFDM symbol period. In the approach advocated in [92] the subtraction of the different transmit antennas' interfering signals is performed in the frequency-domain.

By contrast, in [93] a similar technique was proposed by Li with the aim of simplifying the DDCE approach of [91], which operates in the time-domain. A prerequisite for the operation of this parallel interference cancellation (PIC)-assisted DDCE is the availability of a reliable estimate of the various channel transfer functions for the current OFDM symbol, which are employed in the cancellation process in order to obtain updated channel transfer function estimates for the demodulation of the next OFDM symbol. In order to compensate for the channel's variation as a function of the OFDM symbol index, linear prediction techniques can be employed, as it was also proposed for example in [93]. However, due to the estimator's recursive structure, determining the optimum predictor coefficients is not as straightforward as for the transversal FIR filter-assisted predictor as described in Section 15.2.4 for the single-user DDCE.

A comprehensive overview of further publications on channel transfer factor estimation for OFDM systems supported by multiple transmit antennas is provided in Table 1.3.

---

[1]In the context of the OFDM system the set of K different subcarriers' channel transfer factors is referred to as the channel transfer function, or simply as the channel.

Year	Author	Contribution
'99	Li, Seshadri and Ariyavisitakul [91]	The LS-assisted DDCE proposed exploits the cross-correlation properties of the transmitted subcarrier symbol sequences.
'00	Jeon, Paik and Cho [92]	Frequency-domain PIC-assisted DDCE is studied, which exploits the channel's slow variation versus time.
	Li [93]	Time-domain PIC-assisted DDCE is investigated as a simplification of the LS-assisted DDCE of [91]. Optimum training sequences are proposed for the LS-assisted DDCE of [91].
'01	Mody and Stüber [94]	Channel transfer factor estimation designed for frequency-domain PSAM based on CIR-related domain filtering is studied.
	Gong and Letaief [95]	MMSE-assisted DDCE is advocated which represents an extension of the LS-assisted DDCE of [95]. The MMSE-assisted DDCE is shown to be practical in the context of transmitting consecutive training blocks. Additionally, a low-rank approximation of the MMSE-assisted DDCE is considered.
	Jeon, Paik and Cho [96]	2D MMSE based channel estimation is proposed for frequency-domain PSAM.
	Vook and Thomas [97]	2D MMSE based channel estimation is invoked for frequency-domain PSAM. A complexity reduction is achieved by CIR-related domain based processing.
	Xie and Georghiades [98]	Expectation maximization (EM) based channel transfer factor estimation approach for DDCE.
'02	Li [99]	A more detailed discussion on time-domain PIC-assisted DDCE is provided and optimum training sequences are proposed [93].
	Bölcskei, Heath Jr. and Paulray [100]	Blind channel indentification and equalization using second-order cyclostationary statistics as well as antenna precoding was studied.
	Minn, Kim and Bhargava [101]	A reduced-complexity version of the LS-assisted DDCE of [91] is introduced, based on exploiting the channel's correlation in the frequency-direction, as opposed to invoking the simplified scheme of [99], which exploits the channel's correlation in the time-direction. A similar approach was suggested by Slimane [102] for the specific case of two transmit antennas.
	Komninakis, Fragouli, Sayed and Wesel [103]	Fading channel tracking and equalization was proposed for employment in MIMO systems assisted by Kalman estimation and channel prediction.

Table 1.3: Contributions on channel transfer factor estimation for multiple-transmit antenna assisted OFDM.

1.2.6 Uplink Detection Techniques for Multi-User SDMA-OFDM

Combining adaptive antenna aided techniques with OFDM transmissions was shown to be advantageous for ecxample in the context of suppressing co-channel interference in cellular communications systems. Amongst others, Li, Cimini and Sollenberger [129–131], Kim, Choi and Cho [132], Lin, Cimini and Chuang [133] as well as Münster *et al.* [134] have investigated algorithms designed for multi-user channel estimation and interference suppression.

The related family of Space-Division-Multiple-Access (SDMA) communication systems has recently drawn wide reseach interests. In these systems the L different users' transmitted signals are separated at the base-station (BS) with the aid of their unique, user-specific spatial signature, which is constituted by the P-element vector of channel transfer factors between the users' single transmit antenna and the P different receiver antenna elements at the BS, upon assuming flat-fading channel conditions such as those often experienced in the context of each of the OFDM subcarriers. These wave propgation related issues will be further detailed during our portrayal of the SDMA-MIMO channel model in Section 17.1.3.

A whole host of multi-user detection (MUD) techniques known from Code-Division-Multiple-Access (CDMA) communications lend themselves also to an application in the context of SDMA-OFDM on a per-subcarrier basis. Some of these techniques are the Least-Squares (LS) [113, 119, 127, 135], Minimum Mean-Square Error (MMSE) [105–108, 110, 113, 117, 121, 135–137], Successive Interference Cancellation (SIC) [104, 109, 113, 117, 119, 124, 126, 128, 135, 137], Parallel Interference Cancellation (PIC) [125, 135] and Maximum Likelihood (ML) detection [112, 114–118, 120, 123, 135, 137]. A comprehensive overview of recent publications on MUD techniques for MIMO systems is given in Tables 1.4 and 1.5.

The further structure of our introduction is as follows. In Section 17.1.1 a detailed classification of the different MUD techniques is provided. By contrast, a more simple classification is employed in Section 17.1.2, which reflects the structure of this chapter. Before we embark on the discussion of linear MUD techniques in Section 17.2, the SDMA-MIMO channel model, to be used in our further discussions will be introduced in Section 17.1.3

1.2.7 OFDM applications

Due to their implementational complexity, OFDM applications have been scarce until quite recently. Recently, however, OFDM has been adopted as the new European digital audio broadcasting (DAB) standard [11, 12, 138–140] as well as for the terrestrial digital video broadcasting (DVB) system [47, 141].

For fixed-wire applications, OFDM is employed in the asynchronous digital subscriber line (ADSL) and high-bit-rate digital subscriber line (HDSL) systems [142–145] and it has also been suggested for power line communications systems [146, 147] due to its resilience to time dispersive channels and narrow band interferers.

More recently, OFDM applications were studied within the European 4th Framework Advanced Communications Technologies and Services (ACTS) programme [148]. The MEDIAN project investigated a 155 Mbps wireless asynchronous transfer mode (WATM) network [149–152], while the Magic WAND group [153, 154] developed a wireless local area network (LAN). Hallmann and Rohling [155] presented a range of different OFDM systems that were applicable to the European Telecommunications Standardisation Institute's (ETSI)

Year	Author	Contribution
'96	Foschini [104]	The concept of the BLAST architecture was introduced.
'98	Vook and Baum [105]	SMI-assisted MMSE combining was invoked on an OFDM subcarrier basis.
	Wang and Poor [106]	Robust sub-space based weight vector calculation and tracking was employed for co-channel interference suppression, as an improvement of the SMI-algorithm.
	Wong, Cheng, Letaief and Murch [107]	Optimization of an OFDM system was reported in the context of multiple transmit- and receive antennas upon invoking the maximum SINR criterion. The computational computational was reduced by exploiting the channel's correlation in the frequency-direction.
	Li and Sollenberger [108]	Tracking of the channel correlation matrix' entries was suggested in the context of SMI-assisted MMSE combining for multiple receiver antenna assisted OFDM, by capitalizing on the principles of [68].
'99	Golden, Foschini, Valenzuela and Wolniansky [109]	The SIC detection assisted V-BLAST algorithm was introduced.
	Li and Sollenberger [110]	The system introduced in [108] was further detailed.
	Vandenameele, Van Der Perre, Engels and H. D. Man [111]	A comparative study of different SDMA detection techniques, namely that of MMSE, SIC and ML detection was provided. Further improvements of SIC detection were suggested by adaptively tracking multiple symbol decisions at each detection node.
	Speth and Senst [112]	Soft-bit generation techniques were proposed for MLSE in the context of a coded SDMA-OFDM system.
'00	Sweatman, Thompson, Mulgrew and Grant [113]	Comparisons of various detection algorithms including LS, MMSE, D-BLAST and V-BLAST (SIC detection) were carried out.
	van Nee, van Zelst and Awater [114–116]	The evaluation of ML detection in the context of a Space-Division Multiplexing (SDM) system was provided, considering various simplified ML detection techniques.
	Vandenameele, Van Der Perre, Engels, Gyselinckx and De Man [117]	More detailed discussions were provided on the topics of [111].

Table 1.4: Contributions on multiuser detection techniques designed for multiple transmit antenna assisted OFDM systems.

Year	Author	Contribution
'00	Li, Huang, Lozano and Foschini [118]	Reduced complexity ML detection was proposed for multiple transmit antenna systems employing adaptive antenna grouping and multi-step reduced-complexity detection.
'01	Degen, Walke, Lecomte and Rembold [119]	An overview of various adaptive MIMO techniques was provided. Specifically, pre-distortion was employed at the transmitter, as well as LS- or BLAST detection were used at the receiver or balanced equalization was invoked at both the transmitter and receiver.
	Zhu and Murch [120]	A tight upper bound on the SER performance of ML detection was derived.
	Li, Letaief, Cheng and Cao [121]	Joint adaptive power control and detection was investigated in the context of an OFDM/SDMA system, based on the approach of Farrokhi *et al.* [122].
	van Zelst, van Nee and Awater [123]	Iterative decoding was proposed for the BLAST system following the turbo principle.
	Benjebbour, Murata and Yoshida [124]	The performance of V-BLAST or SIC detection was studied in the context of backward iterative cancellation scheme employed after the conventional forward cancellation stage.
	Sellathurai and Haykin [125]	A simplified D-BLAST was proposed, which used iterative PIC capitalizing on the extrinsic soft-bit information provided by the FEC scheme employed.
	Bhargave, Figueiredo and Eltoft [126]	A detection algorithm was suggested, which followed the concepts of V-BLAST or SIC. However, multiple symbols states are tracked from each detection stage, where - in contrast to [117] - an intermediate decision is made at intermediate detection stages.
	Thoen, Deneire, Van Der Perre and Engels [127]	A constrained LS detector was proposed for OFDM/SDMA, which was based on exploiting the constant modulus property of PSK signals.
'02	Li and Luo [128]	The block error probability of optimally ordered V-BLAST was studied. Furthermore, the block error probability is also investigated for the case of tracking multiple parallel symbol decisions from the first detection stage, following an approach similar to that of [117].

Table 1.5: Contributions on detection techniques for MIMO systems and for multiple transmit antenna assisted OFDM systems.

recent personal communications oriented air interface concept [156].

1.3   Outline of the book

- **Chapter 2**: In this chapter we commence our detailed discourse by demonstrating that OFDM modems can be efficiently implemented by invoking the Fourier transform or the fast Fourier Transform (FFT). A number of basic OFDM design issues are discussed in an accessible style.

- **Chapter 3**: The BER performance of OFDM modems achievable in AWGN channels is studied for a set of different modulation schemes in the subcarriers. The effects of amplitude limiting of the transmitter's output signal, caused by a simple clipping amplifier model, and of finite resolution D/A and A/D conversion on the system performance are investigated. Oscillator phase noise is considered as a source of intersubcarrier interference and its effects on the system performance are demonstrated.

- **Chapter 4**: The effects of time-dispersive frequency-selective Rayleigh fading channels on OFDM transmissions are demonstrated. Channel estimation techniques are presented which support the employment of coherent detection in frequency selective channels. Additionally, differential detection is investigated, and the resulting system performance over the different channels is compared.

- **Chapter 5**: We focuse our attention on the time and frequency synchronisation requirements of OFDM transmissions and the effects of synchronisation errors are demonstrated. Two novel synchronisation algorithms for frame and OFDM symbol synchronisation are suggested and compared. The resulting system performance over fading wideband channels is examined.

- **Chapter 6**: Based on the results of Chapter 4, the employment of adaptive modulation schemes is suggested for duplex point-to-point links over frequency-selective time-varying channels. Different bit allocation schemes are investigated and a simplified sub-band adaptivity OFDM scheme is suggested for alleviating the associated signalling constraints. A range of blind modulation scheme detection algorithms are also investigated and compared. The employment of long-block-length convolutional turbo codes is suggested for improving the system's throughput and the turbo coded adaptive OFDM modem's performance is compared using different sets of parameters. Then the effects of using pre-equalisation at the transmitter are examined, and a set of different pre-equalisation algorithms is introduced. A joint pre-equalisation and adaptive modulation algorithm is proposed and its BER and throughput performance is studied.

- **Chapter 7**: The adaptive OFDM transmission ideas of Chapter 6 are extended further, in order to include adaptive error correction coding, based on redundant residual number system (RRNS) and turbo BCH codes. A joint modulation and code rate adaptation scheme is presented.

- **Chapter 8**: The discussions of **Part II** of the book commence by a rudimentary comparison of OFDM, CDMA and MC-CDMA in Chapter 8.

- **Chapter 9**: Since the properties of spreading sequences are equally important in both multicarrier CDMA and in DS-CDMA, the properties of various spreading sequences are reviewed in Chapter 9.

- **Chapter 10**: The basic characterisation of spreading codes is followed by Chapter 10, analysing the achievable performance of both single- and multi-user detected MC-CDMA.

- **Chapter 11**: One of the main problems associated with the implementation of multi-carrier communication systems is their high Peak-to-Mean Envelope-Power Ratio (PMEPR), requiring highly linear power amplifiers. Hence the envelope power of the MC-CDMA signal is analysed in Chapter 11. Several orthogonal spreading sequences are examined, in order to assess their ability to maintain low PMEPR of the transmitted signal. The effects of reduced PMEPR are investigated in terms of the BER performance and the out-of-band frequency spectrum.

- **Chapter 12**: An adaptive modulation assisted MC-CDMA technique is investigated using both analysis as well as simulation-based studies. Various techniques of optimising the modem mode switching thresholds are compared and the Lagragian optimisation method is shown to provide the best solution. This method results in an SNR-dependent set of switching thresholds, because at high SNRs the activation of high-throughput modem modes may be promoted by lowering their respective activation thresholds, while still maintaining the target BER.

- **Chapter 13** deals with three different types of reduced complexity despreading aided MC-CDMA detection techniques that can be used at the receiver. Their BER performance as well as their achievable computational complexity reduction is characterised.

- **Chapter 14**: In **Part III** of the book our discussions are dedicated to the detailed design of channel transfer function estimation and to the conception of multiuser OFDM systems. We commence our discourse with the portrayal of two-dimensional pilot symbol assisted channel estimation techniques in Chapter 14.

- **Chapter 15**: Our discussions in Chapter 15 continue by reviewing the concepts of 1D- and 2D-MMSE based Decision Directed Channel Estimators (DDCE) contrived for single-user OFDM, which was analysed for example by Edfors *et al.* [62, 69, 157], Sandell [158] and Li *et al.* [68]. Based on the observation that in the context of DDCE the most recently received OFDM symbol is equalized based on a potentially outdated channel transfer function estimate, which was generated during the previous OFDM symbol period, the CIR-related tap *estimation filters* invoked by the 2D-MMSE DDCE proposed by Li *et al.* [68] are substituted by CIR-related tap *prediction filters*. For this configuration we derive the channel predictor's average *a priori* estimation MSE observed in the frequency-domain, as it will be shown in Section 15.2.4.6. In the context of our performance assessments provided in Section 15.3 two methods are compared against each other for evaluating the Wiener prediction filter's coefficients, namely the robust approach as advocated by Li *et al.* [68] and the adaptive approach as proposed by Al-Susa and Ormondroyd [72], based on the Burg-algorithm known from speech coding. As a third- and most promising alternative, the RLS algorithm could be employed, as proposed in the context of our discussions in Chapter 16.

Following our in-depth performance assessment of the CIR-related tap prediction assisted DDCE, both in the context of uncoded and turbo-coded scenarios, combining channel transfer factor prediction-assisted DDCE with AOFDM is proposed in Section 15.4. As a result of the channel transfer factor prediction, AOFDM is rendered attractive also in scenarios having a relatively high OFDM symbol-normalized Doppler frequency. These contributions were published in [159] and [160].

- **Chapter 16** commences in Section 16.4 with an in-depth discussion of Li's Least-Squares (LS) assisted DDCE, which was contrived for space-time coded OFDM systems [91], or more generally for OFDM systems employing multiple transmit antennas encountered in the context of multi-user SDMA-OFDM scenarios. Our contribution in this section is the provision of a sophisticated mathematical description, which provides the standard LS-related solution of the associated estimation problem. In the context of these discussions a necessary condition for the existence of the LS-channel estimates is identified. In contrast to Li's discussions in [91], which provided an expression for the estimation MSE based on sample-spaced CIRs, here we also derived expression for the estimation MSE assuming the more realistic scenario of a non-sample-spaced CIR.

  Motivated by the potentially excessive complexity of the LS-assisted DDCE [91] and by its limitation in terms of the number of users- or transmit antennas supported, we focused our attention in Section 16.5 on the investigation of Parallel Interference Cancellation (PIC) assisted DDCE. We found that the PIC operations can either be performed in the CIR-related domain - as proposed by Li [93] - or in the frequency-domain as proposed by Jeon *et al.* [92]. We found that the frequency-domain PIC appears more advantageous in terms of its lower complexity. In contrast to the contributions of Li [93] and Jeon *et al.* [92], in Section 16.5 we provide an in-depth mathematical analysis with respect to a number of key points. Based on identifying the estimator's recursive structure, expressions are derived for the *a posteriori-* and *a priori* estimation MSE and conditions are provided for the estimator's stability. Furthermore, an iterative procedure is devised for the off-line calculation of the *a priori* predictor coefficients. In order to provide an improved flexibility for the PIC-assisted DDCE with respect to variations of the channel's statistics and in order to increase its resilience to impulsive noise imposed by the erroneous symbol decisions that may be encountered in the DDCE, the RLS algorithm is adopted for the task of predictor coefficient adaptation. Part of this work was published in [161] or it was accepted for publication [162].

- **Chapter 17**: Various linear- and non-linear multi-user detection techniques are compared against each other in terms of their applicability to the problem of detecting the subcarrier-based vectors of the L different users' transmitted symbols encountered in a multi-user SDMA-OFDM system. Specifically, the Least-Squares Error (LSE) and Minimum Mean-Square Error (MMSE) schemes are studied in Section 17.2, while the Successive Interference Cancellation (SIC) scheme and its derivatives, such as M-SIC and partial M-SIC, as well as the Parallel Interference Cancellation (PIC) and the Maximum Likelihood (ML) detection algorithms are considered in Section 17.3. These sections include the different techniques' mathematical derivation, as well as their performance and complexity analysis.

  Specifically, in the context of SIC detection our investigations of the effects of error

propagation occurring through the different detection stages should be emphasized. Motivated by the results of these investigations an improved metric is proposed for the generation of soft-bit values suitable for turbo-decoding. Furthermore, our contributions contrived for hard-decision based turbo-decoding assisted PIC for SDMA-OFDM should be mentioned here, which was published in [163].

Based on the observation that SIC detection as the second-best performing detection approach after ML detection exhibits a potentially high complexity, further investigations are conducted in Section 17.4 for the sake of enhacing the performance of both MMSE- and PIC detection. Specifically, in Section 17.4.1 we discuss the employment of adaptive modulation in the context of an SDMA-OFDM scenario, which is hence termed as SDMA-AOFDM. This scheme will be shown to be effective in the context of an almost 'fully-loaded' system, where the L number of users supported approaches the P number of reception antennas employed at the basestation. This novel scheme was disseminated in [134].

However, the employment of the SDMA-AOFDM scheme is restricted to duplex transmission scenarios having a reverse link, such as those in Time Division Duplexing (TDD). An enhancement of the MMSE- and PIC-assisted detection schemes' performance was achieved with the aid of orthogonal Walsh-Hadamard spreading codes, which will be investigated in Section 17.4.2. These advances were published in [160].

- **Chapter 18**: In the penultimate chapter we provide a few application examples based on powerful turbo coded OFDM systems invoked for the wireless transmission of video telephone signals. In the first system design example turbo coded adaptive OFDM video transmissions are considered, while in the second system various multi-user detection schemes are invoked and their achievable transmission integrity and video performance is quitified as a function of the number of users supported.

- **Chapter 19**: In this chapter we offer detailed conclusions and highlight a range of further research problems.

1.4   Chapter Summary and Conclusions

Here we conclude our brief introduction to OFDM and the review of its evolution since its conception by Chang in 1966 [1]. Numerous seminal contributions have been reviewed in chronological order in Tables 1.1 - 1.5, highlighting the historical development of the subject. These contributions reflect the state-of-the-art at the time of writing in the context of the various OFDM system components, outlining a number of open research topics. Let us now embark on a detailed investigation of the topics introduced in this chapter.

$$*\qquad\qquad*$$

Throughout this monograph we endeavour to highlight the range of contradictory system design trade-offs associated with the conception of OFDM and MC-CDMA sys-

tems. We intend to present the material in an unbiased fashion and sufficiently richly illustrated in terms of the associated design trade-offs so that readers will be able to find recipes and examples for solving their own particular wireless communications problems. In this rapidly evolving field it is a challenge to complete a timely, yet self-contained treatise, since new advances are discovered at an accelerating pace, which should find their way into a timely monograph. Our sincere hope is that you, the readers, will find the book a useful source of information, but above all a catalyst of further research.

Part I

OFDM System Design

Part II

OFDM versus MC-CDMA Systems, Their Spreading Codes and Peak Factor Reduction

Part III

Advanced Topics: Channel Estimation and Multi-user OFDM Systems

Uplink Detection Techniques for Multi-User SDMA-OFDM

17.1 Introduction

Space-Division-Multiple-Access (SDMA) communication systems have recently drawn wide interests. In these systems the L different users' transmitted signals are separated at the base-station (BS) with the aid of their unique, user-specific spatial signature, which is constituted by the P-element vector of channel transfer factors between the users' single transmit antenna and the P different receiver antenna elements at the BS, upon assuming flat-fading channel conditions such as in each of the OFDM subcarriers. This will be further detailed during our portrayal of the SDMA-MIMO channel model in Section 17.1.3.

A whole host of multi-user detection (MUD) techniques known from Code-Division-Multiple-Access (CDMA) communications lend themselves also to an application in the context of SDMA-OFDM on a per-subcarrier basis. Some of these techniques are the Least-Squares (LS) [113, 119, 127, 135], Minimum Mean-Square Error (MMSE) [105–108, 110, 113, 117, 121, 135–137], Successive Interference Cancellation (SIC) [104, 109, 113, 117, 119, 124, 126, 128, 135, 137], Parallel Interference Cancellation (PIC) [125, 135] and Maximum Likelihood (ML) detection [112, 114–118, 120, 123, 135, 137]. A comprehensive overview of recent publications on MUD techniques for MIMO systems is given in Tables 17.1 and 17.2.

The further structure of our introduction is as follows. In Section 17.1.1 a detailed classification of the different MUD techniques is provided. By contrast, a more simple classification is employed in Section 17.1.2, which reflects the structure of this chapter. Before we embark on the discussion of linear MUD techniques in Section 17.2, the SDMA-MIMO channel model, to be used in our further discussions will be introduced in Section 17.1.3

17.1.1 Classification of Multi-User Detection Techniques

The above techniques have been classified in Figure 17.1. Among the different techniques, the ML detection principle shown at the left-hand side of Figure 17.1 is known to exhibit

Year	Author	Contribution
'96	Foschini [104]	The concept of the BLAST architecture was introduced.
'98	Vook and Baum [105]	SMI-assisted MMSE combining was invoked on an OFDM subcarrier basis.
	Wang and Poor [106]	Robust sub-space based weight vector calculation and tracking was employed for co-channel interference suppression, as an improvement of the SMI-algorithm.
	Wong, Cheng, Letaief and Murch [107]	Optimization of an OFDM system was reported in the context of multiple transmit- and receive antennas upon invoking the maximum SINR criterion. The computational computational was reduced by exploiting the channel's correlation in the frequency-direction.
	Li and Sollenberger [108]	Tracking of the channel correlation matrix' entries was suggested in the context of SMI-assisted MMSE combining for multiple receiver antenna assisted OFDM, by capitalizing on the principles of [68].
'99	Golden, Foschini, Valenzuela and Wolniansky [109]	The SIC detection assisted V-BLAST algorithm was introduced.
	Li and Sollenberger [110]	The system introduced in [108] was further detailed.
	Vandenameele, Van Der Perre, Engels and H. D. Man [111]	A comparative study of different SDMA detection techniques, namely that of MMSE, SIC and ML detection was provided. Further improvements of SIC detection were suggested by adaptively tracking multiple symbol decisions at each detection node.
	Speth and Senst [112]	Soft-bit generation techniques were proposed for MLSE in the context of a coded SDMA-OFDM system.
'00	Sweatman, Thompson, Mulgrew and Grant [113]	Comparisons of various detection algorithms including LS, MMSE, D-BLAST and V-BLAST (SIC detection) were carried out.
	van Nee, van Zelst and Awater [114–116]	The evaluation of ML detection in the context of a Space-Division Multiplexing (SDM) system was provided, considering various simplified ML detection techniques.
	Vandenameele, Van Der Perre, Engels, Gyselinckx and De Man [117]	More detailed discussions were provided on the topics of [111].

Table 17.1: Contributions on detection techniques for MIMO systems and more specifically multiple transmit antenna assisted OFDM systems.

Year	Author	Contribution
'00	Li, Huang, Lozano and Foschini [118]	Reduced complexity ML detection was proposed for multiple transmit antenna systems employing adaptive antenna grouping and multi-step reduced-complexity detection.
'01	Degen, Walke, Lecomte and Rembold [119]	An overview of various adaptive MIMO techniques was provided. Specifically, pre-distortion was employed at the transmitter, as well as LS- or BLAST detection were used at the receiver or balanced equalization was invoked at both the transmitter and receiver.
	Zhu and Murch [120]	A tight upper bound on the SER performance of ML detection was derived.
	Li, Letaief, Cheng and Cao [121]	Joint adaptive power control and detection was investigated in the context of an OFDM/SDMA system, based on the approach of Farrokhi *et al.* [122].
	van Zelst, van Nee and Awater [123]	Iterative decoding was proposed for the BLAST system following the turbo principle.
	Benjebbour, Murata and Yoshida [124]	The performance of V-BLAST or SIC detection was studied in the context of backward iterative cancellation scheme employed after the conventional forward cancellation stage.
	Sellathurai and Haykin [125]	A simplified D-BLAST was proposed, which used iterative PIC capitalizing on the extrinsic soft-bit information provided by the FEC scheme employed.
	Bhargave, Figueiredo and Eltoft [126]	A detection algorithm was suggested, which followed the concepts of V-BLAST or SIC. However, multiple symbols states are tracked from each detection stage, where - in contrast to [117] - an intermediate decision is made at intermediate detection stages.
	Thoen, Deneire, Van Der Perre and Engels [127]	A constrained LS detector was proposed for OFDM/SDMA, which was based on exploiting the constant modulus property of PSK signals.
'02	Li and Luo [128]	The block error probability of optimally ordered V-BLAST was studied. Furthermore, the block error probability is also investigated for the case of tracking multiple parallel symbol decisions from the first detection stage, following an approach similar to that of [117].

Table 17.2: Contributions on detection techniques for MIMO systems and for multiple transmit antenna assisted OFDM systems.

Multi-User Detection

Optimum
(M_c^L-dim. classifier)

Sub-Optimum
(M_c-dim. classifiers)

Sequential
(combining/classification)

Embedded
(combining/classification)

ML

LS
MMSE

SIC
PIC
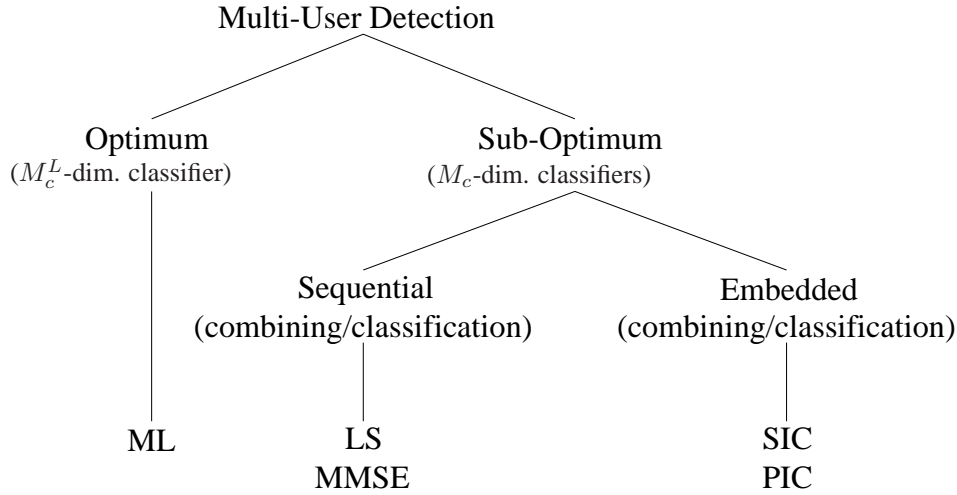
Figure 17.1: Classification of the various MUD techniques discussed in Chapter 17.

the optimum performance, but also imposes the highest complexity. This is, because in ML detection the number of M_c^L trial symbol combinations, which are constituted by all possible combinations of the L different users' transmitted symbols belonging to an M_c-ary constellation, has to be evaluated in terms of the Euclidean distance between the vector of signals actually received by the P different antenna elements and the vector of trial signals, which are generated from all legitimate transmitted symbols, impaired according to the estimated channel.

In order to avoid the potentially excessive complexity of the optimum ML detection, a range of sub-optimum detection techniques have been devised, which are summarized at the right-hand side of Figure 17.1. The philosophy of the suboptimum detectors is to reduce the dimensionality of the classification problem associated with selecting the specific constellation point, which is most likely to have been transmitted by each user.

Specifically, in the context of the LS- and MMSE detection techniques to be detailed in Sections 17.2.2 and 17.2.3, first linear estimates of the different users' transmitted signals are provided with the aid of the weighted combining of the signals received by the different antenna elements at the BS. This is followed by separately demodulating each of the L different users' combiner output signals. Hence, the original M_c^L-dimensional classification problem associated with the optimum ML detection has been reduced to L number of individual classification steps, each having a dimensionality of M_c. This is achieved at the cost of a BER degradation, which is associated with ignoring the residual interference contaminating the linear combiner's output signals.

We note again that in the context of LS- and MMSE detection the linear combining and classification steps are invoked in a sequential manner. However, a significant BER performance improvement can be achieved by embedding the classification process, which is a non-linear operation, into the linear combining process. Two of the most prominent representatives of this family of techniques are the SIC- and the PIC based detectors, which will

Multi-User Detection

Linear   Non-Linear

LS   SIC
MMSE   PIC
                            ML
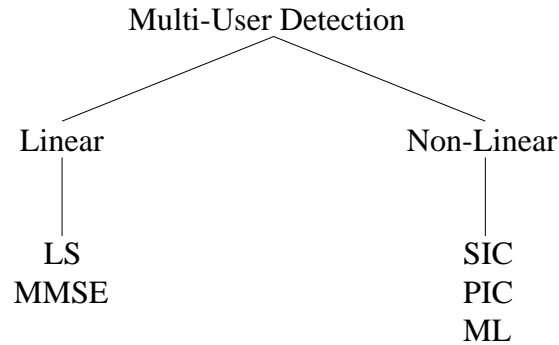
Figure 17.2: Classification of the various MUD techniques

be the topic of Sections 17.3.1 and 17.3.2, respectively.

17.1.2 Outline of Chapter 17

A possible classification of the various MUD techniques to be discussed in this chapter was presented in Figure 17.1. However, an alternative classification, which will serve as a guideline for our forthcoming discussions is portrayed in Figure 17.2. Here we have introduced the classes of linear- and non-linear detection techniques. The rationale of this classification is that in the context of linear detection techniques, such as LS- and MMSE detection, no *a priori* knowledge of the remaining users' transmitted symbols is required for the detection of a specific user. However, in the case of SIC, PIC and ML detection, *a priori* knowledge is involved, which must be provided by the non-linear classification operation involved in the demodulation process.

As shown in Figure 17.2, the further structure of this chapter 17 is as follows. In Section 17.2 the most salient linear detection techniques, namely LS- and MMSE detection will be discussed. These discussions include their MSE- and BER performance analysis in the context of both uncoded and turbo-coded scenarios, as well as the analysis of the computational complexity.

In Section 17.3 we will then embark on a detailed analysis of the family of non-linear detection techniques, namely that of SIC, PIC and ML detection, again, with respect to their BER performance in both uncoded and turbo-coded scenarios. Furthermore, a complexity analysis will be carried out. Specifically, in the context of our analysis of SIC detection and its derivatives, namely of M-SIC and partial M-SIC we will focus our efforts on the effects of error propagation across the different detection stages. These investigations motivated the introduction of a weighted soft-bit metric to be employed in the context of turbo-decoding. Furthermore, in the context of PIC detection we proposed to embed turbo-decoding into the detection process, with the aim of increasing the reliability of the *a priori* symbol estimates employed in the PIC process. A final comparison between the different linear- and non-linear detection techniques in terms of their BER performance and computational complexity will be conducted at the end of Section 17.3.

In an effort to further enhance the performance of the different detection techniques with-
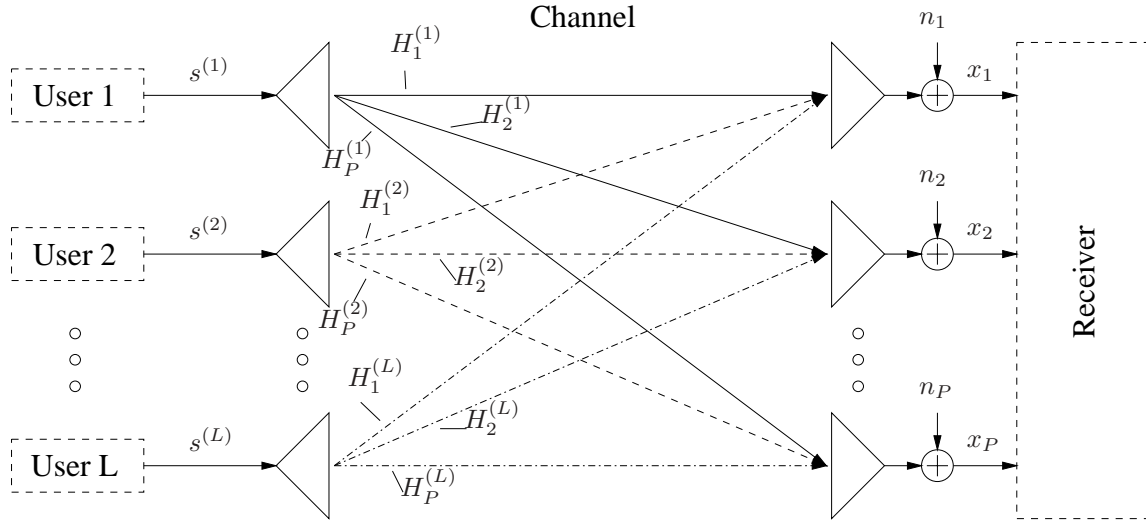
Figure 17.3: Schematic of an SDMA uplink MIMO channel scenario, where each of the L users is equipped with a single transmit antenna and the receiver is assisted by a P-element antenna front-end.

out reducing their effective throughput, as in the case of turbo-coding, the applicability of adaptive modulation and Walsh-Hadamard Transform (WHT) based spreading will be investigated in Section 17.4. Our final conclusions for this chapter will then be offered in Section 17.5.

However, before we embark on the investigation of linear detection techniques in Section 17.2, the SDMA-MIMO channel model will be introduced in the next section.

17.1.3 SDMA-MIMO Channel Model

In Figure 17.3 we have portrayed a Space-Division-Multiple-Access (SDMA) uplink transmission scenario, where each of the L simultaneous users is equipped with a single transmission antenna, while the receiver capitalizes on a P-element antenna front-end. The vector of complex signals, $\mathbf{x}[n, k]$, received by the P-element antenna array in the k-th subcarrier of the n-th OFDM symbol is constituted by the superposition of the independently faded signals associated with the L users sharing the same space-frequency resource. The received signal was corrupted by the Gaussian noise at the array elements. The indices $[n, k]$ have been omitted for notational convenience during our forthcoming discourse, yielding:

$$\mathbf{x} \quad = \quad \mathbf{Hs} + \mathbf{n}, \tag{17.1}$$

where the vector $\mathbf{x} \in \mathbb{C}^{P \times 1}$ of received signals, the vector $\mathbf{s} \in \mathbb{C}^{L \times 1}$ of transmitted signals and the array noise vector $\mathbf{n} \in \mathbb{C}^{P \times 1}$, respectively, are given by:

$$\mathbf{x} = (x_1, x_2, \dots, x_P)^T, \tag{17.2}$$

$$\mathbf{s} = (s^{(1)}, s^{(2)}, \dots, s^{(L)})^T, \tag{17.3}$$

$$\mathbf{n} = (n_1, n_2, \dots, n_P)^T. \tag{17.4}$$

The frequency domain channel transfer factor matrix $\mathbf{H} \in \mathbb{C}^{P \times L}$ is constituted by the set of channel transfer factor vectors $\mathbf{H}^{(l)} \in \mathbb{C}^{P \times 1}$, $l = 1, \dots, L$ of the L users:

$$\mathbf{H} = (\mathbf{H}^{(1)}, \mathbf{H}^{(2)}, \dots, \mathbf{H}^{(L)}), \tag{17.5}$$

each of which hosts the frequency domain channel transfer factors between the single transmitter antenna associated with a particular user l and the reception antenna elements $p = 1, \dots, P$:

$$\mathbf{H}^{(l)} = (H_1^{(l)}, H_2^{(l)}, \dots, H_P^{(l)})^T, \tag{17.6}$$

with $l \in \{1, \dots, L\}$. Regarding the statistical properties of the components associated with the vectors involved in Equation 17.1, we assume that the complex data signal $s^{(l)}$ transmitted by the l-th user has zero-mean and a variance of σ_l^2. The AWGN noise process n_p at any antenna array element p exhibits also zero-mean and a variance of σ_n^2. The frequency domain channel transfer factors $H_p^{(l)}$ of the different array elements $p \in \{1, \dots, P\}$ or users $l \in \{1, \dots, L\}$ are independent, stationary, complex Gaussian distributed processes with zero-mean and unit variance.

17.2 Linear Detection Techniques

The first class of detectors portrayed in this chapter belong to the family of the so-called linear detectors. Their employment is motivated by the observation that in the context of the optimum ML detector to be discussed in Section 17.3.3 a potentially excessive number of M_c^L trial symbol combinations has to be tested in terms of their associated trial signals' Euclidean distance measured from the vector of signals received by the different antenna elements. Recall that L represents the number of simultaneously transmitting users and M_c represents the number of legitimate transmitted symbols. Depending on the L number of simultaneous users supported and the M_c number of constellation points, a practical implementation of the ML detector may become unrealistic, as we will show during our complexity comparison in Section 17.3.4.2. A more practical approach is hence to generate estimates of the different users' transmitted signals with the aid of a linear combiner. These signal estimates would then be demodulated separately for each of the L users upon neglecting the residual interference caused by the remaining users in a specific user's combiner output signal. Hence the dimensionality of the receiver's classification task during demodulation is reduced from evaluating the multi-user Euclidean distance metric M_c^L times to the evaluation of the single-user Euclidean distance metric L times for all the M_c symbols. This reduces the total complexity to evaluating the Euclidean metric LM_c times. A simplified block diagram of the linear detector is also shown in Figure 17.4.
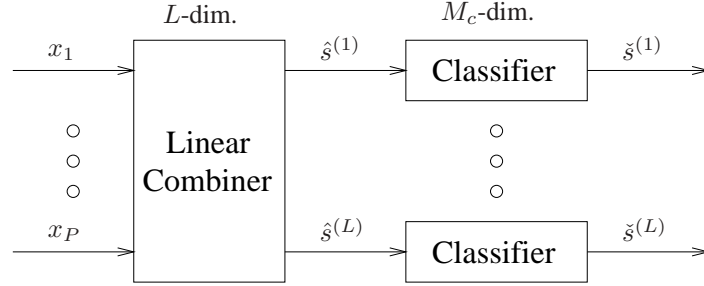
Figure 17.4: Illustration of the main signal paths associated with a linear detector such as LS or MMSE. The signals $x_p, p = 1, \ldots, P$ received by the different antenna elements are fed into the linear combiner, whose associated output vector $\hat{\mathbf{s}}$ of linear signal estimates with elements $\hat{s}^{(l)}, l = 1, \ldots, L$ is defined by Equation 17.7, and the LS- or MMSE-specific weight matrices are given by Equations 17.39 or 17.64 in its right-inverse related form and 17.68 in its left-inverse related form. The l-th user's signal, where $l = 1, \ldots, L$, is then conveyed to a separate classifier or demodulator, at the output of which the amplified constellation point $\check{s}^{(l)}$ most likely transmitted by the l-th user becomes available. The demodulator is described by Equation 17.94. Note that here we have omitted the signal paths associated with the channel transfer factor estimates required by the linear combiner.

Our discussions commence in Section 17.2.1 with the characterization of the linear combiner's output signal and its components. By contrast, in Sections 17.2.2 and 17.2.3 we will focus our attention on two specific linear combiners, namely on the LS combiner and on the MMSE combiner, respectively[1]. These combiners constitute the basis for our discussions on non-linear detection techniques, such as SIC, PIC and transform-based ML detection in Sections 17.3.1, 17.3.2 and 17.3.3. Furthermore, in Section 17.2.4 the process of symbol classification or demodulation - as seen at the right-hand side of Figure 17.4 - is described while in Section 17.2.5 the generation of soft-bit values for turbo-decoding is outlined. The LS and MMSE detectors are characterized in terms of their associated combiner's MSE and SINR as well as the detector's BER performance in Section 17.2.6. This is followed by a detailed complexity analysis in Section 17.2.7. Finally, our conclusions on linear detection techniques will be offered in Section 17.2.8.

17.2.1   Characterization of the Linear Combiner's Output Signal

As the terminology suggests, an estimate $\hat{\mathbf{s}} \in \mathbb{C}^{L \times 1}$ of the vector of transmitted signals $\mathbf{s}$ of the L simultaneous users is generated by linearly combining the signals received by the P different receiver antenna elements with the aid of the weight matrix $\mathbf{W} \in \mathbb{C}^{P \times L}$, resulting in:

$$\hat{\mathbf{s}} = \mathbf{W}^H \mathbf{x}. \tag{17.7}$$

---

[1]Note that in the following the specific linear detector is considered is referred to as the LS- or MMSE-detector, depending on whether LS- or MMSE combining is employed.

In order to gain a further insight into the specific structure of the combiner's output signal on a component basis, let us substitute Equation 17.1 into Equation 17.7 and consider the l-th user's associated vector component:

$$\hat{s}^{(l)} \quad = \quad \mathbf{w}^{(l)H}\mathbf{x} \tag{17.8}$$

$$= \quad \mathbf{w}^{(l)H}(\mathbf{Hs} + \mathbf{n}) \tag{17.9}$$

$$= \quad \mathbf{w}^{(l)H}\mathbf{H}^{(l)}s^{(l)} + \mathbf{w}^{(l)H}\sum_{\substack{i=1 \\ i\neq l}}^{L}\mathbf{H}^{(i)}s^{(i)} + \mathbf{w}^{(l)H}\mathbf{n}, \tag{17.10}$$

where the weight vector $\mathbf{w}^{(l)} \in \mathbb{C}^{P\times 1}$ is the l-th column vector of the weight matrix $\mathbf{W}$. The further structure of Section 17.2.1 is as follows. While in Section 17.2.1.1 we briefly characterize the different additive components of the combiner's output signal, their statistical properties recorded in terms of the different contributions' variances are highlighted in Section 17.2.1.2. On the basis of these, the three most prominent performance measures used for assessing the quality of the combiner's output signal namely, the SINR, the SIR and the SNR will be introduced in Section 17.2.1.3.

17.2.1.1 Description of the Different Signal Components

We observe from Equation 17.10 that the combiner's output signal is constituted by three additive components. More specifically, in Equation 17.10 the first term, namely:

$$\hat{s}_S^{(l)} = \mathbf{w}^{(l)H}\mathbf{H}^{(l)}s^{(l)} \tag{17.11}$$

denotes the desired user's associated contribution, while the second term, namely:

$$\hat{s}_I^{(l)} = \mathbf{w}^{(l)H}\sum_{\substack{i=1 \\ i\neq l}}^{L}\mathbf{H}^{(i)}s^{(i)} \tag{17.12}$$

denotes the interfering users' residual contribution. Finally, the last term, namely:

$$\hat{s}_N^{(l)} = \mathbf{w}^{(l)H}\mathbf{n} \tag{17.13}$$

is related to the AWGN. These components can be further characterized in terms of their variances, which will be further elaborated on in the next section.

17.2.1.2 Statistical Characterization

Specifically, the variance of the desired user's detected signal is given by:

$$\sigma_S^{(l)2} \quad = \quad E\{\hat{s}_S^{(l)H}\hat{s}_S^{(l)}\} \tag{17.14}$$

$$= \quad \mathbf{w}^{(l)H}\mathbf{R}_{a,S}^{(l)}\mathbf{w}^{(l)}, \quad \text{where} \tag{17.15}$$

$$\mathbf{R}_{a,S}^{(l)} \quad = \quad \sigma_l^2\mathbf{H}^{(l)}\mathbf{H}^{(l)H} \in \mathbb{C}^{P\times P} \tag{17.16}$$

is the auto-correlation matrix of the desired user's signal. Following similar calculations, the variance of the interfering users' contribution is given as:

$$\sigma_I^{(l)2} = E\{\hat{s}_I^{(l)H}\hat{s}_I^{(l)}\} \tag{17.17}$$

$$= \mathbf{w}^{(l)H}\mathbf{R}_{a,I}^{(l)}\mathbf{w}^{(l)}, \quad \text{where} \tag{17.18}$$

$$\mathbf{R}_{a,I}^{(l)} = \sum_{\substack{i=1 \\ i \neq l}}^{L} \sigma_i^2 \mathbf{H}^{(i)}\mathbf{H}^{(i)H} \in \mathbb{C}^{P \times P} \tag{17.19}$$

is the auto-correlation matrix of the interfering users' signals. Finally, the residual AWGN related variance can be expressed as:

$$\sigma_N^{(l)2} = E\{\hat{s}_N^{(l)H}\hat{s}_N^{(l)}\} \tag{17.20}$$

$$= \mathbf{w}^{(l)H}\mathbf{R}_{a,N}\mathbf{w}^{(l)}, \quad \text{where} \tag{17.21}$$

$$\mathbf{R}_{a,N} = \sigma_n^2 \mathbf{I} \in \mathbb{C}^{P \times P} \tag{17.22}$$

is the diagonal noise correlation matrix. Specifically, in the context of Equation 17.22 we have exploited again that the AWGN observed at different elements of the receiver antenna array is uncorrelated. For employment at a later stage we will additionally define here the undesired signal's auto-correlation matrix, which is related to the sum of the residual interference plus the AWGN expressed as:

$$\mathbf{R}_{a,I+N}^{(l)} = \mathbf{R}_{a,I}^{(l)} + \mathbf{R}_{a,N}, \tag{17.23}$$

where the matrices $\mathbf{R}_{a,I}^{(l)}$ and $\mathbf{R}_{a,N}$ were given by Equations 17.19 and 17.22, respectively.

17.2.1.3 Performance Measures

Three different performance measures can be defined on the basis of the desired signal's variance $\sigma_S^{(l)2}$, the interfering signal's variance $\sigma_I^{(l)2}$ and the noise variance $\sigma_N^{(l)2}$, which were given by Equations 17.14, 17.17 and 17.20. These measures can be employed for characterizing the quality of the linear combiner's output signal. These are the Signal-to-Interference-plus-Noise Ratio (SINR) at the combiner's output, defined as [136]:

$$\text{SINR}^{(l)} = \frac{\sigma_S^{(l)2}}{\sigma_I^{(l)2} + \sigma_N^{(l)2}} = \frac{\mathbf{w}^{(l)H}\mathbf{R}_{a,S}^{(l)}\mathbf{w}^{(l)}}{\mathbf{w}^{(l)H}\mathbf{R}_{a,I+N}^{(l)}\mathbf{w}^{(l)}}, \tag{17.24}$$

the Signal-to-Interference Ratio (SIR), defined as [136]:

$$\text{SIR}^{(l)} = \frac{\sigma_S^{(l)2}}{\sigma_I^{(l)2}} = \frac{\mathbf{w}^{(l)H}\mathbf{R}_{a,S}^{(l)}\mathbf{w}^{(l)}}{\mathbf{w}^{(l)H}\mathbf{R}_{a,I}^{(l)}\mathbf{w}^{(l)}}, \tag{17.25}$$

and the Signal-to-Noise Ratio (SNR) given by [136]:

$$\text{SNR}^{(l)} \quad = \quad \frac{\sigma_S^{(l)2}}{\sigma_N^{(l)2}} = \frac{\mathbf{w}^{(l)H}\mathbf{R}_{a,S}^{(l)}\mathbf{w}^{(l)}}{\mathbf{w}^{(l)H}\mathbf{R}_{a,N}^{(l)}\mathbf{w}^{(l)}}. \tag{17.26}$$

In the next section we will embark on the portrayal of least-squares error detection, in an effort to compare a number of different criteria that can be invoked for adjusting the detector's associated combiner weight matrix $\mathbf{W}$ introduced in Equation 17.7.

17.2.2 Least-Squares Error Detector

With reference to Figure 17.4, in this section we will derive the Least-Squares (LS) error- or Zero-Forcing (ZF) combiner [113,119,127,135], which attempts to recover the vector $\mathbf{s}[n, k]$ of signals transmitted by the L different users in the k-th subcarrier of the n-th OFDM symbol period, regardless of the signal quality quantified in terms of the SNR at the reception antennas. For simplicity, we will again omit the index $[n, k]$ throughout our forthcoming discourse. Our description of the LS combiner is structured as follows. In Section 17.2.2.1 a simplified model $\hat{\mathbf{x}}$ of the vector $\mathbf{x}$ of signals received by the P different antenna elements is introduced as a function of the estimate $\hat{\mathbf{s}}$ of the vector of L number of transmitted signals. On the basis of this simplified model a cost-function is established in Section 17.2.2.2, which follows the philosophy of the squared model mismatch error. The estimate $\hat{\mathbf{s}}$ of the L different users' transmitted symbols is then determined in Section 17.2.2.3 with the aid of the conjugate-gradient method [90]. Alternatively, the so-called orthogonality principle [90] could be invoked. Furthermore, in Section 17.2.2.4 a condition is provided, which has to be satisfied in order to be able to identify the estimate $\hat{\mathbf{s}}$, while in Sections 17.2.2.5 and 17.2.2.6 expressions are presented for both the squared error measured in the received signal's domain and for the mean-square error evaluated in the transmitted signal's domain.

17.2.2.1 Simplified Model of the Received Signal

Upon assuming perfect knowledge of the channel transfer factor matrix $\mathbf{H}$ an estimate $\hat{\mathbf{x}} \in \mathbb{C}^{P \times 1}$ of the vector of signals received by the P different antenna elements in a specific subcarrier is given similarly to Equation 17.1 by:

$$\hat{\mathbf{x}} = \mathbf{H}\hat{\mathbf{s}}, \tag{17.27}$$

where $\hat{\mathbf{s}} \in \mathbb{C}^{L \times 1}$ is the estimate of the vector of signals transmitted by the L different users, which we are attempting to recover.

17.2.2.2 Least-Squares Error Cost-Function

The estimation error $\Delta\hat{\mathbf{x}} \in \mathbb{C}^{P \times 1}$ in the received signal's domain can hence be expressed as:

$$\Delta\hat{\mathbf{x}} \quad = \quad \mathbf{x} - \hat{\mathbf{x}} \tag{17.28}$$
$$= \quad \mathbf{x} - \mathbf{H}\hat{\mathbf{s}}. \tag{17.29}$$
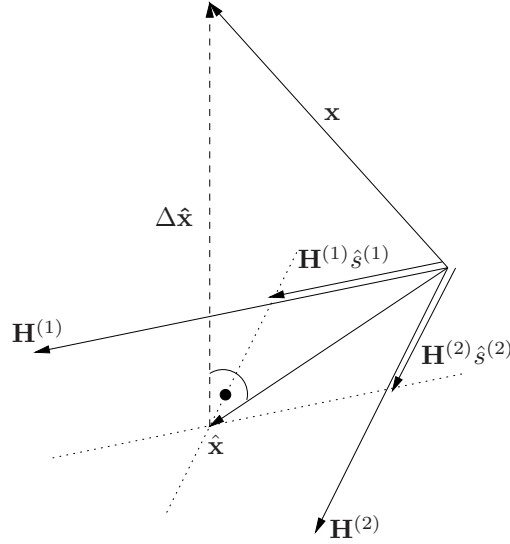
Figure 17.5: Illustration of the principle of LS detection for a scenario of $L = 2$ simultaneous users. The vector $\mathbf{x}$ of received signals is projected onto the vector space spanned by the column vectors $\mathbf{H}^{(1)}$, $\mathbf{H}^{(2)}$ hosted by the channel matrix $\mathbf{H}$.

Correspondingly, the squared error $||\Delta\hat{\mathbf{x}}||_2^2 \in \mathbb{R}$ is given as the inner product of the vector of LS estimation errors formulated in Equation 17.28, namely as:

$$\begin{align} ||\Delta\hat{\mathbf{x}}||_2^2 &= \Delta\hat{\mathbf{x}}^H \Delta\hat{\mathbf{x}} \tag{17.30} \\ &= \mathbf{x}^H\mathbf{x} - 2\Re\mathfrak{e}(\hat{\mathbf{s}}^H \mathbf{p}_{\text{LS}}) + \hat{\mathbf{s}}^H \mathbf{Q}_{\text{LS}}\hat{\mathbf{s}}, \tag{17.31} \end{align}$$

where the 'cross-correlation' vector $\mathbf{p}_{\text{LS}} \in \mathbb{C}^{L \times 1}$ is given by:

$$\mathbf{p}_{\text{LS}} = \mathbf{H}^H\mathbf{x}, \tag{17.32}$$

while the 'auto-correlation' matrix $\mathbf{Q}_{\text{LS}} \in \mathbb{C}^{L \times L}$ is given by[2]:

$$\mathbf{Q}_{\text{LS}} = \mathbf{H}^H\mathbf{H}. \tag{17.33}$$

17.2.2.3   Recovery of the Transmitted Signals by the Gradient Approach

A standard approach designed for determining the desired vector $\hat{\mathbf{s}}$ representing the estimated transmitted signals of the L users is to minimize the squared error given by Equation 17.30. This can be achieved by noting that in the optimum point of operation, associated with the

---

[2]Note that $\mathbf{p}_{\text{LS}}$ and $\mathbf{Q}_{\text{LS}}$ have been intentionally termed 'cross-correlation' vector and 'auto-correlation' matrix, in order to highlight the similarities to the corresponding matrices in the context of MMSE combining, although the expectation operator is not invoked here.

weight matrix having the optimum weights, the conjugate gradient $\nabla^* = \frac{\partial}{\partial \hat{\mathbf{s}}^*} \in \mathbb{C}^{L \times 1}$ of $||\Delta \hat{\mathbf{x}}||_2^2$ with respect to $\hat{\mathbf{s}}$ is equal to zero, which can be expressed as:

$$||\Delta \hat{\mathbf{x}}||_2^2 = \text{Min.} \quad \Longleftrightarrow \quad \nabla^* ||\Delta \hat{\mathbf{x}}||_2^2 \stackrel{!}{=} 0. \tag{17.34}$$

Upon substituting Equation 17.31 into Equation 17.34, after some mathematical manipulations we obtain:

$$\mathbf{Q}_{\text{LS}} \hat{\mathbf{s}}_{\text{LS}} = \mathbf{p}_{\text{LS}} \quad \Longleftrightarrow \quad \hat{\mathbf{s}}_{\text{LS}} = \mathbf{Q}_{\text{LS}}^{-1} \mathbf{p}_{\text{LS}}. \tag{17.35}$$

Here we have specifically exploited that the gradient with respect to the first term of Equation 17.31 is equal to zero, while the gradient with respect to the second term was evaluated by capitalizing on $\frac{\partial}{\partial \mathbf{z}^*} \mathfrak{Re}(\mathbf{z}^H \mathbf{a}) = \frac{1}{2}\mathbf{a}$ [90] for complex valued vectors $\mathbf{z}$ and $\mathbf{a}$. Furthermore, in the context of evaluating the gradient of the last term in Equation 17.31 we have exploited that we have $\frac{\partial}{\partial \mathbf{z}^*} \mathbf{z}^H \mathbf{R} \mathbf{z} = \mathbf{R} \mathbf{z}$ [90] in conjunction with a Hermitian matrix $\mathbf{R}$.

Upon substituting Equations 17.32 and 17.33 into Equation 17.35 we obtain the following expression for the vector $\hat{\mathbf{s}}_{\text{LS}}$ of estimated transmitted signals of the L simultaneous users:

$$\hat{\mathbf{s}}_{\text{LS}} = \mathbf{P}_{\text{LS}} \mathbf{x}, \tag{17.36}$$

where the projection matrix $\mathbf{P}_{\text{LS}} \in \mathbb{C}^{L \times P}$ is given by:

$$\mathbf{P}_{\text{LS}} = (\mathbf{H}^H \mathbf{H})^{-1} \mathbf{H}^H. \tag{17.37}$$

More specifically, the matrix $\mathbf{P}_{\text{LS}}$ projects the vector $\mathbf{x}$ of the P different antenna elements' received signals onto the column space of the channel matrix $\mathbf{H}$ [90]. These principles are further illustrated in Figure 17.5. As a comparison between Equations 17.7 and 17.36 reveals, the least-squares estimation based weight matrix $\mathbf{W}_{\text{LS}} \in \mathbb{C}^{P \times L}$ is hence given by:

$$\begin{aligned} \mathbf{W}_{\text{LS}} &= \mathbf{P}_{\text{LS}}^H & (17.38) \\ &= \mathbf{H}(\mathbf{H}^H \mathbf{H})^{-1}, & (17.39) \end{aligned}$$

while the l-th user's associated weight vector $\mathbf{w}_{\text{LS}}^{(l)}$, which is the l-th column vector of matrix $\mathbf{W}_{\text{LS}}$ can be expressed as:

$$\mathbf{w}_{\text{LS}}^{(l)} = \mathbf{H} \cdot \mathbf{col}^{(l)} \{ (\mathbf{H}^H \mathbf{H})^{-1} \}, \tag{17.40}$$

where $\mathbf{col}^{(l)}\{\}$ denotes the l-th column vector of the matrix enclosed in curly brackets.

17.2.2.4 Condition for Identification

From the literature [90], the projection matrix $\mathbf{P}_{\text{LS}}$ of Equation 17.37 is also known as the Moore-Penrose pseudo-inverse or left-inverse of $\mathbf{H}$ [90], which is denoted by $\mathbf{H}^\dagger$. A sufficient condition for its existence is that the L number of columns of the matrix $\mathbf{H}$ are linearly independent, which implies that we have $rank(\mathbf{H}) = L$. A necessary condition for this is that the P number of rows of $\mathbf{H}$ is equal to or larger than its L number of columns, namely that $P \geq L$. This implies that the maximum number of simultaneous users or transmit an-

tennas supported by the LS combiner must be lower or equal to the P number of receiver antennas.

17.2.2.5   Squared Estimation Error in the Received Signals' Domain

The squared estimation error formulated in the sense of Equation 17.30 and associated with the vector $\hat{\mathbf{s}}_{\mathrm{LS}}$ of least-squares signal estimates is given upon substituting Equation 17.35 into Equation 17.31, resulting in:

$$(||\Delta\hat{\mathbf{x}}||_2^2)_{\mathrm{LS}} = \mathbf{x}^H\mathbf{x} - \mathbf{p}_{\mathrm{LS}}^H\hat{\mathbf{s}}_{\mathrm{LS}}. \tag{17.41}$$

17.2.2.6   Mean-Square Estimation Error in the Transmitted Signals' Domain

By substituting the received signal's model of Equation 17.1 into Equation 17.36 we obtain:

$$\hat{\mathbf{s}}_{\mathrm{LS}} = \mathbf{s} + \mathbf{P}_{\mathrm{LS}}\mathbf{n}, \tag{17.42}$$

which indicates that the LS-estimate $\hat{\mathbf{s}}_{\mathrm{LS}}$ of the transmitted signal vector $\mathbf{s}$ of the L simultaneous users is based on a noise-contaminated version of $\mathbf{s}$. We note that the vector $\mathbf{s}$ of transmitted signals is restored regardless of the potential noise amplification incurred, which coined the term Zero-Forcing (ZF) combiner. Since $E\{\hat{\mathbf{s}}_{\mathrm{LS}}\} = \mathbf{s}$, the vector $\hat{\mathbf{s}}_{\mathrm{LS}}$ is also called an unbiased estimate of $\mathbf{s}$ [90]. Furthermore, from the literature [90] the vector $\hat{\mathbf{s}}_{\mathrm{LS}}$ is also known as the Maximum Likelihood (ML) estimate of $\mathbf{s}$. More specifically, the vector $\hat{\mathbf{s}}_{\mathrm{LS}}$ is a sample of an L-dimensional multi-variate complex Gaussian distribution, namely, $\hat{\mathbf{s}}_{\mathrm{LS}} \sim \mathcal{CN}(\mathbf{s}, \mathbf{R}_{\Delta\hat{\mathbf{s}}_{\mathrm{LS}}})$ ([3]), with the mean vector $\mathbf{s}$ and the covariance matrix $\mathbf{R}_{\Delta\hat{\mathbf{s}}_{\mathrm{LS}}} \in \mathbb{C}^{L\times L}$([4]), given by:

$$\mathbf{R}_{\Delta\hat{\mathbf{s}}_{\mathrm{LS}}} = E\{(\mathbf{P}_{\mathrm{LS}}\mathbf{n})(\mathbf{P}_{\mathrm{LS}}\mathbf{n})^H\} \tag{17.43}$$

$$= \sigma_n^2(\mathbf{H}^H\mathbf{H})^{-1}, \tag{17.44}$$

and where Equation 17.44 has been obtained by substituting Equation 17.37 into Equation 17.43, and by exploiting that $E\{\mathbf{n}\mathbf{n}^H\} = \sigma_n^2\mathbf{I}$. The average estimation Mean-Square Error (MSE) evaluated in the transmitted signals' domain is hence given by:

$$\overline{\mathrm{MSE}}_{\mathrm{LS}} = \frac{1}{L}\mathrm{Trace}(\mathbf{R}_{\Delta\hat{\mathbf{s}}_{\mathrm{LS}}}) \tag{17.45}$$

$$= \frac{1}{L}\sigma_n^2\mathrm{Trace}((\mathbf{H}^H\mathbf{H})^{-1}), \tag{17.46}$$

while the l-th user's associated minimum MSE is given as the l-th diagonal element of the matrix $\mathbf{R}_{\Delta\hat{\mathbf{s}}_{\mathrm{LS}}}$ in Equation 17.43. Hence, according to Equations 17.43 and 17.44 we have:

$$\mathrm{MSE}_{\mathrm{LS}}^{(l)} = \sigma_n^2\mathbf{w}_{\mathrm{LS}}^{(l)H}\mathbf{w}_{\mathrm{LS}}^{(l)} \tag{17.47}$$

$$= \sigma_n^2((\mathbf{H}^H\mathbf{H})^{-1})_{[l,l]}. \tag{17.48}$$

---

[3]The complex Gaussian distribution function is denoted here as $\mathcal{CN}()$, in order to distinguish it from the Gaussian distribution function defined for real-valued random variables.

[4]Note that $\Delta\mathbf{s}_{\mathrm{LS}} = \mathbf{s} - \hat{\mathbf{s}}_{\mathrm{LS}}$.

In the next section the potentially more effective MMSE detection approach will be discussed.

17.2.3 Minimum Mean-Square Error Detector

With reference to Figure 17.4, in contrast to the LS combiner of Section 17.2.2 the Minimum Mean-Square Error (MMSE) detector's associated MMSE combiner [105–108, 110, 113, 117, 121, 135–137] exploits the available statistical knowledge concerning the signals transmitted by the different users, as well as that related to the AWGN at the receiver antenna elements.

The specific structure of Section 17.2.3 is as follows. In Section 17.2.3.1 the mean-square error related cost-function is introduced, which is then employed in Section 17.2.3.2 for deriving the optimum weight matrix with the aid of the conjugate-gradient approach [90]. Furthermore, in Section 17.2.3.3 expressions are provided for the average MSE and the user-specific MSE, respectively, in the context of employing the optimum weight matrix. Our discussions of the MMSE combiner are concluded in Section 17.2.3.4 by reducing the expression derived for the optimum weight matrix to a standard form, which will be shown later in Section 17.2.3.4 to differ only by a scalar factor from the corresponding expressions associated with the Minimum Variance (MV) combiner and also from that of the maximum SINR combiner.

17.2.3.1 Mean-Square Error Cost-Function

In contrast to the derivation of the LS combiner in Section 17.2.2, the cost-function employed here directly reflects the quality of the combiner weights in the transmitted signals' domain. In order to elaborate further, the vector $\Delta\hat{s} \in \mathbb{C}^{L \times 1}$ of the L simultaneous users' estimation errors evaluated in the transmitted signals' domain can be defined as:

$$\Delta\hat{s} = \mathbf{s} - \hat{\mathbf{s}} \tag{17.49}$$

$$= \mathbf{s} - \mathbf{W}^H \mathbf{x}, \tag{17.50}$$

where Equation 17.50 has been obtained by substituting Equation 17.7 into Equation 17.49. Furthermore, the estimation error's auto-correlation matrix $\mathbf{R}_{\Delta\hat{s}} \in \mathbb{C}^{L \times L}$ is given by:

$$\mathbf{R}_{\Delta\hat{s}} = E\{\Delta\hat{s}\Delta\hat{s}^H\} \tag{17.51}$$

$$= \mathbf{P} - \mathbf{R}_c^H \mathbf{W} - \mathbf{W}^H \mathbf{R}_c + \mathbf{W}^H \mathbf{R}_a \mathbf{W}, \tag{17.52}$$

where the cross-correlation matrix $\mathbf{R}_c \in \mathbb{C}^{P \times L}$ of the received and transmitted signals is defined as:

$$\mathbf{R}_c = E\{\mathbf{x}\mathbf{s}^H\} \tag{17.53}$$

$$= \mathbf{HP}. \tag{17.54}$$

Similarly, for the auto-correlation matrix $\mathbf{R}_a \in \mathbb{C}^{P \times P}$ of the received signals we obtain:

$$
\begin{aligned}
\mathbf{R}_a &= E\{\mathbf{x}\mathbf{x}^H\} & (17.55) \\
&= \mathbf{H}\mathbf{P}\mathbf{H}^H + \sigma_n^2 \mathbf{I} & (17.56) \\
&= \sum_{l=1}^{L} \sigma_l^2 \mathbf{H}^{(l)} \mathbf{H}^{(l)H} + \sigma_n^2 \mathbf{I}. & (17.57)
\end{aligned}
$$

Note that clearly the sum of the auto-correlation matrices $\mathbf{R}_{a,S}$, $\mathbf{R}_{a,I}$ and $\mathbf{R}_{a,N}$ given by Equations 17.16, 17.19 and 17.22, respectively, constitutes the auto-correlation matrix $\mathbf{R}_a \in \mathbb{C}^{P \times P}$ of the different reception antennas' associated signals, which can be expressed as:

$$
\mathbf{R}_a = \mathbf{R}_{a,S}^{(l)} + \mathbf{R}_{a,I+N}^{(l)}, \tag{17.58}
$$

where $\mathbf{R}_{a,I+N}^{(l)} = \mathbf{R}_{a,I}^{(l)} + \mathbf{R}_{a,N}$ from Equation 17.23. Furthermore, in Equations 17.54 and 17.56 the matrix $\mathbf{P} \in \mathbb{R}^{L \times L}$ is the diagonal matrix of the different users' associated transmit powers- or signal variances, given by:

$$
\mathbf{P} = Diag(\sigma_1^2, \sigma_2^2, \dots, \sigma_L^2). \tag{17.59}
$$

In the context of deriving Equations 17.54 and 17.56 we have also exploited that $E\{\mathbf{s}\mathbf{s}^H\} = \mathbf{P}$, as well as that $E\{\mathbf{n}\mathbf{n}^H\} = \sigma_n^2 \mathbf{I}$ and that $E\{\mathbf{s}\mathbf{n}^H\} = 0$. On the basis of Equation 17.52, the *total* mean-square estimation error $E\{||\Delta \hat{s}||_2^2\} \in \mathbb{R}$ accumulated for the different users is given by:

$$
\begin{aligned}
E\{||\Delta \hat{s}||_2^2\} &= \mathrm{Trace}(\mathbf{R}_{\Delta \hat{s}}) & (17.60) \\
&= \mathrm{Trace}(\mathbf{P}) - \mathrm{Trace}(\mathbf{R}_c^H \mathbf{W}) - \mathrm{Trace}(\mathbf{W}^H \mathbf{R}_c) + \\
&\quad + \mathrm{Trace}(\mathbf{W}^H \mathbf{R}_a \mathbf{W}). & (17.61)
\end{aligned}
$$

This equation will be employed in the next section in order to optimally adjust the matrix $\mathbf{W}$ of combiner coefficients.

17.2.3.2   Recovery of the Transmitted Signals by the Gradient Approach

Determining the weight matrix on the basis of evaluating the gradient with respect to the different users' total mean-square estimation error given by Equation 17.61 results in the standard form of the MMSE combiner, which is related to the right-inverse of the channel matrix $\mathbf{H}$. This will be further elaborated on in Section 17.2.3.2.1. Alternatively, the weight matrix can be represented in a form related to the left-inverse of the channel matrix $\mathbf{H}$, which had drawn our interest earlier in Section 17.2.2 in the context of the LS combiner characterized by Equations 17.36 and 17.37. The left-inverse related form of the MMSE combiner will be briefly addressed in Section 17.2.3.2.2.

17.2.3.2.1   Right-Inverse Related Form of the MMSE Combiner   Similarly to our proceedings in Section 17.2.2.3, the matrix $\mathbf{W}$ of optimum weights can be determined by noting that when $E\{||\Delta \hat{s}||_2^2\}$ of Equation 17.60 is minimized, its conjugate gradient evaluated with

respect to the weight matrix $\mathbf{W}$ is identical to the zero-matrix. Hence, we obtain the following equation for the matrix $\mathbf{W}_{\text{MMSE}} \in \mathbb{C}^{P \times L}$ of optimum weights:

$$\mathbf{R}_a \mathbf{W}_{\text{MMSE}} = \mathbf{R}_c \quad \Longleftrightarrow \quad \mathbf{W}_{\text{MMSE}} = \mathbf{R}_a^{-1} \mathbf{R}_c. \tag{17.62}$$

More specifically, upon substituting Equations 17.54 and 17.56 into Equation 17.62 we have:

$$\mathbf{W}_{\text{MMSE}} = (\mathbf{HPH}^H + \sigma_n^2 \mathbf{I})^{-1} \mathbf{HP}. \tag{17.63}$$

In the context of deriving the conjugate gradient of Equation 17.61 with respect to the weight matrix $\mathbf{W}$ we have exploited that the constant first term yields a zero contribution, while the remaining terms were evaluated upon noting that $\frac{\partial \text{Trace}(\mathbf{AXB})}{\partial \mathbf{X}} = \mathbf{0}$, as well as that $\frac{\partial \text{Trace}(\mathbf{AX}^H \mathbf{B})}{\partial \overline{\mathbf{X}}} = \mathbf{BA}$ and $\frac{\partial \text{Trace}(\mathbf{X}^H \mathbf{AXB})}{\partial \overline{\mathbf{X}}} = \mathbf{AXB}$ for the complex matrices $\mathbf{A}$, $\mathbf{B}$ and $\mathbf{X}$ [90]. Note that Equation 17.63 can be rewritten as:

$$\mathbf{W}_{\text{MMSE}} = (\mathbf{HP}_{\text{SNR}} \mathbf{H}^H + \mathbf{I})^{-1} \mathbf{HP}_{\text{SNR}}, \tag{17.64}$$

where similarly to Equation 17.59, the matrix $\mathbf{P}_{\text{SNR}} \in \mathbb{R}^{L \times L}$ is the diagonal matrix of the different users' associated SNRs at the receiver antennas, which can be written as:

$$\mathbf{P}_{\text{SNR}} = Diag(\text{SNR}^{(1)}, \text{SNR}^{(2)}, \dots, \text{SNR}^{(L)}), \tag{17.65}$$

and where the l-th user's SNR is given by $\text{SNR}^{(l)} = \frac{\sigma_l^2}{\sigma_n^2}$. Furthermore, note from Equation 17.62 and 17.63 that the l-th user's associated weight vector $\mathbf{w}_{\text{MMSE}}^{(l)} \in \mathbb{C}^{P \times 1}$ is given by:

$$\mathbf{w}_{\text{MMSE}}^{(l)} = \mathbf{R}_a^{-1} \mathbf{H}^{(l)} \sigma_l^2 \tag{17.66}$$

$$= (\mathbf{HPH}^H + \sigma_n^2 \mathbf{I})^{-1} \mathbf{H}^{(l)} \sigma_l^2. \tag{17.67}$$

17.2.3.2.2 Left-Inverse Related Form of the MMSE Combiner
Recall that as demonstrated in Equation 17.22, the auto-correlation matrix of the AWGN is represented by a scaled identity matrix. Hence, it can be shown that an alternative expression with respect to Equation 17.63 for the MMSE combiner's weight matrix is given by:

$$\mathbf{W}_{\text{MMSE}} = \mathbf{HP}_{\text{SNR}} (\mathbf{H}^H \mathbf{HP}_{\text{SNR}} + \mathbf{I})^{-1}. \tag{17.68}$$

Upon substituting $\mathbf{R}_c = \mathbf{HP}$ as defined in Equation 17.54([5]), as well as by substituting $\mathbf{R}_{\overline{a}} \in \mathbb{C}^{L \times L}$([6]) defined as:

$$\mathbf{R}_{\overline{a}} = \mathbf{H}^H \mathbf{HP} + \sigma_n^2 \mathbf{I}, \tag{17.69}$$

---

[5]Recall from Equations 17.59 and 17.65 that $\mathbf{P} = \sigma_n^2 \mathbf{P}_{\text{SNR}}$.

[6]The left-inverse related form of the auto-correlation matrix is denoted here as $\mathbf{R}_{\overline{a}}$ in order to distinguish it from its right-inverse related form, namely $\mathbf{R}_a$, defined in Equation 17.56.

similarly to Equation 17.62 we obtain the following relation:

$$\mathbf{R}_{\bar{a}}^{H} \mathbf{W}_{\text{MMSE}}^{H} = \mathbf{R}_{c}^{H} \quad \Longleftrightarrow \quad \mathbf{W}_{\text{MMSE}}^{H} = \mathbf{R}_{\bar{a}}^{H-1} \mathbf{R}_{c}^{H}. \tag{17.70}$$

In terms of the required numerical accuracy, calculating the weight matrix $\mathbf{W}_{\text{MMSE}}$ by solving the system of equations as shown at the left-hand side of Equation 17.70 is more attractive, than a solution by the direct inversion of the auto-correlation matrix $\mathbf{R}_{\bar{a}}$, as shown at the right-hand side of Equation 17.70.

Note that in contrast to the auto-correlation matrix $\mathbf{R}_{a}$ defined in Equation 17.56, which is the core element of the right-inverse related representation of the weight matrix according to Equation 17.62, the correlation matrix $\mathbf{R}_{\bar{a}}$ defined in Equation 17.69, which was associated with the left-inverse related representation of the weight matrix in Equation 17.70 is not Hermitian. As a result, unfortunately the same computationally efficient methods which can be invoked for solving the system of equations associated with the right-inverse related representation of the weight matrix, namely the auto-correlation matrix's Toeplitz structure are not applicable here. However, a computational advantage is potentially achievable with the advent of the lower dimensionality of the matrix $\mathbf{R}_{\bar{a}} \in \mathbb{C}^{L \times L}$ compared to that of matrix $\mathbf{R}_{a} \in \mathbb{C}^{P \times P}$, provided that we have $P > L$. This property renders the left-inverse related form of the MMSE combiner particularly attractive for its repeated application in each cancellation stage of the SIC detector, which will be discussed in Section 17.3.1.

17.2.3.3 Mean-Square Estimation Error in the Transmitted Signals' Domain

Upon substituting the weight matrix $\mathbf{W}_{\text{MMSE}}$ defined in Equation 17.62 into Equation 17.52 we obtain for the auto-correlation matrix of the estimation errors associated with the different users' transmitted signals in the following expression:

$$\mathbf{R}_{\Delta\hat{\mathbf{s}}_{\text{MMSE}}} = \mathbf{P} - \mathbf{R}_{c}^{H} \mathbf{R}_{a}^{-1} \mathbf{R}_{c} \tag{17.71}$$
$$= \mathbf{P} - \mathbf{R}_{c}^{H} \mathbf{W}_{\text{MMSE}}. \tag{17.72}$$

Hence, following the philosophy of Equation 17.60, the *average* minimum MSE (MMSE) of the L simultaneous users is given by:

$$\overline{\text{MMSE}}_{\text{MMSE}} = \frac{1}{L} \text{Trace}(\mathbf{R}_{\Delta\hat{\mathbf{s}}_{\text{MMSE}}}), \tag{17.73}$$

while the l-th user's MMSE is given as the l-th diagonal element of the estimation errors' auto-correlation matrix $\mathbf{R}_{\Delta\hat{\mathbf{s}}_{\text{MMSE}}}$ defined in Equation 17.71, namely as:

$$\text{MMSE}_{\text{MMSE}}^{(l)} = \sigma_{l}^{2}(1 - \mathbf{H}^{(l)H} \mathbf{R}_{a}^{-1} \mathbf{H}^{(l)} \sigma_{l}^{2}) \tag{17.74}$$
$$= \sigma_{l}^{2}(1 - \mathbf{H}^{(l)H} \mathbf{w}_{\text{MMSE}}^{(l)}). \tag{17.75}$$

17.2.3.4 Optimum Weight Vector in Standard Form

We recall from Equation 17.58 that the received signals' auto-correlation matrix $\mathbf{R}_a$ can be expressed as the sum of the desired- and undesired signals' contributions, namely as:

$$\mathbf{R}_a = \mathbf{R}_{a,S}^{(l)} + \mathbf{R}_{a,I+N}^{(l)}. \tag{17.76}$$

Upon invoking the well-known matrix-inversion lemma- or Sherman-Morrison formula [90], the inverse of the auto-correlation matrix, namely $\mathbf{R}_a^{-1}$, can be rewritten as:

$$\mathbf{R}_a^{-1} = \mathbf{R}_{a,I+N}^{(l)-1} - \frac{\mathbf{R}_{a,I+N}^{(l)-1} \sigma_l^2 \mathbf{H}^{(l)} \mathbf{H}^{(l)H} \mathbf{R}_{a,I+N}^{(l)-1}}{1 + \sigma_l^2 \mathbf{H}^{(l)H} \mathbf{R}_{a,I+N}^{(l)-1} \mathbf{H}^{(l)}}. \tag{17.77}$$

Upon further substituting Equation 17.77 into Equation 17.66 we obtain:

$$\mathbf{w}_{\text{MMSE}}^{(l)} = \beta_{\text{MMSE}} \mathbf{R}_{a,I+N}^{(l)-1} \mathbf{H}^{(l)}, \tag{17.78}$$

where:

$$\beta_{\text{MMSE}} = \frac{\sigma_l^2}{1 + \text{SINR}^{(l)}}, \tag{17.79}$$

and where the achievable SINR is given by:

$$\text{SINR}^{(l)} = \sigma_l^2 \mathbf{H}^{(l)H} \mathbf{R}_{a,I+N}^{(l)-1} \mathbf{H}^{(l)}. \tag{17.80}$$

This is immediately seen by substituting Equation 17.78 into Equation 17.24. It is interesting to note that the SINR given by Equation 17.80 is independent from the factor β_{MMSE} related to the MMSE-criterion. As a consequence, different combining approaches result in achieving the same SINR at the combiner's output [136], provided that their weight vectors can be expressed in the form of Equation 17.78, despite having a constant β, which is potentially different from β_{MMSE} of the MMSE combiner. It was demonstrated in [136] that the most prominent combiners, which obey Equation 17.78 are the MMSE-, the Minimum Variance (MV) and the Maximum SINR combiners. As argued before, all three of these techniques exhibit the same SINR at the combiner's output, although they have different MSEs.

17.2.3.5 Relation between MMSE and MV combining

In order to motivate the employment of the Minimum Variance (MV) combiner let us recall from Section 17.2.2 that the LS combiner's philosophy was to fully recover the original signal transmitted - as illustrated by Equation 17.42 - without relying on any information concerning the AWGN process, which corrupts the signal received by the different antenna elements. By contrast, the philosophy of the MMSE combiner portrayed in Section 17.2.3 was to strike a balance between the recovery of the signals transmitted and the suppression of the AWGN. An attractive compromise is constituted by the MV approach, which aims for recovering the original signals transmitted whilst ensuring a partial suppression of the AWGN based on the knowledge of its statistics. In other words, the l-th user's associated weight vector $\mathbf{w}^{(l)}$ has to be adjusted such, that its transfer factor, which is seen from Equation 17.11 to be equal

to $\mathbf{w}^{(l)H}\mathbf{H}^{(l)}$, assumes a specific predefined value of $g = \mathbf{w}^{(l)H}\mathbf{H}^{(l)}$. The corresponding interference and noise variances of $\sigma_I^{(l)2}$ and $\sigma_N^{(l)2}$ are given by Equations 17.17 and 17.20, respectively.

Usually the MV combiner is derived by minimizing a Lagrangian cost-function, which incorporates both a constraint on the desired user's effective transfer factor, as well as the undesired signal's variance [90,136]. However, as argued in the previous section, the different combiners' associated weight vectors, namely those of the MMSE, MV and Maximum SINR combiners, differ only by a scalar multiplier. Hence, the MV-related weight vector $\mathbf{w}_{\mathrm{MV}}^{(l)}$ of the l-th user can be directly inferred from the MMSE-related weight vector $\mathbf{w}_{\mathrm{MMSE}}^{(l)}$ by simple normalization according to:

$$\mathbf{w}_{\mathrm{MV}}^{(l)} = \frac{g}{\mathbf{w}_{\mathrm{MMSE}}^{(l)H}\mathbf{H}^{(l)}}\mathbf{w}_{\mathrm{MMSE}}^{(l)}. \tag{17.81}$$

Here the term in the nominator denotes the l-th user's gain factor valid in the context of MMSE combining. Upon substituting the MMSE-specific weight vector given by Equation 17.78 into Equation 17.81 we obtain:

$$\mathbf{w}_{\mathrm{MV}}^{(l)} = \beta_{\mathrm{MV}}\mathbf{R}_{a,I+N}^{(l)-1}\mathbf{H}^{(l)}, \tag{17.82}$$

where:

$$\beta_{\mathrm{MV}} = \frac{g}{\mathbf{H}^{(l)H}\mathbf{R}_{a,I+N}^{(l)}\mathbf{H}^{(l)}}. \tag{17.83}$$

Specifically, for $g = 1$ this "normalized MMSE combiner" is also known as the Minimum Variance Distortionless Response (MVDR) combiner.

17.2.4 Demodulation of the Different Users' Combiner Output Signals

As observed at the left-hand side of Figure 17.4, the linear detector is constituted by the linear combiner, which produces estimates of the signals transmitted by the L different users. Based on these linear estimates the task of the classifiers seen at the right-hand side of Figure 17.4 is to determine the complex symbols- or constellation points that are most likely to have been transmitted by the different users.

Our further proceedings are as follows. In Section 17.2.4.1 each user's combiner output signal is approximated as a sample of a complex Gaussian distribution function. This representation is then employed in Section 17.2.4.2 for determining the complex symbol- or constellation point that is most likely to have been transmitted by a specific user.

17.2.4.1 Approximation of a Specific User's Combiner Output Signal as a Sample of a Complex Gaussian Distribution

In Sections 17.2.2, 17.2.3 and 17.2.3.5 various methods of detecting the different users' transmitted signals were discussed namely, the LS- MMSE- and MV techniques, respectively. Common to these techniques was their linear structure, which was conveniently illustrated by Equation 17.10. Specifically, the l-th user's combiner output signal $x_{\mathrm{eff}}^{(l)} = \hat{s}^{(l)}$ is constituted

by a superposition of the desired user's signal $H_{\text{eff}}^{(l)} s^{(l)}$ and of the undesired signal $n_{\text{eff}}^{(l)}$, which is expressed as:

$$x_{\text{eff}}^{(l)} = H_{\text{eff}}^{(l)} s^{(l)} + n_{\text{eff}}^{(l)}. \tag{17.84}$$

Comparing Equation 17.84 with Equation 17.10 reveals that the desired user's effective transfer factor $H_{\text{eff}}^{(l)}$ is given by:

$$H_{\text{eff}}^{(l)} = \mathbf{w}^{(l)H} \mathbf{H}^{(l)}, \tag{17.85}$$

while the effective undesired signal $n_{\text{eff}}^{(l)}$, namely the sum of the $L-1$ interfering users' residual signals plus the residual AWGN, is given by:

$$n_{\text{eff}}^{(l)} = \hat{s}_I^{(l)} + \hat{s}_N^{(l)}. \tag{17.86}$$

The individual components were defined in Equations 17.12 and 17.13, while their associated variances $\sigma_I^{(l)2}$ and $\sigma_N^{(l)2}$ were given by Equations 17.18 and 17.21. The l-th user's combiner output signal can therefore be approximately modeled, as a sample of a complex Gaussian distribution having a mean value of $H_{\text{eff}}^{(l)} s^{(l)}$ and a variance of $\sigma_{n_{\text{eff}}}^{(l)2} = \sigma_I^{(l)2} + \sigma_N^{(l)2}$ which is formulated as, $x_{\text{eff}}^{(l)} \sim \mathcal{CN}(H_{\text{eff}}^{(l)} s^{(l)}, \sigma_{n_{\text{eff}}}^{(l)2})$ ([7]). We note however, that this relationship is only exactly true for an infinite number of interferers, as a result of the Central-Limit Theorem [176]. This complex Gaussian distribution can be expressed as [482]:

$$f\left(x_{\text{eff}}^{(l)} | s^{(l)}, H_{\text{eff}}^{(l)}\right) = \frac{1}{\pi \sigma_{n_{\text{eff}}}^{(l)2}} \exp\left(-\frac{1}{\sigma_{n_{\text{eff}}}^{(l)2}} \left| x_{\text{eff}}^{(l)} - H_{\text{eff}}^{(l)} s^{(l)} \right|^2 \right). \tag{17.87}$$

More explicitly, $P(x_{\text{eff}}^{(l)} | s^{(l)}, H_{\text{eff}}^{(l)}) = f(x_{\text{eff}}^{(l)} | s^{(l)}, H_{\text{eff}}^{(l)})$ denotes the *a priori* probability that $x_{\text{eff}}^{(l)}$ is observed at the l-th user's combiner output under the condition that the symbol $s^{(l)}$ is transmitted over a channel characterized by the effective transfer factor $H_{\text{eff}}^{(l)}$ of Equation 17.85.

17.2.4.2 Determination of a Specific User's Transmitted Symbol by Maximizing the *A Posteriori* Probability

The complex symbol $\check{s}_{\text{ML}\approx}^{(l)}$[8] that is most likely to have been transmitted by the l-th user can be determined upon maximizing the *a posteriori* probability $P(\check{s}^{(l)} | x_{\text{eff}}^{(l)}, H_{\text{eff}}^{(l)})$, that the complex symbol $\check{s}$ was transmitted under the condition that the signal $x_{\text{eff}}^{(l)}$ was observed at the combiner output, for all symbols contained in the trial-set $\mathcal{M}^{(l)}$ given by:

$$\mathcal{M}^{(l)} = \left\{ \check{s}^{(l)} \middle| \frac{\check{s}^{(l)}}{\sigma_l} \in \mathcal{M}_c \right\}. \tag{17.88}$$

---

[7]The complex Gaussian distribution function is denoted here as $\mathcal{CN}()$, in order to distinguish it from the Gaussian distribution function $\mathcal{N}()$ defined for real-valued random variables.

[8]Here we have denoted the most likely transmitted symbol as $\check{s}_{\text{ML}\approx}^{(l)}$, in order to emphasize that the Gaussian approximation was used for modelling the residual interference contaminating the combiner's output signal.

In Equation 17.88 $\mathcal{M}_c$ denotes the set of constellation points associated with the specific modulation scheme employed. In mathematical terms this can be formulated as:

$$\check{s}_{\mathrm{ML}\approx}^{(l)} = arg \max_{\check{s}^{(l)} \in \mathcal{M}^{(l)}} P\left(\check{s}^{(l)} | x_{\mathrm{eff}}^{(l)}, H_{\mathrm{eff}}^{(l)}\right). \tag{17.89}$$

Upon invoking the definition of the conditional probability, the *a posteriori* probability $P(\check{s}^{(l)} | x_{\mathrm{eff}}^{(l)}, H_{\mathrm{eff}}^{(l)})$ seen in Equation 17.89 can be rewritten as:

$$P(\check{s}^{(l)} | x_{\mathrm{eff}}^{(l)}, H_{\mathrm{eff}}^{(l)}) = P(x_{\mathrm{eff}}^{(l)} | \check{s}^{(l)}, H_{\mathrm{eff}}^{(l)}) \frac{P(\check{s}^{(l)})}{P(x_{\mathrm{eff}}^{(l)})}, \tag{17.90}$$

where the total probability $P(x_{\mathrm{eff}}^{(l)})$ follows from the condition that:

$$\sum_{\check{s}^{(l)} \in \mathcal{M}^{(l)}} P(\check{s}^{(l)} | x_{\mathrm{eff}}^{(l)}, H_{\mathrm{eff}}^{(l)}) \stackrel{!}{=} 1, \tag{17.91}$$

which yields:

$$P(x_{\mathrm{eff}}^{(l)}) = \sum_{\check{s}^{(l)} \in \mathcal{M}^{(l)}} P(x_{\mathrm{eff}}^{(l)} | \check{s}^{(l)}, H_{\mathrm{eff}}^{(l)}) P(\check{s}^{(l)}). \tag{17.92}$$

Note that Equation 17.90 in conjunction with Equation 17.92 is also known as Bayes' theorem [90].

Upon substituting Equation 17.90 into Equation 17.89 and by noting again that the *a priori* probability $P(x_{\mathrm{eff}}^{(l)} | \check{s}^{(l)}, H_{\mathrm{eff}}^{(l)})$ is given by the complex Gaussian distribution function of Equation 17.87, namely by $f(x_{\mathrm{eff}}^{(l)} | \check{s}^{(l)}, H_{\mathrm{eff}}^{(l)})$, we obtain for the ML symbol estimate $\check{s}_{\mathrm{ML}\approx}^{(l)}$ the following expression:

$$\check{s}_{\mathrm{ML}\approx}^{(l)} = arg \max_{\check{s}^{(l)} \in \mathcal{M}^{(l)}} P\left(x_{\mathrm{eff}}^{(l)} | \check{s}^{(l)}, H_{\mathrm{eff}}^{(l)}\right) \iff \check{s}_{\mathrm{ML}\approx}^{(l)} = arg \min_{\check{s}^{(l)} \in \mathcal{M}^{(l)}} \left| x_{\mathrm{eff}}^{(l)} - H_{\mathrm{eff}}^{(l)} \check{s}^{(l)} \right|^2. \tag{17.93}$$

Note from Equation 17.93 that determining the ML symbol estimate implies minimizing the Euclidean distance in the argument of the exponential term associated with the Gaussian distribution function of Equation 17.87. In the context of our derivation we have also exploited that we have $P(\check{s}^{(l)}) = \frac{1}{M_c} = const.$, as well as that we have $P(x_{\mathrm{eff}}^{(l)}) = const.$ as seen in Equation 17.91. Hence, these terms are irrelevant in the context of the minimization required by Equation 17.93.

In order to avoid the multiplication of each trial-symbol $\check{s}^{(l)}$ with the effective transfer factor $H_{\mathrm{eff}}^{(l)}$, as required by Equation 17.93, it is legitimate to evaluate:

$$\check{s}_{\mathrm{ML}\approx}^{(l)} = arg \min_{\check{s}^{(l)} \in \mathcal{M}^{(l)}} \left| \frac{1}{H_{\mathrm{eff}}^{(l)}} x_{\mathrm{eff}}^{(l)} - \check{s}^{(l)} \right|^2, \tag{17.94}$$

instead. Note again that if the estimate $x_{\mathrm{eff}}^{(l)}$ at the l-th user's combiner output is generated

with the aid of the MMSE criterion, then the normalized estimate $x_{\text{eff}}^{(l)}/H_{\text{eff}}^{(l)}$ is actually the complex symbol, which would be observed at the output of the MVDR combiner, as described in Section 17.2.3.5. Note however that in the context of MPSK modulation schemes the normalization by the real-valued factor of $H_{\text{eff}}^{(l)}$ is not necessary, since only the signal's phase is of importance to the detection process.

17.2.5 Generation of Soft-Bit Information for Turbo-Decoding

Employing turbo decoding at the receiver is a powerful means of further enhancing the system's BER. Naturally, this is achieved at the cost of a reduction of the system's effective throughput. A prerequisite for the employment of turbo codes is the availability of soft-bit information at the detector's output, whose generation will be discussed in this section.

Our discussions will be based on Equation 17.84, which described the l-th user's combiner output signal $x_{\text{eff}}^{(l)}$ as the superposition of the desired user's signal contribution $s^{(l)}$, which has a gain of $H_{\text{eff}}^{(l)}$, plus the effective noise contribution $n_{\text{eff}}^{(l)}$, which comprises the $L-1$ remaining users' residual interference and the residual AWGN. The residual interference was approximated by a Gaussian process and hence the total variance of the effective noise became $\sigma_{n_{\text{eff}}}^{(l)2} = \sigma_I^{(l)2} + \sigma_N^{(l)2}$.

With respect to Equation 17.84 the soft-bit value or log-likelihood ratio $L_{m\approx}^{(l)}$ associated with the l-th user at the m-th bit-position is given by [90]:

$$L_{m\approx}^{(l)} = \ln \frac{P(b_m^{(l)} = 1|x_{\text{eff}}^{(l)}, H_{\text{eff}}^{(l)})}{P(b_m^{(l)} = 0|x_{\text{eff}}^{(l)}, H_{\text{eff}}^{(l)})}, \tag{17.95}$$

which is the natural logarithm of the quotient of *a posteriori* probabilities that the m-th bit transmitted by the l-th user in the k-th subcarrier is associated with a logical value of $b_m^{(l)} = 1$ or $b_m^{(l)} = 0$. Note that here we have again omitted the index $[n, k]$ for the k-th subcarrier of the n-th OFDM symbol. Equation 17.95 can be further expanded by noting that the *a posteriori* probability that a bit of $b_m^{(l)} = 1$ was transmitted is given by the sum of the *a posteriori* probabilities of those symbols, which are associated with a bit value of $b_m^{(l)} = 1$, again, at the m-th bit position. The *a posteriori* probability that a bit value of $b_m^{(l)} = 0$ was transmitted can be represented equivalently. Hence we obtain:

$$L_{m\approx}^{(l)} = \ln \frac{\sum_{(\check{s}^{(l)}/\sigma_l)\in\mathcal{M}_{cm}^1} P(\check{s}^{(l)}|x_{\text{eff}}^{(l)}, H_{\text{eff}}^{(l)})}{\sum_{(\check{s}^{(l)}/\sigma_l)\in\mathcal{M}_{cm}^0} P(\check{s}^{(l)}|x_{\text{eff}}^{(l)}, H_{\text{eff}}^{(l)})}, \tag{17.96}$$

where $\mathcal{M}_{cm}^b$ denotes the specific subset of the set $\mathcal{M}_c$ of constellation points of the modulation scheme employed, which are associated with a bit value of $b \in \{0, 1\}$ at the m-th bit position. For notational convenience we can define the l-th user's associated set of trial-vectors employed for determining the probability that the m-th transmitted bit exhibits a value of $b \in \{0, 1\}$ as follows:

$$\mathcal{M}_m^{b(l)} = \left\{ \check{s}^{(l)} \,\middle|\, \frac{\check{s}^{(l)}}{\sigma_l} \in \mathcal{M}_{cm}^b \right\}. \tag{17.97}$$

Substituting the Bayes theorem of Equation 17.90 into Equation 17.96 then yields for the l-th user's soft-bit value at the m-th bit position the following expression:

$$L_{m\approx}^{(l)} = \ln \frac{\sum_{\check{s}^{(l)} \in \mathcal{M}_m^{1(l)}} P(x_{\text{eff}}^{(l)} | \check{s}^{(l)}, H_{\text{eff}}^{(l)})}{\sum_{\check{s}^{(l)} \in \mathcal{M}_m^{0(l)}} P(x_{\text{eff}}^{(l)} | \check{s}^{(l)}, H_{\text{eff}}^{(l)})}. \tag{17.98}$$

Here we have exploited that the different trial-symbols $\check{s}^{(l)}$ have the same probability, namely $P(\check{s}^{(l)}) = const.$, $\check{s}^{(l)} \in \mathcal{M}^{(l)}$, where $\mathcal{M}^{(l)} = \mathcal{M}_m^{(0)(l)} \bigcup \mathcal{M}_m^{(1)(l)}$. Upon recalling from Section 17.2.4 that the *a priori* probability $P(x_{\text{eff}}^{(l)} | \check{s}^{(l)}, H_{\text{eff}}^{(l)})$ is given by the complex Gaussian distribution function $f(x_{\text{eff}}^{(l)} | \check{s}^{(l)}, H_{\text{eff}}^{(l)})$ defined in Equation 17.87, we obtain that:

$$L_{m\approx}^{(l)} = \ln \frac{\sum_{\check{s}^{(l)} \in \mathcal{M}_m^{1(l)}} \exp\left(-\frac{1}{\sigma_{n_{\text{eff}}}^2} |x_{\text{eff}}^{(l)} - H_{\text{eff}}^{(l)} \check{s}^{(l)}|^2\right)}{\sum_{\check{s}^{(l)} \in \mathcal{M}_m^{0(l)}} \exp\left(-\frac{1}{\sigma_{n_{\text{eff}}}^2} |x_{\text{eff}}^{(l)} - H_{\text{eff}}^{(l)} \check{s}^{(l)}|^2\right)}. \tag{17.99}$$

Observe that evaluating the l-th user's soft-bit value at the m-th bit position with the aid of Equation 17.99 involves the exponential function, which is computationally demanding.

17.2.5.1   Simplification by Maximum Approximation

In order to avoid the explicit evaluation of the exponential function, a common approach is constituted by the so-called maximum-approximation, which implies that only that specific additive term is retained in the calculation of the numerator and nominator of Equation 17.99, which yields the maximum contribution. It can be readily shown that as a result of this simplification we obtain instead of Equation 17.99 the following expression:

$$L_{m\approx}^{(l)} \quad \approx \quad \frac{1}{\sigma_{n_{\text{eff}}}^{(l)2}} \left[|x_{\text{eff}}^{(l)} - H_{\text{eff}}^{(l)} \check{s}_{m\approx}^{0(l)}|^2 - |x_{\text{eff}}^{(l)} - H_{\text{eff}}^{(l)} \check{s}_{m\approx}^{1(l)}|^2 \right], \tag{17.100}$$

where

$$\check{s}_{m\approx}^{b(l)} = arg \min_{\check{s}^{(l)} \in \mathcal{M}_m^{b(l)}} |x_{\text{eff}}^{(l)} - H_{\text{eff}}^{(l)} \check{s}^{(l)}|^2, \quad b \in \{0, 1\}, \tag{17.101}$$

while the set $\mathcal{M}_m^{b(l)}$ was defined in Equation 17.97. We note that for each soft-bit to be determined, Equation 17.101 has to be invoked twice, namely, once for a bit value of $b = 1$ and once for $b = 0$.

A significant complexity reduction can be achieved by exploiting that $\mathcal{M}^{(l)} = \mathcal{M}_m^{0(l)} \bigcup \mathcal{M}_m^{1(l)}$. Hence, the calculation of the Euclidean distance metric $|x_{\text{eff}}^{(l)} - H_{\text{eff}}^{(l)} \check{s}^{(l)}|^2$ only has to be performed once for the different trial symbols $\check{s}^{(l)} \in \mathcal{M}^{(l)}$, followed by an appropriate selection in the context of the soft-bit generation assisted by Equation 17.101. Specifically half of the symbols $\check{s}_{m\approx}^{b(l)}$ for the different bit polarities $b \in \{0, 1\}$ and bit positions m can be readily inferred by conducting an initial search of the entire set $\mathcal{M}^{(l)}$. This results in the ML estimate $\check{s}_{\text{ML}\approx}^{(l)}$ of the transmitted symbol according to Equation 17.94. The initial ML symbol estimate is constituted by a specific bit representation. The minimization obeying Equation 17.101 has to be conducted over the set of specific symbols, which contain

system parameters	choice
CIR model	3-path indoor WATM of Section 14.3.1
CIR tap fading	OFDM symbol invariant
system model	indoor WATM of Section 14.3.1
channel estimation	ideal
transmit antennas per user	1

Table 17.3: Summary of the system setup; also note that the fading was assumed to be uncorrelated for the different CIR taps associated with the channel between a specific transmitter-receiver antenna pair, as well as uncorrelated for the same CIR tap of different transmitter-receiver antenna pairs.

turbo coding parameters	choice
coding rate R_c	$1/2$
constraint length K_c	3
generator polynomial	$(7, 5)_8$
number of iterations	4

Table 17.4: Summary of the turbo-coding parameters.

the inverted versions of the bits identified during the previously mentioned initial ML symbol search.

17.2.6 Performance Analysis

In the context of our simulations the frame-invariant fading indoor WATM channel- and system model described in Section 14.3.1 will be employed. Furthermore, perfect knowledge of the channel transfer functions associated with the different transmit-receive antenna pairs will be assumed. Note that as a result of performing the detection of the different users' transmitted symbols independently on an OFDM subcarrier-by-subcarrier basis, the performance results presented here for the uncoded system are independent from the indoor WATM channel's specific multipath intensity profile. The advantage of employing the idealistic model of an OFDM symbol invariant fading channel is that the performance results are not impaired by the obfuscating effects of Inter-subCarrier Interference (ICI). Again the general system setup has been summarized in Table 17.3, while in Table 17.4 we have summarized the turbo-coding parameters to be employed in the context of our investigation of turbo-coded systems.

The structure of our performance investigations is as follows. In Section 17.2.6.1 the different detectors, namely LS, MMSE and MV are compared to each other in terms of the achievable MSE at the associated combiner's output, as well as in terms of the BER. By contrast, in Sections 17.2.6.2 and 17.2.6.3 we concentrate on the assessment of the specific MMSE detector's performance in terms of the distribution of the SINR measured at the associated combiner's output, as well as that of the detector's BER performance, respectively. These investigations are conducted as a function of the number of users L and that of the
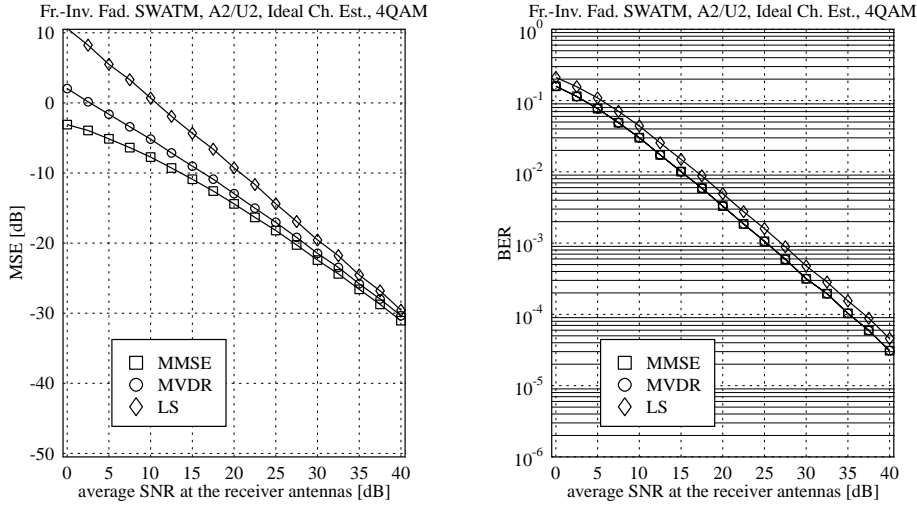
Figure 17.6: Comparison of the different linear detectors, namely, the LS, MMSE and MVDR tech-
niques as a function of the SNR at the reception antennas, with respect to (left:) the
MSE at the combiner's output and (right:) the detector's BER; here we have employed
the configuration of $L = 2$ simultaneous users and $P = 2$ reception antennas at the BS
($A2/U2$); for the basic simulation parameters we refer to Table 17.3

number of reception antennas P. Our investigations are concluded upon evaluating the BER
performance of turbo-coded MMSE detection-assisted SDMA-OFDM in Section 17.2.6.4.

17.2.6.1   MSE and BER Performance Comparison of LS, MMSE and MVDR Detection

At the left-hand side of Figure 17.6 we have portrayed the average MSE performance
recorded at the different detectors' combiner outputs, as a function of the SNR at the re-
ception antennas. More specifically, the MSE was evaluated as the squared error between
the signal transmitted by a specific user and that observed at its associated combiner output,
normalized to the user's signal variance. Here we have considered the scenario of two recep-
tion antennas and two simultaneous SDMA users, each equipped with one transmit antenna,
which we denoted as (A2/U2). As expected, the best MSE performance is exhibited by the
MMSE combiner, closely followed by the MVDR combiner, as seen in Figure 17.6. The
worst MSE performance was exhibited by the LS combiner, which is also widely known as
the zero-forcing combiner. Furthermore, observe that upon increasing the users' SNRs to-
wards infinity, the different combiners' MSE curves merge. This is, because when increasing
the SNR a Wiener filter based combiner effectively operates as an LS combiner, aiming for
minimizing purely the interfering signals' variances, rather than that of the joint noise and
interference contributions. Note that in the context of our simulations the LS combiner's cor-

relation matrix given by Equation 17.33 was regularized [90] upon adding a value of 10^{-6} to its main diagonal elements. This contributed towards mitigating the problems associated with its inversion. By contrast, on the right-hand side of Figure 17.6 we have portrayed the system's BER associated with the different detectors in the context of 4QAM modulation. We observe that both Wiener-filter based detectors, namely, the MMSE and MVDR schemes achieve the same BER performance, as a result of their identical SINR performance as it was highlighted in Sections 17.2.3.4 and 17.2.3.5. Note however that in the context of higher-order QAM modulation schemes, such as 16QAM for example, where also the constellation points' amplitude conveys information, a slight BER performance advantage was observed for the MVDR detector although the corresponding results are not included here for reasons of space economy. Furthermore, similarly to our observations with respect to the different detectors' associated combiner MSE performance, the LS detector performs significantly worse, than the MMSE and the MVDR detectors also in terms of the BER. Hence, in our following discussions we will focus on the MMSE detector, which will also be employed as the core element of SIC and PIC detectors to be discussed in Sections 17.3.1 and 17.3.2, respectively.

17.2.6.2 SINR Performance of MMSE Detection for Different Numbers of Users and Reception Antennas

In order to further characterize the MMSE detector, in Figure 17.7 we have plotted the Probability Density Function (PDF) of the SINR at the combiner's output for different combinations of the number of simultaneous users L and the number of reception antennas P, as well as for SNRs of 0dB, 20dB and 40dB recorded at the reception antennas. Specifically, in the graph seen at the left-hand side of Figure 17.7 we have compared those PDFs against each other, which are associated with the particular configurations of $P = L \in \{2, 3, 4\}$. We observe that at sufficiently high SNRs the SINR distributions become *almost* identical, which is because the different arrangements have the same diversity order. Here we emphasize the expression "almost identical", since at higher SNRs - although visually they appear identical in Figure 17.7 - perceivable differences were found in terms of the corresponding average BER performance for the configurations of A2/U2, A3/U3 as well as A4/U4. More explicitly, upon increasing the MIMO system's order, the BER performance is improved.

By contrast, at the right-hand side of Figure 17.7 we have considered configurations of $P = 4$, $L \in \{2, 3, 4\}$. Here we observe that upon increasing the diversity order, namely by decreasing the L number of SDMA users, while keeping the P number of reception antennas constant, the probability of incurring higher SINRs is increased. The effects of these SINR improvements on the system's BER performance will be further investigated in the next section,

17.2.6.3 BER Performance of MMSE Detection for Different Numbers of Users and Reception Antennas

In Figure 17.8 we have portrayed the BER performance of a 4QAM-modulated MMSE detection-assisted SDMA-OFDM scheme as a function of the SNR at the reception antennas. The curves are further parameterized with the number of simultaneous users L and the number of reception antennas P. Upon decreasing the number of users L while keep-
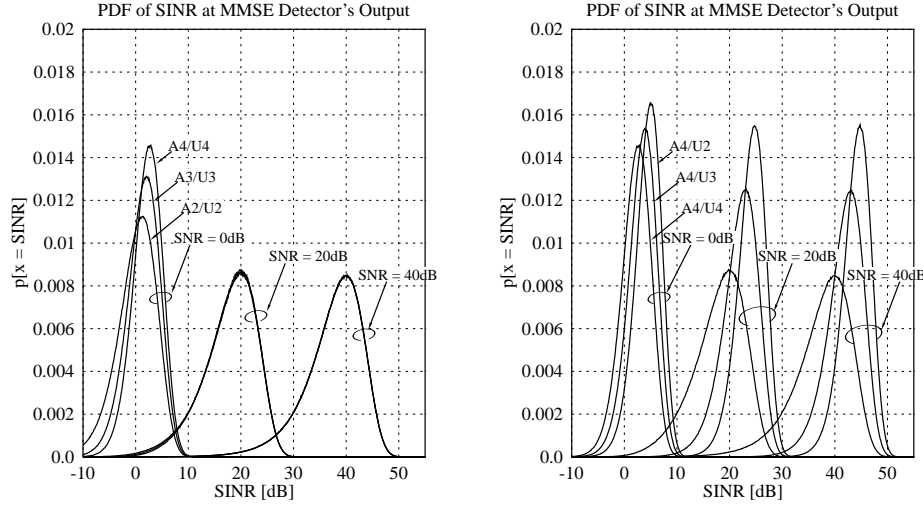
Figure 17.7: Characterization of the MMSE detector in terms of its associated SINR-PDF observed at the combiner's output; (left:) for each configuration the L number of users is identical to the P number of reception antennas, using the configurations of $A2/U2$, $A3/U3$ and $A4/U4$; (right:) the P number of reception antennas is equal to four, while the L number of users is varied, where we have the configurations of $A4/U2$, $A4/U3$ and $A4/U4$; for the basic simulation parameters we refer to Table 17.3.

ing the number of reception antennas P constant, we observe that the BER performance is dramatically improved. This is because the system's diversity order is increased and hence the detector benefits from a degree of freedom for adjusting its associated combiner weights in favour of a better exploitation of the channel's diversity, in favour of a reduction of the AWGN, rather than aiming for the mitigation of the remaining users' interference.

17.2.6.4   BER Performance of Turbo-Coded MMSE Detection-Assisted SDMA-OFDM

Turbo-decoding at the receiver is a powerful means of further enhancing the system's BER performance. This is achieved at the cost of reducing the system's effective throughput and by investing additional computational complexity. The turbo coding parameters were summarized in Table 17.4, but for the reader's convenience they are repeated here. Namely, the coding rate was $R_c = \frac{1}{2}$, the constraint length was $K_c = 3$, the octally represented generator polynomials of $(7, 5)_8$ were used and four iterations were performed. The generation of the soft-bits required for turbo-decoding was discussed earlier in Section 17.2.5.

Our BER simulation results are portrayed in Figure 17.9, at the left-hand side for $P = 2$ reception antennas, while at the right-hand side for $P = 4$ reception antennas, when supporting up to $L = P$ number of users. We observe that compared to the uncoded scenario, whose
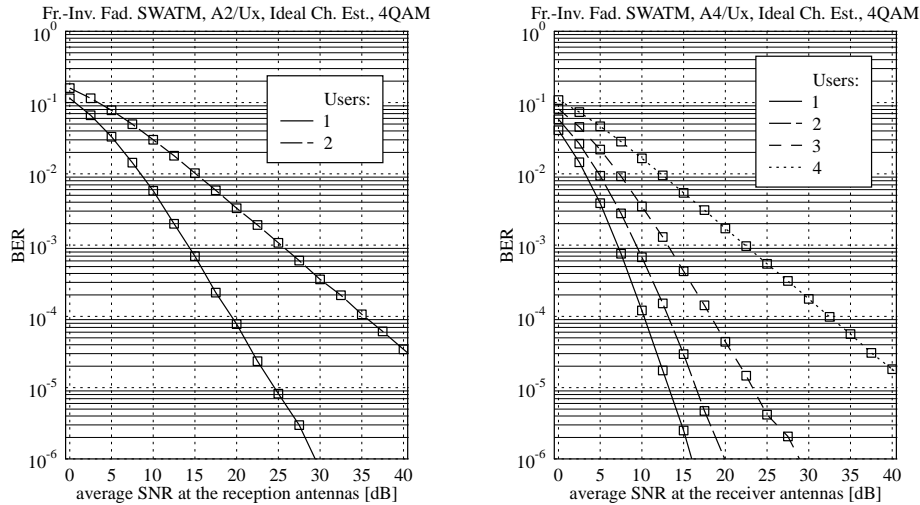
Figure 17.8: BER performance of 4QAM-modulated, MMSE detection-assisted SDMA-OFDM as a function of the SNR at the reception antennas; the curves are further parameterized with the number of simultaneous users L and the number of reception antennas P, where more specifically (left:) two reception antennas, (right:) four reception antennas were employed; for the basic simulation parameters we refer to Table 17.3.

associated simulation results were shown in Figure 17.8 the BER is significantly reduced. To provide an example, for a so-called 'fully loaded' system associated with $L = P = 4$ the SNR at the reception antennas required for a BER of 10^{-5} was around 42dB, while in the context of turbo-decoding the same BER was reached at an SNR of around 13dB. Again, this performance improvement is achieved at the cost of halving the system's throughput and at an additional computational complexity imposed by the turbo-decoder. Furthermore, similarly to the uncoded scenario, upon removing one user from the 'fully loaded' system results in a significant reduction of the BER. This is, because the MMSE combiner has a higher degree of freedom in terms of the choice of the optimum weight matrix, with the beneficial effect of a better suppression of the undesired AWGN.

17.2.7 Complexity Analysis

In this section we will analyse the computational complexity inflicted per subcarrier when evaluating the vector of estimated transmitted signals, followed by hard-decision based demodulation carried out with the aid of minimizing the Euclidean distance metric of Equation 17.94. The structure of this section is as follows. While in Section 17.2.7.1 the LS combiner's complexity is quantified, in Section 17.2.7.2 we will concentrate on the portrayal of the MMSE combiner's complexity. Finally, the computational complexity related to the de-
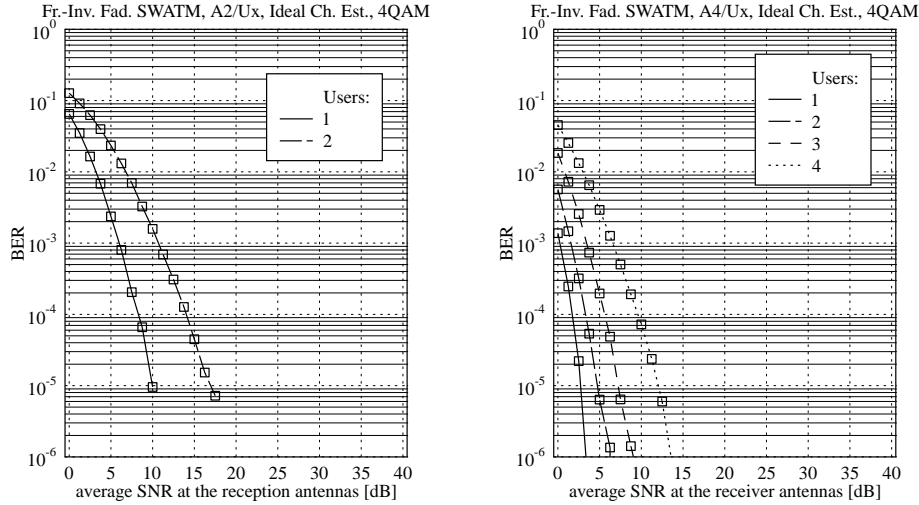
Figure 17.9: BER performance of turbo-coded, 4QAM-modulated, MMSE detection-assisted SDMA-OFDM as a function of the SNR at the reception antennas; the curves are further parameterized with the number of simultaneous users L and the number of reception antennas P, where (left:) two reception antennas, and (right:) four reception antennas were employed, respectively; for the basic simulation parameters and for the turbo-coding parameters we refer to Tables 17.3 and 17.4, respectively.

modulation of the linear combiners' output signals will then be analysed in Section 17.2.7.3.

17.2.7.1   LS Combining

An expression for the LS combiner's associated weight vector was provided in Equation 17.35 for the case of $P \geq L$. First of all, the calculation of the 'auto-correlation' matrix $\mathbf{Q}_{\mathrm{LS}}$ defined in Equation 17.33 requires $L^2 P$ number of complex multiplications and the same number of additions. By contrast, the evaluation of the 'cross-correlation' vector $\mathbf{p}_{\mathrm{LS}}$ requires LP number of complex multiplications and additions. Due to the potentially high condition number [90] of the 'auto-correlation' matrix $\mathbf{Q}_{\mathrm{LS}}$ it is disadvantageous to directly invert it, since it requires a high numerical accuracy. Recall that this direct solution for the vector $\hat{\mathbf{s}}_{\mathrm{LS}}$ was shown at the right-hand side of Equation 17.35.

17.2.7.1.1   LS Combining without Generating the Weight Matrix   In order to circumvent this problem, the preferred method is that of solving the equation system shown at the left-hand side of Equation 17.35. In order to ensure numerical stability, a matrix decomposition based approach such as the Cholesky-, LU- or QR decomposition [90] could be invoked. In the context of the LS solution the most prominent matrix factorization technique is the

QR decomposition. However, here we assume that the LU decomposition technique outlined in [90] is employed. Hence, in a first step the matrix $\mathbf{Q}_{\mathrm{LS}}$ is LU decomposed, imposing a computational complexity of $\frac{1}{3}L^3$ complex multiplications and additions. Then, in a second step the desired vector $\hat{\mathbf{s}}_{\mathrm{LS}}$ is determined with the aid of forward- and backward substitutions using the procedure outlined in [90], which imposes a complexity of L^2 complex multiplications and additions. Hence, the *total* computational complexity of solving Equation 17.35 per subcarrier is given by:

$$C_{\mathrm{LS,direct}}^{(\mathbb{C}*\mathbb{C})} = C_{\mathrm{LS,direct}}^{(\mathbb{C}+\mathbb{C})} = PL + (P+1)L^2 + \frac{1}{3}L^3. \qquad (17.102)$$

Note however that as a result of this procedure the weight matrix $\mathbf{W}_{\mathrm{LS}}$ defined in Equation 17.38 does not become explicitly available, although it might be required for determining the estimation MSE, the SNR or SINR on a subcarrier basis.

17.2.7.1.2 LS Combining Generating the Weight Matrix
As an example, in the context of the SIC detection[9] procedure to be discussed in Section 17.3.1, explicit knowledge of the weight matrix is required for calculating the subcarrier based S(I)NR values employed for selecting the most dominant user to be cancelled next in a specific detection stage. A possible solution for determining $\mathbf{W}_{\mathrm{LS}}$ is first to solve Equation 17.37 for obtaining the projection matrix $\mathbf{P}_{\mathrm{LS}}$, which is related to the weight matrix $\mathbf{W}_{\mathrm{LS}}$ by the Hermitian transpose as seen in Equation 17.38. This step is then followed by appropriately combining the output signals of the array elements according to Equation 17.36. As a consequence, the associated *total* computational complexity would be:

$$C_{\mathrm{LS,W+cmb}}^{(\mathbb{C}*\mathbb{C})} = C_{\mathrm{LS,W+cmb}}^{(\mathbb{C}+\mathbb{C})} = PL + 2PL^2 + \frac{1}{3}L^3. \qquad (17.103)$$

The concomitant increase in computational complexity compared to that quantified by Equation 17.102 is, because in the process of evaluating $\mathbf{W}_{\mathrm{LS}}$ the forward- and backward substitutions as outlined in [90] would have to be carried out for P different matrix right-hand sides.

Note that since the computational complexity is dominated in both cases by the third order as a function of the number of simultaneous users L, increasing this parameter will dramatically increase the associated complexity.

17.2.7.2 MMSE Combining

The second combiner which we will analyse in terms of its computational complexity is the MMSE combiner of Section 17.2.3. Here the relevant equations are the general combiner's formula, namely Equation 17.7, as well as the MMSE-specific expression that has to be evaluated for the determination of the optimum weight matrix, namely, Equation 17.64 or 17.68. Recall that both forms are equivalent to each other. Nonetheless, as argued in Section 17.2.3.2, there is a difference in the dimension of the auto-correlation matrices. Specifically, in the context of the left-inverse related form of the weight matrix given by Equa-

---

[9]The LS detector, or alternatively the MMSE detector could be employed as a baseline detector in each SIC detection stage.

tion 17.68 an auto-correlation matrix $\mathbf{R}_{\overline{a}}$ of dimension $L \times L$ has to be inverted, while in conjunction with the right-inverse related form of Equation 17.64 the auto-correlation matrix $\mathbf{R}_a$ to be inverted is of dimension $P \times P$.

17.2.7.2.1 Left-Inverse Related Form of MMSE Combining without Generating the Weight Matrix

As it was shown earlier in Section 17.2.7.1 for the LS combiner, if the weight matrix $\mathbf{W}_{\text{MMSE}}$ is not explicitly required, a complexity reduction can be achieved in conjunction with the left-inverse related representation of the MMSE combiner by directly solving Equation 17.70 for the vector of the transmitted symbols' estimates. The solution of Equation 17.70 imposes a complexity of:

$$C_{\text{MMSE,direct}}^{(\mathbb{C}*\mathbb{C})} = C_{\text{MMSE,direct}}^{(\mathbb{C}+\mathbb{C})} = PL + (P+1)L^2 + \frac{1}{3}L^3 \tag{17.104}$$

$$C_{\text{MMSE,direct}}^{(\mathbb{R}*\mathbb{C})} = PL \tag{17.105}$$

$$C_{\text{MMSE,direct}}^{(\mathbb{R}+\mathbb{C})} = L. \tag{17.106}$$

which implies a complexity reduction by a factor of $(P-1)L^2$ in terms of the number of complex multiplications and additions.

17.2.7.2.2 Left-Inverse Related Form of MMSE Combining Generating the Weight Matrix

Upon following similar steps, as in the context of our analysis of the LS combiner's complexity, which was considered for the scenario of $P \geq L$ in Section 17.2.7.1, we found that the complexity of the MMSE combiner, as represented by Equation 17.68 in its left-inverse related form can be related to the complexity formula originally derived for the LS combiner namely, to Equation 17.103, which is repeated here for the reader's convenience:

$$C_{\text{MMSE,W+cmb}}^{(\mathbb{C}*\mathbb{C})} = C_{\text{MMSE,W+cmb}}^{(\mathbb{C}+\mathbb{C})} = PL + 2PL^2 + \frac{1}{3}L^3. \tag{17.107}$$

More explicitly, this LS combining related formula quantifies the number of complex multiplications and additions required by Equations 17.37 and 17.7, respectively. However, the MMSE combiner is somewhat more complex, since in Equation 17.68 an additional complexity contribution of mixed real-complex multiplications and additions is incurred due to incorporating the SNR matrix of $\mathbf{P}_{\text{SNR}}$. The number of these operations is given by:

$$C_{\text{MMSE,W+cmb}}^{(\mathbb{R}*\mathbb{C})} = PL \tag{17.108}$$

$$C_{\text{MMSE,W+cmb}}^{(\mathbb{R}+\mathbb{C})} = L. \tag{17.109}$$

17.2.7.3 Demodulation of the Linear Combiner's Output Signal

In addition to the computational complexity associated with the process of linear combining, we also have to account for the complexity imposed by demodulating the different users' associated combiner output signals with the aid of Equation 17.94. More specifically, from Equation 17.94 we infer that evaluating the Euclidean distance metric for a single M_c-ary trial-symbol $\check{s}$ of a subcarrier requires one complex addition, as well as 'half' a complex

multiplication, which is related to the operation of actually calculating the Euclidean norm[10] of the complex-valued difference between the received signal and the trial-symbol. Hence, in the context of M_c number of symbols per trial-set and for L number of simultaneous users to be demodulated, the total computational complexity related to the demodulation of Equation 17.94 is given by:

$$C_{\text{lin,dem}}^{(\mathbb{C}*\mathbb{C})} = \frac{1}{2}LM_c \tag{17.110}$$

$$C_{\text{lin,dem}}^{(\mathbb{C}+\mathbb{C})} = C_{\text{lin,dem}}^{(\mathbb{R}\lessgtr\mathbb{R})} = LM_c, \tag{17.111}$$

where we have introduced the number of real-valued comparisons $C_{\text{lin,dem}}^{(\mathbb{R}\lessgtr\mathbb{R})}$ between the Euclidean distance metric outcomes as a further index of complexity.

17.2.7.4 Simplified Complexity Formulae to be used in the Comparison of the Different Detectors

In Sections 17.2.7.1, 17.2.7.2 and 17.2.7.3 we elaborated on the individual computational complexity exhibited by the LS- and MMSE combiners described in Sections 17.2.2 and 17.2.3, respectively, as well as by the process of demodulating the combiner's output signal as outlined in Section 17.2.4. By contrast, in this section, we will present simplified complexity formulae for the LS- and MMSE detectors, which will be employed in our final comparison of the different detectors' complexities in Section 17.3.4.2. Our aim was to give a more compact representation of the complexity, in terms of the number of complex multiplications and additions, as well as real-valued comparisons. Specifically, in the context of the MMSE detector the number of mixed real-complex multiplications and additions has been expressed in terms of the number of complex multiplications and additions[11] upon weighting them by a factor of $\frac{1}{2}$. Here we assume that the weight matrix is not determined, which allows for a lower-complexity implementation, as argued in the previous sections. Hence, for the LS detector of Equation 17.35 and the associated process of demodulation in Equation 17.94 we obtain the following simplified complexity formulae:

$$C_{\text{LS}}^{\mathbb{C}*\mathbb{C}} = \frac{1}{2}LM_c + PL + (P+1)L^2 + \frac{1}{3}L^3 \tag{17.112}$$

$$C_{\text{LS}}^{\mathbb{C}+\mathbb{C}} = LM_c + PL + (P+1)L^2 + \frac{1}{3}L^3 \tag{17.113}$$

$$C_{\text{LS}}^{\mathbb{R}\lessgtr\mathbb{R}} = LM_c. \tag{17.114}$$

---

[10] $|a_x + ja_y|^2 = (a_x + ja_y) \cdot (a_x + ja_y)^* = a_x^2 + a_y^2$

[11] Here we have neglected the real-valued additions required for evaluating the product of two complex numbers and hence our complexity formulae provide an upper bound estimate.

By contrast, for the left-inverse related form of the MMSE detector in Equation 17.70 plus for the associated demodulation procedure of Equation 17.94 we obtain:

$$C_{\mathrm{MMSE}}^{\mathbb{C}*\mathbb{C}} \;=\; \frac{1}{2}LM_c + \frac{3}{2}PL + (P+1)L^2 + \frac{1}{3}L^3 \tag{17.115}$$

$$C_{\mathrm{MMSE}}^{\mathbb{C}+\mathbb{C}} \;=\; LM_c + \left(P + \frac{1}{2}\right)L + (P+1)L^2 + \frac{1}{3}L^3 \tag{17.116}$$

$$C_{\mathrm{MMSE}}^{\mathbb{R} \lessgtr \mathbb{R}} \;=\; LM_c. \tag{17.117}$$

Again, these simplified formulae will be employed in the context of Section 17.3.4.2 for comparing the different detectors' complexities.

17.2.8   Conclusions on Linear Detection Techniques

In Section 17.2 we have concentrated on the mathematical portrayal, performance- and complexity comparison of the most prominent linear detection techniques, namely on the LS and MMSE procedures of Sections 17.2.2 and 17.2.3, respectively. Our discussions commenced in Section 17.2.1 with the characterization of a linear combiner's output signal and its components, while our more specific discussions in Section 17.2.2 focussed on the LS detector, also known as the ZF detector- or decorrelating detector. Its associated combiner weight matrix was shown in Equation 17.38 to be given as the Hermitian transpose of the Moore-Penrose pseudo-inverse or left-inverse of the channel transfer factor matrix $\mathbf{H}$. In contrast to the calculation of the MMSE related weight matrix, its calculation outlined in Equation 17.38 does not require any statistical information. Although, as shown in Equation 17.42 the transmitted signal is recovered with unit-gain, it is contaminated by the residual AWGN, which is potentially boosted due to the effects of the actual channel matrix. In order to achieve a lower average MSE than that of Equation 17.46, derived for characterizing the LS combiner's output, the MMSE combiner of Section 17.2.3 can be invoked.

As suggested by the terminology, from the set of all linear combiners the MMSE combiner exhibits the lowest MSE at the output. As shown in Section 17.2.3, this is achieved upon incorporating statistical information concerning the transmitted signals' variances and the AWGN variance into the detection process, resulting in a Wiener filter-related weight matrix as evidenced by Equation 17.63 or 17.64. This representation of the weight matrix $\mathbf{W}_{\mathrm{MMSE}}$ is related to the right-inverse of the channel matrix. If the auto-correlation matrix associated with the different antenna elements' AWGN is a scaled unity matrix, then an alternative representation, namely Equation 17.68, can be obtained, which is related to the channel matrix's left-inverse rather than its right-inverse. Depending on the dimensions of the channel transfer factor matrix $\mathbf{H}$ in terms of the L number of users and the P number of reception antenna elements, the left- or right-inverse related form may be preferred in terms of the computational complexity imposed. In the context of these discussions the relation between the MMSE- and MVDR combiner was briefly addressed. Similarly to the LS combiner of Section 17.2.2, the desired signal is recovered with unity gain, while at the same time suppressing the AWGN, again, based upon knowledge of the different users' SNRs encountered at the reception antennas. Specifically, from Equations 17.78 and 17.82 we recall that both the l-th user's MMSE weight vector $\mathbf{w}_{\mathrm{MMSE}}^{(l)}$ and the MVDR combiner's weight vector $\mathbf{w}_{\mathrm{MV}}^{(l)}$ can be represented as the scaled product of the inverse interference-plus-noise correlation matrix

$\mathbf{R}_{a,I+N}^{-1}$ and the desired user's channel vector $\mathbf{H}^{(l)}$. The difference between the two solutions resides in the choice of the scalar factor β, which for the specific case of MMSE detection was given by Equation 17.79, while for MV detection by Equation 17.83. As further argued in Section 17.2.3.4, both solutions exhibit the same SINR, which in turn is identical to that of the maximum SINR combiner [90, 136] not detailed here. The maximum SINR combiner an also be represented in a similar form as Equations 17.79 and 17.83, but with a different value of β. Hence, the Wiener filter-related linear combiners, namely the MMSE, MVDR and maximum SINR combiners maximise the SINR. Furthermore, in Section 17.2.5 the generation of soft-bit information for turbo-decoding was demonstrated.

Our performance assessment with respect to the MSE and SINR at the combiner's output, as well as with respect to the detector's BER was carried out in Section 17.2.6. The curves, which were shown on the left-hand side of Figure 17.6 supported that the MSE at the combiner's output is minimized by the MMSE weight matrix, while a slight MSE degradation was observed for the MVDR weight matrix of Equation 17.81 as a consequence of the requirement to recover the desired user's transmitted signal with a specific gain, which was assumed to be unity in our case. As expected, the worst MSE was exhibited by the LS combiner of Section 17.2.2. In terms of the system's 4QAM-related BER on the right-hand side of Figure 17.6 we observed an identical performance for both Wiener filter related detectors[12], namely for the MMSE and MV detector. Again, as argued in Section 17.2.3.5, their performance was identical, because the different Wiener filter-related detectors achieve the same SINR. However, for the LS detector of Section 17.2.2 a significant performance degradation was also observed in terms of the BER as shown at the right-hand side of Figure 17.6. Our further investigations concentrated on portraying the influence of the relation between the number of users L and the number of reception antennas P on the MMSE detector's SINR and on the associated BER performance. Specifically, from Figures namely, 17.7 and 17.8 we observed that upon decreasing the number of users L, while keeping the number of reception antennas P constant, the PDF of the SINR is shifted towards higher SINRs, while at the same time the system's BER is significantly improved. This is also a motivation for the employment of the successive interference cancellation approach, which will be discussed in Section 17.3.1.

Finally the BER performance of MMSE detection-assisted SDMA-OFDM was analysed in a turbo-coded scenario. The associated BER versus SNR performance curves were portrayed in Figure 17.9. Compared to the uncoded scenario the BER was significantly improved - although at the cost of halving the system's effective throughput. Our estimates of the computational complexity associated with the different linear detectors, namely LS and MMSE were presented in Section 17.2.7. We found that the computational complexity is of third order, namely $\mathcal{O}(3)$ with respect to the number of users L, upon assuming the weight matrix's representation in its left-inverse related form.

17.3 Non-Linear Detection Techniques

In Section 17.2 the family of linear detection techniques was discussed. These detectors aimed at reducing the potentially excessive M_c^L number of evaluations of the multi-user Euclidean distance metric associated with the optimum ML detector to a significantly lower

---

[12]Recall that the linear detector is constituted by the concatenation of the linear combiner and the classifier.

LM_c number of evaluations of the single-user Euclidean distance metric of Equation 17.94. This implies a substantial complexity reduction. Recall that the variable L represents the number of users supported, while M_c is the number of constellation points for the specific modulation scheme employed. As portrayed in the linear detector's block diagram shown in Figure 17.4, the strategy is first to provide linear estimates of the different users' transmitted signals and then to perform the non-linear classification- or demodulation separately for each user. This philosophy was based on the assumption that the different users' associated linear combiner output signals are corrupted only by the residual AWGN, which is however, only an approximation. In fact the linear combiners' output signals in Figure 17.4 also contain residual interference, which is not Gaussian distributed and hence represents an important source of further information.

Instead of sequentially performing the operations of linear combining and classification- or demodulation as in the linear detector's case of Figure 17.4, a more effective strategy is to embed the demodulation into the process of linear combining, which is known from the family of classic channel equalizers as decision-feedback. As a result, the residual multi-user interference observed at the classifier's inputs is reduced. Hence, the classifier's accuracy due to neglecting the residual interference is less impaired. Two of the most prominent multi-user detection techniques known from CDMA communications, which incorporate these ideas are the SIC and PIC detection techniques. These techniques are also applicable in the context of communicating over flat-fading channels as observed for example on an OFDM subcarrier basis. In the context of our portrayal of SIC detection in Section 17.3.1, apart from discussing various techniques for its improvement, a detailed analysis of the effects of error propagation occurring at the different detection stages will be provided. This error propagation analysis motivated the employment of weighted soft-bit metric assisted turbo-decoding. Furthermore, our discussions on PIC detection will be presented in Section 17.3.2. We will demonstrate that a significant enhancement of the PIC detector's performance can be achieved by embedding turbo-decoding into the PIC detection process, instead of simply serially concatenating the PIC detector with the turbo-decoder. Finally, the optimum ML detector will be analysed in Section 17.3.3.

17.3.1   SIC Detection

The philosophy of the Successive Interference Cancellation (SIC) assisted detector [104, 109, 113, 117, 119, 124, 126, 128, 135, 137] is motivated by two observations. First of all, we note that for a specific subcarrier the MSE and SINR at the output of the LS- or MMSE combiner might substantially differ for the different users, depending on their spatial signatures. Secondly, we recall from our investigations in Section 17.2.6.3 that upon increasing the MIMO system's diversity order, e.g. by decreasing the number of simultaneous users L while keeping the number of reception antennas P constant, the MSE performance of the LS- or MMSE combiner and correspondingly the system's BER performance is improved as a consequence of assigning a higher grade of diversity to mitigate the effects of fading. This was illustrated in Figure 17.8. Hence, an attractive strategy, which has recently drawn wide interests is to detect only the specific user having the highest SINR, SIR or SNR in each iteration at the output of the LS- or MMSE combiner. Having detected this user's signal, the corresponding remodulated signal is subtracted from the composite signal received by the different antenna elements. Furthermore, the channel transfer factor matrix - and the SNR matrix formulated in
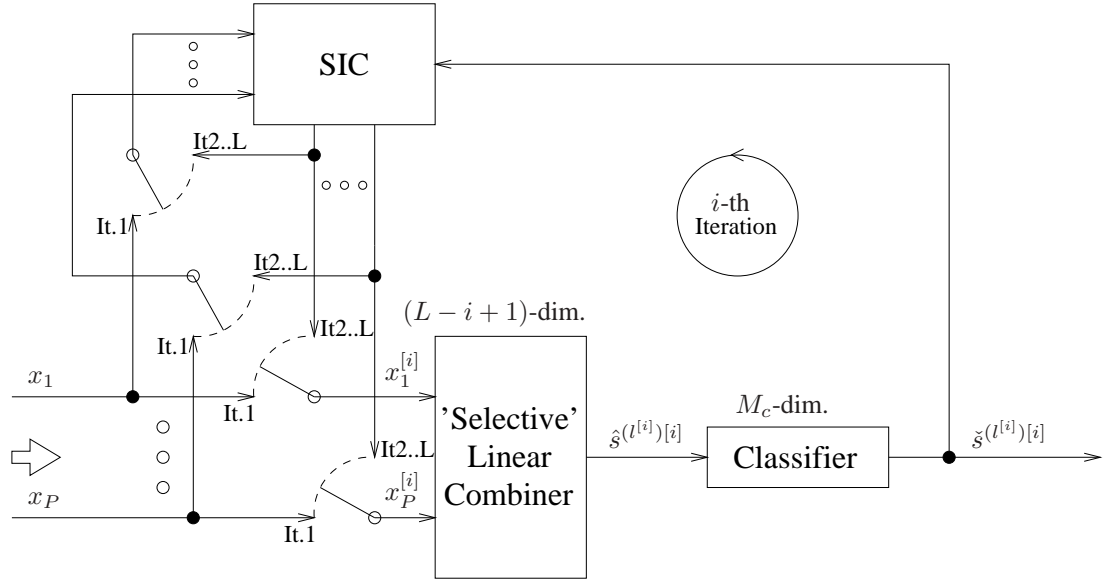
Figure 17.10: Illustration of the main signal paths associated with the standard SIC detector. During the first iteration the signals $x_p, p = 1, \ldots, P$ received by the different antenna elements are directly fed into the 'selective' linear combiner, where we have $\mathbf{x}^{[1]} = \mathbf{x}$ at the detection stage or iteration of $i = 1$. The task of the 'selective' linear combiner is to identify the most dominant remaining user in terms of its SINR at the combiner output - from the set of $(L - i + 1)$ remaining users during the i-th detection stage or iteration - and to provide its signal estimate $\hat{s}^{(l^{[i]})[i]}$ at the combiner's output. This is described by Equations 17.123 and 17.124. The selected $l^{[i]}$-th user's linear signal estimate $\hat{s}^{(l^{[i]})[i]}$ is then classified- or demodulated according to Equation 17.125, yielding the amplified constellation point $\check{s}^{(l^{[i]})[i]}$ that is most likely to have been transmitted by the $l^{[i]}$-th user. Now the corresponding modulated signal can be regenerated. The influence of the $l^{[i]}$-th user's modulated signal is then removed from the vector $\mathbf{x}^{[1]}$ of signals received by the different antenna elements with the aid of the SIC module. This cancellation operation is described by Equation 17.127. The first iteration $(i = 1)$ is deemed to have been completed, when the decontaminated signal appears at the output of the SIC stage. Hence, beginning with the second SIC iteration the 'selective' linear combiner's input, namely the 'decontaminated' vector $\mathbf{x}^{[i]}$ of signals received by the different antenna elements, which contains only the influence of the $(L - i + 1)$ remaining users, is constituted by the output of the SIC module, provided that correct symbol decisions were conducted in the previous detection stages. Note that for the sake of visual clarity here we have omitted the signal paths associated with the channel transfer factor estimates required by the linear combiner and by the SIC module. The role of the switches is to indicate that at the first detection stage the SIC is directly fed with the signals received by the different array elements, while during the remaining iterations of $i = 2, \ldots, L$ with the partially 'decontaminated' composite signal of the remaining $(L - i + 1)$ users.

the context of the MMSE combiner characterized by Equation 17.68 in its left-inverse related form - are updated accordingly.

The further structure of this section is as follows. In Section 17.3.1.1 the standard SIC algorithm is portrayed, which allows only the most likely symbol decision to be retained in each detection stage. This section also includes a detailed analysis of the effects of error propagation, which occurs across the different detection stages. By contrast, in Section 17.3.1.2 M-SIC and its derivatives are discussed, where potentially the M most likely tentative symbol decisions are retained at each detection node of the detection process - as it will be further explained in Section 17.3.1.2.1 - rather than retaining only the most likely symbol decision. Note that each detection node is associated with a specific appropriately updated array output vector of the SIC-aided detection process. Furthermore, in Section 17.3.1.3 the various techniques of soft-bit generation will be discussed and a weighted soft-bit metric will be proposed for employment in turbo-decoding, which is capable of substantially enhancing the performance of turbo-coded SIC detection-assisted SDMA-OFDM systems. Finally, a detailed performance analysis of the standard SIC and that of the M-SIC is offered in terms of the associated system's BER and SER performance both in the context of uncoded and turbo-coded scenarios in Section 17.3.1.4. The complexity of the different detection schemes will be analysed in Section 17.3.1.5. Finally, the summary of Section 17.3.1 will be offered in Section 17.3.1.6 along with our conclusions.

17.3.1.1 Standard SIC

From now on we assume that the MMSE combiner in its specific left-inverse related form as given by Equation 17.68 is assumed to be employed for performing the detection of the most dominant user in each cancellation stage. For the reader's convenience we have repeated here the formula describing the combiner's operation from Equation 17.70:

$$\mathbf{R}_{\overline{a}}^{H}\mathbf{W}_{\text{MMSE}}^{H} = \mathbf{R}_{c}^{H} \quad \Longleftrightarrow \quad \mathbf{W}_{\text{MMSE}}^{H} = \mathbf{R}_{\overline{a}}^{H-1}\mathbf{R}_{c}^{H}, \tag{17.118}$$

where the received signals' auto-correlation matrix $\mathbf{R}_{\overline{a}}$ was defined in Equation 17.69 as:

$$\mathbf{R}_{\overline{a}} = \mathbf{H}^{H}\mathbf{H}\mathbf{P} + \sigma_{n}^{2}\mathbf{I}, \tag{17.119}$$

while the cross-correlation matrix of the transmitted and received signals was given in Equation 17.54 namely:

$$\mathbf{R}_{c} = \mathbf{H}\mathbf{P}. \tag{17.120}$$

It is computationally efficient to refrain from recalculating the correlation matrix $\mathbf{R}_{\overline{a}}$ of Equation 17.119 and the cross-correlation matrix $\mathbf{R}_{c}$ of Equation 17.120 at each cancellation stage. This complexity reduction can be achieved by updating these matrices based on the specific index of the most recently detected user. Nonetheless, these matrices have to be calculated once at the beginning of the SIC detection procedure. The more detailed structure of the SIC detector will be portrayed below.

1) *Initialization*: Initialize the detector upon setting $\mathbf{x}^{[1]} = \mathbf{x} \in \mathbb{C}^{P\times 1}$, as well as upon evaluating $\mathbf{R}_{\overline{a}}^{[1]H} = \mathbf{P}\mathbf{H}^{H}\mathbf{H} + \sigma_{n}^{2}\mathbf{I}$ and $\mathbf{R}_{c}^{[1]H} = \mathbf{P}\mathbf{H}^{H}$. Here the index in the superscript, namely $()^{[i]}$ indicates the detection stage index, which is initially set to $i = 1$.

2) *i-th Detection Stage*: At the beginning of the i-th SIC detection stage, given correct symbol decisions in the previous detection stages, the updated vector $\mathbf{x}^{[i]}$ of received signals only contains the remaining $L^{[i]} = L - i + 1$ users' signal contributions plus the AWGN since the remodulated signals of the previously detected $(i-1)$ users have been deducted from the originally received composite signal of $\mathbf{x}$. Furthermore, the dimension of the auto-correlation matrix $\mathbf{R}_{\overline{a}}^{[i]H}$ - represented here in its Hermitian transposed form - has been reduced to $\mathbf{R}_{\overline{a}}^{[i]H} \in \mathbb{C}^{L^{[i]} \times L^{[i]}}$, while the dimension of the cross-correlation matrix $\mathbf{R}_c^{[1]H}$ also represented in its Hermitian transposed form has been reduced to $\mathbf{R}_c^{[i]H} \in \mathbb{C}^{L^{[i]} \times P}$ upon removing the previously cancelled users' associated entries. This matrix dimension reduction potentially facilitates the reduction of the system's overall complexity. Then the specific steps at the i-th detection stage are as follows:

- *Calculation of the Remaining Users' Weight Matrix*: Generate the $L^{[i]}$ number of remaining users' associated weight matrix upon invoking the MMSE approach, which is represented in its left-inverse related form by:

$$\mathbf{R}_{\overline{a}}^{[i]H}\mathbf{W}_{\text{MMSE}}^{[i]H} = \mathbf{R}_c^{[i]H} \quad \Longleftrightarrow \quad \mathbf{W}_{\text{MMSE}}^{[i]H} = \mathbf{R}_{\overline{a}}^{[i]H-1}\mathbf{R}_c^{[i]H}. \quad (17.121)$$

  Observe in Equation 17.121 that in contrast to Equation 17.119 and 17.120 we have substituted the matrices $\mathbf{R}_{\overline{a}}^H$ and $\mathbf{R}_c^H$ by their reduced-dimensional counterparts associated with the i-th detection stage, namely by $\mathbf{R}_{\overline{a}}^{[i]H}$ and $\mathbf{R}_c^{[i]H}$. The set of $L^{[i]}$ number of remaining users at the i-th detection stage is denoted here by $\mathcal{L}^{[i]}$.

- *Selection of the Most Dominant User*: Calculate the objective function, which could be the SINR, SIR or SNR at the MMSE combiner's output according to Equations 17.24, 17.25 or 17.26, respectively employing the different users' weight vectors. As an example, here we employ the SNR of Equation 17.26, since its calculation is significantly less complex than that of the SINR or SIR given by Equations 17.25 and 17.26. Based on Equation 17.26, the l-th user's associated SNR at the MMSE combiner's output during the i-th detection stage is given by:

$$\text{SNR}^{(l)[i]} = \frac{\mathbf{w}^{(l)[i]H}\mathbf{R}_{a,S}^{(l)}\mathbf{w}^{(l)[i]}}{\mathbf{w}^{(l)[i]H}\mathbf{R}_{a,N}\mathbf{w}^{(l)[i]}} \quad (17.122)$$

  where the auto-correlation matrix $\mathbf{R}_{a,S}^{(l)}$ of the l-th user's channel transfer factors was defined in Equation 17.16, while the noise correlation matrix $\mathbf{R}_{a,N}$ recorded in case of encountering uncorrelated AWGN at the different reception antenna elements of the BS was given in Equation 17.22. Furthermore, the l-th user's weight vector $\mathbf{w}^{(l)[i]}$ is given here in form of the corresponding column vector of the weight matrix $\mathbf{W}_{\text{MMSE}}^{[i]}$, which has been obtained upon solving Equation 17.121.

  The selection of the most dominant user, which is assumed here to be the $l^{[i]}$-th

user, can then be expressed as:

$$l^{[i]} = arg\max_{l \in \mathcal{L}^{[i]}} (\text{SNR}^{(l)[i]}). \tag{17.123}$$

- *Detection of the Most Dominant User*: Under the assumption that the $l^{[i]}$-th user has been found to be the most dominant one among the $L^{[i]}$ remaining users at the i-th detection stage, detect the user's transmitted signal upon invoking Equation 17.8, namely:

$$\hat{\mathbf{s}}^{(l^{[i]})[i]} = \mathbf{w}^{(l^{[i]})[i]H} \mathbf{x}^{[i]}. \tag{17.124}$$

- *Demodulation of the Most Dominant User*: Carry out the demodulation by mapping the detected signal $\hat{\mathbf{s}}^{(l^{[i]})[i]}$[13] to one of the M_c number of constellation points contained in the set $\mathcal{M}_c$ associated with a particular modulation scheme. As shown in Equation 17.94, this involves minimizing the Euclidean distance metric, namely:

$$\check{\mathbf{s}}^{(l^{[i]})[i]} = arg\min_{\check{\mathbf{s}}/\sigma_{l^{[i]}} \in \mathcal{M}_c} \left| \frac{1}{H_{\text{eff}}^{(l^{[i]})[i]}} \hat{\mathbf{s}}^{(l^{[i]})[i]} - \check{\mathbf{s}} \right|^2, \tag{17.125}$$

where the detected user's transfer factor $H_{\text{eff}}^{(l^{[i]})[i]}$ is given by:

$$H_{\text{eff}}^{(l^{[i]})[i]} = \mathbf{w}^{(l^{[i]})[i]H} \mathbf{H}^{(l^{[i]})}. \tag{17.126}$$

Note however that for MPSK modulation schemes the normalization to $H_{\text{eff}}^{(l^{[i]})[i]}$ is not necessary, because the information transmitted is incorporated into the signal's phase. Furthermore, in the context of Equation 17.125 the variance of the $l^{[i]}$-th user's M_c number of legitimate trial symbols is given by $\sigma_{l^{[i]}}^2$. Alternatively the MMSE combiner's output signal $\hat{\mathbf{s}}^{(l^{[i]})[i]}$ can be normalized by $\sigma_{l^{[i]}} = \sqrt{\sigma_{l^{[i]}}^2}$ instead of amplifying the individual constellation points contained in the set $\mathcal{M}_c$.

- *Detector Update by Removing the Most Dominant User's Contribution*: Based on the demodulated signal $\check{\mathbf{s}}^{(l^{[i]})[i]}$, the $l^{[i]}$-th user's remodulated contribution is removed from the current vector of composite received signals, yielding:

$$\mathbf{x}^{[i+1]} = \mathbf{x}^{[i]} - \mathbf{H}^{(l^{[i]})} \check{\mathbf{s}}^{(l^{[i]})[i]}. \tag{17.127}$$

Furthermore, the influence of the $l^{[i]}$-th user's associated channel transfer factor vector $\mathbf{H}^{(l^{[i]})}$ is eliminated from the auto-correlation matrix $\mathbf{R}_{\overline{a}}^{[i]H}$, yielding the reduced-dimensional matrix of:

$$\mathbf{R}_{\overline{a}}^{[i]H} \longrightarrow \mathbf{R}_{\overline{a}}^{[i+1]H} \in \mathbb{C}^{(L^{[i]}-1) \times (L^{[i]}-1)}, \tag{17.128}$$

---

[13]Note that while the superscript in round brackets denotes the user index, the superscript in squared brackets denotes the detection stage or iteration index.

Description	Instruction
Initialization	$\mathbf{x}^{[1]} = \mathbf{x};\ \mathbf{R}_{\overline{a}}^{[1]H} = \mathbf{P}\mathbf{H}^H\mathbf{H} + \sigma_n^2\mathbf{I};\ \mathbf{R}_c^{[1]H} = \mathbf{P}\mathbf{H}^H;\ L^{[1]} = L$
i-th iteration:	
Weight calc.	$\mathbf{R}_{\overline{a}}^{[i]H}\mathbf{W}_{\text{MMSE}}^{[i]H} = \mathbf{R}_c^{[i]H} \iff \mathbf{W}_{\text{MMSE}}^{[i]H} = \mathbf{R}_{\overline{a}}^{[i]H-1}\mathbf{R}_c^{[i]H}$
Selection	$\text{SNR}^{(l)[i]} = \frac{\mathbf{w}^{(l)[i]H}\mathbf{R}_{a,S}^{(l)}\mathbf{w}^{(l)[i]}}{\mathbf{w}^{(l)[i]H}\mathbf{R}_{a,N}\mathbf{w}^{(l)[i]}},\ l \in \mathcal{L}^{[i]},\ l^{[i]} = \underset{l \in \mathcal{L}^{[i]}}{argmax}(\text{SNR}^{(l)[i]})$
Combining	$\hat{\mathbf{s}}^{(l^{[i]})[i]} = \mathbf{w}^{(l^{[i]})[i]H}\mathbf{x}^{[i]}$
Demodulation	$\check{\mathbf{s}}^{(l^{[i]})[i]} = arg\underset{\check{\mathbf{s}}/\sigma_{l^{[i]}} \in \mathcal{M}_c}{min}\left\vert\frac{1}{H_{\text{eff}}^{(l^{[i]})[i]}}\hat{\mathbf{s}}^{(l^{[i]})[i]} - \check{\mathbf{s}}\right\vert^2,\ H_{\text{eff}}^{(l^{[i]})[i]} = \mathbf{w}^{(l^{[i]})[i]H}\mathbf{H}^{(l^{[i]})}$
Updating	$\mathbf{x}^{[i+1]} = \mathbf{x}^{[i]} - \mathbf{H}^{(l^{[i]})}\check{\mathbf{s}}^{(l^{[i]})[i]}$
	$\mathbf{R}_{\overline{a}}^{[i]H} \longrightarrow \mathbf{R}_{\overline{a}}^{[i+1]H} \in \mathbb{C}^{(L^{[i]}-1)\times(L^{[i]}-1)}$
	$\mathbf{R}_c^{[i]H} \longrightarrow \mathbf{R}_c^{[i+1]H} \in \mathbb{C}^{(L^{[i]}-1)\times P}$
	$L^{[i+1]} = L^{[i]} - 1$
Return	Start $(i+1)$-th iteration

Table 17.5: Summary of the standard SIC detector's operation in the context of employing MMSE combining and the SNR as an objective funtion for the selection of the most dominant user at each detection stage.

as well as from the cross-correlation matrix $\mathbf{R}_c^{[i]H}$, yielding the reduced-dimensional matrix of:

$$\mathbf{R}_c^{[i]H} \longrightarrow \mathbf{R}_c^{[i+1]H} \in \mathbb{C}^{(L^{[i]}-1)\times P}. \qquad (17.129)$$

More specifically, this is achieved by removing the $\acute{l}^{[i]}$-th row and column from the matrix $\mathbf{R}_{\overline{a}}^{[i]H}$ as well as by eliminating the $\acute{l}^{[i]}$-th row from the matrix $\mathbf{R}_c^{[i]H}$, where the index $\acute{l}^{[i]}$ denotes the position of the column vector $\mathbf{H}^{(l^{[i]})}$ in the hypothetic reduced-size channel transfer factor matrix $\mathbf{H}^{[i]}$, which is associated with the i-th detection stage.

3) Commence the $(i+1)$-th iteration by returning to Step (2). Iterate, until all the L users have been detected.

We have summarized the standard SIC algorithm once again in Table 17.5. Furthermore, a simplified block diagram of the SIC detector was portrayed in Figure 17.10. Note that here we have omitted the signal paths associated with supplying of the channel transfer factor estimates to the linear combiner and to the SIC module. In the next section a higher-complexity strategy is proposed for further enhancing the standard SIC detector's performance.

17.3.1.2 M-SIC and its Derivatives

As we will highlight in Section 17.3.1.4, the standard SIC detector's performance is impaired as a result of the error-propagation occuring between the different consecutive detection stages. Hence efficient countermeasures capable of significantly reducing these effects
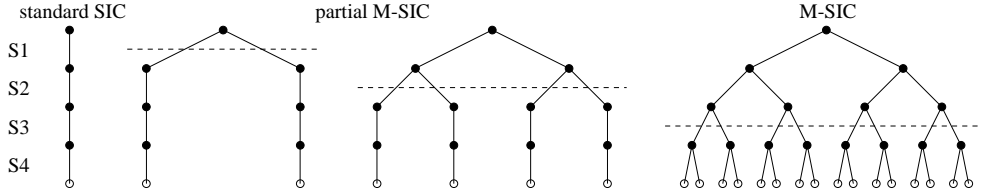
Figure 17.11: Illustration of the (left:) standard SIC, (middle:) partial M-SIC retaining multiple branches per detection node up to the first- and second detection stage, (right:) M-SIC with multiple tentative symbol decisions per detection node at all detection stages; here we have assumed that $M = 2$; in the graph each *detection node* represents an updated vector of signals received by the different antenna elements, for which also the linear combining - but not the array weight calculation has to be performed separately; furthermore, each *branch* represents a tentative symbol decision made at a given detection stage.

will be the topic of this section. Specifically in Section 17.3.1.2.1 M-SIC will be investigated, while partial M-SIC in Section 17.3.1.2.2 and Selective Decision Insertion (SDI) M-SIC in Section 17.3.1.2.3.

17.3.1.2.1 M-SIC A viable strategy of reducing the error propagation effects is to track from each detection stage not only the single most likely symbol decision, but an increased number of $M \leq M_c$ most likely tentative symbol decisions, where M_c denotes the number of constellation points associated with a specific modulation scheme. To provide an example, for $M = 2$ in the first detection stage we have a total of $M = 2$ possible symbol decisions, while in the second detection stage $M^2 = 4$ tentative symbol decisions and correspondingly, in the i-th detection stage we encounter M^i possible tentative symbol decisions. Following our description of the standard SIC detector in Table 17.5, associated with each tentative symbol decision there is a specific updated vector of signals, generated by cancelling the effects of the most dominant $L - i + 1$ number of users from the P-dimensional vector of signals received by the P number of different antenna elements. Hence, in the following detection stage the MMSE combining has to be performed separately for the different updated P-dimensional vectors of received signals. Correspondingly, the number of parallel tentative symbol decisions to be tracked is increased by the factor of M compared to that of the current detection stage. This process can conveniently be portrayed with the aid of a tree-structure, as shown at the right-hand side of Figure 17.11, where, again, we have assumed that $M = 2$ was used. Specifically, each detection node represents an updated P-dimensional vector of signals received by the P different antenna elements, while the branches are associated with the various tentative symbol decisions at the $i = 1, \dots, L$ detection stages. Note that the first detection node at the top of the figure is associated with the original P-dimensional vector of signals received by the different antenna elements. In the final detection stage, after the subtraction of the least dominant user's estimated P-dimensional signal contribution, a decision must be made concerning which specific combination of L number of symbols - represented by the branches connecting the different detection nodes - has most likely been transmitted by the L different users in the specific subcarrier considered. A suitable criterion for performing

this decision is given by the Euclidean distance between the original P-dimensional vector of signals received by the P different antenna elements and the estimated P-dimensional vector of received signals based on the tentative symbol decisions and upon taking into account the effects of the channel. The same decision metric is employed also by the ML detector, which will be discussed in Section 17.3.3. Note furthermore, that this distance measure is identical to the Euclidean norm of the P-dimensional vector of residual signals after the subtraction of the last detected user's P-dimensional signal contribution vector.

The performance improvement potentially observed for the M-SIC scheme compared to the standard SIC arrangement is achieved at the cost of a significantly increased computational complexity. This is since the number of parallel tentative symbol decisions associated with a specific detection stage is a factor of M higher than that of the previous detection stage, and hence in the last detection stage we potentially have to consider M^L number of different tentative symbol decisions. Again, this implies that the approach of the M-SIC scheme resembles that of the ML detector to be discussed in Section 17.3.3.

17.3.1.2.2 Partial M-SIC A viable approach of further reducing the associated computational complexity is motivated by the observation that for sufficiently high SNRs the standard SIC detector's performance is predetermined by the bit- or symbol-error probabilities incurred during the first detection stage. This is, because if the most dominant user's associated symbol decision is erroneous, its effects potentially propagate to all other users' decisions conducted in the following detection stages. Furthermore, as observed previously in the context of our investigations of the MMSE detector's performance in Section 17.2.6.3 as a function of the number of simultaneous users L and the number of reception antennas P the highest performance gain in terms of the achievable SNR reduction at the reception antennas, whilst maintaining a specific BER is observed upon removing the first user from a fully loaded system. An example of such a fully loaded system is that supporting four simultaneous users with the aid of four reception antennas. Hence we conclude that the symbol error probability specifically of the first detection stage should be as low as possible, while the tentative symbol decisions carried out at later detection stages become automatically more reliable as a result of the system's increased diversity order due to removing the previously detected users.

Hence, our suggestion is to retain $M > 1$ number of tentative symbol decisions at each detection node, characterized by its associated updated P-dimensional vector of received signals only up to the specific $L_{\text{pM-SIC}}$-th stage in the detection process. By contrast, at later detection stages only one symbol decision is retained at each detection node, as in the standard SIC scheme. This philosophy is further highlighted with the aid of the two graphs at the centre of Figure 17.11. Specifically, in the illustration second from the left of Figure 17.11 we have portrayed the case of retaining two tentative symbol decisions per detection node only in the first detection stage, while in the illustration second from the right-hand side of Figure 17.11 two tentative symbol decisions per detection node are retained in both of the first two detection stages.

17.3.1.2.3 Selective-Decision-Insertion Aided M-SIC In order to even further reduce the computational complexity an improved strategy termed Selective-Decision-Insertion (SDI) can be applied, which was initially proposed in [117, 137]. The philosophy of the

SDI technique is that of tracking additional tentative symbol decisions only in those $N_{\text{SDI}}^{[1]}$ number of subcarriers, which exhibit the lowest SINR during the first detection stage, since these are most likely to cause symbol errors.

17.3.1.3 Generation of Soft-Bit Information for Turbo-Decoding

In Section 17.2.5 we elaborated on the process of soft-bit generation supporting the employment of turbo-decoding in the context of linear detection techniques, such as the LS and MMSE schemes. Specifically, we capitalized on the assumption that the residual interference at the combiner's output is Gaussian, which enabled us to employ the same strategies for generating the soft-bit values, as in a single-user scenario. In Section 17.3.1.3.1 we will demonstrate that the soft-bit generation process designed for the non-linear SIC detector can be based on that of the linear detection schemes, although, as shown in Section 17.3.1.3.2 a further performance enhancement can be achieved upon accounting for the effects of error propagation, which occur through the different detection stages, as it will be demonstrated in Section 17.3.1.4.2.

17.3.1.3.1 Generation of Rudimentary Soft-Bits As it was highlighted in Section 17.3.1.1, at each stage of the standard SIC-related detection process we generate estimates of the remaining users' transmitted signals with the aid of a linear combiner. Hence, a feasible approach employed for generating soft-bit values is to invoke the linear combiner's output signals of the most dominant user as it was demonstrated in Section 17.2.5. More specifically, the $l^{[i]}$-th user's soft-bit values - where the superscript i in $()^{[i]}$ indicates that this particular user was found to be the most dominant remaining user during the i-th detection stage - can be generated upon invoking the associated combiner output signal $x_{\text{eff}}^{(l^{[i]})[i]} = \hat{s}^{(l^{[i]})[i]}$ defined in the context of Equation 17.95 namely:

$$L_{m\approx}^{(l^{[i]})[i]} = \ln \frac{P(b_m^{(l^{[i]})[i]} = 1|x_{\text{eff}}^{(l^{[i]})[i]}, H_{\text{eff}}^{(l^{[i]})[i]})}{P(b_m^{(l^{[i]})[i]} = 0|x_{\text{eff}}^{(l^{[i]})[i]}, H_{\text{eff}}^{(l^{[i]})[i]})}, \qquad (17.130)$$

where $H_{\text{eff}}^{(l^{[i]})[i]} = \mathbf{w}^{(l^{[i]})[i]H}\mathbf{H}^{(l^{[i]})}$, as given by Equation 17.126 is the l-th detected user's effective channel transfer factor.

However, generating the soft-bit values of the $l^{[i]}$-th user - whose associated signal is linearly detected during the i-th detection stage - with the aid of Equation 17.130 inherently assumes that the signal components of those users, which have already been detected and demodulated during the previous SIC detection stages, have been correctly removed from the P-dimensional vector $\mathbf{x}^{[1]} = \mathbf{x}$ of signals received by the P different antenna elements for the successful employment of this principle. A necessary condition is that the associated symbol decisions were free of errors, namely that we had $s^{(l^{[j]})} = \check{s}^{(l^{[j]})[j]}$, $j = 1, \ldots, i-1$. Naturally, this assumption only holds with a certain probability. In the sequel our aim will be to estimate this probability and draw our further conclusions.

17.3.1.3.2 Generation of Weighted Soft-Bits To elaborate a little further, during the first detection stage the probability that the $l^{[1]}$-th user, which was found to be the most dominant one, has been correctly demodulated is given by the *a posteriori* probability of

$P(\check{s}^{(l^{[1]})[1]}|x_{\text{eff}}^{(l^{[1]})[1]}, H_{\text{eff}}^{(l^{[1]})[1]})$. Hence, by contrast during the second detection stage the probability that the $l^{[2]}$-th user, which was found to be the most dominant one among the $L-1$ remaining users, has been correctly demodulated is given by the *a posteriori* probability of $P(\check{s}^{(l^{[2]})[2]}|x_{\text{eff}}^{(l^{[2]})[2]}, H_{\text{eff}}^{(l^{[2]})[2]})$, conditioned on a correct symbol decision during the first detection stage.

Furthermore, since we have $P(x_{\text{eff}}^{(l^{[2]})[2]}|x_{\text{eff}}^{(l^{[1]})[1]}) = P(s^{(l^{[1]})[1]}|x_{\text{eff}}^{(l^{[1]})[1]})$, where we have exploited that $P(H_{\text{eff}}^{(l^{[1]})[1]}) = P(H_{\text{eff}}^{(l^{[2]})[2]}) = 1$, we obtain an estimate for the probability of the joint event that $\check{s}^{(l^{[1]})[1]}$ and $\check{s}^{(l^{[2]})[2]}$ are the correct symbol decisions at the first and second detection stages, respectively, which can be expressed as:

$$P(\check{s}^{(l^{[2]})[2]}, \check{s}^{(l^{[1]})[1]}|x_{\text{eff}}^{(l^{[1]})[1]}) = P(\check{s}^{(l^{[2]})[2]}|x_{\text{eff}}^{(l^{[2]})[2]})P(\check{s}^{(l^{[1]})[1]}|x_{\text{eff}}^{(l^{[1]})[1]}). \qquad (17.131)$$

More generally, for the demodulated symbols of the first i number of detection stages we have the joint probability:

$$P_{\text{joint}}^{[i]} = P(\check{s}^{(l^{[i]})[i]}, \dots, \check{s}^{(l^{[1]})[1]}|x_{\text{eff}}^{(l^{[1]})[1]}) = \prod_{j=1}^{i} P(\check{s}^{(l^{[j]})[j]}|x_{\text{eff}}^{(l^{[1]})[1]}). \qquad (17.132)$$

Note however that this is only an estimate of the true joint probability, since for a finite number of users the residual interference at a specific stage's combiner output is potentially non-Gaussian, which is particularly the case, if an error has occurred in one of the detection stages.

The estimated joint probability $P_{\text{joint}}^{[i]}$ of correct symbol decisions during the first i number of detection stages, which was given by Equation 17.132, can be invoked as a measure of confidence for the soft-bit values generated during the $(i+1)$-th detection stage. Specifically, it is expected that if an error has occurred during one of the detection stages, then the soft-bit values produced with the aid of Equation 17.130 for the following detection stages will be relatively unreliable. Hence, a viable approach of mitigating these effects is the employment of weighting, namely by weighting of the *a posteriori* probabilities that a bit having a polarity of $b \in \{0,1\}$ has been transmitted, as seen in the numerator and denominator of Equation 17.130, yielding:

$$L_{m\approx}^{(l^{[i]})[i]}\Big|_{\text{weight}} = \ln \frac{P(b_m^{(l^{[i]})[i]} = 1|x_{\text{eff}}^{(l^{[i]})[i]}, H_{\text{eff}}^{(l^{[i]})[i]}) \cdot P_{\text{joint}}^{[i-1]} + \frac{1}{2}(1 - P_{\text{joint}}^{[i-1]})}{P(b_m^{(l^{[i]})[i]} = 0|x_{\text{eff}}^{(l^{[i]})[i]}, H_{\text{eff}}^{(l^{[i]})[i]}) \cdot P_{\text{joint}}^{[i-1]} + \frac{1}{2}(1 - P_{\text{joint}}^{[i-1]})}. \qquad (17.133)$$

We observe that if $P_{\text{joint}}^{[i-1]}$ approaches unity, which reflects a high confidence in having no symbol errors during the previous $(i-1)$ number of detection stages, then the expression of Equation 17.133 transforms into that of Equation 17.130, which was based on the assumption of benefitting from the perfect removal of the previously detected users' signal contributions. By contrast, if $P_{\text{joint}}^{[i-1]}$ tends towards zero, which indicates a high probability of encountering symbol errors in the SIC process, then the bit probabilities $P(b_m^{(l^{[i]})[i]}|x_{\text{eff}}^{(l^{[i]})[i]}, H_{\text{eff}}^{(l^{[i]})[i]})$, $b_m^{(l^{[i]})[i]} \in \{0,1\}$ are potentially unreliable and hence should be de-weighted. This has the effect that the L-value in Equation 17.133 tends to zero.

The advantage of weighted soft-bits will be demonstrated in the context of our investigations on turbo-coded SIC schemes in Section 17.3.1.4.7.

17.3.1.4   Performance Analysis

In this section the standard SIC algorithm and its derivative, namely the M-SIC scheme will be investigated in terms of their achievable Bit Error-Ratio (BER) and Symbol Error-Ratio (SER)[14] performance. Again, the frame-invariant fading indoor WATM channel model and its associated OFDM system model described in Section 14.3.1 were invoked and ideal knowledge of the channel transfer functions associated with the different transmit-receive antenna pairs was assumed. The aim of stipulating a frame-invariant fading channel was that of avoiding the obfuscating effects of Inter-subCarrier Interference (ICI). Note that as a result of this assumption in the uncoded scenario the different detectors' BER and SER performance curves are independent from the indoor SWATM channel's specific multipath intensity profile. For a summary of the basic simulation setup we refer to Table 17.3.

The structure of Section 17.3.1.4 is as follows. In Section 17.3.1.4.1 standard SIC and M-SIC are characterized in terms of their BER and SER performance for different numbers of communicating users and receiver antennas. Furthermore, in an effort to illustrate the effects of error-propagation across the different detection stages, in Section 17.3.1.4.2 more detailed investigations are conducted with respect to the associated system's SER performance, which is evaluated on a detection stage-by-stage basis. These investigations are further extended in Section 17.3.1.4.3 to the scenario, where an error-free remodulated reference signal is employed in the context of updating the vector of signals received by the different antenna elements in each detection stage. In order to further augment our understanding of the effects of error-propagation, in Section 17.3.1.4.4 the detection stages' symbol-error event probabilities are analysed. More specifically, each error-event is captured as the unique combination of the presence of a symbol error ("1") - or the absence of a symbol error ("0") at the different detection stages. Furthermore, in Section 17.3.1.4.5 the SER performance of the partial M-SIC scheme is analysed with respect to the detection stage $L_{\mathrm{pM\text{-}SIC}}$ up to which the M most likely symbol decisions are retained at each detection node of the detection process. Finally, in Section 17.3.1.4.6 the technique of SDI-M-SIC is characterized briefly. Explicitly we will quantify the effect of the $N_{\mathrm{SDI}}^{[1]}$ number of subcarriers for which $M = 2$ tentative symbol decisions are made during the first SIC detection stage. Our performance assessments will be concluded in Section 17.3.1.4.7 with the analysis of turbo-decoded, standard SIC detection-assisted SDMA-OFDM systems.

17.3.1.4.1   BER and SER Performance of Standard SIC and M-SIC for Different Numbers of Users and Receiver Antennas

In Figure 17.12 we have portrayed the BER- as well as the SER performance as a function of the SNR at the reception antennas. Specifically, at the left-hand side of Figure 17.12 we characterized the standard SIC, while at the right-hand side of Figure 17.12 the M-SIC scheme. The results of Figure 17.12 are also parameterized for the different configurations by the number of users L and by the number of reception antennas P, which were assumed here to be identical. Furthermore, both the SINR as well as the SNR recorded at the MMSE combiner's output are considered as potential alternatives for performing the selection of the most dominant user at each detection stage.

---

[14]Note that here we refer to the symbol transmitted on an OFDM subcarrier basis.
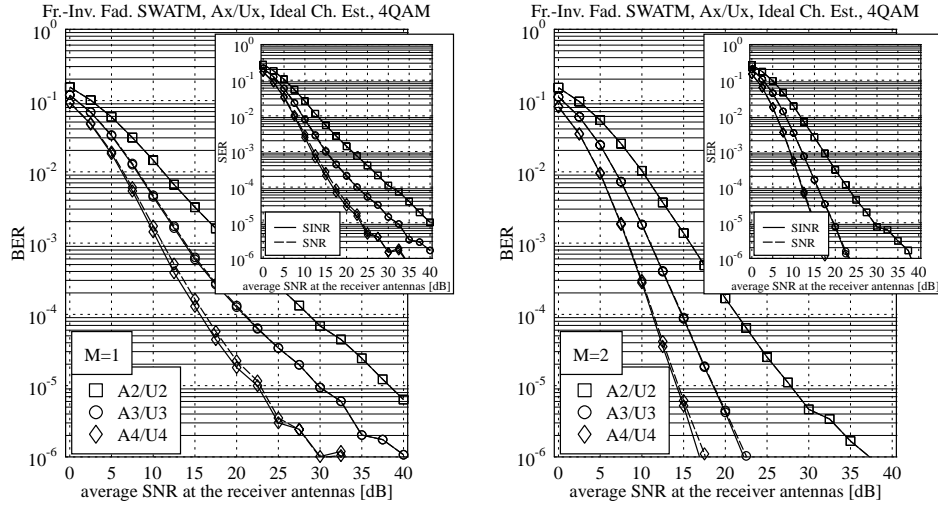
Figure 17.12: BER and SER performance of 4QAM-modulated (left:) standard SIC and (right:) M-SIC ($M = 2$) detection-assisted SDMA-OFDM as a function of the SNR recorded at the reception antennas and parameterized for the different system configurations in terms of the number of users L and the number of reception antennas P; two different measures, namely the SINR and the SNR at the combiner's output were employed for performing the selection of the most dominant user at each detection stage; for the basic simulation parameters we refer to Table 17.3.

For both detectors, namely for the standard SIC and for the M-SIC scheme the general trend is that by increasing the MIMO system's order upon employing for example four reception antennas for supporting four simultaneous users (A4/U4) instead of two reception antennas for supporting two simultaneous users (A2/U2), the system's performance evaluated in terms of the achievable BER and SER is significantly improved. This is, because in the context of encountering correct symbol decisions at the different stages of the detection process, the associated MIMO system's diversity order, namely the ratio between the number of transmit- and receive antennas, is increased. As argued in Sections 17.2.6.2 and 17.2.6.3, this has the effect of providing a higher degree of freedom at the MMSE combiner of each detection stage for adjusting the reception antennas' weights, which results in a more efficient suppression of the AWGN. Furthermore, for a MIMO system having a higher order, at a specific detection stage there is also the choice between a larger number of users to be selected as the most dominant user to be detected next, which also implies additional diversity. We also observe in Figure 17.12 that compared to standard SIC the M-SIC scheme retaining $M = 2$ tentative 4QAM symbol decisions out of the $M_c = 4$ legitimate symbols exhibits a significant performance advantage, which is achieved at the cost of an increased computational complexity. Hence, potential complexity reduction strategies, namely partial M-SIC
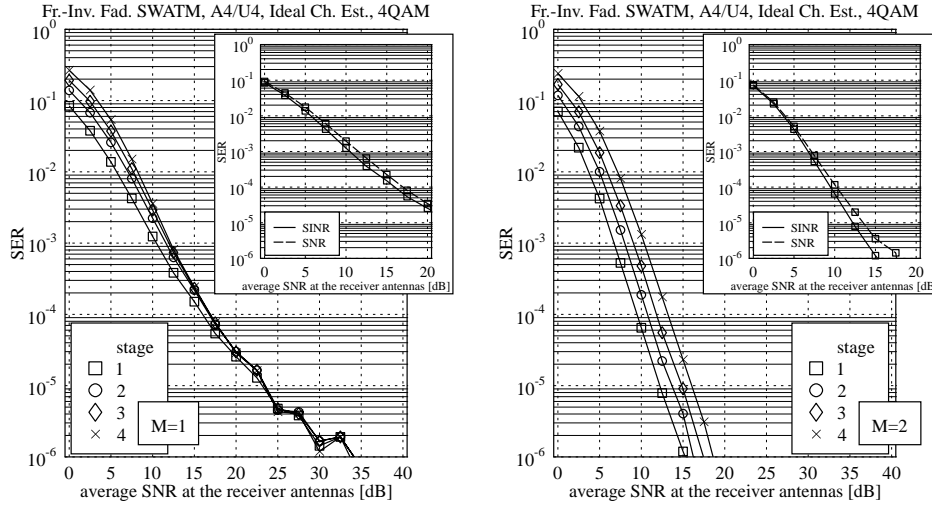
Figure 17.13: SER performance observed in different detection stages in the context of 4QAM-modulated (left:) standard SIC and (right:) M-SIC ($M = 2$) detection-assisted SDMA-OFDM as a function of the SNR at the reception antennas; here a system configuration of $L = 4$ simultaneous users and $P = 4$ reception antennas is considered; in the smaller-sized sub-figures two measures, namely the SINR and the SNR evaluated at the combiner's output are compared against each other in terms of performing the selection of the most dominant user at each detection stage; for the basic simulation parameters we refer to Table 17.3.

and SDI-M-SIC will be characterized in Section 17.3.1.4.5 and 17.3.1.4.6.

With respect to the different objective measures, namely the SNR and SINR, employed for performing the selection of the most dominant user at each stage of the detection process a slight advantage is observed in favour of the SINR measure, although only for the system configurations of a higher order. In the context of these configurations the residual interference was apparently higher than for the system configurations supporting a lower number of users. In the next section we will focus our attention further on the effects of error propagation between the different detection stages.

17.3.1.4.2 SER Performance of Standard SIC and M-SIC on a Per-Detection Stage Basis In this section we will further investigate the effects of error propagation across the different detection stages. Hence at the left-hand side of Figure 17.13 we have portrayed the SER associated with the different detection stages for standard SIC, while at the right-hand side of Figure 17.13 for the M-SIC scheme. In the context of the simulation results presented in each of the larger graphs the SINR was invoked as the metric used for performing the selection of the most dominant user at each stage of the detection process. By contrast, in

the smaller-sized sub-graphs of Figure 17.13, we have compared the SINR and SNR criteria against each other, at the first detection stage.

More specifically, for the standard SIC we observe at the left-hand side of Figure 17.13 that upon traversing through the different detection stages the SER is significantly increased at lower SNRs, while at higher SNRs the different detection stages' SERs become virtually identical. As it will be supported by our forthcoming analysis of the standard SIC detector's SER recorded in the context of an error-free reference signal, a viable explanation of this phenomenon is that the majority of symbol errors caused by the early detection stages propagates to the later stages. In other words, only a comparably small additional error contribution is caused by the later detection stages, which is a consequence of the increased diversity order associated with the gradually decreasing number of undetected user symbols. For the M-SIC scheme at the right-hand side of Figure 17.13 a similar behaviour is observed, although, for higher SNRs the different detection stages' SER performance curves do not merge. This is, because at each detection stage the SER contribution induced by the error propagation from previous detection stages is of a similar significance as the additional contribution due to the AWGN.

17.3.1.4.3 SER Performance of Standard SIC and M-SIC on a Per-Detection Stage Basis for an Error-Free Reference

In order to further highlight the associated error propagation effects, let us stipulate the availability of an ideal, error-free remodulated reference during the subtraction of the most recently detected user's contribution from the P-dimensional vector of signals received by the P different antenna elements. Corresponding to this scenario at the left-hand side of Figure 17.14 we have plotted the SER versus SNR performance of various system configurations parameterized again with the number of simultaneous users L, each equipped with one transmit antenna, which was assumed for each configuration to be identical to the number of reception antennas P, namely we had $L = P$. In contrast to the curves presented in Figure 17.12, which are repeated here as a benchmarker, the error propagation between the different detection stages was prevented due to the employment of an error-free remodulated reference. Again, the standard SIC detector with $M = 1$ is considered here. As a result of the idealistic nature of the reference, the system's SER performance is significantly improved compared to the more realistic case of an imperfect, potentially error-contaminated remodulated reference. The corresponding SER performance curves recorded during the different detection stages are shown at the right-hand side of Figure 17.14, where again, in the reduced-sized sub-figure we have plotted the curves associated with an imperfect remodulated reference. These curves were originally shown at the left-hand side of Figure 17.13. For the error-free remodulated reference related curves we observe at the higher-index detection stages that for SNRs up to 7.5dB only a relatively modest SER degradation is encountered, when compared to the previous detection stages. This phenomenon is in contrast to the more distinct degradation observed in conjunction with the original curves generated in the context of a potentially error-contaminated remodulated reference. This was a result of the effects of error propagation. The residual SER degradation observed in Figure 17.14 for the SNR range up to 7.5dB is attributed to the process of ranking the remaining users' SINRs, where the most dominant remaining user is detected and consequently during the last detection stages only the weaker users are still to be detected. By contrast, at higher SNRs this trend is reversed. Specifically, the SER achieved during the last detection stages is far lower than that of the first detection stages, which is a result of the implicit increase
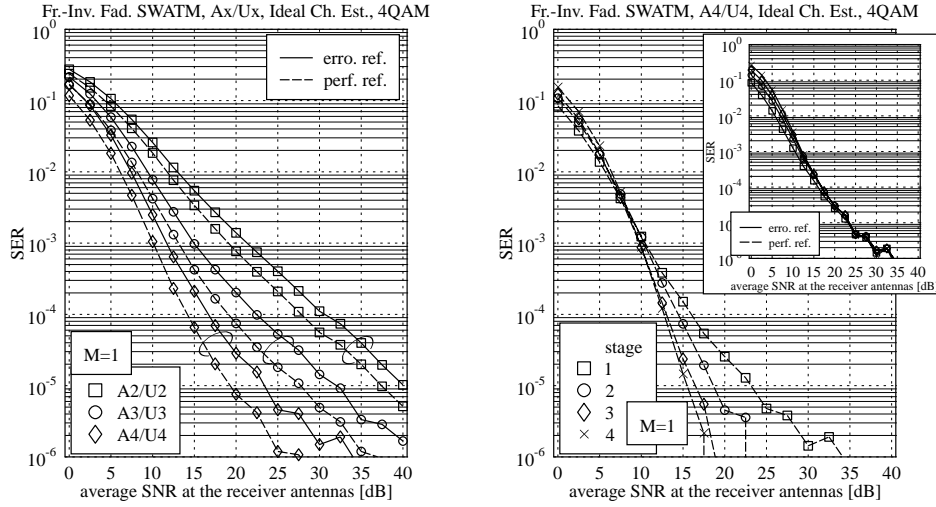
Figure 17.14: (left:) SER performance of 4QAM-modulated standard SIC detection-assisted SDMA-OFDM as a function of the SNR at the reception antennas, parameterized with the number of simultaneous users L and the number of reception antennas P, where $L = P$; (right:) SER performance of standard SIC recorded separately for each detection stage in the context of a scenario of $L = P = 4$; an ideal, error-free reference is employed in the subtractive interference cancellation process associated with each detection stage, while the curves associated with the more realistic error-contaminated reference have been plotted as a benchmarker; the SINR was invoked as the metric for the selection of the most dominant user at each detection stage; for the basic simulation parameters we refer to Table 17.3.

of the system's diversity order. Again, as also supported by the BER curves of Figure 17.8, for a lower number of users the MMSE combiner employed at each detection stage is less restricted in terms of the specific choice of the receiver antenna weights, which results in a more efficient suppression of the AWGN.

17.3.1.4.4 Evaluation of the Error-Propagation-Related Event Probabilities In order to obtain an even further insight into the effects of error propagation across the different detection stages, we have measured the probabilities of the various symbol error events. More specifically, the error-event associated with index j can be defined as the following vector:

$$E_j = \mathbf{e}_j = (e_{L-1}, \dots, e_i, \dots, e_0), \quad e_i \in \{0, 1\}, \tag{17.134}$$
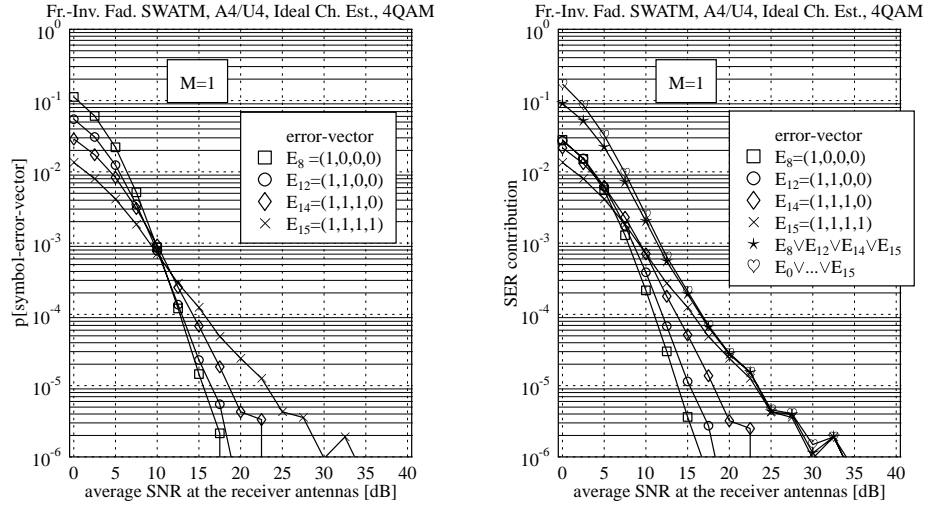
Figure 17.15: (left:) Probability- and (right:) SER contribution of the different significant error-vectors as a function of the SNR measured at the reception antennas; here 4QAM-modulated standard SIC detection-assisted SDMA-OFDM is considered in the context of a scenario of $L = 4$ simultaneous users and $P = 4$ reception antennas (A4/U4); the SINR was invoked as the metric for the selection of the most dominant user at each detection stage; for the basic simulation parameters we refer to Table 17.3.

where the index j is given by interpreting the vector $\mathbf{e}_j$ as a binary number, yielding:

$$j = \sum_{i=0}^{L-1} \left\{ \begin{array}{ll} 2^i & \wedge e_i = 1 \\ 0 & \wedge e_i = 0 \end{array} \right. . \tag{17.135}$$

Explicitly, in case of an error at the i-th detection stage we have $e_i = 1$. In the context of our evaluations we have focussed on four specific symbol error events, which are suitable for further demonstrating the effects of error propagation through the different detection stages. These error events are $E_8 = (1, 0, 0, 0)$, $E_{12} = (1, 1, 0, 0)$, as well as $E_{14} = (1, 1, 1, 0)$ and $E_{15} = (1, 1, 1, 1)$, where E_8 indicates encountering an error event during the last detection stage. The corresponding probabilities of these events as a function of the SNR recorded at the reception antennas are portrayed at the left-hand side of Figure 17.15 for the standard SIC scheme. Here we observe that for SNRs below the cross-over point near 10dB the specific error propagation events, which extend from the first detection stage to the last stage are less likely than those events which commence in one of the last stages of the detection process.

This phenomenon can be explained as follows. Even for SNRs as low as 0dB, the probability of an AWGN-induced symbol error at a specific detection stage is far lower than the

probability of incurring an error-free detection. Hence, the event having the highest probability is that of no symbol errors at all detection stages, which is denoted as E_0. The next most likely class of error events - assuming the independence of encountering decision errors at the different detection stages, as we also assumed in the case of an error-free reference - is constituted by those events which host a symbol error only in one of the detection stages. As highlighted earlier in the context of our description of the graph at the right-hand side of Figure 17.14, for relatively low SNRs it is more likely to incur symbol errors during the higher-index detection stages than in the lower-index stages, which was attributed to the process of ranking the users at the different detection stages. This effect is even further augmented here as a result of the associated error-propagation phenomenon. More explicitly, the probability of incurring an error event during the first detection stage only, which is indicated by $E_1 = (0, 0, 0, 1)$ is likely to be lower than the probability of encountering the error event of $E_{15} = (1, 1, 1, 1)$ due to the error-propagation effects, although in case of independent errors the probability of the latter would be expected to be significantly lower. Hence, following these argumentations, among the four different error events considered here, the event of $E_8 = (1, 0, 0, 0)$, which is associated with incurring a symbol error only in the last detection stage appears with the highest probability at low to medium SNRs of up to 10dB. By contrast, for higher SNRs the reverse behaviour is observed, namely that the event of incurring symbol errors in all detection stages occurs with the highest probability. This is because upon increasing the SNR, the probability of incurring a symbol error in the last detection stage decreases far more rapidly than the probability of incurring a symbol error in the first detection stage due to its interference-contaminated nature, despite detecting the highest-power user first. As argued earlier, this is also a consequence of the higher diversity order available for the MMSE combiner during the last detection stages, which is due to removing the interference imposed by other users during the previous detection stages.

On the right-hand side of Figure 17.15 we have related the different symbol error events to their SER contribution. For this purpose we have weighted the event probabilities presented at the left-hand side of Figure 17.15 by their relative contribution to the average SER. More specifically, for errors events which host a symbol error in a single detection stage only, the weighting factor is $1/L$, while correspondingly for two symbol errors we have $2/L$ and so on. Additionally, we have plotted here the joint contribution of the four most significant error events, as well as the total average SER, which is the joint contribution of all error events. While for lower SNRs some difference is observed between the SER predicted with the aid of the four most significant error events, namely $E_8 \vee E_{12} \vee E_{14} \vee E_{15}$ and the actual SER curves associated with $E_1 \vee \ldots \vee E_{15}$, at higher SNRs the former events of $E_8 \vee E_{12} \vee E_{14} \vee E_{15}$ closely predict the actual SER. A plausible interpretation of this phenomenon is that at higher SNRs the SER is constituted by error propagation events, which is even further augmented, since the MMSE combiner does not take into account the extra non-Gaussian "noise" caused by symbol errors encountered in previous detection stages. This problem results in a noise amplification, a phenomenon, which is also known from zero-forcing combiners.

17.3.1.4.5 SER Performance of the Partial M-SIC   As observed in the previous sections, the M-SIC scheme described in Section 17.3.1.2.1 is capable of significantly outperforming the standard SIC arrangement, which was found to suffer from the consequences of error-propagation between the different detection stages. Furthermore, compared to the optimum ML detection scheme the performance degradation was observed to be less than 0.5dB
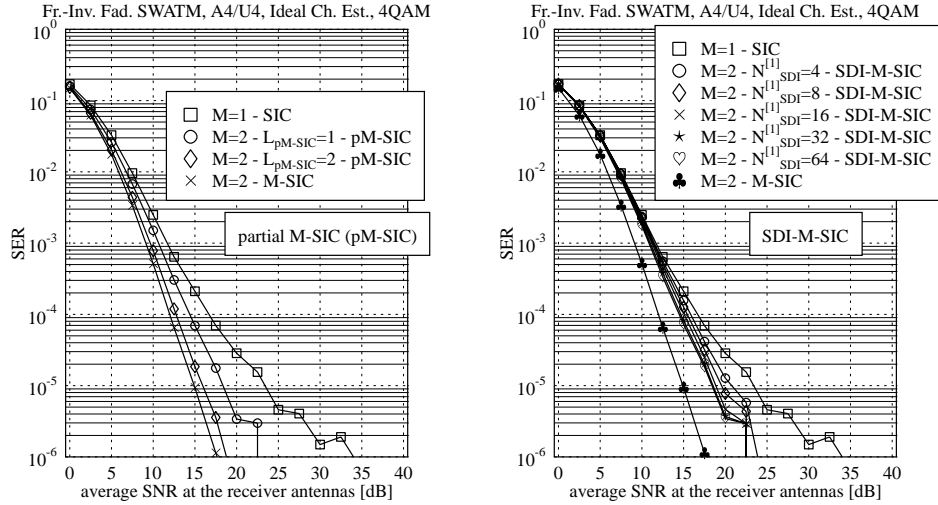
Figure 17.16: SER performance as a function of the SNR recorded at the reception antennas of 4QAM-modulated (left:) partial M-SIC ($M = 2$) detection-assisted SDMA-OFDM, parameterized with the index of the detection stage up to which multiple tentative symbol decisions are retained at each detection node of the detection process and (right:) SDI-M-SIC ($M = 2$) detection-assisted SDMA-OFDM, parameterized with the $N_{\text{SDI}}^{[1]}$ number of subcarriers associated with multiple tentative symbol decisions during the first detection stage; here a system configuration of $L = 4$ simultaneous users and $P = 4$ reception antennas (A4/U4) is considered; the SINR was employed as the metric for the selection of the most dominant user at each detection stage; for the basic simulation parameters we refer to Table 17.3.

in terms of the SNR at the receiver antennas required at a specific SER. This impressive performance was achieved at the cost of a significantly increased computational complexity compared to standard SIC. In order to reduce this potentially excessive complexity, it was proposed in Section 17.3.1.2.2 to retain $M > 1$ symbol decisions at each detection node, characterized by its associated updated vector of received signals up to the specific $L_{\text{pM-SIC}}$-th stage in the detection process, where the updating process implied cancelling the effects of the remodulated tentatively demodulated symbols from the composite multiuser signal. By contrast, at higher-index detection stages only one symbol decision would be tracked from each detection node, as in the standard SIC scheme. These principles were illustrated in Figure 17.11.

The benefits of employing this strategy have again been verified here with the aid of simulations, as shown at the left-hand side of Figure 17.16. Again, we have plotted the performance of standard SIC ($M = 1$) as a benchmarker. Also note that the case of tracking multiple decisions per detection node in the first three detection stages is equivalent to the

original M-SIC and hence it does not yield a complexity reduction. However, employing multiple tentative symbol decisions only at the first two detection stages will be shown to yield a significant complexity reduction in Section 17.3.1.5.2, which is achieved at the modest cost of increasing the SNR required for maintaining an SER of 10^{-5} by only about 1dB.

17.3.1.4.6 SER Performance of Selective-Decision-Insertion Aided M-SIC The philosophy of the SDI technique [117, 137] of Section 17.3.1.2 is that of tracking additional tentative symbol decisions only in those $N_{\mathrm{SDI}}^{[1]}$ number of subcarriers, which exhibit the lowest SINR during the first detection stage, since these are most likely to cause symbol errors. As it was argued in the context of Figure 17.15, the employment of this approach is motivated by the observation that at higher SNRs symbol errors are mainly caused during the first detection stage because of the higher number of interfering users than at later stages. Again, we have evaluated the performance of this strategy with the aid of computer simulations. The associated SER performance results as a function of the SNR measured at the reception antennas and further parameterized with the number of low-quality subcarriers N_{SDI} where $M = 2$ tentative symbol decisions are retained during the first detection stage are shown at the right-hand side of Figure 17.16. By contrast, in all other subcarriers only one symbol decision is retained at each detection node for the sake of maintaining a low complexity. As a reference at the right-hand side of Figure 17.16 we have again plotted the SER performance curves associated with the partial M-SIC, as well as that of the original M-SIC, as shown at the left-hand side of Figure 17.16. We observe that when the $N_{\mathrm{SDI}}^{[1]} = 64$ number of lowest-quality subcarriers classified in terms of the SINR experienced during the first detection stage are associated with $M = 2$ tentative symbol decisions during this specific detection stage, then a similar SER performance is observed, to the significantly more complex scenario, where all subcarriers are associated with $M = 2$ tentative symbol decisions during the first detection stage. This is because by retaining multiple tentative symbol decisions exclusively during the first detection stage, only the probability of those error propagation events is reduced, which are caused during the first detection stage and these are likely to be those associated with the $N_{\mathrm{SDI}}^{[1]}$ number of lowest-SINR subcarriers.

However, compared to the SER performance of the M-SIC, the performance degradation incurred by the first-stage SDI-M-SIC characterized at the right-hand side of Figure 17.16 is substantial. In order to achieve further performance improvements, additional tentative symbol decisions could also be retained during the higher-index detection stages although naturally at the cost of a higher complexity.

17.3.1.4.7 BER Performance of Turbo-Coded SIC Detection-Assisted SDMA-OFDM As demonstrated in Section 17.2.6.4 in the context of MMSE detection-assisted SDMA-OFDM employing turbo-decoding at the receiver is a powerful means of further enhancing the system's BER performance. Naturally, this is achieved at the cost of reducing the system's effective throughput and by investing an additional amount of computational complexity. The relevant turbo coding parameters were summarized in Table 17.4, but for the reader's convenience they are repeated here: the coding rate was $R_c = \frac{1}{2}$, the constraint length was $K_c = 3$, the octally represented generator polynomials of $(7, 5)_8$ were used and four turbo decoding iterations were performed.

Our discussions will first of all concentrate on a comparison between the various methods
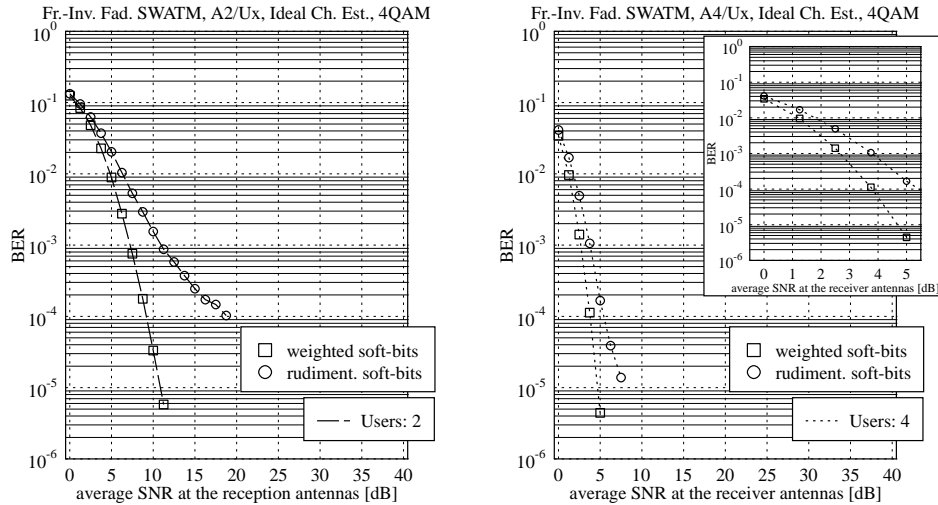
Figure 17.17: BER performance of turbo-coded, 4QAM-modulated, standard SIC detection-assisted SDMA-OFDM as a function of the SNR recorded at the reception antennas for the *rudimentary soft-bit generation* approach as suggested by Equation 17.130 and for the *weighted soft-bit generation* approach of Equation 17.133; the curves are further parameterized with the number of simultaneous users and reception antennas using $L = P$, where more specifically (left:) two reception antennas, (right:) and four reception antennas were employed; in the smaller-sized sub-figure we have magnified the range of SNRs between 0dB and 5dB; for the basic simulation parameters and the turbo-coding parameters we refer to Tables 17.3 and 17.4, respectively.

of soft-bit generation, namely on the rudimentary approach of Equation 17.130 and on the weighted approach of Equation 17.133. The associated BER versus SNR simulation results valid for a scenario of $L = P = 2$ and $L = P = 4$ number of simultaneous users and reception antennas are portrayed at the left- and right-hand side of Figure 17.17, respectively. In both scenarios a significant performance advantage is observed for the weighted soft-bit generation approach, which attempts to take into account the effects of error propagation through the different SIC detection stages upon de-weighting potentially unreliable soft-bit values. For the lower-order SDMA scenario of $L = P = 2$ the performance improvement achieved by the weighted soft-bit generation is even more dramatic than for the scenario of $L = P = 4$. This is, because for the lower-order scenario the probability that a symbol error is incurred during the first detection stage is higher than for the higher-order scenario, since the latter system benefits more substantially from the increased grade of diversity experienced in conjunction with the higher number of users, supported by a higher number of antennas. Hence, weighting of the soft-bits is more effective in scenarios supporting a lower number of users with the aid of less antennas.
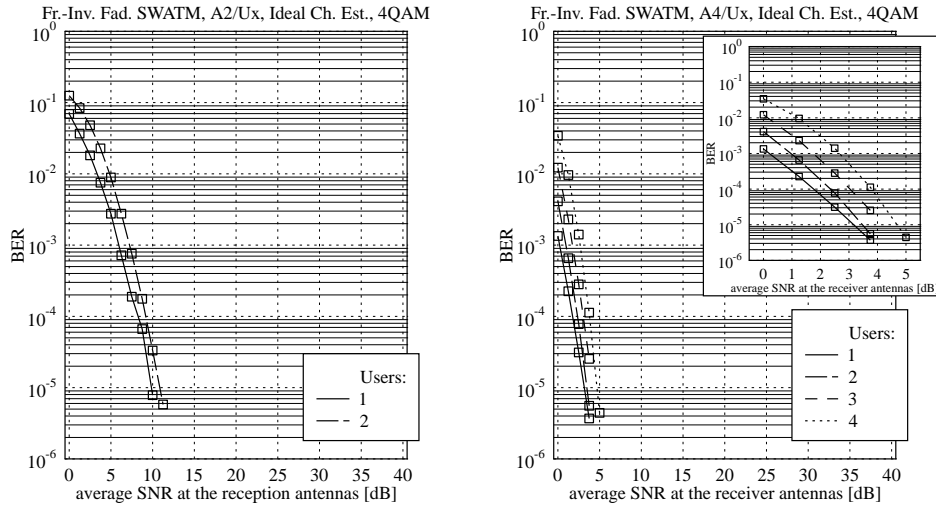
Figure 17.18: BER performance of turbo-coded, 4QAM-modulated, standard SIC detection-assisted SDMA-OFDM as a function of the SNR recorded at the reception antennas; the curves are further parameterized with the number of simultaneous users L and the number of reception antennas P, where more specifically (left:) two reception antennas, (right:) and four reception antennas were employed; in the smaller-sized sub-figure we have magnified the range of SNRs between 0dB and 5dB; for the basic simulation parameters and the turbo-coding parameters we refer to Tables 17.3 and 17.4, respectively.

Having found that the weighted soft-bit metric of Equation 17.133 is the advantageous one in terms of the system's associated BER performance, further investigations were conducted with respect to different scenarios in terms of the number of simultaneous users L and the number of reception antennas P. The corresponding simulation results are shown in Figure 17.18 again, on the left-hand side for $P = 2$ reception antennas while at the right-hand side for $P = 4$ reception antennas. Similarly to our observations discussed in the context of turbo-coded MMSE detection-assisted SDMA-OFDM in Section 17.2.6.4, the system's BER performance is improved upon decreasing the number of simultaneous users L. Again, this is because, the associated MMSE combiner of each detection stage is less constrained with respect to the specific choice of the antenna array weights and hence more of the channel's diversity potential can be dedicated to mitigating the effects of AWGN, rather than to suppressing the undesired co-channel users.

17.3.1.5   Complexity Analysis

In this section we will analyse the computational complexity exhibited by the various forms of the SIC algorithm on a per-subcarrier basis. The specific structure of this section is as

follows. In Section 17.3.1.5.1 the computational complexity of the standard SIC algorithm will be investigated, while in Sections 17.3.1.5.2 and 17.3.1.5.3 the complexity of the M-SIC and partial M-SIC schemes will be analysed, respectively.

17.3.1.5.1 Complexity of Standard SIC   Here we assume that at each stage of the detection process the MMSE combiner is employed in its specific left-inverse related representation as described in Section 17.2.3.2.2. As highlighted in Section 17.3.1.1, a prerequisite for the calculation of the weight matrix $\mathbf{W}_{\text{MMSE}}^{[i]H}$ according to Equation 17.118 in the i-th detection stage, is the availability of the left-inverse related correlation matrix $\mathbf{R}_{\bar{a}}^{[i]H}$ defined in Equation 17.119, and the knowledge of the cross-correlation matrix $\mathbf{R}_{c}^{[i]H}$ defined in Equation 17.120, which were employed in the context of our description of the SIC detector in Section 17.3.1.1 in their Hermitian transposed form. It was highlighted furthermore in the same section that instead of entirely recalculating these matrices at the beginning of each detection stage on the basis of the current reduced-size channel transfer factor matrix $\mathbf{H}^{[i]}$, it is computationally more advantageous to calculate these matrices only once at the beginning of the detection process and then eliminate the most recently detected user's influence at the end of each detection stage. This is achieved by removing the $\acute{l}^{[i]}$-th row- and column from the matrix $\mathbf{R}_{\bar{a}}^{[i]H}$ and by eliminating the $\acute{l}^{[i]}$-th column from the matrix $\mathbf{R}_{c}^{[i]H}$, respectively, followed by appropriately rearranging these matrices with the result of a reduced dimensionality. Note that $\acute{l}^{[i]}$ is the column vector index of the reduced-size channel transfer factor matrix $\mathbf{H}^{[i]}$, which is associated with the most recently detected user, namely the $l^{[i]}$-th user. Let us now consider the individual steps one by one.

- *Initialization*: Specifically, the computational overhead incurred in terms of the number of complex - as well as mixed real-complex multiplications and additions at the beginning of the detection process required for the computation of the auto-correlation matrices $\mathbf{R}_{\bar{a}}^{[1]H}$ and $\mathbf{R}_{c}^{[1]H}$ is given by:

$$C_{\text{SIC,stp}}^{(\mathbb{C}*\mathbb{C})} = C_{\text{SIC,stp}}^{(\mathbb{C}+\mathbb{C})} = PL^2 \tag{17.136}$$

$$C_{\text{SIC,stp}}^{(\mathbb{R}*\mathbb{C})} = PL \tag{17.137}$$

$$C_{\text{SIC,stp}}^{(\mathbb{R}+\mathbb{C})} = L. \tag{17.138}$$

- *Weight Calculation*: Furthermore, during the i-th detection stage Equation 17.118 has to be solved for the weight matrix $\mathbf{W}_{\text{MMSE}}^{[i]H}$ with the aid of the LU-decomposition [90]. More specifically, the LU decomposition implies factorizing the reduced-size correlation matrix $\mathbf{R}_{\bar{a}}^{[i]H} \in \mathbb{C}^{L^{[i]} \times L^{[i]}}$ into a lower (L) and upper (U) triangular matrix, followed by forward- and backward substitutions as outlined in [90]. The associated computational complexity becomes:

$$C_{\text{SIC,w}}^{(\mathbb{C}*\mathbb{C})[i]} = C_{\text{SIC,w}}^{(\mathbb{C}+\mathbb{C})[i]} = PL^{[i]2} + \frac{1}{3}L^{[i]3}. \tag{17.139}$$

Upon taking into account the reduction of the number of users to be detected and the corresponding reduction of the channel matrix' dimension across the different detection stages, the total complexity imposed by calculating the weight matrices defined in

Equation 17.121 is given by:

$$C_{\text{SIC,w}}^{(\mathbb{C}*\mathbb{C})} = C_{\text{SIC,w}}^{(\mathbb{C}+\mathbb{C})} = P \sum_{L^{[i]}=1}^{L} (L^{[i]})^2 + \frac{1}{3} \sum_{L^{[i]}=1}^{L} (L^{[i]})^3 \tag{17.140}$$

$$= \frac{1}{3} P(2L+1)\alpha_{\text{SIC}} + \frac{1}{3} \alpha_{\text{SIC}}^2, \tag{17.141}$$

where the factor α_{SIC} is defined as:

$$\alpha_{\text{SIC}} = \sum_{i=1}^{L} i = \frac{1}{2} L(L+1). \tag{17.142}$$

Here we have exploited that [468] $\sum_{i=1}^{n} i = n(n+1)/2$ and $\sum_{i=1}^{n} i^2 = n(n+1)(2n+1)/6$ as well as $\sum_{i=1}^{n} i^3 = n^2(n+1)^2/4$.

- *Selection*: As the metric employed for the selection of the most dominant user we opted for the SNR at the combiner's output, as given by Equation 17.26. The rationale of this choice was that we demonstrated in Section 17.3.1.4.1 that the employment of the SNR only imposes a marginal performance loss compared to employing the SINR as the dominant user ranking metric. Here we have found that the number of complex multiplications and additions, as well as the number of real divisions and multiplications and the number of comparisons required is given by:

$$C_{\text{SIC,obj}}^{(\mathbb{C}*\mathbb{C})} = (\alpha_{\text{SIC}} - 1)(2P + 1) \tag{17.143}$$

$$C_{\text{SIC,obj}}^{(\mathbb{C}+\mathbb{C})} = (\alpha_{\text{SIC}} - 1)(2P) \tag{17.144}$$

$$C_{\text{SIC,obj}}^{(\mathbb{R}/\mathbb{R})} = C_{\text{SIC,obj}}^{(\mathbb{R}*\mathbb{R})} = C_{\text{SIC,obj}}^{(\mathbb{R}\lessgtr\mathbb{R})} = (\alpha_{\text{SIC}} - 1). \tag{17.145}$$

In this context we implicitly assumed that the SNR calculation associated with the selection of the most dominant user is not required in the last detection stage, since only a single user remains to be detected.

- *Combining*: Furthermore, the linear combining at each stage of the successive cancellation process - carried out with the aid of Equation 17.124 - necessitates the following number of complex multiplications and additions as given by:

$$C_{\text{SIC,cmb}}^{(\mathbb{C}*\mathbb{C})} = C_{\text{SIC,cmb}}^{(\mathbb{C}+\mathbb{C})} = LP. \tag{17.146}$$

- *Demodulation*: In addition, the process of MPSK-related demodulation[15], which is realized with the aid of Equation 17.125, exhibits a total complexity of:

$$C_{\text{SIC,dem}}^{(\mathbb{C}*\mathbb{C})} = \frac{1}{2} LM_c \tag{17.147}$$

$$C_{\text{SIC,dem}}^{(\mathbb{C}+\mathbb{C})} = C_{\text{SIC,dem}}^{(\mathbb{R}\lessgtr\mathbb{R})} = LM_c, \tag{17.148}$$

---

[15]In the context of the MPSK modulation scheme the normalization of the MMSE combiner's output signal is avoided.

where again, we have included the number of comparisons between the outcomes of the Euclidean distance metric as an additional factor increasing the complexity.

- *Updating*: Finally, the process of updating the vector of signals received by the different antenna elements according to Equation 17.127 by cancelling the effects of the remodulated signal of a specific user from the composite multiuser signal imposes a total complexity of:

$$C_{\text{SIC,upd}}^{(\mathbb{C}*\mathbb{C})} = C_{\text{SIC,upd}}^{(\mathbb{C}+\mathbb{C})} = (L-1)P, \tag{17.149}$$

where again, no updating or remodulated signal cancellation is required during last detection stage. Here we have also taken into account the average number of explicit data transfers, which was quantified as:

$$C_{\text{SIC,upd}}^{\Rightarrow} = L\left[(L+1)\left[\frac{1}{9}(2L+1) - \frac{3}{4}\right] + \frac{5}{6}\right] + \frac{1}{4}PL(L-1). \tag{17.150}$$

More explicitly, the first term corresponds to rearranging the auto-correlation matrix $\mathbf{R}_{\bar{a}}^{[i]H}$, while the second terms is associated with rearranging the cross-correlation matrix $\mathbf{R}_{c}^{[i]H}$ at the end of each detection stage, $i = 1, \ldots, L$.

Upon combining the different contributions given in the previous equations, we obtain for the total complexity of the standard SIC detector as a function of the number of users L, the number of reception antennas P and the number of constellation points M_c the following expressions:

$$C_{\text{SIC}}^{(\mathbb{C}*\mathbb{C})} = \frac{1}{2}LM_c + [P(L-3) - 1] + \frac{1}{3}[3 + P(2L+13)]\alpha_{\text{SIC}} + \frac{1}{3}\alpha_{\text{SIC}}^2 \tag{17.151}$$

$$C_{\text{SIC}}^{(\mathbb{C}+\mathbb{C})} = LM_c + [P(L-3) - 1] + \frac{1}{3}[3 + P(2L+13)]\alpha_{\text{SIC}} + \frac{1}{3}\alpha_{\text{SIC}}^2 \tag{17.152}$$

$$C_{\text{SIC}}^{(\mathbb{R}\lessgtr\mathbb{R})} = (\alpha_{\text{SIC}} - 1) + LM_c \tag{17.153}$$

$$C_{\text{SIC}}^{(\mathbb{R}*\mathbb{C})} = PL \tag{17.154}$$

$$C_{\text{SIC}}^{(\mathbb{R}+\mathbb{C})} = L \tag{17.155}$$

$$C_{\text{SIC}}^{(\mathbb{R}/\mathbb{R})} = C_{\text{SIC}}^{(\mathbb{R}*\mathbb{R})} = (\alpha_{\text{SIC}} - 1) \tag{17.156}$$

where again, $\alpha_{\text{SIC}} = \frac{1}{2}L(L+1)$ was defined in Equation 17.142. In order to further simplify the complexity analysis, it is reasonable to assume that mixed real-complex multiplications[16] and additions are only half as complex as those performed on two complex variables, while the multiplication of two real-valued variables exhibits only one fourth of the complexity. Hence, a slightly simplified characterization of the standard SIC detector's complexity is

---

[16]Here we neglect that the multiplication of two complex numbers involves real-valued additions as well. Hence our simplified formulae are to be understood as an upperbound estimate of the complexity.

given by:

$$C_{\text{SIC}}^{(\mathbb{C}*\mathbb{C})} = \frac{1}{2}LM_c + \left[P\left(\frac{3}{2}L - 3\right) - \frac{5}{4}\right] + \frac{1}{3}\left[\frac{15}{4} + P\left(2L + 13\right)\right]\alpha_{\text{SIC}} + \frac{1}{3}\alpha_{\text{SIC}}^2 \quad (17.157)$$

$$C_{\text{SIC}}^{(\mathbb{C}+\mathbb{C})} = L\left(M_c + \frac{1}{2}\right) + P(L - 3) + \frac{1}{3}P(2L + 13)\alpha_{\text{SIC}} + \frac{1}{3}\alpha_{\text{SIC}}^2 \quad (17.158)$$

$$C_{\text{SIC}}^{(\mathbb{R}\lessgtr\mathbb{R})} = (\alpha_{\text{SIC}} - 1) + LM_c \quad (17.159)$$

$$C_{\text{SIC}}^{(\mathbb{R}/\mathbb{R})} = (\alpha_{\text{SIC}} - 1). \quad (17.160)$$

17.3.1.5.2   Complexity of M-SIC   As argued in Section 17.3.1.4.2, the standard SIC algorithm suffers from error propagation, especially in those subcarriers, where the S(I)NR observed at the selected user's associated combiner output during the first detection stage is relatively low. A viable strategy of improving the achievable performance and of further reducing the BER/SER is that of allowing not only the single most likely constellation point to be selected from the constellation during a specific detection stage's demodulation process, but rather to retain the $M > 1$ number of most likely constellation points. As a result, in the i-th stage $M^{(i-1)}$ number of detection and demodulation operations has to be performed. This also requires M^i number of updating or interference cancellation operations with respect to the local vector $\mathbf{x}^{[i]}$ of received signals. The complexity contribution required for evaluating the weight matrices and SNR estimates, namely 'Initialization', 'Weight Calculation' and 'Selection' of Section 17.3.1.5.1 remains unchanged.

- *Combining*: More specifically, the computational complexity associated with the operation of combining hence becomes:

$$C_{\text{M-SIC,cmb}}^{(\mathbb{C}*\mathbb{C})} = C_{\text{M-SIC,cmb}}^{(\mathbb{C}+\mathbb{C})} = \beta_{\text{M-SIC}}P, \quad (17.161)$$

  where the factor $\beta_{\text{M-SIC}}$, which corresponds to the total number of different detection nodes in the detection process is given by:

$$\beta_{\text{M-SIC}} = \sum_{i=0}^{L-1} M^i = \begin{cases} L & \wedge M = 1 \\ \frac{M^L - 1}{M - 1} & \wedge M > 1. \end{cases} \quad (17.162)$$

  This is the formula characterizing a geometrical series [468].

- *Demodulation*: For the MPSK-related demodulation operation we have:

$$C_{\text{M-SIC,dem}}^{(\mathbb{C}*\mathbb{C})} = \frac{1}{2}\beta_{\text{M-SIC}}M_c \quad (17.163)$$

$$C_{\text{M-SIC,dem}}^{(\mathbb{C}+\mathbb{C})} = \beta_{\text{M-SIC}}M_c, \quad (17.164)$$

  where the factor $\beta_{\text{M-SIC}}$ was given by Equation 17.162. Additionally, it is also useful to take into account the number of comparisons to be carried out in the context of the demodulation process invoked at the different detection stages. Here we have to differ-

entiate between the first $L-1$ detection stages and the last detection stage. Specifically, during the first $L-1$ stages of Figure 17.11 there are:

$$\gamma_{\text{M-SIC,i}} = \sum_{i=0}^{L-2} M^i = \begin{cases} L-1 & \wedge M = 1 \\ \frac{M^{(L-1)}-1}{M-1} & \wedge M > 1, \end{cases} \qquad (17.165)$$

number of different detection nodes, each of which is associated with selecting the M number of most likely tentative symbol decisions out of the M_c number of possible symbol decisions associated with the specific modulation scheme employed. The number of comparisons per detection node required by this operation is given by:

$$\delta_{\text{M-SIC,i}} = \sum_{i=M_c-(M-1)}^{M_c} i = \frac{1}{2}M(1 + 2M_c - M), \qquad (17.166)$$

which could potentially be further reduced with the aid of more effective binary tree-based search methods[17]. By contrast, during the last detection stage we incur:

$$\gamma_{\text{M-SIC,ii}} = \begin{cases} 1 & \wedge M = 1 \\ M^{(L-1)} & \wedge M > 1 \end{cases} \qquad (17.167)$$

number of different detection nodes, each of which is associated with the selection of the single most likely symbol decision. This imposes a total number of comparisons per detection node, which is given by:

$$\delta_{\text{M-SIC,ii}} = M_c. \qquad (17.168)$$

The final operation in the M-SIC detection process is to select the specific symbol vector from the various possible symbol vectors defined by the different tentative symbol decisions retained at each detection node, whose associated Euclidean distance metric is the lowest during the last detection stage. This requires an additional $M^{(L-1)} - 1$ number of comparisons. Hence, the total number of demodulation-related comparisons during the entire detection process is given by:

$$C_{\text{M-SIC,dem}}^{(\mathbb{R} \lessgtr \mathbb{R})} = \epsilon_{\text{M-SIC}}, \qquad (17.169)$$

where:

$$\epsilon_{\text{M-SIC}} = \gamma_{\text{M-SIC,i}}\delta_{\text{M-SIC,i}} + \gamma_{\text{M-SIC,ii}}\delta_{\text{M-SIC,ii}} + M^{(L-1)} - 1. \qquad (17.170)$$

- *Updating*: Furthermore, for the total number of updating operations with respect to the vector of signals received by the different antenna elements which implies cancelling the effects of the remodulated signal from the composite multiuser signal as seen in

---

[17]From the literature it is well-known that recursive search algorithms, such as 'quick-sort' require a potentially lower number of comparisons than those based on the principles of 'sorting by selection'.

Equation 17.127 we obtain:

$$C_{\text{M-SIC,upd}}^{(\mathbb{C}*\mathbb{C})} = C_{\text{M-SIC,upd}}^{(\mathbb{C}+\mathbb{C})} = \zeta_{\text{M-SIC}}P, \tag{17.171}$$

where $\zeta_{\text{M-SIC}}$ is defined here as:

$$\zeta_{\text{M-SIC}} = \sum_{i=1}^{L-1} M^i = \begin{cases} L-1 & \wedge\ M = 1 \\ M\frac{M^{(L-1)}-1}{M-1} & \wedge\ M > 1. \end{cases} \tag{17.172}$$

Upon additionally recalling the complexity-related contributions corresponding to the initialization, weight calculation and selection from Section 17.3.1.5.1, the M-SIC detector's complexity is characterized by the following equations:

$$\begin{aligned} C_{\text{M-SIC}}^{(\mathbb{C}*\mathbb{C})} &= \frac{1}{2}\beta_{\text{M-SIC}}M_c + \left[P\left(\beta_{\text{M-SIC}} + \zeta_{\text{M-SIC}} - \frac{1}{2}L - 2\right) - \frac{5}{4}\right] + \\ &\quad + \frac{1}{3}\left[\frac{15}{4} + P\left(2L + 13\right)\right]\alpha_{\text{SIC}} + \frac{1}{3}\alpha_{\text{SIC}}^2 \end{aligned} \tag{17.173}$$

$$\begin{aligned} C_{\text{M-SIC}}^{(\mathbb{C}+\mathbb{C})} &= \beta_{\text{M-SIC}}M_c + L\left(\frac{1}{2} - P\right) + P(\beta_{\text{M-SIC}} + \zeta_{\text{M-SIC}} - 2) + \\ &\quad + \frac{1}{3}P(2L+13)\alpha_{\text{SIC}} + \frac{1}{3}\alpha_{\text{SIC}}^2 \end{aligned} \tag{17.174}$$

$$C_{\text{M-SIC}}^{(\mathbb{R}/\mathbb{R})} = (\alpha_{\text{SIC}} - 1) \tag{17.175}$$

$$C_{\text{M-SIC}}^{(\mathbb{R}\lessgtr\mathbb{R})} = (\alpha_{\text{SIC}} - 1) + \epsilon_{\text{M-SIC}}. \tag{17.176}$$

where again, α_{SIC}, $\beta_{\text{M-SIC}}$, as well as $\gamma_{\text{M-SIC,i}}$, $\delta_{\text{M-SIC,i}}$ and $\gamma_{\text{M-SIC,ii}}$, $\delta_{\text{M-SIC,ii}}$ and additionally $\epsilon_{\text{M-SIC}}$, $\zeta_{\text{M-SIC}}$ were given by Equations 17.142, 17.162, as well as 17.165, 17.166 and 17.167, 17.168 and also Equations 17.170, 17.172, respectively. In the context of these equations we have once again taken into account that mixed real-complex multiplications and additions are only half as complex as the corresponding operations associated with two complex numbers[18].

17.3.1.5.3 Complexity of Partial M-SIC In this section we will briefly assess the computational complexity of partial M-SIC. We recall from Section 17.3.1.2.2 that in contrast to the M-SIC described in Section 17.3.1.2.1, the M most likely symbol decisions per detection node are only retained up to the specific $L' = L_{\text{pM-SIC}}$-th detection stage. By contrast, for the higher-index detection stages only the single most likely symbol decision per detection node is retained, as in the case of the standard SIC scheme, which was described in Section 17.3.1.1. This implies that for $L' = 1$ the partial M-SIC detector is identical to the standard SIC detector, while for $L' = L$ the M-SIC detector is obtained. The analysis of the partial M-SIC's complexity follows a similar procedure to that applied in Section 17.3.1.5.2 in the case of the M-SIC scheme. The difference resides in the specific composition of the factors $\beta_{\text{M-SIC}}$ and $\gamma_{\text{pM-SIC,i}}$, $\gamma_{\text{pM-SIC,ii}}$, as well as $\epsilon_{\text{pM-SIC}}$ and $\zeta_{\text{pM-SIC}}$, which were defined for M-SIC in

---

[18]Again, this neglects that the multiplication of two complex numbers also involves real-valued additions.

Equations 17.162 and 17.165, 17.167 as well as 17.170, 17.172. By contrast, here we have:

$$\beta_{\text{pM-SIC}} = \sum_{i=0}^{L'-1} M^i + \sum_{i=L'}^{L-1} M^{L'-1} = \begin{cases} L & \wedge\, M = 1 \\ \frac{M^{L'}-1}{M-1} + (L - L')M^{L'-1} & \wedge\, M > 1, \end{cases} \quad (17.177)$$

as well as:

$$\gamma_{\text{pM-SIC,i}} = \sum_{i=0}^{L'-2} M^i = \begin{cases} L' - 1 & \wedge\, M = 1 \\ \frac{M^{L'-1}-1}{M-1} & \wedge\, M > 1, \end{cases} \quad (17.178)$$

and:

$$\gamma_{\text{pM-SIC,ii}} = \sum_{i=L'-1}^{L-1} M^{(L'-1)} = (L - L' + 1)M^{(L'-1)}. \quad (17.179)$$

Hence, similarly to Equation 17.169 the total number of demodulation-related comparisons during the entire detection process is given by:

$$C_{\text{pM-SIC,dem}}^{(\mathbb{R}\lessgtr\mathbb{R})} = \epsilon_{\text{pM-SIC}}, \quad (17.180)$$

where we have:

$$\epsilon_{\text{pM-SIC}} = \gamma_{\text{pM-SIC,i}}\delta_{\text{pM-SIC,i}} + \gamma_{\text{pM-SIC,ii}}\delta_{\text{pM-SIC,ii}} + M^{(L'-1)} - 1, \quad (17.181)$$

and $\delta_{\text{pM-SIC,i}} = \delta_{\text{M-SIC,i}}$ as well as $\delta_{\text{pM-SIC,ii}} = \delta_{\text{M-SIC,ii}}$. Furthermore, the interference-cancellation based updating-related factor $\zeta_{\text{pM-SIC}}$ is given by:

$$\zeta_{\text{pM-SIC}} = \sum_{i=1}^{L'-1} M^i + \sum_{i=L'}^{L-1} M^{L'-1} = \begin{cases} L - 1 & \wedge\, M = 1 \\ M\frac{M^{L'-1}-1}{M-1} + (L - L')M^{(L'-1)} & \wedge\, M > 1. \end{cases}$$
$$(17.182)$$

In order to obtain the expressions for the total complexity associated with partial M-SIC, the variables $\beta_{\text{M-SIC}}$, $\gamma_{\text{M-SIC,i}}$, $\gamma_{\text{M-SIC,ii}}$, $\epsilon_{\text{M-SIC}}$ and $\zeta_{\text{pM-SIC}}$ employed in the context of Equations 17.173, 17.174, 17.175, 17.176 have to be substituted against the corresponding partial M-SIC-specific expressions defined in this section.

17.3.1.5.4 Complexity Comparison of the Different SIC Detectors   In this section the different SIC-related detection techniques, namely standard SIC, M-SIC and partial M-SIC will be compared against each other on the basis of the complexity formulae developed in the previous sections. In the context of our evaluations the M_c number of constellation points associated with the modulation scheme employed was assumed to be $M_c = 4$, which is the case for example for 4QAM modulation. The M-SIC retained $M = 2$ number of symbol decisions at each detection node. In the context of the 4QAM modulation scheme we found that further increasing the M number of tentative symbol decisions per detection node retained does not yield a significant additional performance improvement.
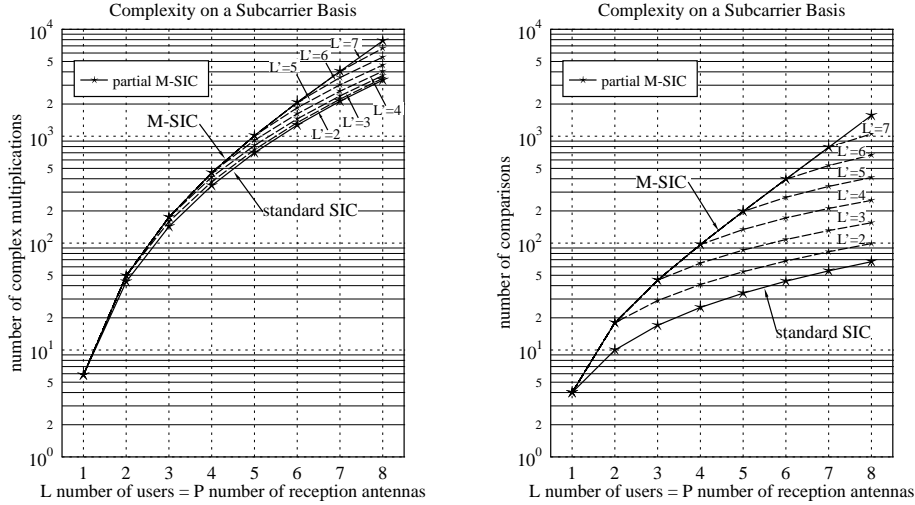
Figure 17.19: Complexity of standard SIC, M-SIC and partial M-SIC in terms of (left:) the number of complex multiplications $C^{(\mathbb{C}*\mathbb{C})}$ and (right:) the number of real-valued comparisons $C^{(\mathbb{R}\lessgtr\mathbb{R})}$ recorded on a subcarrier basis, as a function of the number of simultaneous users L, which was assumed to be equal to the number of reception antennas P; the curves related to partial M-SIC are further parameterized with the index of the detection stage namely, $L' = L_{\text{pM-SIC}}$, up to which M number of tentative symbol decisions per detection node were retained; specifically for M-SIC and partial M-SIC the number of retained tentative symbol decisions per detection node was equal to $M = 2$, while in all scenarios $M_c = 4$ constellation points were assumed, which is for example the case in the context of 4QAM modulation.

Specifically, on the left-hand side of Figure 17.19 we have compared standard SIC against the M-SIC scheme as well as to the partial M-SIC arrangement in terms of the number of complex multiplications imposed on a subcarrier basis, as a function of the number of simultaneous users L, which was assumed here to be equal to the number of reception antennas P. Furthermore, the curves associated with the partial M-SIC scheme are additionally parameterized with the index of the detection stage, namely $L' = L_{\text{pM-SIC}}$, up to which the M most likely tentative symbol decisions per detection node were retained. By contrast, for the higher-index detection stages only one symbol decision per detection node was retained. The curves associated with the different detection techniques in Figure 17.19 were generated with the aid of the complexity formulae given by Equations 17.157 as well as 17.173. For the partial M-SIC scheme furthermore the specific variables have to be substituted into Equation 17.173. The number of complex additions associated with the different detectors has not been illustrated here, since these values were found only to differ slightly from those of the number of complex multiplications. As expected, it is evidenced by Figure 17.19 that the M-

description	$C_{\text{SIC}}^{(\mathbb{C}*\mathbb{C})}$	$C_{\text{SIC}}^{(\mathbb{C}+\mathbb{C})}$	$C_{\text{SIC}}^{(\mathbb{R}\lessgtr\mathbb{R})}$	$C_{\text{M-SIC}}^{(\mathbb{C}*\mathbb{C})}$	$C_{\text{M-SIC}}^{(\mathbb{C}+\mathbb{C})}$	$C_{\text{M-SIC}}^{(\mathbb{R}\lessgtr\mathbb{R})}$
initialization:	72	66	-	%	%	%
weight calc.	$153.3\dot{3}$	$153.3\dot{3}$	-	%	%	%
selection	83.25	72	9	%	%	%
combining	16	16	-	60	60	-
demodulation	8	16	16	30	60	88
updating	12	12	-	56	56	-
→ total	345	$335.3\dot{3}$	25	454.58	$467.3\dot{3}$	97

Table 17.6: Computational complexity of the different processing steps involved in standard SIC (columns $1 \ldots 3$) and M-SIC (columns $4 \ldots 6$) for a scenario of $L = P = 4$ simultaneous users- and reception antennas; specifically for M-SIC the number of tentative symbol decisions per detection node was equal to $M = 2$, while in all scenarios $M_c = 4$ constellation points were assumed, which is for example the case with 4QAM modulation.

SIC detector may become significantly more complex than standard SIC, depending on the number of simultaneous users L. While for a scenario of $L = P = 4$ the complexity of the M-SIC scheme is observed in Figure 17.19 to be higher than that of standard SIC by about 32%, for a scenario of $L = P = 8$ the M-SIC is by a factor of about 2.32 or equivalently, by about 132% more complex. This is a result of the exponential growth of the number of demodulation and updating operations associated with the M-SIC scheme, when increasing the number of users L as seen in Figure 17.19. As expected, the complexity of partial M-SIC is shown in Figure 17.19 to be between that of standard SIC and M-SIC for $1 < L' < L$.

Similar observations can also be inferred for the computational complexity in terms of the number of comparisons between real-valued numbers, as portrayed at the right-hand side of Figure 17.19. Here the complexity difference between standard SIC and M-SIC is even more dramatic. While for a scenario of $L = P = 4$ the M-SIC is a factor 3.88 more complex than standard SIC, for a scenario of $L = P = 8$ this factor is as high as 23.32. Again, the partial M-SIC is capable of significantly reducing the complexity - also depending on the cut-off level L' - although this is achieved at the cost of a performance degradation, as it was observed in Section 17.3.1.4.5.

In order to further characterize the complexity of the standard SIC- and that of the M-SIC detector, in Table 17.6 we have listed the complexity-related contribution of the different components involved in the detection process for a scenario of $L = P = 4$. Note that the process of initialization, weight calculation and selection - as described in Section 17.3.1.1 - is identical for both the standard- and the M-SIC detector, which is indicated by "%" in the corresponding entries of Table 17.6. However, as argued earlier in this section, the computational complexity related to the operations of demodulation, combining and updating is significantly increased for the M-SIC scheme compared to standard SIC due to the high number of detection nodes.

17.3.1.6   Summary and Conclusions on SIC Detection Techniques

Our discussions commenced in Section 17.3.1 with a portrayal and characterization of standard SIC based detection and its derivatives, namely the M-SIC and partial M-SIC detection schemes in the context of both uncoded and turbo-coded scenarios. More specifically, standard SIC detection was detailed in Section 17.3.1.1. Its associated block diagram was portrayed in Figure 17.10 and the most significant equations were summarized in Table 17.5. As a result of the SIC detector's strategy of detecting only the most dominant user having the highest SINR, SIR or SNR at its associated linear combiner's output, the dimensionality of the associated symbol classification- or demodulation was reduced to evaluating the single-user Euclidean distance metric of Equation 17.125 LM_c times in contrast to calculating the multi-user Euclidean distance metric of Equation 17.223 M_c^L-times, as in the case of joint optimum ML detection.

The performance of the SIC detector critically relies on correct symbol decisions at the different detection stages, otherwise potentially catastrophic error propagation is encountered. An attractive strategy of reducing these effects is that of tracking multiple symbols decisions from each detection node. The philosophy of this technique was addressed in Section 17.3.1.2. Specifically in Section 17.3.1.2.1 we considered M-SIC, where the M number of most likely tentative symbol decisions were tracked from all detection nodes in the detection 'tree' of Figure 17.11.

In an effort to reduce the potentially high computational complexity of M-SIC compared to that of standard SIC and motivated by the observation that the highest symbol error probabilities are associated with the 'early' or low-index detection stages, in Section 17.3.1.2.2 the partial M-SIC was briefly characterized. Recall that at higher SNRs for the detection stages encountered towards the end of the detection process the symbol error probability is lower than for the detection process at the beginning, provided that error-free symbol decisions were encountered in the previous detection stages. This is because towards the end of the detection process the MIMO system's effective diversity order is increased. More specifically, the principle of partial M-SIC was to track the $M > 1$ number of most likely tentative symbol decisions per detection node only during the first few detection stages. By contrast, for the later detection stages only one symbol decision per detection node was made, as in the case of standard SIC. The philosophy of these techniques was further augmented with the aid of Figure 17.11, which illustrates the associated detection trees for the specific scenario of $L = 4$ users and for retaining $M = 2$ number of tentative symbol decisions per detection node in case of M-SIC and partial M-SIC. Specifically, the graph at the left-hand side of Figure 17.11 was associated with standard SIC, while that at the right-hand side of Figure 17.11 with M-SIC. Finally, in the centre of Figure 17.11 the various partial M-SIC related detection 'trees' were portrayed. A further reduction of the computational complexity could potentially be achieved with the aid of the SDI-M-SIC technique [117, 137], which was briefly addressed in Section 17.3.1.2.3.

Our further deliberations in Section 17.3.1.3 then addressed the problem of SIC-specific soft-bit generation required for turbo-decoding. Based on our observation of the effects of error propagation through the different SIC detection stages the weighted soft-bit metric of Equation 17.133 was proposed. It was demonstrated later in Section 17.3.1.4.7 that the employment of this weighted soft-bit metric resulted in a significant BER performance improvement in scenarios, where the number of users L is of similar value to the number of BS

reception antenna elements P.

Our performance analysis of the various SIC-related detection techniques was conducted in Section 17.3.1.4. Specifically, in Section 17.3.1.4.1 our discussions commenced with the analysis of the BER and SER performance of standard SIC and M-SIC, parameterized with the number of users L and the number of reception antennas P. A significant performance improvement was observed in Figure 17.12 upon increasing the SDMA-MIMO system's order under the constraint of $L = P$. This was a result of the higher 'diversity' of users in terms of their different received signal quality observed at each detection stage. Furthermore, we found that using the SINR instead of the SNR at the linear combiner's output for selecting the most dominant user from the set of remaining users at each SIC detection stage had a modest, but noticeable beneficial effect at low BERs in conjunction with more than three users.

Our further investigations conducted in Section 17.3.1.4.2 then focused on the analysis of the SER encountered at each detection stage, again for both the standard SIC and the M-SIC. As it was shown for the standard SIC scheme at the left-hand side of Figure 17.13, the SER monotonously increases upon approaching the last detection stage. Our explanation of this phenomenon was that the symbol error probability encountered at a specific detection stage is composed of the symbol error probability of the previous stage plus an 'additional' error probability, which is related to the effects of the residual AWGN at the specific stage considered under the assumption that no symbol errors have occurred in the previous detection stages. For higher SNRs we observed that the different detection stages' SER curves merge, since the 'AWGN'-related symbol error contribution is decreased for the higher-index detection stages, which is a result of the system's increased grade of diversity. For M-SIC similar SER curves were shown at the right-hand side of Figure 17.13.

In order to further highlight the effects of error propagation through the different SIC detection stages, in Section 17.3.1.4.3 the standard SIC detector's SER performance was portrayed in the context employing error-free symbol decisions in the SIC module of Figure 17.10. Specifically at the left-hand side of Figure 17.14 the SER results were averaged over the different detection stages, while at the right-hand side of Figure 17.14 the SER results were portrayed on a per-detection stage basis. Compared to the more realistic case of employing an imperfect, potentially error-contaminated remodulated reference the SER improvement is substantial, which provided a further motivation for mitigating the effects of error-propagation for example with the aid of the M-SIC scheme of Section 17.3.1.2.

In an effort to further characterize the effects of error-propagation, in Section 17.3.1.4.4 we have analysed the probability of the various symbol error events, namely that a symbol error has occurred in the first detection stage, while the symbol decisions carried out during the higher-index detection stages were error-free. The associated probabilities of the various error-events at the reception antennas were shown at the left-hand side of Figure 17.15 as a function of the SNR, while at the right-hand side their contribution to the total SER was portrayed. From these curves we inferred that for higher SNRs the SER is governed by specific error-events, which originated from the first detection-stage, followed by those events, which commenced in the second stage and so on.

This was the main motivation for employing partial M-SIC, which was characterized in terms of its SER in Section 17.3.1.4.5, specifically at the left-hand side of Figure 17.16. Here we observed that in a scenario of $L = P = 4$ users and reception antennas as well as at an SER of 10^{-5} achieved by the partial M-SIC scheme up to and including the second detection stage, the SNR must be only a modest 1dB higher than that required by the M-SIC

arrangement, while at the same time halving the complexity.

Furthermore, in Section 17.3.1.4.6 SDI-M-SIC was discussed and compared to both standard SIC and M-SIC at the right-hand side of Figure 17.16. The philosophy of SDI-M-SIC was to allow the employment of M-SIC or partial M-SIC only in a limited number of low-quality OFDM subcarriers, namely in those, which exhibit the lowest SINR during the first detection stage, while using standard SIC in all other subcarriers. In our specific example we employed partial M-SIC, where multiple tentative symbol decisions per detection node were permitted only during the first detection stage. In the context of the indoor WATM channel model of Section 14.3.1 it was shown at the right-hand side of Figure 17.16 that a modest number of $N_{\mathrm{SDI}}^{[1]} = 64$ decision-insertion related subcarriers is sufficient for closely approximating the performance of the partial M-SIC scheme. This corresponded to $1/8$-th of the total subcarriers.

Finally, in Section 17.3.1.4.7 the BER performance of turbo-coded standard SIC detection-assisted SDMA-OFDM was analysed. Specifically, in the context of Figure 17.17 we have compared the benefits of employing the rudimentary soft-bit metric of Equation 17.130 against those of the improved soft-bit metric of Equation 17.133, which accounted for the effects of error-propagation through the different detection stages. The employment of the weighted soft-bit metric of Equation 17.133 was found to be particularly beneficial in the context of a 'fully-loaded' SDMA-OFDM system, where the number of users L equals the number of reception antennas P. Further BER performance results related to the weighted soft-bit metric were presented in Figure 17.18, which characterized the influence of the number of users L on the SDMA-OFDM system's BER performance. Here we observed that the BER curves associated with different numbers of users were within an SNR range of 2dB at a BER of 10^{-5}. This is an indication of the higher quality of the soft-bit estimates.

Our discussions in Section 17.3.1 were concluded in Section 17.3.1.5 with the aid of a complexity analysis of standard SIC, M-SIC and partial M-SIC, which were the topics of Sections 17.3.1.5.1, 17.3.1.5.2 and 17.3.1.5.3. Specifically, the associated complexity formulae of standard SIC, which reflect the number of complex multiplications and additions as well as real-valued comparisons and divisions were given by Equations 17.157, 17.158, 17.159 and 17.160, respectively. Furthermore, the corresponding complexity formulae of M-SIC were given by Equations 17.173, 17.174, 17.175 and 17.176, respectively. Based on these equations the different SIC detectors' complexities were graphically compared in Figure 17.19. Specifically at the left-hand side of Figure 17.19 we have plotted the number of complex multiplications, while at the right-hand side the number of real-valued comparisons required. We observed that standard SIC exhibits the lowest complexity, while M-SIC the highest complexity. A compromise in terms of both the achievable BER performance and the complexity imposed is achieved with the aid of the partial M-SIC scheme. In order to support our analysis, the corresponding numerical complexity values were provided in Table 17.5 for the standard SIC and the M-SIC.

17.3.2 PIC Detection

One of the key justifications for proposing SIC was that upon decreasing the number of users during the successive detection stages a higher grade of antenna array diversity potential can be dedicated by the MMSE combiner to the mitigation of the serious channel transfer factor fades, rather than to suppressing the interfering signal sources. Hence the highest
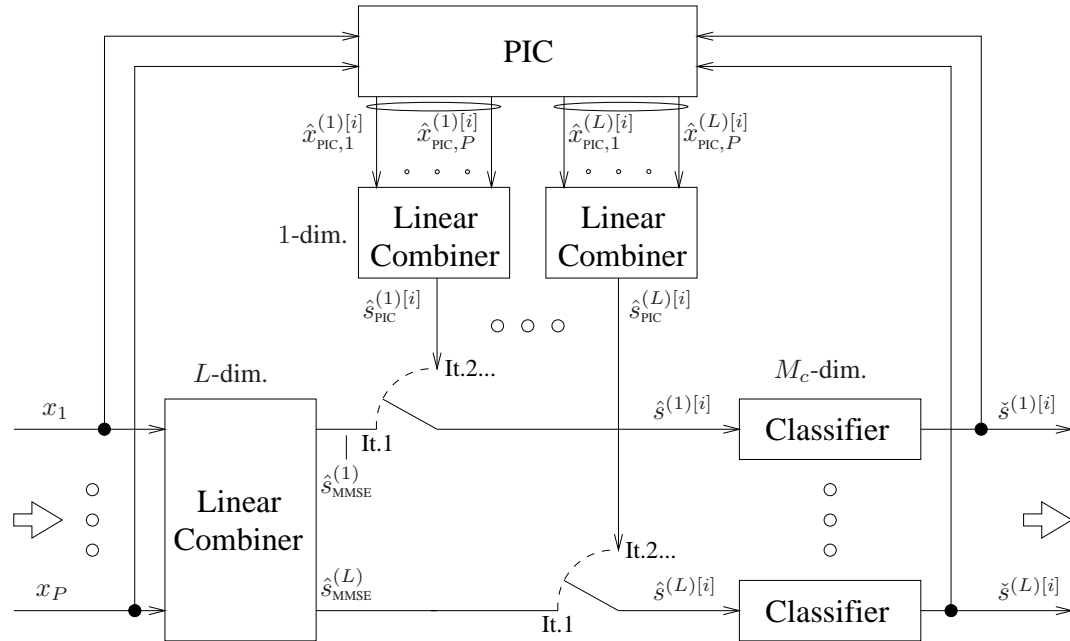
Figure 17.20: Illustration of the main signal paths associated with the hard-decision based PIC detector. The signals $x_p, p = 1, \ldots, P$ received by the different antenna elements are fed into the MMSE linear combiner described by Equations 17.185 and 17.186, which is active only during the first PIC detection stage. Furthermore, the signals $x_p, p = 1, \ldots, P$ are fed into the PIC module described by Equation 17.189, which is active for all PIC iterations associated with $i \geq 2$. The outputs $\check{s}^{(l)[i]}, l = 1, \ldots, L$ of the bank of M_c-ary symbol classifiers or demodulators obeying Equations 17.187 and 17.193 are then fed back to the PIC module seen at the top of the figure. According to Equation 17.189, P different signals $\hat{x}_{\text{PIC},p}^{(l)[i]}, p = 1, \ldots, P$, namely the potentially interference-free i.e. 'decontaminated' antenna output signals are available for the l-th user at the output of the PIC module, which are again linearly combined with the aid of Equations 17.191 and 17.192, in order to form the estimate $\hat{s}_{\text{PIC}}^{(l)[i]}$ of the signal transmitted by the l-th user, where $l = 1, \ldots, L$. Note that for the sake of visual clarity here we have omitted the signal paths associated with the channel transfer factor estimates required by the linear combiners and the PIC module. Also note than in our specific case the linear combiner employed is the MMSE combiner of Section 17.2.3

array noise mitigation is achieved during the last SIC iteration, when after correct detection and subtraction of all the co-channel users' remodulated signals, the interference-free array output vector is constituted by the transmitted signal of the least dominant user plus an array noise contribution. The above interference cancellation principle - which was portrayed in the context of SIC in Section 17.3.1 - can be invoked also in form of a PIC scheme [125,135].

The outline of this section is as follows. Our discussions commence in Section 17.3.2.1 with the description of the PIC detector's structure in the context of an uncoded scenario, while in Section 17.3.2.2 the principles of turbo-coded PIC are discussed. This is followed in Section 17.3.2.3 by the analysis of its performance in both an uncoded- and a turbo-coded scenario, while in Section 17.3.2.4 the analysis of the detector's complexity is carried out. A summary and conclusions will be offered in Section 17.3.2.5.

17.3.2.1 Uncoded PIC

In this section we will highlight the PIC detector's structure, which is depicted in Figure 17.20. Let us commence our discussions upon recalling from Equation 17.1 the specific structure of the vector $\mathbf{x} \in \mathbb{C}^{P \times 1}$ of signals received by the different antenna elements, namely that we have:

$$\mathbf{x} \quad = \quad \mathbf{H}\mathbf{s} + \mathbf{n} \tag{17.183}$$

$$= \quad \mathbf{H}^{(l)}s^{(l)} + \sum_{\substack{i=1 \\ i \neq l}}^{L} \mathbf{H}^{(i)}s^{(i)} + \mathbf{n}, \tag{17.184}$$

where again, $\mathbf{H} \in \mathbb{C}^{P \times L}$ is the channel transfer factor matrix, $\mathbf{s} \in \mathbb{C}^{L \times 1}$ is the composite multiuser vector of signals transmitted by the L different users and $\mathbf{n} \in \mathbb{C}^{P \times 1}$ is the vector of AWGN contributions encountered at the P different antenna elements. Specifically, from the component representation given by Equation 17.184 we observe that the array output vector $\mathbf{x}$ is composed of the l-th user's signal contribution vector and the $L-1$ interfering users' signal contribution vectors plus the AWGN vector. Hence, if initial estimates $\check{s}^{(i)}, i \in \{1, \dots, L\} \setminus \{l\}$ of the interfering users' transmitted signals would be available, a noisy estimate $\hat{\mathbf{x}}^{(l)}$ of the l-th user's signal contribution could be obtained upon removing the $L-1$ interfering users' estimated signal contributions given by $\mathbf{H}^{(i)}\check{s}^{(i)}, i \in \{1, \dots, L\} \setminus \{l\}$ from the vector $\mathbf{x}$ of signals received by the different antenna elements. An estimate $\hat{s}^{(l)}$ of the l-th user's transmitted signal could then be inferred by linear antenna diversity combining. The more specific processing steps of the PIC detector proposed here will be further detailed in the following sections with reference to Figure 17.20.

First-Stage - MMSE Detection

- *Combining*: During the first PIC iteration seen in Figure 17.20 each user is detected by means of the MMSE combiner, where the linear combiner's output vector $\hat{\mathbf{s}}_{\text{MMSE}} \in \mathbb{C}^{L \times 1}$ is given according to Equation 17.50 by:

$$\hat{\mathbf{s}}_{\text{MMSE}} = \mathbf{W}_{\text{MMSE}}^{[1]H}\mathbf{x}, \tag{17.185}$$

and the weight matrix $\mathbf{W}_{\text{MMSE}}^{[1]} \in \mathbb{C}^{L \times L}$ is given in its left-inverse related form according

to Equation 17.68 as:

$$\mathbf{W}_{\text{MMSE}}^{[1]} = \mathbf{H}\mathbf{P}_{\text{SNR}}(\mathbf{H}^H\mathbf{H}\mathbf{P}_{\text{SNR}} + \mathbf{I})^{-1}, \qquad (17.186)$$

where $\mathbf{P}_{\text{SNR}} \in \mathbb{C}^{L \times L}$ is the diagonal-shaped SNR matrix.

- *Classification/Demodulation*: Then the linear combiner's output vector $\hat{\mathbf{s}}^{[1]} = \hat{\mathbf{s}}_{\text{MMSE}}$ is demodulated, with the aid of the blocks seen at the bottom right-hand corner of Figure 17.20, resulting in the vector $\check{\mathbf{s}}^{[1]} \in \mathbb{C}^{L \times 1}$ of symbols that are most likely to have been transmitted by the L different users. More specifically, as shown in Section 17.2.4, the demodulation is carried out upon evaluating Equation 17.94, namely:

$$\check{s}^{(l)[1]} = arg \min_{\check{s}/\sigma_l \in \mathcal{M}_c} \left| \frac{1}{H_{\text{eff}}^{(l)[1]}} \hat{s}^{(l)[1]} - \check{s} \right|^2 , \ l = 1, \dots, L, \qquad (17.187)$$

where the l-th user's effective channel transfer factor $H_{\text{eff}}^{(l)[1]}$ is given by:

$$H_{\text{eff}}^{(l)[1]} = \mathbf{w}_{\text{MMSE}}^{(l)[1]}\mathbf{H}^{(l)}, \qquad (17.188)$$

and the l-th user's weight vector $\mathbf{w}_{\text{MMSE}}^{(l)[1]}$ is the l-th column vector of the weight matrix $\mathbf{W}_{\text{MMSE}}^{[1]}$. Equation 17.187 implies calculating the Euclidean distance between each of the normalized elements[19] of the combiner's output vector $\hat{\mathbf{s}}^{[i]}$ namely, $\hat{s}^{(l)[i]}, l = 1, \dots, L$, and all of the legitimate trial-symbols, which are the amplified constellation points contained in the set $\mathcal{M}_c$, associated with the specific modulation scheme employed. According to the ML principle that specific trial-symbol is retained as the most likely transmitted one for the l-th user, which exhibits the smallest Euclidean distance from the combiner's normalized output signal $\hat{s}^{(l)}$. However, as argued in Section 17.2.4, this decision principle is based on the assumption, that the residual interference contaminating the combiner's output signal is also Gaussian, which in general is not the case. Hence the demodulation principle formulated according to Equation 17.187 is sub-optimum.

i-th Stage: PIC Detection

- *Parallel Interference Cancellation*: During the i-th PIC iteration seen in Figure 17.20, where $i \geq 2$ a potentially improved estimate $\hat{s}_{\text{PIC}}^{(l)[i]}$ of the complex symbol $s^{(l)}$ transmitted by the l-th user is obtained upon subtracting in a first step the $L - 1$ interfering users' estimated signal contributions, from the original vector $\mathbf{x}$ of signals received by the different antenna elements, which can be expressed as:

$$\hat{\mathbf{x}}_{\text{PIC}}^{(l)[i]} = \mathbf{x} - \sum_{\substack{j=1 \\ j \neq l}}^{L} \mathbf{H}^{(j)}\check{s}^{(j)[i-1]}. \qquad (17.189)$$

---

[19]The normalization is not necessary in the context of employing MPSK modulation schemes in the absence of turbo-decoding.

This operation takes place within the PIC block shown at the top of Figure 17.20. Provided that correct tentative symbol decisions were made during the previous detection stage, namely we have $\check{s}^{(j)[i-1]} = s^{(j)}, j \in \{1, \dots, L\} \setminus \{l\}$ for the $L-1$ interfering users, the estimated array output vector $\hat{\mathbf{x}}_{\text{PIC}}^{(l)[i]} \in \mathbb{C}^{P \times 1}$ will only consist of the l-th user's namely the desired user's signal contribution vector $\mathbf{H}^{(l)}s^{(l)}$ plus the AWGN vector $\mathbf{n}$, which is expressed as:

$$\hat{\mathbf{x}}_{\text{PIC}}^{(l)[i]} = \mathbf{H}^{(l)}s^{(l)} + \mathbf{n} \quad \wedge \check{s}^{(j)[i-1]} = s^{(j)}, j \in \{1, \dots, L\} \setminus \{l\}. \qquad (17.190)$$

- *Combining*: The final task is hence to extract an estimate $\hat{s}_{\text{PIC}}^{(l)[i]}$ of the signal $s^{(l)}$ transmitted by the l-th user from the l-th user's PIC-related array output vector $\hat{\mathbf{x}}_{\text{PIC}}^{(l)[i]}$. This can be achieved upon invoking once again the left-inverse related MMSE combiner, seen below the PIC block at the top of Figure 17.20, whose associated weight matrix was given by Equation 17.186 for the more general case of detecting L users. As observed in Equation 17.190, the signal vector $\hat{\mathbf{x}}_{\text{PIC}}^{(l)[i]}$ at the output of the PIC block at the top of Figure 17.20 is now potentially free of interference. Hence the channel transfer factor matrix $\mathbf{H}$ and the SNR matrix $\mathbf{P}_{\text{SNR}}$ defined in Equation 17.65, which are integral parts of the MMSE-related weight matrix according to Equation 17.186, have to be substituted by the l-th user's related components namely, by $\mathbf{H}^{(l)}$ and $\text{SNR}^{(l)} = \frac{\sigma_l^2}{\sigma_n^2}$. This results in the weight vector $\mathbf{w}_{\text{MMSE}}^{(l)[i]}$, given by:

$$\mathbf{w}_{\text{MMSE}}^{(l)[i]} = \frac{\mathbf{H}^{(l)}}{||\mathbf{H}^{(l)}||_2^2 + \frac{1}{\text{SNR}^{(l)}}}. \qquad (17.191)$$

With the aid of the weight vector of Equation 17.191 an estimate $\hat{s}^{(l)[i]} = \hat{s}_{\text{PIC}}^{(l)[i]}$ of the l-th user's transmitted signal $s^{(l)}$ can then be extracted from the vector $\hat{\mathbf{x}}_{\text{PIC}}^{(l)[i]}$ seen at the output of the linear MMSE combiner in the centre of Figure 17.20 - similarly to Equation 17.185 - as follows:

$$\hat{s}_{\text{PIC}}^{(l)[i]} = \mathbf{w}_{\text{MMSE}}^{(l)[i]H} \hat{\mathbf{x}}_{\text{PIC}}^{(l)[i]}. \qquad (17.192)$$

- *Classification/Demodulation*: The above PIC and MMSE-combining steps are again followed by the classification, demodulation stage seen at the right of Figure 17.20, which obeys:

$$\check{s}^{(l)[i]} = arg \min_{\check{s}/\sigma_l \in \mathcal{M}_c} \left| \frac{1}{H_{\text{eff}}^{(l)[i]}} \hat{s}^{(l)[i]} - \check{s} \right|^2, \quad l = 1, \dots, L, \qquad (17.193)$$

where the l-th user's effective channel transfer factor $H_{\text{eff}}^{(l)[i]}$ is given by:

$$H_{\text{eff}}^{(l)[i]} = \mathbf{w}_{\text{MMSE}}^{(l)[i]} \mathbf{H}^{(l)}. \qquad (17.194)$$

In other words, Equation 17.193 delivers the symbol $\check{s}^{(l)[i]}$ that is most likely to have been transmitted by the l-th user. The i-th PIC iteration described above potentially

description	instruction
First-Stage - MMSE Det.	
Calc. MMSE weight matrix	$\mathbf{W}_{\text{MMSE}}^{[1]} = \mathbf{H}\mathbf{P}_{\text{SNR}}(\mathbf{H}^H\mathbf{H}\mathbf{P}_{\text{SNR}} + \mathbf{I})^{-1} \in \mathbb{C}^{P \times L}$
Detection	$\hat{\mathbf{s}}_{\text{MMSE}} = \mathbf{W}_{\text{MMSE}}^{[1]H}\mathbf{x} \in \mathbb{C}^{L \times 1}, \quad \hat{s}^{(l)[1]} = \hat{s}_{\text{MMSE}}, \; l = 1, \dots, L$
Demodulation, $l = 1, \dots, L$	$\check{s}^{(l)[1]} = arg \min_{\check{s}/\sigma_l \in \mathcal{M}_c} \left| \frac{1}{H_{\text{eff}}^{(l)[1]}}\hat{s}^{(l)[1]} - \check{s} \right|^2, H_{\text{eff}}^{(l)[1]} = \mathbf{w}_{\text{MMSE}}^{(l)[1]}\mathbf{H}^{(l)}$
i-th Stage - PIC ($l = 1, .., L$)	
Subtraction	$\hat{\mathbf{x}}_{\text{PIC}}^{(l)[i]} = \mathbf{x} - \sum_{\substack{j=1 \\ j \neq l}}^{L} \mathbf{H}^{(j)}\check{s}^{(j)[i-1]} \in \mathbb{C}^{P \times 1}$
Calc. MMSE weight vectors	$\mathbf{w}_{\text{MMSE}}^{(l)[i]} = \frac{\mathbf{H}^{(l)}}{\|\mathbf{H}^{(l)}\|_2^2 + \frac{1}{\text{SNR}^{(l)}}} \in \mathbb{C}^{P \times 1}$
Detection	$\hat{s}_{\text{PIC}}^{(l)[i]} = \mathbf{w}_{\text{MMSE}}^{(l)[i]H}\hat{\mathbf{x}}_{\text{PIC}}^{(l)[i]}, \quad \hat{s}^{(l)[i]} = \hat{s}_{\text{PIC}}^{(l)[i]}$
Demodulation	$\check{s}^{(l)[i]} = arg \min_{\check{s}/\sigma_l \in \mathcal{M}_c} \left| \frac{1}{H_{\text{eff}}^{(l)[i]}}\hat{s}^{(l)[i]} - \check{s} \right|^2, H_{\text{eff}}^{(l)[i]} = \mathbf{w}_{\text{MMSE}}^{(l)[i]H}\mathbf{H}^{(l)}$

Table 17.7: Summary of the standard hard-decision based PIC detector.

has to be performed for all the different SDMA users namely, for $l = 1, \dots, L$.

We have summarized the steps of the PIC algorithm once again in Table 17.7, while the schematic of the PIC detector was provided in Figure 17.20. Note however that for the sake of visual clarity in the context of this simplified schematic we have omitted the signal paths associated with the channel transfer factor estimates required by the linear combiners and within the PIC module.

17.3.2.2   Turbo-Coded PIC

In the context of our investigations concerning uncoded PIC detection assisted SDMA-OFDM in Section 17.3.2.3.1 we will highlight that the system's relatively poor performance compared to that of uncoded SIC detection-assisted SDMA-OFDM, discussed in Section 17.3.1.4.1, is related to the effects of 'error propagation' *between the different users' symbol estimates* during the second PIC detection stage. This is, because if amongst the L different users' tentative symbol decisions made during the first PIC stage there is a specific subcarrier, which has an unreliable tentative symbol decision while all the $L - 1$ remaining users' tentative symbol decisions are relatively reliable, then after the second PIC detection stage all of these $L - 1$ users' symbol decisions will become potentially unreliable. By contrast, the single user's tentative symbol decision, which was unreliable after the first detection stage is expected to become more reliable.

In Sections 17.2.6.4 and 17.3.1.4.7 we demonstrated in the context of both MMSE- and SIC detection-assisted SDMA-OFDM that turbo-decoding at the receiver is a powerful means of further enhancing the system's BER performance. Specifically, the turbo-decoder was incorporated into the system by simply feeding the demodulator's soft-bit output into the turbo-decoder. Recall that the generation of the soft-bits required for turbo-decoding was discussed earlier in Section 17.2.5 and 17.3.1.3, respectively. In the context of the associated simulations four turbo decoding iterations were performed by the turbo-decoder, followed

by slicing or hard-decision of the turbo-decoder's 'source'-related soft-output bits. Here we note explicitly that the turbo-iterations were entirely performed within the turbo-decoder, without invoking again the system's remaining components. The turbo coding parameters were summarized in Table 17.4.

Similarly to the MMSE and SIC schemes, in order to enhance the BER performance of PIC detection-assisted SDMA-OFDM a trivial approach would be to feed the turbo-decoder with the demodulator's soft-bit output after the PIC detection process and again, to perform a number of iterations within the turbo-decoder, followed by slicing the turbo-decoder's 'source'-related soft-output bits. However, recall our observation that for some users the reliability of the second PIC detection stage's symbol decisions might be degraded compared to that of the first PIC detection stage due to feeding potentially unreliable tentative symbol decisions into the second PIC detection stage. Hence it is potentially beneficial to embed the turbo-decoding into the PIC detection process. To be more specific, after the first detection stage - based on the different users' soft-bit values derived from the associated MMSE combiner's output signals, as it was demonstrated in Section 17.2.5, only a fraction of the total number of turbo-decoding iterations is performed. A reference signal is then generated upon slicing and remodulating the turbo-decoder's 'source- plus parity'-related *a posteriori* soft-output bits for the following second PIC detection stage. Our experiments revealed that it is less effective to slice, *reencode* and remodulate only the 'source'-related *a posteriori* soft-output bits. After the second PIC detection stage, again, soft-bits would again be generated, which are fed into the turbo-decoder, followed by a number of turbo-iterations and a final slicing of the 'source'-related soft-output bits. These constitute the PIC receiver's output bits. Alternatively, further PIC iterations could be performed, but in the context of the hard-decision- or slicing based PIC scheme employed here no additional performance gain was observed.

A further BER performance improvement can potentially be achieved upon feeding soft-bit values, rather than sliced bits, into the second PIC detection stage following the concepts of turbo-equalization [125] instead of the hard-decision based remodulated reference signals.

17.3.2.3   Performance Analysis

In this section the PIC algorithm will be investigated with respect to its BER performance in both a scenario without channel coding, as well as a scenario where turbo-coding is employed. Specifically, the interference cancellation process carried out during the PIC detector's second stage will be shown to benefit from the less error-contaminated first stage tentative symbol decisions. Again, the frame-invariant fading indoor WATM channel model and its associated OFDM system model described in Section 14.3.1 were invoked and ideal knowledge of the channel transfer functions associated with the different transmit-receive antenna pairs was assumed. For a summary of the basic simulation setup we refer again to Table 17.3.

The further structure of Section 17.3.2.3 is as follows. While in Section 17.3.2.3.1 the PIC detection assisted SDMA-OFDM system's BER performance is considered without employing channel coding, our simulation results for the turbo-coded scenario will be discussed in Section 17.3.2.3.2.

17.3.2.3.1   BER Performance of Uncoded PIC Detection-Assisted SDMA-OFDM for Different Numbers of Users and Receiver Antennas   In Figure 17.21 we have portrayed
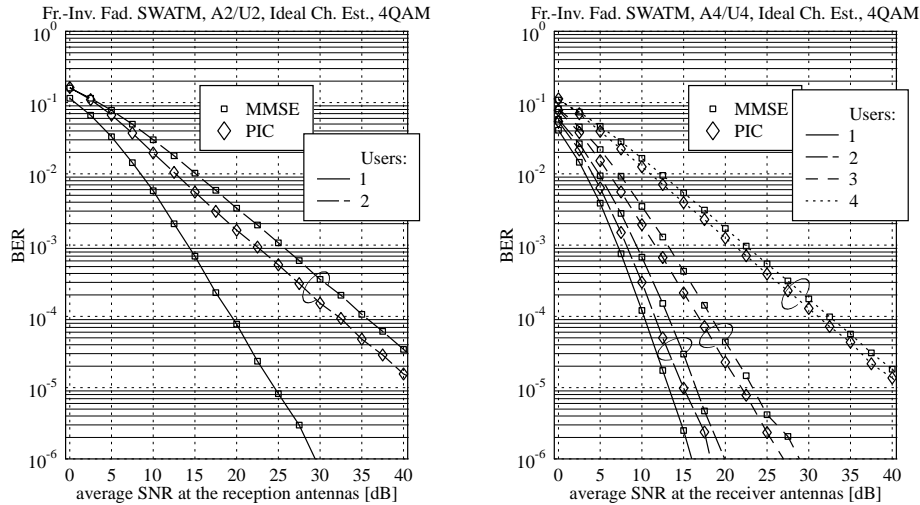
Figure 17.21: BER performance of 4QAM-modulated, PIC detection-assisted SDMA-OFDM as a function of the SNR encountered at the reception antennas for (left:) $P = 2$ reception antennas and up to $L = 2$ simultaneous users and (right:) $P = 4$ reception antennas and up to $L = 4$ simultaneous users; additionally, we have plotted the BER performance of MMSE detection-assisted SDMA-OFDM; for the basic simulation parameters we refer to Table 17.3.

the BER- as well as the SER performance of 4QAM-modulated PIC detection-assisted SDMA-OFDM as a function of the SNR encountered at the reception antennas. Specifically, in the context of the curves shown at the left-hand side of Figure 17.21 $P = 2$ reception antennas and up to $L = 2$ simultaneous users were assumed. By contrast, the curves at the right-hand side of Figure 17.21 characterize the scenario of $P = 4$ reception antennas supporting up to $L = 4$ simultaneous users. The MMSE detection-related BER performance curves, which were shown earlier in Figure 17.8 have again been plotted as a reference. We observe that upon increasing the SNR, the PIC detection-assisted system's BER performance exhibits the same trends as that of the MMSE detector, although a specific BER performance is achieved at consistently lower SNRs. The highest SNR gain achievable with the advent of employing PIC detection compared to MMSE detection is approximately 3.03dB at a BER of 10^{-4}, which was observed here for the basic SDMA scenario of $P = 2$ reception antennas and $L = 2$ simultaneous users (A2/U2). By contrast, for the higher-order SDMA scenario of $P = 4$ reception antennas the highest SNR gain of 1.61dB is observed for $L = 2$ simultaneous users namely, while for $L = 3$ and $L = 4$ users the SNR gains are approximately 1.43dB and 1.25dB, again, at a BER of 10^{-4}. The reason for the reduction of the SNR gain along with increasing the number of simultaneous users L is, because upon supporting more users the probability of an erroneous first-stage tentative symbol decision among one of the
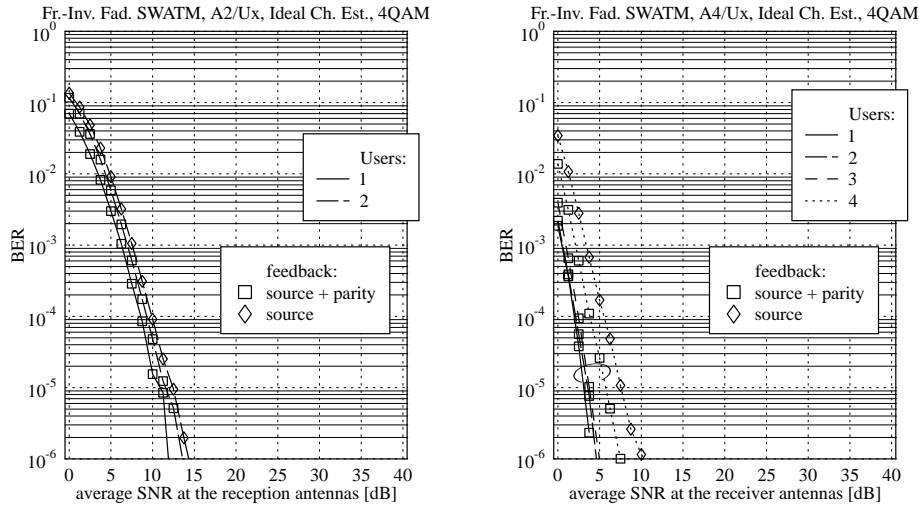
Figure 17.22: BER performance of turbo-coded, 4QAM-modulated, PIC detection-assisted SDMA-OFDM as a function of the SNR recorded at the reception antennas for (left:) $P = 2$ reception antennas and up to $L = 2$ simultaneous users and (right:) $P = 4$ reception antennas and up to $L = 4$ simultaneous users. Two methods of generating the remodulated reference signal were employed by the PIC module of Figure 17.20, namely a 'source'-related *a posteriori* soft-output based reference and a 'source- plus parity'-related *a posteriori* soft-output based reference. For the list of basic simulation parameters we refer to Table 17.3.

users is increased. Hence also the users benefitting from correct tentative symbol decisions during the first detection stage are more likely to be corrupted. As mentioned before, in an effort to render the first-stage tentative symbol decisions more reliable, channel coding can be employed. Hence, in the next section we will concentrate our attention on characterizing the PIC detection-assisted system's BER performance in a turbo-coded scenario.

17.3.2.3.2 BER Performance of Turbo-Coded PIC Detection-Assisted SDMA-OFDM for Different Numbers of Users and Receiver Antennas As demonstrated in Sections 17.2.6.4 and 17.3.1.4.7 in the context of turbo-coded MMSE- and SIC detection-assisted SDMA-OFDM, employing turbo-decoding at the receiver is a powerful means of further enhancing the system's BER performance. Again, this is achieved at the cost of reducing the system's effective throughput and by imposing additional computational complexity.

In the context of PIC detection-assisted SDMA-OFDM we conjectured in Section 17.3.2.2 that instead of simply concatenating PIC detection and turbo-decoding as we did in the case of turbo-coded MMSE- or SIC detection-assisted SDMA-OFDM, it is potentially more beneficial to embed the turbo-decoding into the PIC detection process. As a

result, a set of more accurate remodulated reference signals can be obtained for the second PIC detection stage.

More explicitly, a fraction of the total number of affordable turbo-decoding iterations would be performed after the first PIC detection stage, while the rest of the turbo iterations is carried out during the second PIC detection stage. More explicitly, in order to render the associated BER performance results comparable to those of turbo-coded MMSE-, SIC and ML detection-assisted SDMA-OFDM presented in Sections 17.2.6.4, 17.3.1.4.7 and 17.3.3.4.2, respectively, it is useful to split the total number of turbo iterations available between the turbo-decoding conducted after the first- and the second PIC detection stage. Since four turbo iterations were employed in our previous investigations, a plausible choice is to assign two iterations to both the first- and the second PIC detection stage. An equal splitting of the number of turbo iterations is also motivated by the observation that the most significant BER improvement due to turbo decoding is achieved during the first few turbo-decoding iterations.

The other relevant turbo coding parameters were summarized in Table 17.4, but for the reader's convenience they are repeated: the coding rate was $R_c = \frac{1}{2}$, the constraint length was $K_c = 3$, and octally represented generator polynomials of $(7, 5)_8$ were used. Again, a total of four turbo iterations was performed.

Our BER simulation results are portrayed in Figure 17.22 at the left-hand side for $P = 2$ reception antennas, while at the right-hand side for $P = 4$ reception antennas, when supporting up to $L = P$ number of users. Two methods of generating the remodulated reference- or reconstructed received signal used in the PIC module of Figure 17.20 are compared against each other. Specifically in the first case we used slicing, reencoding, interleaving and remodulating only for the 'source'-related *a posteriori* soft-output bits, while in the second scenario we employed slicing, interleaving and remodulating for the 'source- plus parity'-related *a posteriori* soft-output bits of the turbo-decoder. As expected, compared to the uncoded scenario, whose associated simulation results were shown in Figure 17.21, the BER is significantly reduced for both methods of generating the remodulated reference signal. However, for the 'source- plus parity' related remodulated reference signal of the second scenario a performance advantage of about 1.8dB was observed in Figure 17.22 at a BER of 10^{-5} compared to the 'source'-related reference based scenario. In general, note the significant BER performance difference in favour of the scenario of four reception antennas and three simultaneous users, compared to supporting four simultaneous users. The explanation of this phenomenon is that in the scenario supporting a lower number of users the tentative symbol decisions provided by the first PIC detection stage are more reliable. This is a result of the higher relative diversity order encountered by the MMSE combiner, which constitutes the first detection stage of the PIC process, as argued in Section 17.3.2.1. Hence the effects of 'error propagation' between the different users' signals during the second PIC detection stage are reduced.

17.3.2.4 Complexity Analysis

In this section we will analyse the complexity exhibited by the PIC detector described in Section 17.3.2.1, which was also summarized in Table 17.7. We will consider each step of Section 17.3.2.1 and Table 17.7 in terms of the associated complexity.

First-Stage - MMSE Detection:

- *Combining*: In the standard PIC algorithm of Section 17.3.2.1 the MMSE-related weight matrix $\mathbf{W}_{\text{MMSE}}^{[1]}$ to be employed for detection during the first PIC iteration does not explicitly have to be made available. Hence, according to Equations 17.104, 17.105 and 17.106 an initial estimate $\hat{\mathbf{s}}^{[1]}$ of the vector $\mathbf{s}$ of signals transmitted by the different users can be obtained, which imposes a computational complexity quantified in terms of the number of complex multiplications and additions, as follows:

$$C_{\text{PIC,direct}}^{[1](\mathbb{C}*\mathbb{C})} = C_{\text{PIC,direct}}^{[1](\mathbb{C}+\mathbb{C})} = PL + (P+1)L^2 + \frac{1}{3}L^3 \qquad (17.195)$$

$$C_{\text{PIC,direct}}^{[1](\mathbb{R}*\mathbb{C})} = PL \qquad (17.196)$$

$$C_{\text{PIC,direct}}^{[1](\mathbb{R}+\mathbb{C})} = L. \qquad (17.197)$$

- *Demodulation*: Furthermore, the demodulation operation carried out during the first PIC iteration, which follows the philosophy of Equation 17.187, imposes a computational complexity of:

$$C_{\text{PIC,dem}}^{[1](\mathbb{C}*\mathbb{C})} = \frac{1}{2}LM_c \qquad (17.198)$$

$$C_{\text{PIC,dem}}^{[1](\mathbb{C}+\mathbb{C})} = C_{\text{PIC,dem}}^{[1](\mathbb{R}\lessgtr\mathbb{R})} = LM_c, \qquad (17.199)$$

where M_c is the number of constellation points contained in the set $\mathcal{M}_c$. Note that the number of complex multiplications has been weighted by a factor of $\frac{1}{2}$ in order to account for the reduced complexity associated with calculating the product between a complex number and its conjugate complex value in the context of the Euclidean distance metric evaluation of Equation 17.187.

Second-Stage - PIC Detection:

- *Parallel Interference Cancellation*: As observed in Table 17.7 the second PIC iteration commences by the operation of parallel interference cancellation, described by Equation 17.189, which is associated with a complexity of:

$$C_{\text{PIC,sub}}^{[2](\mathbb{C}*\mathbb{C})} = LP \qquad (17.200)$$

$$C_{\text{PIC,sub}}^{[2](\mathbb{C}+\mathbb{C})} = L(\log_2 L)P. \qquad (17.201)$$

Here we have assumed that the parallel subtraction based interference cancellation is organized in form of a binary tree. This reduces the complexity $C_{\text{PIC,sub}}^{[2](\mathbb{C}+\mathbb{C})}$ from originally $L(L-1)P$ complex additions associated with a linear implementation to that of $L(\log_2 L)P$.

- *Combining*: Then operation of combining was described by Equations 17.191 and 17.192. A complexity reduction is achieved, when employing constant-modulus M-PSK modulation schemes. Then it is sufficient to perform the combining of the different users' associated signals by multiplying them with the Hermitian transpose of the their associated channel vectors, which results in:

$$C_{\text{PIC,cmb-MPSK}}^{[2](\mathbb{C}*\mathbb{C})} = C_{\text{PIC,cmb-MPSK}}^{[2](\mathbb{C}+\mathbb{C})} = PL. \qquad (17.202)$$

By contrast, in the more general case of QAM modulation schemes it can be shown that we have:

$$C_{\text{PIC,cmb-QAM}}^{[2](\mathbb{C}*\mathbb{C})} = \frac{3}{2}LP \tag{17.203}$$

$$C_{\text{PIC,cmb-QAM}}^{[2](\mathbb{C}+\mathbb{C})} = 2LP \tag{17.204}$$

$$C_{\text{PIC,cmb-QAM}}^{[2](\mathbb{R}/\mathbb{C})} = C_{\text{PIC,cmb-QAM}}^{[2](\mathbb{R}+\mathbb{R})} = L, \tag{17.205}$$

where the number of complex multiplications inflicted by calculating the Euclidean norm $||\mathbf{H}^{(l)}||_2^2$ has, again, been weighted by a factor of $\frac{1}{2}$ in order to account for the reduced complexity of calculating the product of a complex number with its conjugate complex value.

- *Demodulation*: In a final step, the different users' estimated signals are again demodulated according to Equation 17.193, which requires a computational complexity of:

$$C_{\text{PIC,dem}}^{[2](\mathbb{C}*\mathbb{C})} = \frac{1}{2}LM_c \tag{17.206}$$

$$C_{\text{PIC,dem}}^{[2](\mathbb{C}+\mathbb{C})} = C_{\text{PIC,dem}}^{[2](\mathbb{R}\lessgtr\mathbb{R})} = LM_c. \tag{17.207}$$

Hence, upon combining the different implementational complex contributions we obtain the following expression for the total computational complexity:

$$C_{\text{PIC}}^{\mathbb{C}*\mathbb{C}} = LM_c + 5PL + (P+1)L^2 + \frac{1}{3}L^3 \tag{17.208}$$

$$C_{\text{PIC}}^{\mathbb{C}+\mathbb{C}} = 2L(M_c + \frac{1}{2}) + (4 + \log_2 L)PL + (P+1)L^2 + \frac{1}{3}L^3 \tag{17.209}$$

$$C_{\text{PIC}}^{\mathbb{R}\lessgtr\mathbb{R}} = 2LM_c \tag{17.210}$$

$$C_{\text{PIC}}^{\mathbb{R}/\mathbb{C}} = L, \tag{17.211}$$

where again, mixed real-complex multiplications and additions as well as real additions were assumed to have half the complexity of those, which involve complex numbers[20].

17.3.2.5 Summary and Conclusions on PIC Detection

In Section 17.3.2.5 PIC assisted detection of SDMA-OFDM was introduced and characterized with respect to its BER performance in the context of both uncoded and turbo-coded scenarios. Furthermore, its complexity was analysed.

The employment of PIC detection was motivated by two observations. In Section 17.3.1.6 we found that SIC based detection is capable of significantly outperforming MMSE detection in terms of the system's BER performance. This was a result of increasing the system's diversity order by successively removing the already detected users' remodulated signal contributions from the vector $\mathbf{x}$ of composite multiuser signals received by the different BS antenna elements. A substantial computational complexity was associated with the calculation of the

---

[20]Here we have again neglected that no real-valued additions are required in the context of real-complex multiplications and hence our calculation produces an upper-bound estimate of the complexity imposed

linear combiner's weight matrix at each detection stage according to Equation 17.121, and with the calculation of the remaining users' SINRs according to Equation 17.122, which was followed by the selection of the most dominant user according to Equation 17.123. Hence, in our quest for alternative, potentially less complex detection techniques, PIC detection was considered.

As shown in the PIC detector's block diagram of Figure 17.20 and as described in Section 17.3.2.1, during the first PIC iteration linear MMSE estimates of the different users' transmitted signals were generated with the aid of a linear combiner, obeying Equations 17.185 and 17.186. These linear estimates seen in Figure 17.20 were demodulated, as shown in Equation 17.187, and employed in the context of the PIC module seen at the bottom left corner of Figure 17.20 as a reference for reconstructing the different users' transmitted signal contributions. A potentially more accurate estimate of the l-th user's transmitted signal, where $l = 1, \ldots, L$, was then generated during the next PIC iteration by subtracting the $L - 1$ remaining users' reconstructed signal contributions from the vector $\mathbf{x}$ of received composite multiuser signals as suggested by Equation 17.189. These operations were followed by diversity combining, obeying Equations 17.191 and 17.192 and demodulation, described by Equation 17.193, in order to obtain the specific constellation point that is most likely to have been transmitted. Provided that correct tentative symbol decisions were made for all the $L - 1$ remaining users in the previous PIC iteration, an improved linear MMSE estimate of the l-th user's transmitted signal would becomes available at the associated demodulator's input. This procedure has to be invoked for all the L different users. These processing steps were also summarized in Table 17.7 and in Figure 17.20.

Motivated by the PIC detector's relatively limited BER improvement compared to MMSE detection in the context of an uncoded scenario, in Section 17.3.2.2 we proposed to embed turbo-decoding into the PIC iteration, instead of simply concatenating the PIC detector and the turbo-decoder. As a result of this embedded turbo-decoding operation we expected to reduce the effects of 'error-propagation' in the PIC module of Figure 17.20. In these experiments soft-bits were generated for turbo-decoding as it was described in Section 17.2.5 in the context of MMSE detection. This procedure was similar to the single-user scenario. Hence, there still remains some potential for further further improvement. In the context of turbo-decoding a sliced reference was generated for employment in the PIC module, which was the result of performing hard-decisions on the turbo-decoder's 'source'-related soft-output bits followed by reencoding. An alternative strategy was that of performing hard-decisions on both the source- and the parity-related soft-output bits, which was shown in our performance investigations in Section 17.3.2.3.2 to be advantageous.

Our BER performance studies were conducted in Section 17.3.2.3. Specifically, Figure 17.21 characterized an uncoded scenario, while Figure 17.22 was recorded in the context of a turbo-coded scenario, again upon portraying the influence of the number of users L and the number of reception antennas P. For the uncoded scenario the SNR performance improvement compared to a system employing MMSE detection was at most 3.03dB, in a scenario of $L = P = 2$, while for a scenario of $L = P = 4$ the corresponding gain was at least 1.25dB. For a turbo-coded scenario the SNR improvement was more substantial. This will be further detailed in the context of our final comparison of all the different detectors in Section 17.3.4.1.

In order to conclude our discussions, the computational complexity imposed by PIC detection was analysed in Section 17.3.2.4, which resulted in Equations 17.208, 17.209 and

M_c^L-dim.

x_1 → | Classifier | → $\check{s}^{(1)}$

x_P → | | → $\check{s}^{(L)}$
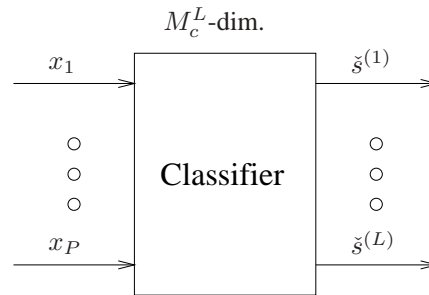
Figure 17.23: Representation of the optimum ML detector. In contrast to the sub-optimum linear- and non-linear detectors, namely LS and MMSE discussed in Sections 17.2.2 and 17.2.3, respectively, as well as SIC and PIC discussed in Sections 17.3.1 and 17.3.2, respectively, the L different users' complex symbols most likely transmitted are *jointly* detected. This is achieved upon evaluating the M_c^L number of trial-symbols in terms of their multi-user Euclidean distance metric with respect to the vector **x** of the signals received by the different antenna elements, namely Equation 17.223. A disadvantage is the associated computational complexity, which might be excessive.

17.210, describing the number of complex multiplications and additions, as well as real-valued comparisons. These equations were invoked in our graphical portrayal of the different detectors' implementational complexities in Section 17.3.4.2.

17.3.3 ML Detection

In this section we will outline the philosophy of the Maximum Likelihood (ML) detector [112, 114–118, 120, 123, 135, 137], which is optimum from a statistical point of view. An associated disadvantage is its potentially excessive computational complexity, which results from the strategy of jointly detecting the L different users. This implies assessing the M_c^L possible combinations of symbols transmitted by the L different users by evaluating their Euclidean distance from the received signal, upon taking into account the effects of the channel. The stylized ML detector has once again been portrayed in Figure 17.23.

The structure of this section is as follows. In Section 17.3.3.1 the philosophy of standard ML detection will be portrayed. In scenarios, where the number of users L is lower than the number of reception antennas P, a complexity reduction can be achieved by transforming the vector of composite multiuser signals received by the different antenna elements first to the so-called 'trial-space' with the aid of a linear transform, as it will be discussed in Section 17.3.3.2. In an attempt to further enhance the system's BER performance turbo-coding can be invoked. The generation of the soft-bit information required will be discussed in Section 17.3.3.3, where a further reduction of the computational complexity can be achieved by applying the well-known maximum approximation. Our BER performance investigation will be conducted in Section 17.3.3.4 for both uncoded as well as turbo-coded scenarios. Furthermore, estimates of the computational complexity imposed will be provided in Section 17.3.3.5. A summary and conclusions will be offered in Section 17.3.3.6

17.3.3.1   Standard ML Detection

The structure of our discussions on the ML detector is as follows. In Section 17.3.3.1.1 the vector $\mathbf{x}$ of received signals is interpreted as a manifestation of a multi-variate complex Gaussian distribution function $f(\mathbf{x}|\check{\mathbf{s}}, \mathbf{H})$, which reflects the *a priori* probability that the vector $\mathbf{x}$ was received. Furthermore, in Section 17.3.3.1.2 it will be shown that determining the desired vector of symbols $\check{\mathbf{s}}_{\text{ML}}$ that is most likely to have been transmitted by the L different users is equivalent to maximizing the transmitted symbols' *a posteriori* probability. However, it will be demonstrated with the aid of the Bayes theorem [90] that this is equivalent to maximizing the *a priori* probability, which again, is available in terms of the Gaussian distribution function.

17.3.3.1.1   Representation of the Vector of Received Signals as a Sample of a Multi-Variate Complex Gaussian Distribution Function
In order to commence our discussions, let us recall from Equation 17.1 the definition of the vector $\mathbf{x}$ of signals received by the P different antenna elements, namely that we have:

$$\mathbf{x} = \mathbf{Hs} + \mathbf{n}, \tag{17.212}$$

where again, we have omitted the index $[n, k]$, which denotes the k-th subcarrier of the n-th OFDM symbol. We observe that $\mathbf{x} \sim \mathcal{CN}(\mathbf{Hs}, \mathbf{R_n})$, namely $\mathbf{x}$ is a sample of an L-dimensional multi-variate complex Gaussian distribution, having a vector of mean values given by $\mathbf{Hs}$ and a covariance matrix of $\mathbf{R_n} \in \mathbb{C}^{P \times P}$, where the latter is given by:

$$\mathbf{R_n} = E\{\mathbf{nn}^H\} \tag{17.213}$$
$$= \sigma_n^2 \mathbf{I}, \tag{17.214}$$

implying that the different noise contributions are assumed to be uncorrelated. This multi-variate complex Gaussian distribution function can be expressed as [482]:

$$f(\mathbf{x}|\mathbf{s}, \mathbf{H}) = \frac{1}{\pi^P |\mathbf{R_n}|} \exp\left(-(\mathbf{x} - \mathbf{Hs})^H \mathbf{R_n}^{-1}(\mathbf{x} - \mathbf{Hs})\right) \tag{17.215}$$

$$= \frac{1}{\pi^P (\sigma_n^2)^P} \exp\left(-\frac{1}{\sigma_n^2}||\mathbf{x} - \mathbf{Hs}||_2^2\right), \tag{17.216}$$

where Equation 17.216 was obtained by substituting Equation 17.214 into Equation 17.215. The representation of the complex Gaussian distribution function is legitimate, since again, the noise at the different receiver antenna elements is assumed to be uncorrelated. More explicitly, $P(\mathbf{x}|\mathbf{s}, \mathbf{H}) = f(\mathbf{x}|\mathbf{s}, \mathbf{H})$ denotes the *a priori* probability that the vector $\mathbf{x}$ has been received by the BS antenna elements under the condition that the vector $\mathbf{s}$ was transmitted by the different users over a channel characterized by the matrix $\mathbf{H}$.

17.3.3.1.2   Determination of the Vector of Transmitted Symbols by Maximizing the *A Posteriori* Probability
In simple verbal terms the ML detector finds the specific L-dimensional vector of M_c-ary symbols, which is most likely to have been transmitted. In more formal terms ML detection is based on the idea of maximizing the *a posteriori* probability $P(\check{\mathbf{s}}|\mathbf{x}, \mathbf{H})$ that the specific vector $\check{\mathbf{s}} \in \mathbb{C}^{L \times 1}$ of the different users' symbols - which is

an element of the set $\mathcal{M}^L$ of trial-vectors - was transmitted over the SDMA-MIMO channel characterized by the channel transfer factor matrix $\mathbf{H} \in \mathbb{C}^{P \times L}$ under the condition that the vector $\mathbf{x} \in \mathbb{C}^{P \times 1}$ was received by the different BS receiver antenna elements. This maximization procedure can be expressed as:

$$\check{\mathbf{s}}_{\text{ML}} = arg\max_{\check{\mathbf{s}} \in \mathcal{M}^L} P(\check{\mathbf{s}}|\mathbf{x}, \mathbf{H}), \tag{17.217}$$

where the set $\mathcal{M}^L$ of trial-vectors is given by:

$$\mathcal{M}^L = \left\{ \check{\mathbf{s}} = \begin{pmatrix} \check{s}^{(1)} \\ \vdots \\ \check{s}^{(L)} \end{pmatrix} \middle| \frac{\check{s}^{(1)}}{\sigma_1}, \dots, \frac{\check{s}^{(L)}}{\sigma_L} \in \mathcal{M}_c \right\}, \tag{17.218}$$

and where $\sigma_l = \sqrt{\sigma_l^2}$ denotes the l-th user's standard deviation, while $\mathcal{M}_c$ denotes the set of complex constellations points associated with the specific modulation scheme employed.

The maximization procedure obeying Equation 17.217 involves knowledge of the *a posteriori* probabilities $P(\check{\mathbf{s}}|\mathbf{x}, \mathbf{H}), \check{\mathbf{s}} \in \mathcal{M}^L$, which can be obtained from the *a priori* probabilities $P(\mathbf{x}|\check{\mathbf{s}}, \mathbf{H})$ with the aid of the Bayes' theorem [90], namely:

$$P(\check{\mathbf{s}}|\mathbf{x}, \mathbf{H}) = P(\mathbf{x}|\check{\mathbf{s}}, \mathbf{H}) \frac{P(\check{\mathbf{s}})}{P(\mathbf{x})}, \tag{17.219}$$

where all symbol vector probabilities are assumed to be identical, i.e. we have $P(\check{\mathbf{s}}) = \frac{1}{M_c^L} = const.$, and for the total probability $P(\mathbf{x})$ we have:

$$P(\mathbf{x}) = \sum_{\check{\mathbf{s}} \in \mathcal{M}^L} P(\mathbf{x}|\check{\mathbf{s}}, \mathbf{H}) P(\check{\mathbf{s}}) = const., \tag{17.220}$$

which follows from the simple fact that all probabilities have to sum to unity, i.e. that:

$$\sum_{\check{\mathbf{s}} \in \mathcal{M}^L} P(\check{\mathbf{s}}|\mathbf{x}, \mathbf{H}) \overset{!}{=} 1. \tag{17.221}$$

Hence, upon substituting Equation 17.219 into Equation 17.217 and exploiting that we have $P(\check{\mathbf{s}}) = const.$ as well as that $P(\mathbf{x}) = const.$ for all $\check{\mathbf{s}} \in \mathcal{M}^L$, we obtain:

$$\check{\mathbf{s}}_{\text{ML}} = arg\max_{\check{\mathbf{s}} \in \mathcal{M}^L} P(\check{\mathbf{s}}|\mathbf{x}, \mathbf{H}) \iff \check{\mathbf{s}}_{\text{ML}} = arg\max_{\check{\mathbf{s}} \in \mathcal{M}^L} P(\mathbf{x}|\check{\mathbf{s}}, \mathbf{H}), \tag{17.222}$$

where $P(\mathbf{x}|\check{\mathbf{s}}, \mathbf{H}) = f(\mathbf{x}|\check{\mathbf{s}}, \mathbf{H})$ was given by Equation 17.216. Note from Equation 17.216 that maximizing $f(\mathbf{x}|\check{\mathbf{s}}, \mathbf{H})$ is equivalent to minimizing the Euclidean distance metric $||\mathbf{x} - \mathbf{H}\check{\mathbf{s}}||_2^2 \, \forall \, \check{\mathbf{s}} \in \mathcal{M}^L$, and hence we have:

$$\check{\mathbf{s}}_{\text{ML}} = arg\max_{\check{\mathbf{s}} \in \mathcal{M}^L} P(\check{\mathbf{s}}|\mathbf{x}, \mathbf{H}) \iff \check{\mathbf{s}}_{\text{ML}} = arg\min_{\check{\mathbf{s}} \in \mathcal{M}^L} ||\mathbf{x} - \mathbf{H}\check{\mathbf{s}}||_2^2. \tag{17.223}$$

Note however that the complexity associated with evaluating Equation 17.223 might potentially be excessive, depending on the M_c^L number of vectors contained in the trial-set $\mathcal{M}^L$.

An attractive strategy of reducing the complexity in the context of scenarios, where the L number of users is lower than the P number of BS reception antenna elements will be outlined in the next section.

17.3.3.2   Transform-Based ML Detection

As observed in Equation 17.223, determining the ML symbol estimate requires comparing the Euclidean distance between the vector $\mathbf{x}$ of signals actually received by the different antenna elements and the vector $\mathbf{H\check{s}}$ of signals, which would be received in the absence of AWGN, for all the different vectors $\check{s}$ of symbol combinations contained in the set $\mathcal{M}^L$. In order to potentially reduce the computational complexity in a specific scenario, where the L number of users is lower than the P number of reception antenna elements, it was proposed in [112] to transform the vector $\mathbf{x}$ of received signals first to the trial-domain[21] with the aid of a linear transform and then to perform the calculation of the Euclidean distance directly in the trial-domain. More explicitly applying this transform-based approach results in a potentially lower complexity than that associated with evaluating Equation 17.223. A linear transform which yields a particularly simple form of the Euclidean distance metric to be evaluated is based on the left-inverse- or Moore-Penrose pseudo-inverse of the channel matrix $\mathbf{H}$, which was discussed in Section 17.2.2. The resultant vector is also known as the LS estimate or ML estimate of the vector $\mathbf{s}$ of transmitted signals. More specifically, the LS estimate $\hat{\mathbf{s}}_{LS}$ was given by Equation 17.36, namely by:

$$\hat{\mathbf{s}}_{LS} = \mathbf{P}_{LS}\mathbf{x}, \tag{17.224}$$

with the associated projection matrix $\mathbf{P}_{LS}$ defined in Equation 17.37 as:

$$\mathbf{P}_{LS} = (\mathbf{H}^H\mathbf{H})^{-1}\mathbf{H}^H. \tag{17.225}$$

Furthermore, it was shown in Equation 17.42 that the LS combiner's output vector $\mathbf{s}_{LS}$ is composed of the vector $\mathbf{s}$ of transmitted signals plus an additional contribution due to the AWGN encountered at the array elements, which is formulated as:

$$\hat{\mathbf{s}}_{LS} = \mathbf{s} + \mathbf{P}_{LS}\mathbf{n}. \tag{17.226}$$

Recall from Equation 17.44 that the noise at the LS combiner's output is correlated, having a covariance matrix $\mathbf{R}_{\Delta\hat{\mathbf{s}}_{LS}}$ expressed in the form of:

$$\mathbf{R}_{\Delta\hat{\mathbf{s}}_{LS}} = \frac{1}{\sigma_n^2}(\mathbf{H}^H\mathbf{H})^{-1}. \tag{17.227}$$

Hence, in equivalence to Equation 17.215, the multi-variate complex Gaussian distribution function, which reflects the probability that the vector $\hat{\mathbf{s}}_{LS}$ is observed at the output of the linear combiner under the condition that the vector $\mathbf{s}$ was transmitted over a channel characterized

---

[21]The trial-domain is equal to the transmitted signal's domain.

by the channel transfer factor matrix $\mathbf{H}$ is given by:

$$f(\hat{\mathbf{s}}_{\text{LS}}|\mathbf{s}, \mathbf{H}) = \frac{1}{\pi^P |\mathbf{R}_{\Delta\hat{\mathbf{s}}_{\text{LS}}}|} \exp\left(-(\hat{\mathbf{s}}_{\text{LS}} - \mathbf{s})^H \mathbf{R}_{\Delta\hat{\mathbf{s}}_{\text{LS}}}^{-1} (\hat{\mathbf{s}}_{\text{LS}} - \mathbf{s})\right). \tag{17.228}$$

Upon following the steps outlined in the context of Section 17.3.3.1, the vector $\check{\mathbf{s}}_{\text{ML}}$ of symbols that is most likely to have been transmitted is then given by:

$$\check{\mathbf{s}}_{\text{ML}} = arg \max_{\check{\mathbf{s}} \in \mathcal{M}^L} P(\check{\mathbf{s}}|\mathbf{x}, \mathbf{H}) \quad \Longleftrightarrow \quad \check{\mathbf{s}}_{\text{ML}} = arg \min_{\check{\mathbf{s}} \in \mathcal{M}^L} (\hat{\mathbf{s}}_{\text{LS}} - \check{\mathbf{s}})^H \mathbf{R}_{\Delta\hat{\mathbf{s}}_{\text{LS}}}^{-1} (\hat{\mathbf{s}}_{\text{LS}} - \check{\mathbf{s}}). \tag{17.229}$$

As a result of the linear properties of the transform applied in Equation 17.224 to the vector $\mathbf{x}$ of signals received by the different antenna elements, the same symbol detection error probability is achieved as with the aid of the standard approach of Equation 17.223, however at a potentially lower complexity. Note however, that a necessary condition for the existence of the projection matrix $\mathbf{P}_{\text{LS}}$ is that the number of users L must be lower than or equal to the number of reception antenna elements P, which imposes a limitation compared to the standard ML detector of Section 17.3.3.1.

17.3.3.3 ML-Assisted Soft-Bit Generation for Turbo-Decoding

Turbo coding based error protection of the different subcarriers hosted by an OFDM symbol is a powerful means of further enhancing the system's BER performance. This is achieved at the cost of reducing the system's effective throughput and increasing the system's complexity. A prerequisite for performing turbo decoding at the receiver is the availability of soft-bit information. As suggested in [112], it is desirable in terms of keeping the computational complexity as low as possible to perform the turbo trellis-decoding separately for the different users. This is, because the joint trellis-decoding of the different users' transmitted signals would potentially require an excessive number of trellis decisions and hence impose a high complexity.

17.3.3.3.1 Standard ML-Assisted Soft-Bit Generation Following the concepts of Equation 17.95 the soft-bit value or log-likelihood ratio- or LLR-value associated with the l-th user at the m-th bit-position is given by:

$$L_m^{(l)} = \ln \frac{P(b_m^{(l)} = 1|\mathbf{x}, \mathbf{H})}{P(b_m^{(l)} = 0|\mathbf{x}, \mathbf{H})}, \tag{17.230}$$

which is the natural logarithm of the quotient of probabilities that the bit considered assumes either a value of $b_m^{(l)} = 1$ or $b_m^{(l)} = 0$. Note that here we have again omitted the index $[n, k]$ for the k-th subcarrier of the n-th OFDM symbol, which is associated with the different variables. Equation 17.230 can be further expanded by noting that the probability that a binary bit value of $b_m^{(l)} = 1$ was transmitted at the m-th bit position associated with the l-th user in the k-th subcarrier is given by the sum of the probabilities of those symbol combinations, where the l-th user's transmitted symbol is associated with a bit value of $b_m^{(l)} = 1$. The probability that

a bit value of $b_m^{(l)} = 0$ was transmitted can be expanded equivalently. Hence we obtain:

$$L_m^{(l)} = \ln \frac{\sum_{\check{s}^{(1)}/\sigma_1 \in \mathcal{M}_c} \cdots \sum_{\check{s}^{(l)}/\sigma_l \in \mathcal{M}_{cm}^1} \cdots \sum_{\check{s}^{(L)}/\sigma_L \in \mathcal{M}_c} P(\check{\mathbf{s}}|\mathbf{x}, \mathbf{H})}{\sum_{\check{s}^{(1)}/\sigma_1 \in \mathcal{M}_c} \cdots \sum_{\check{s}^{(l)}/\sigma_l \in \mathcal{M}_{cm}^0} \cdots \sum_{\check{s}^{(L)}/\sigma_L \in \mathcal{M}_c} P(\check{\mathbf{s}}|\mathbf{x}, \mathbf{H})}, \qquad (17.231)$$

where $\mathcal{M}_{cm}^b$ denotes the specific subset of the set $\mathcal{M}_c$ of constellation points of the modulation scheme employed, which are associated with a bit value of $b \in \{0, 1\}$ at the m-th bit position. For notational convenience we can define the l-th user's associated set of trial-vectors employed for determining the probability that the m-th transmitted bit exhibits a value of $b \in \{0, 1\}$ as follows:

$$\mathcal{M}_m^{b(l)L} = \left\{ \check{\mathbf{s}} = \begin{pmatrix} \check{s}^{(1)} \\ \vdots \\ \check{s}^{(L)} \end{pmatrix} \middle| \frac{\check{s}^{(1)}}{\sigma_1} \in \mathcal{M}_c, \ldots, \frac{\check{s}^{(l)}}{\sigma_l} \in \mathcal{M}_{cm}^b, \ldots, \frac{\check{s}^{(L)}}{\sigma_L} \in \mathcal{M}_c \right\}.$$
$$(17.232)$$

Upon invoking again Bayes' theorem given by Equation 17.219, namely that:

$$P(\check{\mathbf{s}}|\mathbf{x}, \mathbf{H}) = P(\mathbf{x}|\check{\mathbf{s}}, \mathbf{H}) \frac{P(\check{\mathbf{s}})}{P(\mathbf{x})}, \qquad (17.233)$$

and re-substituting Equation 17.233 into Equation 17.231 we obtain the following expression for the l-th user's soft-bit value at the m-th bit position:

$$L_m^{(l)} = \ln \frac{\sum_{\check{\mathbf{s}} \in \mathcal{M}_m^{1(l)L}} P(\mathbf{x}|\check{\mathbf{s}}, \mathbf{H})}{\sum_{\check{\mathbf{s}} \in \mathcal{M}_m^{0(l)L}} P(\mathbf{x}|\check{\mathbf{s}}, \mathbf{H})}. \qquad (17.234)$$

Here we have exploited that the different symbol combination vectors $\check{\mathbf{s}}$ have the same probability namely that $P(\check{\mathbf{s}}) = const.$, $\check{\mathbf{s}} \in \mathcal{M}^L$. Upon recalling from Section 17.3.3.1 that the probability $P(\mathbf{x}|\check{\mathbf{s}}, \mathbf{H})$ is given by the multi-variate complex Gaussian distribution function $f(\mathbf{x}|\check{\mathbf{s}}, \mathbf{H})$ defined in Equation 17.216, we obtain:

$$L_m^{(l)} = \ln \frac{\sum_{\check{\mathbf{s}} \in \mathcal{M}_m^{1(l)L}} \exp\left(-\frac{1}{\sigma_n^2}||\mathbf{x} - \mathbf{H}\check{\mathbf{s}}||_2^2\right)}{\sum_{\check{\mathbf{s}} \in \mathcal{M}_m^{0(l)L}} \exp\left(-\frac{1}{\sigma_n^2}||\mathbf{x} - \mathbf{H}\check{\mathbf{s}}||_2^2\right)}. \qquad (17.235)$$

Observe that evaluating the l-th user's soft-bit value based on its LLR at the m-th bit position with the aid of Equation 17.235 involves the exponential function, which might be computationally expensive.

17.3.3.3.2   Simplification by Maximum Approximation   In order to avoid the explicit evaluation of the exponential function in Equation 17.235, a common approach is the employment of the so-called maximum-approximation, which implies that only that specific additive term is retained in the calculation of the numerator and nominator of Equation 17.235, which yields the maximum contribution. It can be readily shown that as a result of this simplification

we obtain instead of Equation 17.235 the following expression:

$$L_m^{(l)} \approx \frac{1}{\sigma_n^2}\left[||\mathbf{x}-\mathbf{H}\check{\mathbf{s}}_m^{0(l)}||_2^2 - ||\mathbf{x}-\mathbf{H}\check{\mathbf{s}}_m^{1(l)}||_2^2\right], \qquad (17.236)$$

where

$$\check{\mathbf{s}}_m^{b(l)} = arg \min_{\check{\mathbf{s}}\in\mathcal{M}_m^{b(l)L}}||\mathbf{x}-\mathbf{H}\check{\mathbf{s}}||_2^2, \quad b\in\{0,1\}, \qquad (17.237)$$

while the set $\mathcal{M}_m^{b(l)L}$ was defined in Equation 17.232. We note that for each soft-bit to be determined, Equation 17.237 has to be invoked twice, once for a bit status of $b=1$ and once for $b=0$.

Observe however, that a significant complexity reduction can be achieved by exploiting that the union of the two subspaces associated with the binary bit values of 0 and 1 of the L users at bit position m constitutes the entire trial space, namely that $\mathcal{M}^L = \mathcal{M}_m^{0(l)L}\bigcup\mathcal{M}_m^{1(l)L}$. Hence, the calculation of the Euclidean distance metric $||\mathbf{x}-\mathbf{H}\check{\mathbf{s}}||_2^2$ has to be performed only once for the different trial vectors $\check{\mathbf{s}}\in\mathcal{M}^L$, followed by an appropriate selection in the context of the soft-bit generation assisted by Equation 17.237. Specifically, in a first step the Euclidean distance metric can be determined for half of the vectors $\check{\mathbf{s}}_m^{b(l)}$ associated with the different bit polarities $b\in\{0,1\}$ and bit positions m by searching the entire set $\mathcal{M}^L$, which results in the ML estimate $\check{\mathbf{s}}_{\text{ML}}$ of the vectors of transmitted symbols according to Equation 17.223. This initial L-dimensional, M_c-ary ML symbol estimate is given by a specific bit vector. The inverse of this ML bit vector contains the specific bit polarities, for which the further minimization according to Equation 17.237 still has to be conducted.

17.3.3.4   Performance Analysis

In this section the BER performance of ML detection-assisted SDMA-OFDM will be investigated in both a lower-complexity, higher effective throughput scenario using no channel coding, as well as in a higher-complexity, lower throughput scenario where turbo-coding is employed. Again, the frame-invariant fading indoor WATM channel model and its associated OFDM system model described in Section 14.3.1 were invoked and ideal knowledge of the channel transfer functions associated with the different transmit-receive antenna pairs was assumed. For a summary of the basic simulation setup we refer again to Table 17.3. The further structure of Section 17.3.3.4 is as follows. While in Section 17.3.3.4.1 the ML detection-assisted SDMA-OFDM system's BER performance is considered in the uncoded scenario, our simulation results characterizing the turbo-coded scheme will be discussed in Section 17.3.3.4.2.

17.3.3.4.1   BER Performance of ML Detection-Assisted SDMA-OFDM for Different Numbers of Users and Reception Antennas   In Figure 17.24 we have portrayed the BER performance of ML detection-assisted OFDM as a function of the SNR encountered at the reception antennas. Specifically, the curves at the left-hand side of Figure 17.24 are parameterized with both the number of users L and the number of reception antennas P, where only scenarios associated with $L \leq P$ are considered. We observe that upon increasing the MIMO
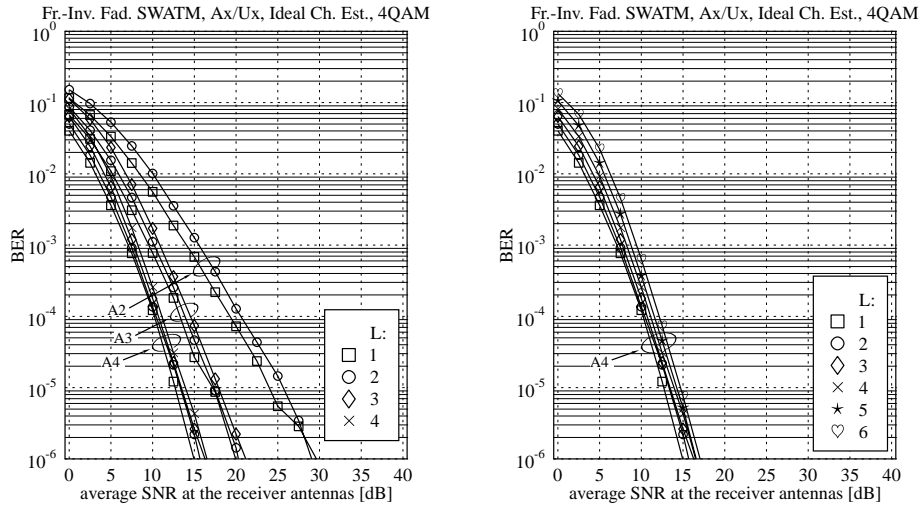
Figure 17.24: BER performance of 4QAM-modulated, ML detection-assisted SDMA-OFDM as a function of the SNR encountered at the reception antennas; (left:) the curves are further parameterized with the number of simultaneous users L and the number of reception antennas P, using the configurations of A2/U1..2, A3/U1..3 and A4/U1..4; (right:) the curves are parameterized with the L number of users for a fixed number of $P = 4$ reception antennas, namely using configurations of A4/U1..6; for the basic simulation parameters we refer to Table 17.3.

system's order, namely by considering a system of four reception antennas and four simultaneous users compared to a system of two reception antennas and two simultaneous users, the system's BER performance is significantly improved. This is in contrast to the behaviour observed for the MMSE detector in Figure 17.8, where a more modest improvement was observed, but it follows similar trends to those exhibited by the SIC detector characterized in Figure 17.12. More specifically, the ML detector benefits from the higher grade of diversity provided by a higher-order MIMO system. Also observe that by increasing the number of users L at a fixed number of reception antennas P, the system's performance degrades gracefully. More explicitly, the performance difference between the lowest-complexity system supporting one user and that of a "fully loaded" system associated with $L = P$ users is less than 2dB, which is in contrast to the significant degradation observed for the MMSE detector in Figure 17.8.

Our further investigations were conducted with respect to supporting L number of users, which was higher than the P number of reception antennas. By contrast, employing a configuration, where $L > P$ was prohibited in the context of the linear detectors, such as the LS or MMSE as well as the MMSE-based SIC and PIC schemes. The associated simulation results are portrayed at the right-hand side of Figure 17.24 for a scenario of $P = 4$ recep-
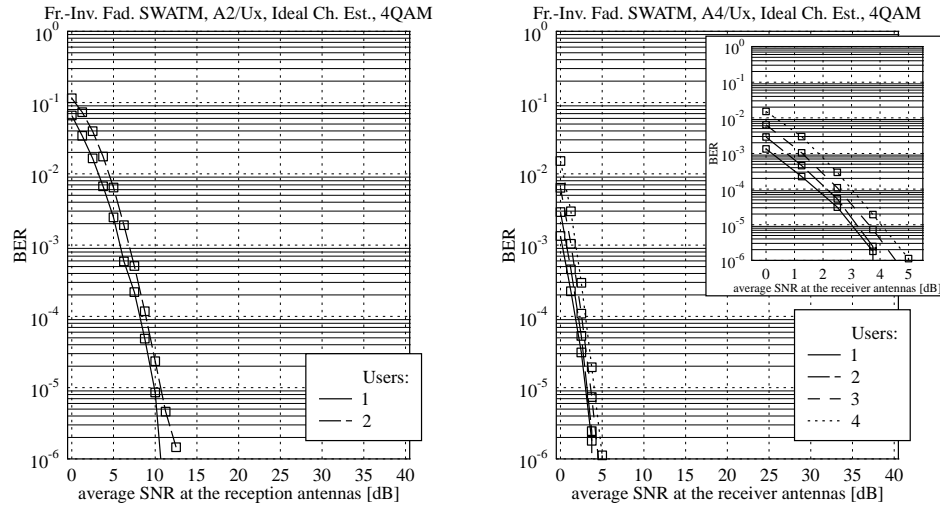
Figure 17.25: BER performance of turbo-coded, 4QAM-modulated, ML detection-assisted SDMA-OFDM as a function of the SNR recorded at the reception antennas; the curves are further parameterized with the number of simultaneous users L and the number of reception antennas P, where more specifically (left:) two reception antennas and (right:) four reception antennas were employed; for the basic simulation- and turbo-coding parameters we refer to Tables 17.3 and 17.4, respectively.

tion antennas, supporting up to $L = 6$ simultaneous users. Here we observe again that the performance degradation incurred upon increasing the number of users L beyond the number of reception antennas P is gradual. This is in contrast to the more abrupt degradation, which would potentially be observed in conjunction with MMSE-based detection schemes, when allowing for example five simultaneous users instead of four users in a scenario of four reception antennas.

17.3.3.4.2 BER Performance of Turbo-Coded ML Detection-Assisted SDMA-OFDM for Different Numbers of Users and Reception Antennas As it was shown in Sections 17.2.6.4, 17.3.1.4.7 and 17.3.2.3.2 for MMSE, SIC and PIC detection-assisted SDMA-OFDM systems, respectively, the employment of turbo-decoding at the receiver is a powerful means of further enhancing the system's BER performance. This is achieved at the cost of a reduction of the system's effective throughput and by investing additional computational complexity. The associated turbo coding parameters were summarized in Table 17.4, but for the reader's convenience they will be repeated here: the coding rate was $R_c = \frac{1}{2}$, the constraint length was $K_c = 3$, the octally represented generator polynomials of $(7, 5)_8$ were used and 4 iterations were performed. The generation of the soft-bits required for turbo-decoding

in the context of ML detection was discussed earlier in Section 17.3.3.3.

Our BER simulation results are portrayed in Figure 17.25, at the left-hand side for $P = 2$ reception antennas, while at the right-hand side for $P = 4$ reception antennas and up to $L = P$ number of simultaneous users. Again, we observe that compared to the uncoded scenario, whose associated BER simulation results were shown in Figure 17.24, the SNR at the reception antennas required for maintaining a specific BER is significantly reduced. In order to provide an example, in the context of a scenario associated with $L = P = 2$ and in the absence of channel coding an SNR of about 25.7dB is required for maintaining a target BER of 10^{-5}, while with the assistance of turbo-coding this target BER is reached at a reduced SNR of about 10.6dB. Similarly, for a scenario of $L = P = 4$ the corresponding SNRs for the uncoded and coded case are given by 13.9dB and 4dB, respectively.

17.3.3.5 Complexity Analysis

The structure of our complexity analysis of the ML-related detection techniques is as follows. While in Section 17.3.3.5.1 the complexity of standard ML detection is discussed, we will focus our attention in Section 17.3.3.5.2 on the analysis of transform-based ML detection. Our discussions will be concluded in Section 17.3.3.5.3 by elaborating on the complexity associated with the generation of soft-bits to be used in the context of turbo-coded ML detection-assisted SDMA-OFDM.

17.3.3.5.1 Complexity of Standard ML Detection   As observed in Equation 17.223, an M_c^L number of symbols combinations has to be compared in terms of the Euclidean distance metric for the detection of the different users' transmitted symbols in a specific OFDM subcarrier. This imposes a computational complexity quantified in terms of the number of complex multiplications, additions as well as real-valued comparisons, which is given by:

$$C_{\text{ML}}^{(\mathbb{C}*\mathbb{C})} = M_c^L P \left(\frac{1}{2} + L \right) \tag{17.238}$$

$$C_{\text{ML}}^{(\mathbb{C}+\mathbb{C})} = M_c^L P \left(\frac{3}{2} + L \right) \tag{17.239}$$

$$C_{\text{ML}}^{(\mathbb{R} \lessgtr \mathbb{R})} = M_c^L, \tag{17.240}$$

where again, the number of complex multiplications and additions involved in actually calculating the Euclidean norm $||.||_2^2$ has been weighted with a factor of $\frac{1}{2}$, because the multiplication of a complex number with its conjugate complex value inflicts two real-valued multiplications[22]. Note however that the number of multiplications $M_c^L P L$ required in the context of evaluating the term $\mathbf{H}\check{\mathbf{s}}$ in Equation 17.223 for the M_c^L number of different trial vectors can be reduced to $M_c P L$ by evaluating $\mathbf{H}^{(l)} \check{s}^{(l)}$, $\check{s}^{(l)} \in \mathcal{M}_c$, $l = 1, \ldots, L$ and storing the resultant vectors in a lookup table. A similar technique could also be applied for reducing the number of complex multiplications in the context of the transform-based ML detection technique of Section 17.3.3.2, as it will be discussed in the next section.

---

[22]$(a_x + j a_y) \cdot (a_x - j a_y) = a_x^2 + a_y^2$

17.3.3.5.2 Complexity of Transform-Based ML Detection The transform-based ML detection technique of Equation 17.229 capitalized on the LS estimate $\hat{s}_{LS}$ of the vector $\mathbf{x}$ of signals received by the different antenna elements. This estimate was provided with the aid of Equation 17.224 which employs the projection matrix $\mathbf{P}_{LS}$ given by Equation 17.225. Furthermore, in the transform-based ML detection process obeying Equation 17.229 explicit knowledge of the error- or noise covariance matrix $\mathbf{R}_{\Delta\hat{s}_{LS}}$ given by Equation 17.213, was required for describing the statistical properties of the LS combiner's vector of output signals.

Hence, it is a reasonable strategy to determine the error covariance matrix $\mathbf{R}_{\Delta\hat{s}_{LS}}$ first with the aid of Equation 17.213. This imposes a computational complexity given by:

$$C^{(\mathbb{C}*\mathbb{C})}_{\text{ML-trf,err-cov}} = C^{(\mathbb{C}+\mathbb{C})}_{\text{ML-trf,err-cov}} = PL^2 + \frac{4}{3}L^3, \qquad (17.241)$$

where the second term accounts for performing the direct inversion in Equation 17.213 with the aid of the LU decomposition [90]. Specifically, the LU decomposition [90] itself requires a complexity of $\frac{1}{3}L^3$ complex multiplications and additions, while the ensuing forward- and backward substitutions as outlined in [90] contribute another $L \cdot L^2$ number of complex multiplications and additions. The LU decomposition technique is only used here for a baseline comparison - more efficient techniques of performing the matrix inversion are known from the literature. Common to most of these matrix inversion techniques is that they are associated with a complexity order of $\mathcal{O}(m^3)$, where m is the dimension of the square matrix to be inverted.

Generating the LS estimate $\hat{s}_{LS}$ of the vector $\mathbf{s}$ of transmitted signals with the aid of Equations 17.224 and 17.225, where the latter can be simplified upon substituting the expression of Equation 17.213 derived for the error covariance matrix $\mathbf{R}_{\Delta\hat{s}_{LS}}$ imposes an additional complexity of:

$$C^{(\mathbb{C}*\mathbb{C})}_{\text{ML-trf,LS-est}} = C^{(\mathbb{C}+\mathbb{C})}_{\text{ML-trf,LS-est}} = PL + L^2. \qquad (17.242)$$

The major part of the computational complexity, however, is imposed - similarly to standard ML detection - by evaluating the M_c^L number of possible trial vectors $\check{s} \in \mathcal{M}^L$ with the aid of Equation 17.229. This inflicts an additional number of operations given by:

$$C^{(\mathbb{C}*\mathbb{C})}_{\text{ML-trf,trial}} = M_c^L L \left(\frac{1}{2} + L\right) \qquad (17.243)$$

$$C^{(\mathbb{C}+\mathbb{C})}_{\text{ML-trf,trial}} = M_c^L L \left(\frac{3}{2} + L\right) \qquad (17.244)$$

$$C^{(\mathbb{R}\lessgtr\mathbb{R})}_{\text{ML-trf,trial}} = M_c^L. \qquad (17.245)$$

Upon combining the different contributions quantified in this section, the total complexity of

the transform-based ML detector becomes:

$$C_{\text{ML-trf}}^{(\mathbb{C}*\mathbb{C})} \quad = \quad PL + (P+1)L^2 + \frac{4}{3}L^3 + M_c^L L \left(\frac{1}{2} + L \right) \tag{17.246}$$

$$C_{\text{ML-trf}}^{(\mathbb{C}+\mathbb{C})} \quad = \quad PL + (P+1)L^2 + \frac{4}{3}L^3 + M_c^L L \left(\frac{3}{2} + L \right) \tag{17.247}$$

$$C_{\text{ML-trf}}^{(\mathbb{R} \lessgtr \mathbb{R})} \quad = \quad M_c^L. \tag{17.248}$$

A comparison between the equations associated with the standard ML detector and the transform-based ML detector reveals that employing the latter is only recommended, when the number of users L is smaller than the number of reception antenna elements P, but even then it still depends on the particular scenario, whether the latter is really advantageous.

In conclusion, particularly in the context of the higher-order QAM modulation schemes, such as for example 16QAM and in conjunction with a relatively high number of simultaneous users the computational complexity might become prohibitive for the application of the ML detector.

17.3.3.5.3 Complexity of ML-Assisted Maximum Approximation Based Soft-Bit Generation

In this section the complexity of maximum approximation based soft-bit generation will be analysed which was discussed in Section 17.3.3.3.2. We argued that the soft-bit generation procedure commences by evaluating the Euclidean distance metric, which is part of Equations 17.223 and 17.237, for all the different vectors of symbols contained in the set $\mathcal{M}^L$. The computational complexity of this processing step expressed in terms of the number of complex multiplications and additions was already quantified in Equations 17.238 and 17.239. Additionally, a substantial number of comparisons has to be carried out between the real-valued metric values, which constitute an integral part of the search across the different subsets of symbols denoted by $\mathcal{M}_m^{b(l)L}$ according to Equation 17.237. As argued in Section 17.3.3.3.2, this complexity can be halved by determining in a first step the ML symbol estimate and its associated bit vector with the aid of Equation 17.223. This complexity is quantified in terms of the number of comparisons between real-valued metric values, as given by Equation 17.240, namely M_c^L. Furthermore, in the second step a $L \log_2 M_c$ number of search steps - where $\log_2 M_c$ is the number of bits per symbol - has to be conducted across a set of dimension $M_c^L/2$ each. Hence the total complexity is given by:

$$C_{\text{ML-soft}}^{(\mathbb{C}*\mathbb{C})} \quad = \quad C_{\text{ML}}^{(\mathbb{C}*\mathbb{C})} = M_c^L P \left(\frac{1}{2} + L \right) \tag{17.249}$$

$$C_{\text{ML-soft}}^{(\mathbb{C}+\mathbb{C})} \quad = \quad C_{\text{ML}}^{(\mathbb{C}+\mathbb{C})} = M_c^L P \left(\frac{3}{2} + L \right) \tag{17.250}$$

$$C_{\text{ML-soft}}^{(\mathbb{R} \lessgtr \mathbb{R})} \quad = \quad C_{\text{ML}}^{(\mathbb{R} \lessgtr \mathbb{R})} (1 + \frac{1}{2} L \log_2 M_c) \tag{17.251}$$

$$= \quad M_c^L (1 + \frac{1}{2} L \log_2 M_c) \tag{17.252}$$

$$C_{\text{ML-soft}}^{(\mathbb{R}+\mathbb{R})} \quad = \quad L \log_2 M_c, \tag{17.253}$$

where the contribution $C_{\text{ML-soft}}^{(\mathbb{R}+\mathbb{R})}$ accounts for performing the subtraction of the metric values as shown in Equation 17.236.

17.3.3.6 Summary and Conclusions on ML Detection

In Section 17.3.3 the ML detector was discussed, which is optimum from a statistical point of view. That specific vector $\check{\mathbf{s}}_{\text{ML}}$ of the different users' symbols is deemed to be optimum at the output of the ML detector, which exhibits the highest *a posteriori* probability of $P(\check{\mathbf{s}}_{\text{ML}}|\mathbf{x}, \mathbf{H})$ amongst the M_c^L number of trial-vectors contained in the set $\mathcal{M}^L$ defined by Equation 17.218. Recall from Section 17.3.3.1.2 that the *a posteriori* probability $P(\check{\mathbf{s}}_{\text{ML}}|\mathbf{x}, \mathbf{H})$ can be expressed with the aid of the Bayesian theorem of Equation 17.219, in terms of the *a priori* probability $P(\mathbf{x}|\check{\mathbf{s}}_{\text{ML}}, \mathbf{H})$, which is given by the multi-variate complex Gaussian distribution function, of Equation 17.216. Identifying the optimum trial-vector $\check{\mathbf{s}}_{\text{ML}}$ is equivalent to minimizing the Euclidean distance between the vector $\mathbf{x}$ of received signals and the trial-vector $\check{\mathbf{s}}$ transmitted over the MIMO channel described by the channel transfer factor matrix $\mathbf{H}$ for all trial-vectors contained in the set $\mathcal{M}^L$ as it was highlighted in Equation 17.223.

The computational complexity associated with this minimization process is potentially excessive, since all the number of M_c^L trial-vectors contained in the set $\mathcal{M}^L$ have to be compared to each other in terms of the Euclidean distance metric of Equation 17.223. Provided that the number of users L is lower than the number of BS reception antenna elements P, a reduction of the complexity can be achieved by transforming the vector $\mathbf{x}$ of received signals first to the trial-space with the aid of the linear transform of Equation 17.224, instead of transforming each trial-vector $\check{\mathbf{s}} \in \mathcal{M}^L$ separately to the received signal's space upon multiplication with the channel transfer factor matrix $\mathbf{H}$. These discussions were conducted in the context of Section 17.3.3.2.

Furthermore, in Section 17.3.3.3 the principles of ML detection-assisted soft-bit generation for employment in turbo-decoding were discussed, where a complexity reduction was achieved by applying the maximum approximation.

The ML detector's associated BER performance evaluated in the context of both a low-complexity, higher effective throughput uncoded- and a higher-complexity, lower-throughput turbo-coded scenario was the topic of Section 17.3.3.4. Specifically, in Section 17.3.3.4.1 the influence of the number of users L and the number of BS reception antennas P on the BER performance of 4QAM-modulated ML detection-assisted SDMA-OFDM was analysed. We found that as shown at the left-hand side of Figure 17.24 - regardless of the number of users L - upon increasing the number of reception antennas P, the ML detector's associated BER performance was significantly improved. This was a result of the increased grade of channel diversity available. Furthermore, as shown at the right-hand side of Figure 17.24 the ML detector also exhibited a high resilience against the increase of the number of users L. Specifically, for a scenario of $P = 4$ reception antennas the BER curves of one to six users were confined an narrow interval of about 2.5dB. This performance trend is in contrast to that observed for the linear combining based detectors, such as the LS and MMSE as well as SIC and PIC schemes, where a necessary condition of high integrity detection is that $L \leq P$. Furthermore, our BER performance results recorded for the turbo-coding based system were presented in Figure 17.25, as part of Section 17.3.3.4.2.

Finally our analysis of the ML detector's computational complexity was conducted in Section 17.3.3.5. Specifically, in Section 17.3.3.5.1 we analysed the complexity of standard

ML detection, where the number of complex multiplications and additions as well as real-valued comparisons was given by Equations 17.238, 17.239 and 17.240, respectively. As expected, these complexities were proportional to the number of vectors M_c^L contained in the trial-set $\mathcal{M}^L$. Furthermore, in Section 17.3.3.5.2 the complexity of transform-based ML detection was evaluated. The associated complexity formulae were given by Equations 17.246, 17.247 and 17.248. It was clear from these equations that the transform based ML detection may only be preferred against standard ML detection, if the number of users L is lower than the number of reception antennas P. Our analysis of the complexity of ML-assisted maximum approximation based soft-bit generation in Section 17.3.3.5.3 revealed that compared to standard ML detection the complexity quantified in terms of the number of real-valued comparisons due to comparing the values of the Euclidean distance metric across subsets of the set $\mathcal{M}^L$ of trial-vectors is significantly increased.

17.3.4   Final Comparison of the Different Detection Techniques

In this section a final comparison of the different linear- and non-linear detection techniques namely, that of the MMSE, standard SIC, M-SIC, PIC and ML schemes will be carried out, which were described and characterized in Sections 17.2.3, 17.3.1.1, 17.3.1.2, 17.3.2 and 17.3.3, respectively. Again, as in previous sections, our comparison will focus on the system's BER performance in both an uncoded- and a turbo-coded scenario, which will be the topic of Section 17.3.4.1. By contrast in Section 17.3.4.2 a comparison between the different detectors' complexities will be carried out.

17.3.4.1   BER Performance Comparison of the Different Detection Techniques in Uncoded and Turbo-Coded Scenarios

In Figure 17.26 we have compared the different detectors' SDMA-OFDM related BER performance, at the left-hand side for the uncoded scenario and at the right-hand side for the turbo-coded scenario.

   Let us first of all focus our attention on the uncoded scenario. As expected, the best performance is exhibited by the most complex ML detector, closely followed by the M-SIC scheme, where $M = 2$. By contrast, a significant BER degradation is observed for the standard SIC scheme potentially as a result of the effects of error propagation through the different detection stages, a phenomenon which was analysed in Section 17.3.1.4.2. The second worst performance is exhibited by the PIC arrangement, while a further degradation by about 1.25dB is incurred upon employing the rudimentary MMSE detection, as argued earlier in Section 17.3.2.3.1. Specifically, the PIC detector's performance was impaired by the lower-power users, potentially propagating errors to those users, which benefitted from a relatively high SNR at the first-stage combiner output. An attractive approach of significantly improving the PIC detector's performance in the context of an SDMA-OFDM system is that of employing channel decoding after the first detection stage, as it was suggested in Section 17.3.2.2.

   Let us now summarize our observations inferred in the context of the turbo-coded scenario, portrayed at the right-hand side of Figure 17.26. Again, the SDMA-OFDM system exhibits the best BER performance in the context of employing soft-bit values, which are generated with the aid of the ML-related metric of Section 17.3.3.3. Note that here we em-
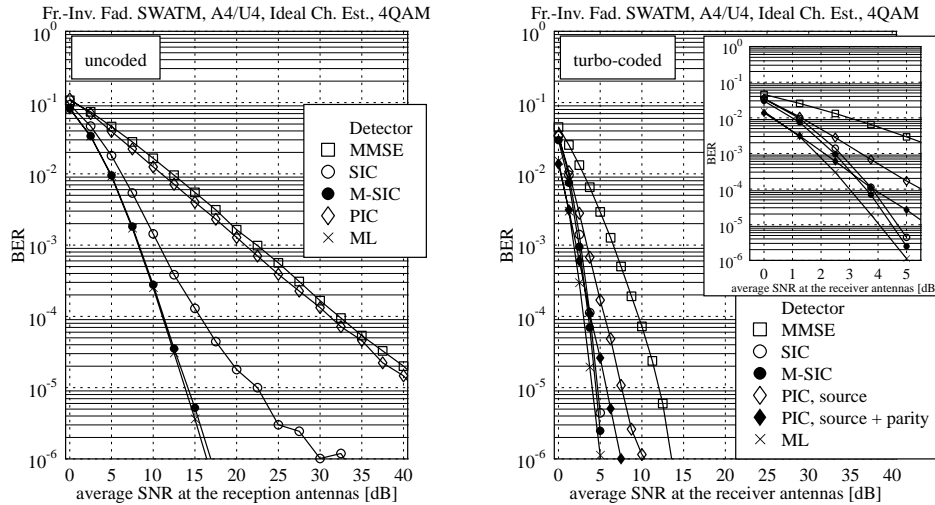
Figure 17.26: BER performance of (left): uncoded and (right:) turbo-coded, 4QAM-modulated, MMSE, standard SIC, M-SIC (M=2), PIC and ML detection assisted SDMA-OFDM as a function of the SNR at the reception antennas; in the context of the turbo-coded scenario both a PIC scheme capitalizing on a 'source'-related reference and a 'source-plus parity'-related reference are compared against each other; $L = P = 4$ simultaneous users and reception antennas were employed; for the list of basic simulation- and turbo-coding parameters we refer to Tables 17.3 and 17.4, respectively.

ployed the simplified, maximum-approximation based formula of Equation 17.236. By contrast, a modest SNR degradation of only around 0.6dB is observed for the M-SIC (M=2) and of about 0.8dB for the standard SIC scheme, both recorded at a BER of 10^{-4}. Again, the SIC detector's soft-bit values were generated with the aid of the weighted soft-bit metric of Equation 17.133. These performance trends are closely followed by the BER performance evaluated in the context of PIC aided soft-bit generation, where we have compared two different approaches of generating the PIC-related remodulated reference- or feedback signals against each other. Recall from Section 17.3.2.3.2 that the 'source'-related reference generation implied slicing, reencoding, interleaving and remodulating the 'source'-related *a posteriori* soft-output bits of the turbo-decoder. By contrast, the 'source- plus parity'-related remodulated reference implied slicing, interleaving and remodulating the 'source- plus parity'-related *a posteriori* soft-output bits of the turbo-decoder. The performance degradation of the 'source-plus parity'-related reference assisted PIC scheme compared to standard SIC is observed in Figure 17.26 to be about 1dB, while for the 'source'-related reference assisted PIC scheme an SNR degradation of 2.8dB is observed compared to standard SIC. Again, for MMSE detection-assisted SDMA-OFDM the worst performance is observed, namely an additional SNR degradation of about 4.3dB, compared to the 'source'-related reference assisted PIC
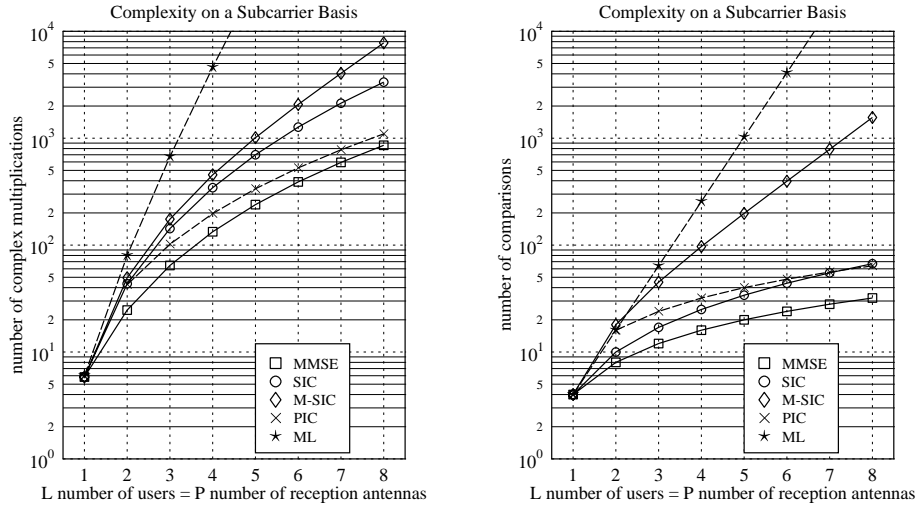
Figure 17.27: Complexity of the MMSE, standard SIC, M-SIC, PIC and ML detection schemes in terms of (left:) the $C^{(\mathbb{C}*\mathbb{C})}$ number of complex multiplications and (right:) the $C^{(\mathbb{R}\lessgtr\mathbb{R})}$ number of real-valued comparisons on a subcarrier basis, as a function of the number of simultaneous users L, which was assumed here to be equal to the number of reception antennas P; specifically for M-SIC the number of tentative symbol decisions per detection node was equal to $M = 2$, while in all scenarios $M_c = 4$ constellation points were assumed, which is for example the case in the context of 4QAM modulation.

arrangement.

17.3.4.2 Complexity Comparison of the Different Detection Techniques

Having compared the various detection techniques, namely MMSE, SIC, M-SIC, PIC and ML in terms of the associated system's BER performance, in this section we will compare them with respect to their computational complexity. Here we will concentrate on the previously introduced two measures of complexity namely, the number of complex multiplications, as well as the number of comparisons between real-valued variables, which occur in the process of demodulation and during the selection of the most dominant user in each of the SIC's detection stages. In the context of our evaluations the number of constellation points associated with the modulation scheme employed was assumed to be $M_c = 4$, which is the case for example in 4QAM modulation, while for the M-SIC the number of symbols retained at each detection node was $M = 2$.

Specifically, at the left-hand side of Figure 17.19 we have compared the MMSE[23], stan-

---

[23]The LS detector's complexity has not been portrayed here explicitly, since it is only marginally less complex than the MMSE detector.

	MMSE	std. SIC	M-ass. SIC	PIC	ML
$C^{\mathbb{C}*\mathbb{C}}$	133.3̇3̇	344.58	454.58	197.3̇3̇	4608
$C^{\mathbb{C}+\mathbb{C}}$	135.3̇3̇	335.3̇3̇	467.3̄3̄	233.3̇3̇	5632
$C^{\mathbb{C}\lessgtr\mathbb{C}}$	16	25	97	32	256

Table 17.8: Computational complexity of the different detection schemes, namely MMSE, standard SIC, M-SIC, PIC and ML detection quantified in terms of the number of complex multiplications and additions $C^{\mathbb{C}*\mathbb{C}}$, $C^{\mathbb{C}+\mathbb{C}}$ as well as the number of real-valued comparisons $C^{\mathbb{R}\lessgtr\mathbb{R}}$ for a scenario of $L = P = 4$ simultaneous users- and reception antennas; specifically for M-SIC the number of tentative symbol decisions per detection node was equal to $M = 2$, while in all scenarios $M_c = 4$ constellation points were assumed, which is for example the case in conjunction with 4QAM modulation.

dard SIC, M-SIC, PIC and the ML detection schemes in terms of the number of complex multiplications $C^{\mathbb{C}*\mathbb{C}}$ incurred on a subcarrier basis, as a function of the number of simultaneous users L, which was assumed here to be equal to the number of reception antennas P. The curves associated with the different detection techniques were generated with the aid of the complexity formulae given by Equations 17.115, 17.157, 17.173, 17.208 and 17.238, respectively. As expected, the lowest computational complexity expressed in terms of the number of multiplications is exhibited by the MMSE detector, followed by PIC, standard SIC and M-SIC, while the highest complexity is exhibited by the optimum ML detector.

Similar observations can also be made for the computational complexity quantified in terms of the number of comparisons between real-valued numbers $C^{(\mathbb{R}\lessgtr\mathbb{R})}$, as portrayed at the right-hand side of Figure 17.27. Here the associated complexity formulae were given for the MMSE, standard SIC, M-SIC, PIC and ML detection schemes by Equations 17.117, 17.159, 17.176, 17.210 and 17.240, respectively. We observe a similar ranking of the different detectors in terms of their associated complexity, as previously seen at the left-hand side of Figure 17.27 in terms of the associated performance. An exception is given by the number of comparisons associated with the PIC detector, which was found to be higher in the context of lower-order SDMA scenarios than for the standard SIC detector. The reason for this trend is that the PIC detector's complexity is increased compared to that of the MMSE detector, since the demodulation of each user's signal has to be performed twice, namely during the first- and the second detection stage. By contrast, the complexity of the standard SIC is increased compared to MMSE, since in each detection stage the most dominant user has to be selected from the set of remaining users.

The number of complex additions associated with the different detectors has not been illustrated here, since these values were found only to differ slightly from those characterizing the number of complex multiplications.

In order to further support our comparison of the different detectors in terms of their associated computational complexity, we have summarized in Table 17.8 the number of complex multiplications and additions, as well as real-valued comparisons imposed in a scenario of $L = 4$ simultaneous users and $P = 4$ reception antenna elements.

17.4   Performance Enhancement

The BER reduction observed in the context of turbo-coded SDMA-OFDM in conjunction with various detection techniques, namely MMSE, SIC, PIC and ML detection in Sections 17.2.6.4, 17.3.1.4.7, 17.3.2.3.2 and 17.3.3.4.2 was achieved at the cost of a substantial reduction of the system's effective throughput, namely by 50% upon employing half-rate turbo-coding. This loss in throughput could have however been compensated upon employing a higher-order modulation scheme, namely 16QAM instead of 4QAM, thus further increasing the computational complexity. Obviously there is a trade-off between the BER performance, the throughput and the computational complexity.

In this section we will study potential techniques for further enhancing the BER performance of SDMA-OFDM on the uplink channel to the basestation, *without* reducing the system's effective throughput. The techniques envisaged are constant throughput adaptive modulation as well as Walsh-Hadamard Transform (WHT) spreading across the different subcarriers. Both of these techniques have been recognized as being effective for exploiting the diversity offered by a wideband channel. Specifically adaptive modulation has widely been discussed in the context of single-user OFDM systems, namely in [2], and furthermore it was also successfully employed in conjunction with decision-directed channel prediction in Section 15.4. On the other hand, spreading the transmitted signal by means of orthogonal codes has been extensively discussed in the context of single- and multi-carrier CDMA systems, potentially supporting multiple simultaneous users. In our contribution however, spreading is employed for further exploiting the channel's diversity potential, while multiple users are supported with the aid of the multiple BS receiver antennas.

The further structure of this section is as follows. In Section 17.4.1 adaptive modulation assisted SDMA-OFDM- or in short form SDMA-AOFDM will be discussed. We will then embark in Section 17.4.2 on a discussion of WHT spreading assisted SDMA-OFDM- or again, in short form SDMA-WHTS-OFDM.

17.4.1   Adaptive Modulation Assisted SDMA-OFDM

In order to commence our discussions, let us briefly review in the next section the concepts of adaptive modulation as employed in the context of a single-user OFDM scenario.

17.4.1.1   Outline of the Adaptive Single-User Receiver

Adaptive modulation employed in single-user OFDM systems has previously been discussed in Section 15.4 in the context of our assessment of channel transfer function prediction techniques. Recall that invoking adaptive modulation was motivated by the observation that the BER performance of an OFDM modem, which employs a fixed-mode modulation scheme is severely degraded due to the deep frequency-domain channel transfer function fades experienced. This deficiency of the fixed-mode modems may be mitigated by assigning a more robust, but lower throughput modulation mode to those subcarriers, which are severely affected by the deep fades. By contrast, a potentially less robust, but higher throughput modulation mode may be assigned to the higher quality subcarriers.

A prerequisite of performing the modulation mode assignment during the n-th uplink[24]

---

[24]Unless otherwise stated, we refer to 'uplink OFDM symbol period' simply as 'OFDM symbol period'.

OFDM symbol period for employment during the $(n + 1)$-th OFDM symbol period is the availability of a reliable estimate of the channel transfer function to be experienced by the OFDM symbol received during $(n + 1)$-th OFDM symbol period. The simplest approach to subcarrier channel quality estimation would be to employ the pilot-based- or decision-directed channel estimate[25] for the n-th OFDM symbol period as an *a priori* estimate of the channel experienced during the $(n + 1)$-th OFDM symbol period. However, as shown in Section 15.4 depending on the OFDM symbol normalized Doppler frequency of the channel this *a priori* estimate may result in an inaccurate assignment of the modulation modes to the different subcarriers, which is a consequence of the channel variations incurred between the two OFDM symbol periods.

A significant improvement leading to a more accurate *a priori* channel estimate for the $(n + 1)$-th OFDM symbol period could however be achieved with the aid of the decision-directed Wiener-filter based channel prediction techniques discussed in Section 15. As a result of the modulation mode adaptation portrayed the BER performance of the AOFDM modem was observed in Figure 15.19 to be significantly improved compared to that of an OFDM modem having the same throughput, but using a fixed modulation mode. At the same time, relatively rapidly varying channels having a high OFDM symbol normalized Doppler frequency could be supported.

Motivated by the successful employment of constant throughput adaptive modulation techniques in the context of single-user OFDM systems, we will now investigate their potential for employment in multi-user SDMA-OFDM systems. We will focus our attention on employing a linear detector at the receiver, which exhibits the highest potential of achieving a significant BER performance improvement with the aid of adaptive modulation techniques.

The further structure of this section is as follows. Our discussions commence in Section 17.4.1.2 with the outline of the adaptive multi-user receiver's structure. This is followed in Section 17.4.1.3 by an assessment of the system's BER performance. Our summary and conclusions will be offered in Section 17.4.1.4.

17.4.1.2 Outline of the Adaptive Multi-User SDMA-OFDM Receiver

In Figure 17.28 we have portrayed the basic block diagram of the adaptive multi-user SDMA-OFDM receiver employed at the BS. During the n-th OFDM symbol period, after removing of the cyclic OFDM prefix- or guard interval, which is not shown here, the complex time-domain signals received by the P different BS antenna elements are independently subjected to the FFT, which delivers the frequency-domain- or subcarrier based representation of the signals received, namely $x_p[n, k]$, where $p = 1, \ldots, P$ and $k = 0, \ldots, K - 1$. Note that for notational convenience the subcarrier index k has been omitted in Figure 17.28.

The various signals $x_p[n, k]$ are then conveyed to the linear combiner, represented by Equation 17.7, which produces linear estimates $\hat{s}^{(l)}[n, k]$ of the signals transmitted by the L different users, namely $l = 1, \ldots, L$, separately for each subcarrier. The combiner weights were already generated during the $(n - 1)$-th OFDM symbol period for employment during the n-th OFDM symbol period.

The linear signal estimates $\hat{s}^{(l)}[n, k]$ are then conveyed to the adaptive classifiers, which deliver the sliced symbols $\check{s}^{(l)}[n, k]$ that are most likely to have been transmitted according to the Euclidean distance metric of Equation 17.94. Again, this classification takes place

---

[25] Again, we synonymously use the expressions 'channel estimate' and 'channel transfer function estimate'.
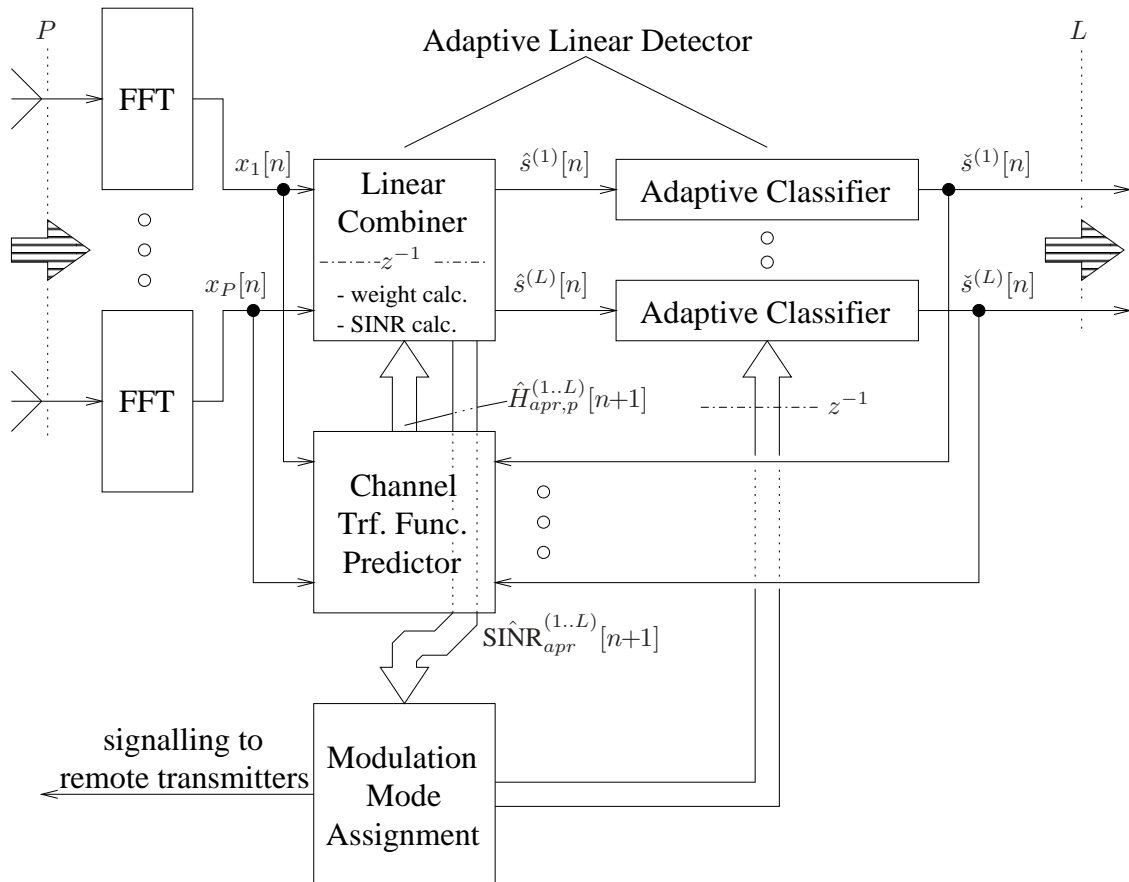
Figure 17.28: Block diagram of the adaptive multi-user SDMA-OFDM receiver, which is supported by a P-element antenna front-end in order to facilitate the separation of the L number of simultaneous users' associated signals at the BS's receiver. The subcarrier index k, where $k = 0, \ldots, K - 1$ has been omitted for reasons of simplicity.

separately for the different users $l = 1, \ldots, L$ and subcarriers $k = 0, \ldots, K - 1$. Note that the classifiers of the adaptive OFDM modem require side information concerning the subcarrier- or subband modulation mode assignment employed, which was generated during the previous OFDM symbol period and was locally stored at the receiver. The sliced symbols are then demapped to their bit-representation not shown in Figure 17.28, in order to obtain the bits transmitted.

Furthermore, the sliced symbols $\check{s}^{(l)}[n, k]$ of Figure 17.28 are conveyed together with the received subcarrier symbols $x_p[n, k]$ to the channel transfer function predictor, which generates the *a priori* estimates $\hat{H}^{(l)}_{apr,p}[n + 1, k]$ of the channel transfer factors $H^{(l)}_p[n + 1, k]$, associated with the $L \cdot P$ number of SDMA-MIMO channels portrayed in Figure 17.3 during the $(n + 1)$-th OFDM symbol period. However, these *a priori* channel transfer factor estimates $\hat{H}^{(l)}_{apr,p}[n+1, k]$ have already been employed during the n-th OFDM symbol period for generating the matrices $\hat{\mathbf{W}}_{apr}[n + 1, k]$, $k = 0, \ldots, K - 1$ of the combiner weights associated with the $(n + 1)$-th OFDM symbol period, upon invoking Equations 17.64 or 17.68[26].

Furthermore, the combiner weights are then employed in conjunction with Equation 17.24 for obtaining *a priori* estimates of the subcarrier-based SINRs, namely of $\hat{\text{SINR}}^{(l)}_{apr}[n + 1, k]$, potentially observed by the L different users at the linear combiner's output during the $(n+1)$-th OFDM symbol period. These *a priori* subcarrier SINR estimates are required for computing the different users' modulation mode assignments to be employed during the $(n + 1)$-th uplink OFDM symbol period. The algorithm used for performing the modem mode assignment was summarized earlier in Section 15.4.1.1. Note that the updated modulation mode assignment is conveyed to the remote transmitters during the next downlink OFDM symbol period.

17.4.1.3   Performance Assessment

In this section we will briefly assess the BER performance of MMSE detection-assisted SDMA-AOFDM. Again, we employed the indoor WATM system- and channel model of Section 14.3.1, where the fading was OFDM symbol invariant in order to avoid the obfuscating effects of inter-subcarrier interference.

Furthermore, perfect channel prediction was invoked, namely perfect knowledge of the channel transfer functions experienced during $(n + 1)$-th OFDM symbol period was made available during the n-th OFDM symbol period for calculating the MMSE combiner's weights to be employed during the $(n + 1)$-th OFDM symbol period. The number of BS receiver antennas P was equal to four. A total of 32 subbands each hosting 16 subcarriers was employed in the context of AOFDM, which capitalized on four modulation modes, namely 'no transmission', BPSK, 4QAM and 16QAM.

Our simulation results are portrayed in Figure 17.29. On the left-hand side of Figure 17.29 we have compared SDMA-OFDM using fixed 4QAM modulation against 32 Subband (Sb)-SDMA-AOFDM having the same throughput, namely 1024 Bit per OFDM Symbol (BPOS). Note that here we have neglected the signalling overhead required for transmitting side infor-

---

[26]Here the combiner weight matrix for a specific subcarrier is represented by $\hat{\mathbf{W}}_{apr}$ instead of $\mathbf{W}$ as in Equations 17.64 and 17.68, in order to indicate that its calculation is based on the imperfect estimates delivered by the *a priori* channel transfer function predictor.
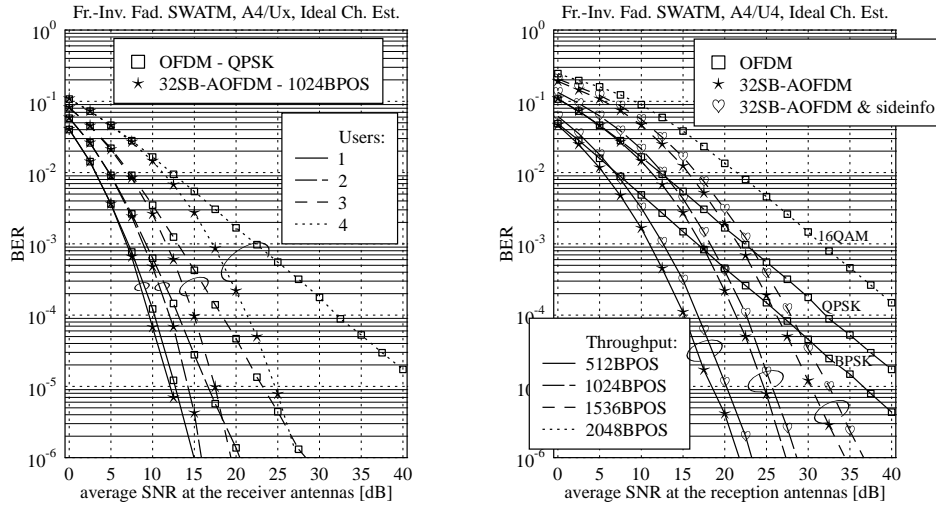
Figure 17.29: BER performance of MMSE detection-assisted SDMA-AOFDM as a function of the SNR recorded at the reception antennas. The curves are further parameterized with the number of simultaneous users L while the number of reception antennas P was fixed to four. Specifically, on the (left:) we have compared SDMA-OFDM using fixed 4QAM modulation to 32 Subband (Sb) AOFDM having the same throughput. Furthermore, on the (right:) we have compared SDMA-OFDM using fixed BPSK, 4QAM or 16QAM modulation to 32Sb-AOFDM having equivalent throughputs, upon once neglecting ('32Sb-AOFDM')- and once incorporating ('32Sb-AOFDM & sideinfo') the additional overhead required for transmitting side-information for the reverse link. Note that in the context of the 512-subcarrier indoor WATM system model of Section 14.3.1 employed here, fixed BPSK-, 4QAM- or 16QAM modulation assisted OFDM is associated with throughputs of 512, 1024 or 2048 Bit per OFDM Symbol (BPOS). Perfect channel transfer function prediction was employed.

mation related to the modulation mode assignment to be employed during the next downlink OFDM symbol period. The BER curves are parameterized with the number of users L. The highest beneficial impact of adaptive modulation is observed for a 'fully loaded' SDMA-AOFDM system, where the number of users equals the number of BS receiver antennas. The is because for a lower number of users the effective channel - namely the SDMA-MIMO channel concatenated with the linear combiner - experienced by the different users across the various subcarriers fluctuates less dramatically. The justification of this observation is that the linear combiner is capable of dedicating more of the channel's diversity potential to mitigating the serious frequency-domain channel fades, rather than to suppressing the interference imposed by the undesired co-channel users. As a result, the benefits of adaptive modulation are eroded.

Having found that adaptive modulation is rendered attractive only in the context of an almost fully loaded SDMA-OFDM scenario, we will now focus our attention further on the BER performance of 32Sb-SDMA-AOFDM in the context of a scenario of four simultaneous users and reception antennas. Here we have considered both cases, namely that where no side-information is transmitted as in the context of the results presented on the left-hand side of Figure 17.29, and that, where explicit side-information related to the modulation mode assignment to be used on the next downlink OFDM symbol period is received from the remote transmitters. Upon assuming that the AOFDM modem supports four modulation modes, namely 'no transmission', BPSK, 4QAM and 16QAM, a total number of two bits per subband are required. This number is increased to four bits upon assuming the employment of half-rate error-correction coding. Hence, in the context of 32Sb-SDMA-AOFDM the transmission overhead required for signalling the modulation mode assignment to be used on the reverse link is equal to 128 bit per OFDM symbol and user. Hence, for the effective system throughputs of 512, 1024 and 1536 BPOS the total target throughputs of the AOFDM modem are 640, 1152 and 1664 BPOS, respectively. From the BER curves shown at the right-hand side of Figure 17.29 we infer that in the context of the more realistic arrangement of transmitting explicit side-information the SNR required for attaining a specific BER is increased by a maximum of about 2dB, compared to the rather idealistic scenario, which neglects the transmission of side-information. Note furthermore that compared to the SDMA-OFDM schemes using fixed BPSK and 4QAM modulation modes, which support throughputs of 512 and 1024 BPOS the BER reduction achieved by AOFDM at a fixed SNR or equivalently, the SNR reduction attained at a specific BER is substantial. To provide an example, for a throughput of 1024 BPOS the SNR reduction due to employing SDMA-AOFDM compared to SDMA-OFDM using fixed 4QAM modulation is around 16dB at a BER of 10^{-5}, upon considering explicit side-information in the AOFDM transmissions.

17.4.1.4 Summary and Conclusions

In summary, in Section 17.4.1 we have described and characterized adaptive modulation assisted SDMA-OFDM. More specifically, in Section 17.4.1.1 adaptive modulation employed in single-user scenarios such as those described in Section 15.4 was briefly revisited. Furthermore, in Section 17.4.1.2 the architecture of multi-user SDMA-AOFDM receiver was detailed in the context of employing linear detection techniques, such as MMSE. Its simplified block diagram was shown in Figure 17.28. Our BER performance assessment was then conducted in Section 17.4.1.3. We found that the employment of adaptive modulation

in SDMA-OFDM is useful only in the context of an almost fully-loaded SDMA-OFDM scenario, where the number of users L approaches the number of receiver antennas P. Using the indoor WATM system- and channel parameters as described in Section 14.3.1, the SNR advantage owing to employing 32Sb-SDMA-AOFDM having an effective throughput of 1024 BPOS compared to SDMA-OFDM using fixed 4QAM modulation was around 16dB at a BER of 10^{-5} in the context of assuming perfect channel transfer function prediction.

In our further experiments, which are not explicitly described here for reasons of space economy, we found that PIC detection, which was discussed in Section 17.3.2 is also amenable to employment in conjunction with adaptive modulation techniques, resulting in a similar BER improvement as recorded in the context of MMSE detection. The modulation mode assignment to be used would be based on the SNR or SINR observed at the output of the linear combiner, which constitutes the first PIC stage, as it was shown in Figure 17.20. By contrast, in the context of the SIC detection scheme investigated in Section 17.3.1 the employment of adaptive modulation techniques turned out to be less attractive. This is because the effects of deep channel transfer function fades experienced by some of the subcarriers have already been mitigated by detecting in each SIC stage only the most dominant remaining user. Similarly, the advantages of adaptive modulation are also expected to erode in the context of ML detection. In the next section we consider an alternative frequency-domain fading counter measure, namely that of averaging the effects of fading, rather than accommodating them.

17.4.2   Walsh-Hadamard Transform Spreading Assisted SDMA-OFDM

Spreading the information symbols to be transmitted with the aid of orthogonal codes is the basis of supporting multiple-access capabilities in the context of single- and multicarrier CDMA (MC-CDMA) systems [483]. Instead of transmitting each complex symbol delivered by the modulator separately on a specific subcarrier in the context of multi-carrier OFDM modems, its influence is spread over several subcarriers with the aid of orthogonal multi-chip spreading codes. The advantage of employing orthogonal codes for performing the spreading is related to the resultant simple receiver design. A prominent class of orthogonal codes, which have been often used in CDMA systems is constituted by the family of orthogonal Walsh codes [483], which are particularly attractive, since the operation of spreading with the aid of these codes can be implemented in form of a 'fast' transform, which takes advantage of the codes' recursive structure, similarly to the FFT.

Note however, that in the context of our discussions presented in this section, we are more interested in spreading as a means of exploiting the wideband channel's diversity potential, rather than in its ability of supporting multiple users, since multiple users are supported in the context of the SDMA-OFDM receiver with the aid of the P-element antenna array and the associated detection techniques.

Due to the operations of spreading and despreading combined with MMSE based frequency-domain equalization the adverse effects of the low-SNR subcarriers on the average BER performance is potentially improved. This is a direct consequence of spreading, because even if the signal corresponding to a specific chip is obliterated by a deep frequency-domain channel fade, after despreading its effects are spread over the Walsh-Hadamard Transform (WHT) length. Hence there is a high chance of still recovering all the partially affected subcarrier symbols without errors.
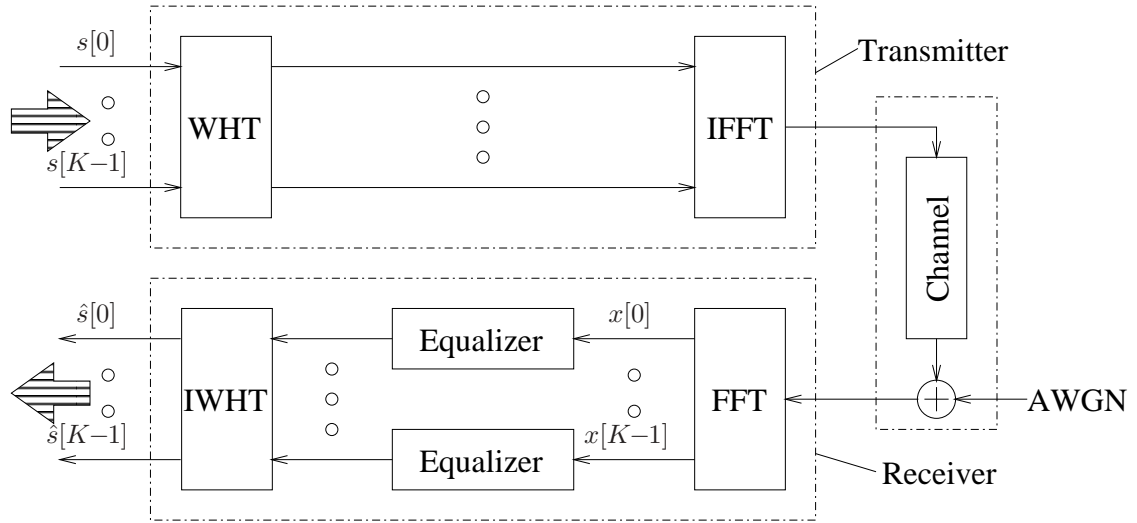
Figure 17.30: Simplified block diagram of the single-user WHTS-OFDM scenario. For reasons of notational simplicity the OFDM symbol index n and the static index $()_{MC}$ have been removed from the different variables.

The further structure of this section is as follows. In Section 17.4.2.1 the structure of the WHT spreading assisted single-user OFDM receiver is outlined. Specifically, we will demonstrate the separability of the operations of frequency-domain channel transfer factor equalization and despreading in the context of orthogonal codes. In Section 17.4.2.2 we will then describe the WHT spreading (WHTS) assisted multi-user SDMA-OFDM (SDMA-WHTS-OFDM) receiver's specific structure. The BER performance assessment of SDMA-WHTS-OFDM cast in the context of employing either MMSE- or PIC detection at the receiver will then be conducted in Section 17.4.2.3. Our conclusions will be offered in Section 17.4.2.4.

17.4.2.1 Outline of WHTS Assisted Single User OFDM Receiver

In Figure 17.30 we have portrayed the simplified block diagram of the single-user WHTS-OFDM transmission scenario. More specifically, at the top of Figure 17.30 the WHTS-OFDM transmitter is shown, which consists of WHT-assisted spreading, followed by the OFDM-related IFFT based modulator. The IFFT assisted modulator's output samples are then conveyed - upon neglecting here the further OFDM transmitter processing steps - through the stylized AWGN contaminated transmission channel, as shown at the right-hand side of Figure 17.30. The WHTS-OFDM receiver shown at the bottom of Figure 17.30 then performs the OFDM-related FFT-aided demodulation of the incoming signal samples, followed by subcarrier-based channel transfer factor equalization and despreading with the aid of the inverse WHT (IWHT). As we will show in the context of the forthcoming derivations, the separation of the WHTS-OFDM receiver into subcarrier-based equalization and despreading is a consequence of the orthogonality of the Walsh codes employed.

The further structure of this section is as follows. Our discussions commence in Section 17.4.2.1.1 with an outline of the WHT matrix's specific properties, namely its unitary nature. Furthermore, in Section 17.4.2.1.2 the WHTS-OFDM receiver's design will be outlined. We will highlight that due to the WHT matrix's unitary nature the processes of channel transfer function equalization and despreading can be conducted separately.

17.4.2.1.1 Properties of the Walsh-Hadamard Transform   The lowest-dimensional WHT from which the higher dimensional WHTs can be recursively derived, is given by the WHT_2 transform, which is described by the following unitary matrix:

$$\mathbf{U}_{\mathrm{WHT2}} = \frac{1}{\sqrt{2}} \begin{pmatrix} 1 & 1 \\ 1 & -1 \end{pmatrix}. \tag{17.254}$$

More generally, the N-th order WHT is given by the following recursive expression:

$$\mathbf{U}_{\mathrm{WHT}N} = \frac{1}{\sqrt{2}} \begin{pmatrix} 1 \cdot \mathbf{U}_{\mathrm{WHT}N-1} & 1 \cdot \mathbf{U}_{\mathrm{WHT}N-1} \\ 1 \cdot \mathbf{U}_{\mathrm{WHT}N-1} & -1 \cdot \mathbf{U}_{\mathrm{WHT}N-1} \end{pmatrix}, \tag{17.255}$$

as a function of the $(N-1)$-th order WHT matrix, namely $\mathbf{U}_{\mathrm{WHT}N-1}$. Note that the column vectors of matrix $\mathbf{U}_{\mathrm{WHT}N}$ represent the orthogonal Walsh code vectors, for which we have:

$$col_i\{\mathbf{U}_{\mathrm{WHT}N}\} \cdot col_j\{\mathbf{U}_{\mathrm{WHT}N}\} = \begin{cases} 1 & i = j \\ 0 & i \neq j \end{cases}. \tag{17.256}$$

This implies that $\mathbf{U}_{\mathrm{WHT}N}$ is an orthogonal matrix, namely that we have [90]:

$$\mathbf{U}_{\mathrm{WHT}N}^T \mathbf{U}_{\mathrm{WHT}N} = \mathbf{I}, \tag{17.257}$$

which therefore allows us to conclude that $\mathbf{U}_{\mathrm{WHT}N}$ is also unitary, satisfying [90]:

$$\mathbf{U}_{\mathrm{WHT}N}^H \mathbf{U}_{\mathrm{WHT}N} = \mathbf{I}. \tag{17.258}$$

The unitary property allows us to separate the signal processing at the receiver into the operations of subcarrier-based channel transfer factor equalization followed by despreading, as it will be demonstrated in the next section.

17.4.2.1.2 Receiver Design   The vector $\mathbf{x}[n] \in \mathbb{C}^{K \times 1}$ of complex signals observed in the K different subcarriers at the output of the receiver's FFT-based demodulation is given for the WHT-OFDM system portrayed in Figure 17.30 by:

$$\mathbf{x}[n] = \mathbf{H}[n]\mathbf{U}_{\mathrm{WHT}}\mathbf{s}[n] + \mathbf{n}[n], \tag{17.259}$$

where $\mathbf{H}[n] \in \mathbb{C}^{K \times K}$ is the diagonal matrix of subcarrier channel transfer factors, namely:

$$\mathbf{H}[n] = diag\left(H[0], H[1], \ldots, H[K-1]\right), \tag{17.260}$$

and $\mathbf{U}_{\text{WHT}} \in \mathbb{C}^{K \times K}$ is the unitary WHT matrix[27] of K-th order, which was defined by Equation 17.255. Furthermore, in Equation 17.259 $\mathbf{s}[n] \in \mathbb{C}^{K \times 1}$ denotes the vector of transmitted subcarrier symbols, namely:

$$\mathbf{s}[n] = (s[0], s[1], \dots, s[K-1])^T, \tag{17.261}$$

and $\mathbf{n}[n] \in \mathbb{C}^{K \times 1}$ is the vector of subcarrier-related AWGN samples, namely:

$$\mathbf{n}[n] = (n[0], n[1], \dots, n[K-1])^T. \tag{17.262}$$

Note that in the context of the above definitions we have omitted the OFDM symbol index $[n]$ for reasons of notational simplicity.

Equation 17.259 can be transferred into standard form, namely to:

$$\mathbf{x}[n] = \mathbf{H}_{\text{WHT}}[n]\mathbf{s}[n] + \mathbf{n}[n], \tag{17.263}$$

by considering the product of the diagonal channel matrix $\mathbf{H}[n]$ and the WHT matrix $\mathbf{U}_{\text{WHT}}$ as the effective channel matrix $\mathbf{H}_{\text{WHT}}[n] \in \mathbb{C}^{K \times K}$, namely by introducing:

$$\mathbf{H}_{\text{WHT}}[n] = \mathbf{H}[n]\mathbf{U}_{\text{WHT}}. \tag{17.264}$$

Note that Equation 17.263 exhibits the same structure as Equation 17.1, describing the SDMA-MIMO channel scenario on a subcarrier basis. Hence the same techniques can be invoked for recovering the vector $\mathbf{s}[n]$ of symbols transmitted over the K different OFDM subcarriers. These detection techniques were investigated in Sections 17.2 and 17.3 for recovering the symbols transmitted by the L different users on a subcarrier basis in the context of SDMA-OFDM.

Here we will focus our attention on the case of linear equalization, namely where an estimate $\hat{\mathbf{s}}[n] \in \mathbb{C}^{K \times 1}$ of the vector of transmitted subcarrier symbols $\mathbf{s}[n]$ is obtained by linearly combining the complex signals received in the different subcarriers, which are represented by the vector $\mathbf{x}[n]$. The combining can be achieved with the aid of the weight matrix $\mathbf{W}[n] \in \mathbb{C}^{K \times K}$, as shown in Equation 17.7, namely:

$$\hat{\mathbf{s}}[n] = \mathbf{W}^H[n]\mathbf{x}[n]. \tag{17.265}$$

In the context of the MMSE criterion we obtain - as demonstrated earlier in Equation 17.63 - the weight matrix $\mathbf{W}_{\text{MMSE}}[n] \in \mathbb{C}^{K \times K}$, which is given in its right-inverse related form as follows:

$$\mathbf{W}_{\text{MMSE}}[n] = (\mathbf{H}_{\text{WHT}}[n]\mathbf{P}_{\text{MC}}\mathbf{H}_{\text{WHT}}^H[n] + \sigma_n^2 \mathbf{I})^{-1}\mathbf{H}_{\text{WHT}}[n]\mathbf{P}_{\text{MC}}. \tag{17.266}$$

In Equation 17.266 the diagonal matrix $\mathbf{P}_{\text{MC}} \in \mathbb{R}^{K \times K}$ of transmit powers associated with the different subcarriers is given for an equal power allocation by:

$$\mathbf{P}_{\text{MC}} = \sigma_s^2 \mathbf{I}, \tag{17.267}$$

where σ_s^2 denotes the signal variance, and σ_n^2 is the AWGN variance. Upon substituting

---

[27]Note that here we have omitted the lower case index, which indicates the order of the WHT.

Equations 17.264 and 17.267 into Equation 17.266 we obtain the following equation for the weight matrix $\mathbf{W}_{\text{MMSE}}[n]$:

$$\mathbf{W}_{\text{MMSE}}[n] = \mathbf{E}_{\text{MMSE}}[n]\mathbf{U}_{\text{WHT}}, \tag{17.268}$$

where the *channel-related equalizer matrix* $\mathbf{E}_{\text{MMSE}}[n] \in \mathbb{C}^{K \times K}$ is given by:

$$\mathbf{E}_{\text{MMSE}}[n] = (\mathbf{H}[n]\mathbf{H}^H[n] + \frac{\sigma_n^2}{\sigma_s^2}\mathbf{I})^{-1}\mathbf{H}[n]. \tag{17.269}$$

This matrix describes the operation of the equalizer seen in Figure 17.30. Here we have capitalized on the unitary nature of the matrix $\mathbf{U}_{\text{WHT}}$, as reflected by Equation 17.258. Note that $\mathbf{E}_{\text{MMSE}}[n]$ given by Equation 17.269 is a diagonal matrix, where the k-th diagonal element is given by:

$$\mathbf{E}_{\text{MMSE}}[n]|_{(k,k)} = \frac{H[n,k]}{|H[n,k]|^2 + \frac{\sigma_n^2}{\sigma_s^2}}, \tag{17.270}$$

and where $H[n,k]$ is the k-th subcarrier's channel transfer factor. Upon substituting Equation 17.268 into Equation 17.265 the MMSE combining related vector $\hat{\mathbf{s}}_{\text{MMSE}}[n] \in \mathbb{C}^{K \times 1}$ of the transmitted subcarrier symbols' estimates is given by:

$$\hat{\mathbf{s}}_{\text{MMSE}}[n] = \mathbf{U}_{\text{WHT}}^H \mathbf{E}_{\text{MMSE}}^H[n]\mathbf{x}[n]. \tag{17.271}$$

Note in Equation 17.271 that the receiver's operation is separated into two steps. The first step is the subcarrier-based one-tap equalization, which is carried out by multiplying the FFT-based OFDM demodulator's output vector $\mathbf{x}[n]$ in Figure 17.30 by the Hermitian transpose of the diagonal matrix $\mathbf{E}_{\text{MMSE}}[n]$ of Equation 17.269. The second step is the IWHT based despreading based on multiplying with the unitary matrix $\mathbf{U}_{\text{WHT}}^H = \mathbf{U}_{\text{WHT}}$, which was also shown in Figure 17.30.

Following the philosophy of Equation 17.73 it can be demonstrated furthermore that the signal estimation MSE averaged over the different subcarrier-related components of $\hat{\mathbf{s}}_{\text{MMSE}}[n]$ is given by:

$$\overline{\text{MMSE}}_{\text{MMSE}}[n] = \sigma_s^2 \left(1 - \frac{1}{K}\sum_{k=0}^{K-1} H_{\text{MMSE}}[n,k]\right), \tag{17.272}$$

where the k-th subcarrier's effective 'channel' transfer factor $H_{\text{MMSE}}[n,k]$, includes both the effects of the channel and that of the one-tap equalization at the receiver, namely:

$$H_{\text{MMSE}}[n,k] = \frac{|H[n,k]|^2}{|H[n,k]|^2 + \frac{\sigma_n^2}{\sigma_s^2}}. \tag{17.273}$$

In the context of deriving Equation 17.272 we have exploited only that $\text{Trace}(\mathbf{U}^H\mathbf{A}\mathbf{U}) = \text{Trace}(\mathbf{A})$ for a unitary matrix $\mathbf{U}$ and for an arbitrary matrix $\mathbf{A}$ [472]. Note however that in the specific case of employing the WHT as the unitary transform, an estimation MSE identical

to that averaged over an OFDM symbol, namely that quantified by Equation 17.272 is also observed for each individual subcarrier. This could be shown by following the philosophy of Equation 17.74. Furthermore, it can be demonstrated that after IWHT assisted despreading, as seen in Figure 17.30 the subcarrier based SINR is identical for all the different subcarriers, which is given by:

$$\text{SINR}_{\text{WHT,MMSE}}[n] = \frac{\sigma^2_{S,\text{WHT,MMSE}}[n]}{\sigma^2_{I,\text{WHT,MMSE}}[n] + \sigma^2_{N,\text{WHT,MMSE}}[n]}, \tag{17.274}$$

where we have:

$$\sigma^2_{S,\text{WHT,MMSE}}[n] = \frac{1}{K^2}\left(\sum_{k=1}^{K} H_{\text{MMSE}}[n,k]\right)^2 \sigma^2_s \tag{17.275}$$

$$\sigma^2_{I,\text{WHT,MMSE}}[n] = \frac{1}{K^2}\left(\sum_{k=0}^{K-1}\left[(K-1)H_{\text{MMSE}}[n,k] - \sum_{\substack{k'=0\\k'\neq k}}^{K-1} H_{\text{MMSE}}[n,k']\right]H_{\text{MMSE}}[n,k]\right)\sigma^2_s \tag{17.276}$$

$$\sigma^2_{N,\text{WHT,MMSE}}[n] = \frac{1}{K}\left(\sum_{k=1}^{K} \frac{H_{\text{MMSE}}[n,k]}{\left(|H[n,k]|^2 + \frac{\sigma^2_n}{\sigma^2_s}\right)^2}\right)\sigma^2_n. \tag{17.277}$$

In the next section we will embark on describing the multi-user SDMA-WHTS-OFDM receiver.

17.4.2.2 Outline of the WHTS Assisted Multi-User SDMA-OFDM Receiver

In the previous section we have demonstrated in the context of a single-user WHTS-OFDM receiver that the operations of linear frequency-domain channel transfer factor equalization and despreading can be sequentially performed. Similar derivations can also be conducted in the context of the multi-user SDMA-WHTS-OFDM scenario, resulting in the receiver design shown in Figure 17.31. Following the design concepts of the multi-user SDMA-AOFDM receiver, shown in Figure 17.28, we have included a decision-directed channel transfer function predictor in Figure 17.31 for providing the channel estimates required by the linear combiner.

Again, as seen in Figure 17.31, blocks of K consecutive samples of the signals received by the P number of BS antenna elements are independently subjected to a K-point FFT, which yields the signal samples' frequency-domain representation, namely $x_p[n,k]$, $p = 1,\ldots,P$, $k = 0,\ldots,K-1$. Following this step linear combining is performed on a per subcarrier basis with the aid of Equation 17.7 in order obtain estimates $\hat{s}^{(l)}[n,k]$ of the signals $s^{(l)}[n,k]$ transmitted by the L different users, where $l = 1,\ldots,L$. Recall that the combiner matrix associated with the MMSE criterion was given in its right-inverse related form by Equation 17.63. Following the design concepts of the single-user WHTS-OFDM receiver shown in Figure 17.30, the linear signal estimates associated with the L different users are independently subjected to despreading by means of a K-point IWHT, which results in the despread signal estimates $\hat{s}^{(l)}_{\text{IWHT}}[n,k]$ of Figure 17.31. These are classified separately for each subcarrier and each user with the aid of Equation 17.94 in order to obtain the complex symbols $\check{s}^{(l)}[n,k]$ that are most likely to have been transmitted. In the context of the receiver
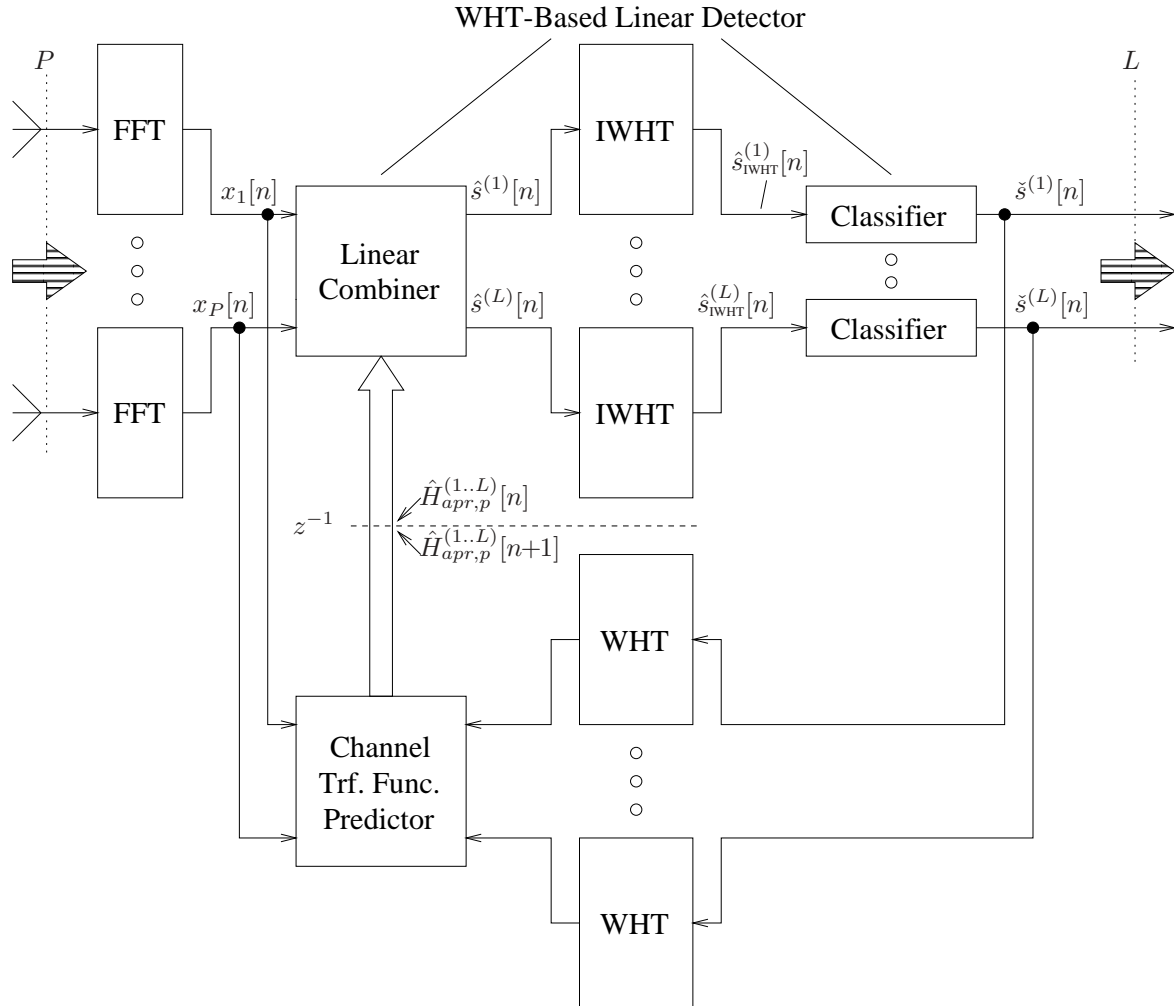
Figure 17.31: Block diagram of the linear combining assisted multi-user SDMA-WHTS-OFDM receiver, which is supported by a P-element antenna front-end in order to facilitate the separation of the L number of simultaneous users' associated signals at the receiver. Decision-directed channel transfer function prediction is performed in order to facilitate the separation of the different users' transmitted signals with the aid of the linear combiner. The subcarrier index k, where $k = 0, \ldots, K - 1$ has been omitted for reasons of notational simplicity.
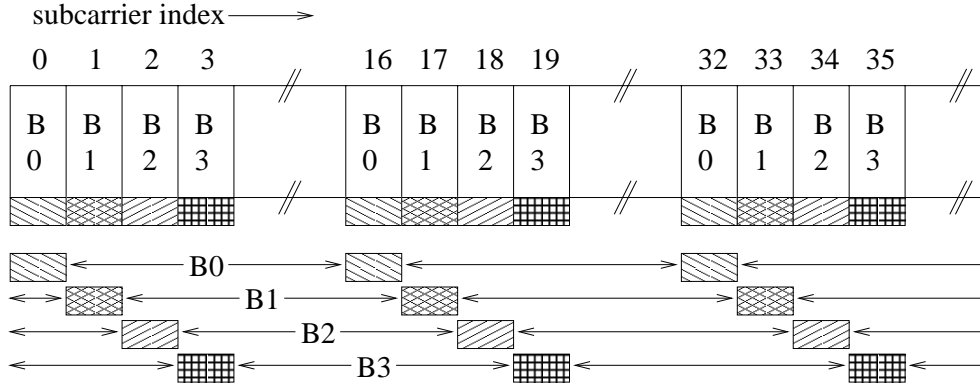
Figure 17.32: Illustration of WHT based subcarrier spreading using a limited WHT blocksize M_{WHT}, which is typically a fraction of the total number of subcarriers K hosted by the OFDM symbol for the sake of low implementational complexity.

design proposed here and depicted in Figure 17.31, *a priori* estimates of the channel transfer factors $H_p^{(l)}[n, k]$ employed in the calculation of the different subcarriers' weight matrices according to Equation 17.63 are again generated upon feeding back the current OFDM symbol's subcarrier symbol decisions, which are subjected to WHT based spreading in order to regenerate the complex symbols transmitted by the L different users in each subcarrier.

Since the employment of WHTs having a high transform length, such as for example 512, as required in case of the indoor WATM system model employed in our investigations in Section 17.4.2.3 would impose a high computational complexity, we partition the OFDM symbol into several WHTs as seen in Figure 17.32. This is also justified by the observation that most of the channel's frequency-domain diversity potential can be exploited with the aid of a relatively short spreading length, as illustrated in Figure 17.33. Furthermore, depending on the particular power delay profile of the channel, the OFDM symbol bandwidth of K subcarriers can be divided into K/M_{WHT} interleaved blocks of size M_{WHT} each, which are separately subjected to the WHT. More specifically, the i-th WHT block of an OFDM symbol contains subcarriers having indices j given by:

$$j = i + r \frac{K}{M_{\text{WHT}}}, \qquad 0 \le r \le M_{\text{WHT}} - 1, \tag{17.278}$$

where according to our definition both the first WHT block and the first OFDM subcarrier are represented by an index of zero. In Figure 17.32 we have further illustrated the operation of WHT based spreading applied to blocks of an identical size, where each block hosts only a fraction of the total number of subcarriers K associated with the OFDM symbol. More specifically, in this particular example the OFDM symbol is composed of 16 interleaved WHT blocks and the specific subcarriers, which are 16 frequency positions apart from each other belong to the same WHT block.
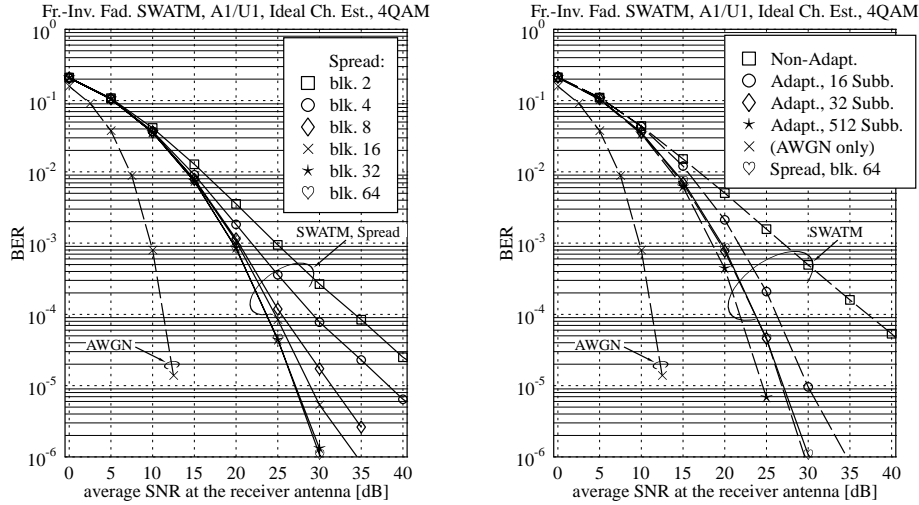
Figure 17.33: (Left:) BER performance of a WHT spreading assisted 4QAM modulated single reception antenna, single user OFDM system parameterised with the spreading blocksize. (Right:) BER performance comparison between a 4QAM modulated single reception antenna, single user standard OFDM system, an OFDM system employing four-mode ('no transmission', BPSK, 4QAM, 16QAM), constant-throughput, zero-delay signalling based adaptive modulation using 16 or 512 subbands, and a Walsh-Hadamard spreading assisted OFDM system. The simulations were conducted in the context of the 'frame-invariant' fading indoor WATM system- and channel model of Section 14.3.1. Ideal channel transfer function knowledge was assumed. The BER performance of 4QAM signalling over an AWGN channel has been plotted as a reference.

17.4.2.3 Performance Assessment

Our performance investigations of WHTS-OFDM are conducted separately for single- and multi-user OFDM scenarios. Specifically in Section 17.4.2.3.1 we will demonstrate the influence of the spreading code length on the WHTS-OFDM system's performance. Furthermore, a comparison between WHTS-OFDM and AOFDM is also carried out. Our investigations of multi-user SDMA-WHTS-OFDM cast in the context of MMSE- and PIC detection will then be conducted in Section 17.4.2.3.2.

17.4.2.3.1 Single-User WHTS-OFDM Simulation results have been obtained for the indoor WATM system- and channel model of Section 14.3.1. We commenced our investigations by assessing the impact of Walsh-Hadamard spreading using different spreading code lengths on the BER performance of a 4QAM single reception antenna, single user OFDM system in the indoor WATM channel environment. MMSE-based frequency domain channel equaliza-

tion, as described in Section 17.4.2.1.2, was performed at the receiver. The corresponding results are portrayed at the left-hand side of Figure 17.33. We observe that as a consequence of the residual 'multiple-access' interference imposed by the spread signals of the different subcarriers hosted by each WHT block, the BER performance is not particularly sensitive to the WHT block length, provided that it is in excess of 32 subcarriers for the SNRs of our interest. It should be noted that the benefit of spreading is directly related to the frequency-domain diversity potential offered by a specific dispersive channel. More specifically, the higher the channel's delay spread, the less separated are the frequency-domain fades, hence tolerating a lower WHT length, while achieving as high a randomization of the frequency-domain fading effects as possible.

In our next investigations we compared the BER performance of the WHT assisted OFDM system to a non-spread OFDM system and to an OFDM system employing adaptive modulation [2], under the constraint of having a target throughput equivalent to that of the fixed mode 4QAM modulated OFDM system. The modulation mode adaptation regime employed a total of four modes, namely 'no transmission', BPSK, 4QAM and 16QAM transmission. In order to reduce the signalling overhead required, the modulation modes were assigned on a subband basis, where each subband hosted either one or a number of subcarriers. Specifically, using one subcarrier per subband allowed us to determine the upperbound performance of the system. Furthermore, the best-case scenario of perfect channel transfer function knowledge was invoked in the process of determining the optimum modulation mode assignment. The corresponding simulation results are illustrated at the right-hand side of Figure 17.33. We observe that in the specific indoor WATM channel environment, assuming the separation of the total bandwidth into 32 equal-sized subbands, each hosting 16 subcarriers, the OFDM system employing adaptive modulation exhibits a similar performance to that of the spread OFDM system for a WHT blocksize of 64 subcarriers. By contrast, a hypothetic system assigning the best-matching individual modulation mode to each subcarrier outperformed the WHT OFDM scheme by about 2dB in terms of the required SNR. Hence, taking also into account the signalling overhead required by the adaptive modulation scheme, as well as its limited applicability restricted to relatively slowly varying channels in the absence of channel transfer function prediction techniques, we conclude that subcarrier spreading is a more convenient approach to exploiting the wideband channel's diversity potential.

17.4.2.3.2   Multi-User SDMA-WHTS-OFDM   Our further aim was to investigate the applicability of WHT based spreading in the context of an SDMA-OFDM system, where the signals of L simultaneous users each equipped with one transmission antenna are separated at the BS with the aid of a P-element antenna array. The design of the corresponding receiver was outlined in Section 17.4.2.2. In our investigations we invoked the MMSE- and PIC based multi-user detection approaches of Sections 17.2.3 and 17.3.2, while SIC described in Section 17.3.1 was not directly applicable to a spread OFDM system. This is because in a specific subcarrier or subband in each iteration the highest-power user is detected first, followed by the subtraction of its sliced and remodulated signal from the residual composite multi-user signal received by each antenna. Since the WHT based spreading is performed across subcarriers spaced apart from each other as far as possible for the sake of maximising the achievable frequency-domain diversity effect, these subcarriers would potentially require a different SIC detection order. Hence not all the symbols of a specific user contained in a WHT block are available at the same time for demodulation. Simulation results have been obtained for a two
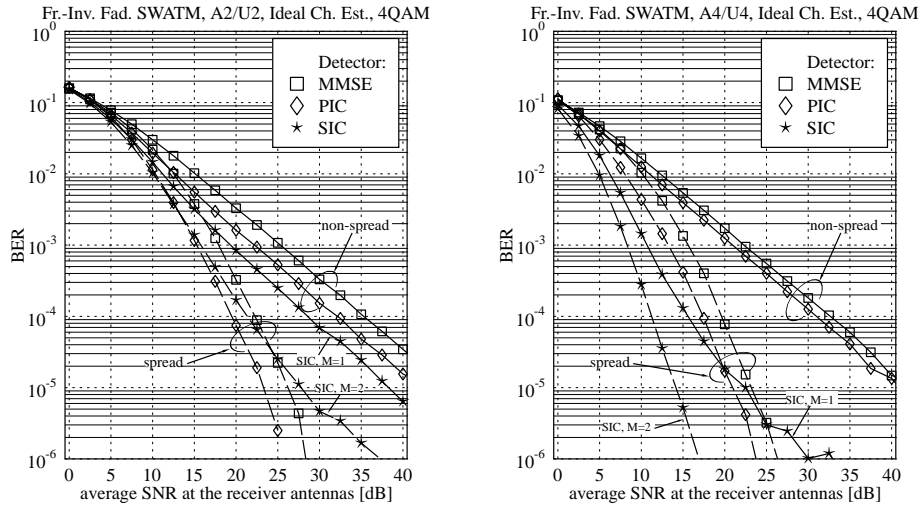
Figure 17.34: BER performance comparison between 4QAM modulated MMSE, PIC or SIC detection-
assisted SDMA-OFDM systems as a function of the SNR at the reception antennas,
(left:) for a $L = P = 2$ number of simultaneous users and reception antennas, while
(right:) for a $L = P = 4$ number of simultaneous users and reception antennas. The
systems employing MMSE and PIC multi-user detection were further assisted by Walsh-
Hadamard spreading using a blocksize of 16 subcarriers. Ideal channel transfer function
knowledge was assumed. The simulations were conducted in the context of the frame-
invariant fading indoor WATM system- and channel model described in Section 14.3.1.

reception antenna, two user SDMA scenario. The results are portrayed at the left-hand side
of Figure 17.34. We observe that both the MMSE and the PIC detector using WHT based
spreading outperform the M-SIC detector in the non-spread case, which tracked $M = 1$ or
$M = 2$ tentative symbol decisions from each detection node as shown in Figure 17.11. Note
that the least complex multi-user receiver, namely the MMSE detector performed about 2.5dB
worse on average, than PIC, which was also observed in the non-spread scenario. Again, by
contrast, in case of a four reception antenna, four user SDMA scenario characterized at the
right-hand side of Figure 17.34, the $(M = 2)$-SIC detector applied in the non-spread scenario
outperforms both spreading assisted arrangements, namely those employing MMSE and PIC
based detection. However, compared to the standard $(M = 1)$-SIC detector, at sufficiently
high SNRs both the MMSE and PIC detection assisted SDMA-OFDM systems exhibit a bet-
ter BER performance. This is achieved at a significantly lower complexity than that of the SIC
scheme, upon assuming that a 'fast' implementation of the WHT is employed for performing
the spreading.

17.4.2.4 Summary and Conclusions

In Section 17.4.2 WHT spreading assisted OFDM was discussed in the context of both single- and multi-user OFDM scenarios. Our discussions commenced in Section 17.4.2.1 with an outline of the WHTS-OFDM receiver's structure in the context of the single-user scenario. Specifically, in Section 17.4.2.1.1 the WHT's properties, namely its recursive structure, as reflected by Equation 17.255, which allows for a 'fast' implementation, similarly to the FFT, were described. Of further interest was the WHT matrix' unitary nature, as described by Equation 17.258, which follows from the orthogonality of the different Walsh code vectors. Next we highlighted in Section 17.4.2.1.2 that the unitary nature of the WHT matrix facilitates a particularly simple receiver design in the context of linear channel transfer function equalization. The block diagram of the single-user WHTS-OFDM receiver was shown at the bottom of Figure 17.30. Specifically, the IWHT based despreading was shown to be decoupled from the channel transfer factor equalization. This was also demonstrated in the context of the formal derivation of a linear estimate $\hat{\mathbf{s}}_{\text{MC,MMSE}}$ of the vector $\mathbf{s}_{\text{MC}}$ of signals transmitted in the K different subcarriers, which was formulated in Equation 17.271. Furthermore, we found that the signal estimation MSE at the receiver's output is identical for the different subcarriers, which was given by Equation 17.272. We also found that the SINR at the receiver's output, which is given by Equation 17.274, is identical for the different subcarriers.

In Section 17.4.2.2 we then embarked on the description of the multi-user SDMA-WHTS-OFDM receiver's structure shown in Figure 17.31, which followed the same design concepts as the single-user WHTS-OFDM receiver. Specifically the multi-user SDMA scheme employed a sequential equalization- or combining scheme, followed by WHT despreading, implemented separately for the different users. In order to reduce the computational complexity, we found that it was attractive to perform the spreading separately for K/M_{WHT} number of 'interleaved' blocks of size M_{WHT} subcarriers each, as it was shown in Figure 17.32, instead of implementing it for a single larger-size block of K subcarriers, without incurring a noticeable increase of the BER.

The evaluation of the single-user WHTS-OFDM and multi-user SDMA-WHTS-OFDM systems' BER performance was then carried out in Section 17.4.2.3. Specifically, in Figure 17.33 of Section 17.4.2.3.1 we found that already for relatively small spreading block lengths, namely 64 subcarriers per block employed in the context of the indoor WATM channel of Figure 14.3.1, the wideband channel's diversity can be exploited, while a further increase of the spreading length did not yield a significant BER improvement, as shown at the left-hand side of Figure 17.33. This was because by increasing the spreading block length, the channel transfer factors associated with neighbouring subcarriers contained in a block became more similar. Furthermore, our BER comparisons portrayed at the right-hand side of Figure 17.33 revealed that WHTS-OFDM is also more attractive than AOFDM. More explicitly, AOFDM is capable of slightly outperforming WHTS-OFDM, but only for an unrealistically high number of subbands, namely in excess of 64, when neglecting the transmission of side-information and by assuming perfect channel transfer function knowledge in the modulation mode assignment, the AOFDM is capable of slightly outperforming WHTS-AOFDM.

Our BER performance assessment of multi-user WHTS-OFDM was then conducted in the context of Figure 17.34 for scenarios of two BS reception antennas and two simultaneous users as well as for four reception antennas and four simultaneous users, as shown at the left-hand- and right-hand side of Figure 17.34, respectively. Various detection techniques

were compared against each other, namely MMSE, PIC and SIC detection, noting that in the context of the latter WHTS was not directly applicable. We found that in the lower-dimensional SDMA-OFDM scenario of two users both PIC- as well as MMSE detection-assisted SDMA-WHTS-OFDM are capable of outperforming $(M = 1)$- and $(M = 2)$-aided SIC detection-assisted SDMA-OFDM, while in the higher-dimensional SDMA-OFDM scenario $(M = 2)$-SIC detection-assisted SDMA-OFDM performed best, while at the same time exhibiting by far the highest complexity. By contrast, at sufficiently high SNRs $(M = 1)$-SIC detection-assisted SDMA-OFDM was outperformed by both PIC- as well as MMSE detection-assisted SDMA-WHTS-OFDM, while at the same time exhibiting a potentially far lower computational complexity, than the SIC detection-assisted systems.

17.5   Chapter Summary and Conclusions

In this section our summary and conclusions will be provided for this chapter, where we discussed a range of uplink detection techniques designed for multi-user SDMA-OFDM. The specific structure of this section is as follows. In Section 17.5.1 the motivation of employing of multiple reception antenna assisted SDMA receivers is reviewed, which is followed in Section 17.5.2 by a summary of the family of linear detection schemes. Our summary and conclusions related to the set of non-linear detection schemes will be offered in Section 17.5.3. Finally our overall comparison between the different detection schemes investigated will then be offered in Section 17.5.3.4. This is followed in Section 17.5.3.5 by our conclusions on the suite of performance enhancement techniques studied.

17.5.1   Review of the Motivation for Multiple Reception Antenna SDMA Receivers

During the past few decades a variety of Multiple Access (MA) techniques, such as Time Division Multiple Access (TDMA), Frequency Division Multiple Access (FDMA), Code Division Multiple Access (CDMA) have found favour in the various wireless communications systems. More recently Space Division Multiple Access (SDMA) has been proposed for supporting multiple users in OFDM-based communications system. In the context of the more conventional techniques, namely TDMA, FDMA and CDMA, both the mobiles as well as the basestation are typically equipped with a single transmit- and receive antenna, respectively. The access of the different users to the finite capacity transmission channel is then facilitated in TDMA by allowing each user to access the channel's entire bandwidth for a finite time duration, namely for the duration of a time-slot. By contrast, in FDMA we assign each user a frequency slot. Finally, in CDMA all users share the same frequency band and we facilitate the separation of the different users' transmitted signals with the aid of unique, user-specific spreading codes.

Alternatively, all users could potentially share the same frequency band, as in CDMA, and we could exploit for their separation that the different users' transmitted signals experience different channel transfer functions. The separation of the different users based on their unique channel transfer function constitutes the principle of a minimalistic SDMA scheme. More specifically, in the context of each of the flat-fading OFDM subcarriers, the channel matrix $\mathbf{H}$ associated with the scenario of $L > 1$ different users and $P = 1$ receiver antenna

is of unity rank. Hence, only the ML detector is capable of separating the different users' transmitted signals, upon inflicting a potentially large complexity.

In order to render SDMA amenable to employment of lower complexity linear combining-based multi-user detection techniques, such as the LS, MMSE, SIC and PIC detection arrangements discussed in Sections 17.2.2, 17.2.3, 17.3.1 and 17.3.2, respectively, a viable strategy is to increase the P number of receiver antennas, such that we have $P \geq L$. Hence the channel matrix $\mathbf{H}$ is of 'full rank' with respect to the number of users L. In other words, we have $L = rank(\mathbf{H})$, which facilitates the linear separation of the different users' transmitted signals based on their spatial signature. More specifically, the spatial signature of a particular user is constituted by the set of channel transfer factors between the user's single transmit antenna and the P number of different receiver antennas, again, upon assuming flat-fading channel conditions for each of the OFDM subcarriers. This Multiple-Input Multiple-Output (MIMO) channel scenario was further detailed in Section 17.1.3, where for simplicity we assumed that the fading experienced by each of the MIMO sub-channels associated with a specific transmitter-receiver antenna pair is independent from that of the other MIMO sub-channels.

Our more specific discussions of multi-user detection techniques applicable to SDMA-OFDM were separated into the subclasses of linear- and non-linear detection techniques of Sections 17.2 and 17.3, respectively. As argued in Sections 17.1.1 and 17.1.2 the rationale of this classification was that in the context of linear detection techniques, such as the LS- and MMSE detection schemes discussed in Section 17.2, no *a priori* knowledge of the remaining users' transmitted symbols is required for the detection of a specific user. However, in the case of the SIC, PIC and ML detection techniques discussed in Section 17.3, *a priori* knowledge of the likely values of the symbol is involved, which must be provided by the non-linear classification or decision operation involved in the demodulation process.

17.5.2 Summary and Conclusions Related to Linear Detectors

The typical structure of a linear detector was highlighted in Figure 17.4. More specifically, in a first step linear estimates of the L different users' transmitted signals are obtained by appropriately combining the signals received by the P different antenna elements. In a next step these signal estimates are classified- or demodulated in order to determine the complex symbol- or constellation point that is most likely to have been transmitted by each user. As a result of the user signal separation facilitated with the aid of the linear combiner, the process of classification is substantially simplified compared to that of the multi-user ML detector discussed in Section 17.3.3. Instead of evaluating the multi-user Euclidean distance metric associated with the multi-user ML detector M_c^L number of times, in case of the linear detector the single-user Euclidean distance metric has to be evaluated LM_c number of times, which constitutes a complexity reduction. However, this complexity reduction is achieved at the cost of a significant performance degradation in the context of the linear detector compared to that of the optimum ML detector, since the effects of the residual interference contaminating the linear combiner's output signals are neglected by the former.

The linear combiner's associated weight matrix can be adjusted according to a number of different criteria. Explicitly, the Least-Squares (LS) error- and the Minimum Mean-Square Error (MMSE) criteria were investigated in Sections 17.2.2 and 17.2.3, respectively. More specifically, as it was detailed in Section 17.2.2, the LS detector's associated LS combiner

generates linear estimates of the signals transmitted by the different users based solely on the knowledge of the channel's frequency-domain transfer factors. In contrast to the LS combiner, the MMSE detector's associated MMSE combiner, which belongs to the class of Wiener-filter related combiners, as argued in Section 17.2.3.4, additionally capitalizes on statistical knowledge of the AWGN process, which contaminates the signals received by the P number of different antenna elements. As the terminology suggests, the MMSE combiner achieves the minimum signal estimation MSE. However, the transmitted signals to be estimated cannot be recovered with a unity gain, which is in contrast to the LS combiner. As argued in Section 17.2.3.5, this non-unity gain may be compensated by normalizing the MMSE combiner's output signals, at the cost of increasing the estimation MSE. The resultant normalized combiner weight vectors were identical to those of the MV combiner.

Our analysis of the LS- and MMSE detector's MSE and BER performance characterized in Section 17.2.6 underlined the MMSE detector's advantage compared to the LS detector in terms of achieving a lower signal estimation MSE and BER, as it was shown in Figure 17.6. Furthermore, we found that upon decreasing the number of simultaneous SDMA users L, while keeping the number of reception antennas P constant, the MMSE detector's performance quantified in terms of the SINR and BER was significantly improved, as it was shown in Figures 17.7 and 17.8. A further BER reduction was achieved with the aid of turbo-coding, as it was shown in Figure 17.9, although as usual, this was achieved at the cost of reducing each SDMA user's effective throughput, while also imposing further additional computational complexity.

Our detailed analysis of the different linear detectors' computational complexity provided in Section 17.2.7 revealed that the MMSE detector is slightly more complex than the LS detector. However, the general trend is that the complexity is proportional to the cube of the number of users L, as in case of LS detection or MMSE detection implemented in its left-inverse related form. A similar cubically proportional complexity dependence is valid also with respect to the number of reception antennas P, as in case of the MMSE detection implemented in its right-inverse related form.

For a more detailed summary and conclusions related to the family of linear detection techniques we refer to Section 17.2.8.

17.5.3   Summary and Conclusions Related to Non-Linear Detectors

Our summary and conclusions on non-linear detectors are separated into Sections 17.5.3.1, 17.5.3.2 and 17.5.3.3, considering SIC, PIC and ML detection, respectively.

17.5.3.1   SIC Detection

The employment of SIC detection was motivated earlier in the context of our performance analysis of MMSE detection in Section 17.2.6.3 by the specific observation that upon decreasing the number of simultaneous users L, while keeping the number of reception antennas P constant, the MMSE detector's BER performance was improved. This was because for a lower number of SDMA users the associated MMSE combiner was less constrained with respect to the specific choice of the combiner weights optimized for suppressing the interfering users' signal contributions. This allowed for a more effective noise mitigation. The same principle can be invoked in the context of an iterative detector, namely the standard SIC de-

tector of Figure 17.10, where in each iteration- or cancellation stage only the most dominant user having for example the highest SNR, SIR or SINR at the linear combiner's output was detected. The detected user's influence is eliminated from the partially decontaminated vector of signals received by the different antenna elements, upon invoking the detected user's remodulated signal. This principle was further detailed in Section 17.3.1.1.

In the context of the BER and SER performance results of Section 17.3.1.4 we found that the standard SIC detector suffers from the effects of error propagation across the different detection stages. In fact, it was observed that if a symbol error occurred in one of the lower-index detection stages, then there was a relatively high probability that symbol errors also occurred in the higher-index detection stages. By contrast, if correct symbol decisions were made in the lower-index detection stages, then the probability that an error occurred in one of the higher-index detection stages was lower, than for the lower-index detection stages. This was a consequence of the MIMO channel's increased diversity order in the context of the higher-index detection stages, following the removal of the signal contributions of those users, which had already been detected. In order to mitigate the effects of error propagation across the different detection stages, the standard SIC detector was appropriately modified.

More specifically, in the context of the M-SIC scheme discussed in Section 17.3.1.2 an $M > 1$ number of tentative symbol decisions are tracked from each detection node. Consequently, after the detection of the last user a decision has to be made as to which of the $M^{(i-1)}$ number of vectors of the different users' tentative symbols is most likely to have been transmitted. The significant performance advantage offered by M-SIC compared to standard SIC is achieved at the cost of an increased computational complexity, which is related to the additional number of 'decontamination'- and demodulation operations associated with the increased number of detection nodes involved.

Based on the observation that symbol error propagation events are predominantly triggered by the lower-index detection stages, as it was evidenced by Figure 17.16, a viable strategy of reducing the complexity of M-SIC is to restrict the employment of $M > 1$ number of tentative symbol decision per detection node to the lower-index detection stages, while at the higher-index detection stages employing $M = 1$. This strategy was discussed in Section 17.3.1.2.2 and it was termed partial M-SIC- or pM-SIC.

A further complexity reduction was achieved in Section 17.3.1.2.3 by restricting the employment of M-SIC- or partial M-SIC to those specific OFDM subcarriers, which exhibited a relatively low SINR during the first detection stage, while using standard SIC in conjunction with $M = 1$ in the subcarriers exhibiting a higher SINR. This strategy, which was initially proposed in [117, 137] was termed as Selective-Decision-Insertion M-SIC (SDI-M-SIC).

Our further discussions presented in Section 17.3.1.3 addressed the task of soft-bit generation in the context of standard SIC. While our rudimentary approach in Section 17.3.1.3.1 followed the philosophy of soft-bit generation contrived for the MMSE detection technique, as discussed in Section 17.2.5, the improved 'weighted' soft-bit metric of Section 17.3.1.3.2 additionally accounted for the effects of error-propagation across the different SIC stages. More specifically, in case of relatively unreliable symbol decisions generated during the previous SIC detection stages a viable strategy is to de-emphasize the soft-bits generated for the current detection stage by appropriately decreasing their value and thus indicating a low associated confidence.

The assessment of the BER and SER performance exhibited by the standard SIC, M-SIC, pM-SIC and SDI-M-SIC schemes was conducted in Section 17.3.1.4. Specifically, we found

in Figure 17.12 that the BER and SER performance of SIC- and M-SIC detection was significantly improved upon increasing the $L = P$ number of users and reception antennas of the 'fully loaded' SDMA-OFDM system. This is, because for a higher number of users, the SIC detector benefits from selecting the most dominant user from a larger 'pool' of different users at a specific detection stage, with the desirable effect of reducing the probability of incurring a low-SINR user as the most dominant user. Furthermore, in Figure 17.12 we found that upon employing M-SIC instead of standard SIC, a further substantial reduction of the BER or SER can be achieved. Using the SINR instead of the SNR recorded at the linear combiner's output in each detection stage for identifying the most dominant user yielded a noticeable BER or SER reduction, although only for SDMA scenarios, where the number of users and reception antennas was in excess of four. The effects of error propagation were detailed in Sections 17.3.1.4.2, 17.3.1.4.3 and 17.3.1.4.4. Furthermore, the SER performance of both pM-SIC and SDI-M-SIC was evaluated in Sections 17.3.1.4.5 and 17.3.1.4.6 with associated Figure 17.16. These schemes were employed for reducing the potentially substantial computational complexity associated with M-SIC. Specifically, in the context of an SDMA scenario supporting $L = 4$ simultaneous users with the aid of $P = 4$ reception antennas we found that employing $M = 2$ tentative symbol decisions per detection node during the first two detection stages ($L_{\text{pM-SIC}} = 2$) of pM-SIC, which was reduced to $M = 1$ symbol decision per detection node during the higher-index detection stages, results in an SNR degradation of approximately 1dB at an SER of 10^{-5}. This 1dB SNR degradation was the price of halving the computational complexity quantified in terms of the number of comparisons to be conducted, as it was shown with the aid of Figure 17.19. Our performance assessment of SDI-pM-SIC was the topic of Section 17.16, which demonstrated that in the context of the specific indoor WATM channel model of Section 14.3.1, SDI-pM-SIC yields the same SER performance as pM-SIC ($L_{\text{pM-SIC}} = 1$)[28], provided that in the context of SDI-pM-SIC pM-SIC is employed in the $N_{\text{SDI}}^{[1]} = 64$ number of lowest-SINR subcarriers recorded during the first detection stage, while using standard SIC in the remaining subcarriers. The performance assessment of the various SIC schemes was concluded with the evaluation of the BER performance exhibited by turbo-coded standard SIC detection-assisted SDMA-OFDM in Figures 17.17 and 17.18, which conveniently highlighted the benefits of the weighted soft-bit metric in comparison to the standard soft-bit metric, both of which were outlined in Section 17.3.1.3.

Finally, an analysis of the computational complexity exhibited by the various SIC schemes was carried out in Section 17.3.1.5. Specifically, in Figure 17.19 it was demonstrated that amongst the various successive interference cancellation based detectors the standard SIC detector is the least complex one, while M-SIC exhibits the highest complexity. A compromise between performance and complexity is constituted by the partial M-SIC scheme. For a more detailed summary and conclusions we refer to Section 17.3.1.6.

17.5.3.2 PIC Detection

The employment of the PIC detection scheme discussed in Section 17.3.2 was partially motivated by the SIC detector's potentially high complexity, which is related to the requirement of identifying the most dominant user - as well as recalculating the selected user's weight vector - in each detection stage, as outlined in Section 17.3.1. Furthermore, we found in the

---

[28]This implied using $M = 2$ tentative symbol decisions at the first detection stage, which was reduced to employing $M = 1$ symbol decision during the remaining detection stages.

context of SIC detection that the highest AWGN mitigation was achieved by the linear combiner employed in each of the SIC detection stages, during its last detection stage, following the successful removal of all interfering co-channel users' contributions.

As a consequence, the PIC scheme portrayed in Figure 17.20 was investigated. In the context of this arrangement tentative estimates of the different users' transmitted signals were generated with the aid of a linear combiner, which was the MMSE combiner of Section 17.2.3 in our specific case. These signal estimates were then demodulated in order to obtain tentative symbol decisions, which were remodulated and subtracted from the vector of signals received by the different antenna elements, upon taking into account the effects of the channel. As a result, a potentially interference-free vector of received signals was obtained for each user, provided that correct symbol decisions were made for the remaining users. Hence, the MMSE combiners, which were employed for obtaining improved signal estimates from the decontaminated array output vectors became then capable of more effectively suppressing the AWGN. This principle was further detailed in Section 17.3.2.1.

However, in the context of our performance study provided in Section 17.3.2.3 we found that in the absence of channel coding the detector performs only slightly better, than the MMSE detector. Specifically, in the context of the 'fully loaded' SDMA scenario of four reception antennas supporting four simultaneous SDMA users, as characterized in Figure 17.21, the SNR advantage of PIC detection over MMSE detection when aiming for maintaining a BER of 10^{-4} was as low as 1.25dB, while for a 'minimalistic' SDMA scenario of two reception antennas and two simultaneous users an SNR advantage of 3.03dB was observed at the same BER. The relatively modest SNR improvement of 1.25dB was related to the effect that if the symbol decisions obtained during the first detection stage were erroneous even for a single user, then during the PIC process of Figure 17.20 the remaining users' received signals were imperfectly decontaminated. This phenomenon had the effect of potentially incurring erroneous symbol decisions for all the other users as well during the following demodulation process.

In order to combat these effects it was proposed in Section 17.3.2.2 to combine the PIC detection scheme with turbo-decoding, incorporated into the classification module of Figure 17.20. A remodulated reference signal to be used in the PIC process may be generated based on the original information bit-positions or 'source'-related soft-output bits of the turbo-decoder, requiring the slicing, re-encoding and remodulation of these bits. Alternatively, the 'source- plus parity'-related soft-output bits may be sliced and remodulated, which exhibited a slight advantage in Figure 17.22 in terms of the system's BER performance. In order to render the associated BER simulation results presented in Figure 17.22 comparable to those of the other detectors we decided to equally split the total affordable number of PIC iterations into those employed during the first- and the second PIC stage. Compared to turbo-coded MMSE detection-assisted SDMA-OFDM a dramatic performance advantage was achieved with the aid of this arrangement, as it was shown in our final performance comparison of the different detection schemes portrayed in Figure 17.26.

A detailed complexity analysis of the PIC detector was conducted in Section 17.3.2.4 and based on these equations it became obvious in our final comparison of the different detectors' complexities quantified in Figure 17.27 that the PIC detector constitutes an attractive design compromise between the MMSE- and standard SIC detectors. For a more detailed summary and conclusions on PIC detection we refer to Section 17.3.2.5.

17.5.3.3 ML Detection

In Section 17.3.3 the optimum ML detector was described and characterized. As argued in Section 17.3.3.1, ML detection is based on the strategy of maximizing the *a posteriori* probability $P(\check{s}|\mathbf{x}, \mathbf{H})$ that a hypothetic 'L-user' vector of symbols $\check{s}$ was composed of the individual symbols transmitted by the L different users over a channel characterized by the matrix $\mathbf{H}$ defined in Equation 17.212, conditioned on the vector $\mathbf{x}$ of signals received by the P different antenna elements. The maximization of the likelihood metric was carried out over the entire set $\mathcal{M}^L$ of M_c^L number of hypothetic 'L-user' symbol vectors constituted by the L different users' M_c-ary constellations. With the aid of Bayes' theorem [90] and upon exploiting that the different symbol combination vectors were transmitted with equal probability, it was furthermore shown that maximizing the *a posteriori* probability $P(\check{s}|\mathbf{x}, \mathbf{H})$ is equivalent to maximizing the *a priori* probability $P(\mathbf{x}|\check{s}, \mathbf{H})$, which is the probability that the signal vector $\mathbf{x}$ was received by the different antenna elements, conditioned on transmitting the hypothetic 'L-user' symbol vector $\check{s}$. It was furthermore shown that the *a priori* probability $P(\mathbf{x}|\check{s}, \mathbf{H})$ is given by the multi-variate complex Gaussian distribution function $f(\mathbf{x}|\check{s}, \mathbf{H})$, which is defined by its vector of mean values and by its covariance matrix. Hence, it was argued that maximization of the *a priori* probability $P(\mathbf{x}|\check{s}, \mathbf{H})$ is equivalent to minimizing the argument of the exponential function of Equation 17.216 constituting the multi-variate complex Gaussian distribution function. This involved minimizing the Euclidean distance between the vector $\mathbf{x}$ of received signals and the hypothetic 'L-user' vector of transmitted signals $\check{s}$, upon taking into account the effects of the MIMO channel described by the channel matrix $\mathbf{H}$ of Equation 17.212, again for all trial-vectors contained in the set $\mathcal{M}^L$ of M_c^L number of 'L-user' symbol vectors.

As part of minimizing the multi-user Euclidean distance metric, each of the M_c^L different hypothetic trial-vectors $\check{s} \in \mathcal{M}^L$ has to be transformed to the received signal's space upon multiplication with the channel matrix $\mathbf{H}$ of Equation 17.212. It was demonstrated in Section 17.3.3.1 that if the number of simultaneous users L is significantly lower than the number of receiver antennas P, the associated complexity can potentially be reduced upon transforming each trial-vector first to the received signal's space with the aid of a linear transform, followed by evaluating a modified Euclidean distance metric. It was shown in Section 17.3.3.2 that a particularly suitable transform is the LS-related transform matrix of Equation 17.225, which delivers a noise-contaminated unity-gain estimate of the 'L-user' vector of transmitted signals, simplifying the Euclidean distance metric employed.

Furthermore, the generation of soft-bit values for turbo-decoding at the receiver was alluded to in Section 17.3.3.3 based on the assumption of employing a separate trellis decoding of the different users' signals.

The BER performance of both the uncoded and turbo-coded scenarios was then characterized in Section 17.3.3.4. Specifically, in Figure 17.24 we found for the uncoded scenario that the ML detector's performance is relatively insensitive to the number of users L, given a fixed number of reception antennas P. In contrast to the linear combining based detectors discussed in this chapter, even when increasing the number of users beyond the number of reception antennas, the performance degradation is graceful. Furthermore, we found that similarly to the SIC detector's behaviour recorded when increasing the number of reception antennas, the ML detector's BER performance was significantly improved owing to the higher degree of diversity provided by a MIMO system of a higher order. Again, for the turbo-coded

scenario we observed in Figure 17.25 a substantially improved BER performance compared to that of the uncoded scenario. For example, for the 'fully loaded' system of four reception antennas supporting four simultaneous users the BER at an SNR of 5dB was as low as 10^{-6}.

Our complexity analysis documented in Section 17.3.3.5 revealed that the ML detector's complexity is proportional to the M_c^L number of symbol combinations constituted by the L different users' M_c-ary trial symbols. For a more detailed summary and conclusions were refer to Section 17.3.3.6.

17.5.3.4 Overall Comparison of the Different Detection Techniques

Our final comparison of the different linear- and non-linear detection techniques in both uncoded- and turbo-coded scenarios was documented in Section 17.3.4. Specifically the achievable BER performance was documented in Figure 17.26, while the associated computational complexity, in Figure 17.27.

The essence of this comparison was that in all investigated scenarios - as expected - the ML detector constituted the best performing, but highest complexity solution, while the MMSE detector was the worst-performing, lowest-complexity solution.

A compromise in terms of performance and complexity was provided by the class of SIC detectors and its derivatives as documented in Section 17.3.1. While in the uncoded scenario of Figure 17.26 the M-SIC (M=2) scheme performed almost identically to the ML detector, a substantial performance degradation was observed in Figure 17.26 for the lower-complexity standard SIC detector. A trade-off between the performance and the complexity associated with the standard SIC and M-SIC schemes of Sections 17.3.1.1 and 17.3.1.2.1 was achievable with the aid of the partial M-SIC or SDI-M-SIC arrangements of Sections 17.3.1.2.2 and 17.3.1.2.3. The associated performance results were, however, not repeated in Figure 17.26. By contrast, in the turbo-coded scenario, both detectors, namely the standard SIC and M-SIC (M=2) schemes of Sections 17.3.1.1 and 17.3.1.2.1 performed within a range of 1dB in excess of the SNR required by turbo-coded ML detection-assisted SDMA-OFDM, when maintaining a specific BER.

While PIC detection was unattractive in the uncoded scenario, owing to its relatively modest BER improvement compared to MMSE detection, in the turbo-coded scenario a significant BER improvement was achieved. However, for the range of BERs of our interest, namely below 10^{-4}, the PIC detector's performance was worse than that of turbo-coded standard SIC. This was related to the imperfections of the soft-bit estimates employed and hence there is still some potential for its improvement. Note that this performance improvement was achieved, while exhibiting a lower complexity, than that of standard SIC.

17.5.3.5 Summary and Conclusions Related to Performance Enhancement Techniques

In order to render the less complex, but also less powerful detection techniques, such as MMSE and PIC also more attractive for employment in uncoded scenarios, the performance enhancement techniques of Section 17.4.1 may be invoked, which are well-known from the field of single reception antenna based communications systems. Specifically, constant throughput adaptive modulation as well as Walsh-Hadamard spreading using orthogonal spreading codes may be employed. While AOFDM capitalizes on the difference of the

different subcarriers' channel quality offered by the wide-band channel, spreading aims for averaging the subcarriers' quality differences.

17.5.3.5.1 Adaptive Modulation Assisted SDMA-OFDM   Adaptive modulation employed in the context of OFDM - which we termed as AOFDM - is based on the idea of assigning a more robust, lower-throughput modulation mode to those subcarriers, which are likely to cause symbol errors in the context of a fixed-mode transceiver as a result of their associated low SNR. By contrast, a less robust, higher throughput modulation mode is assigned to the higher-quality subcarriers. These concepts were further elaborated on in Section 17.4.1. In the context of our associated BER performance investigations conducted in Section 17.4.1.3 we found that as shown in Figure 17.29, the employment of adaptive modulation in an MMSE detection-assisted SDMA-OFDM system is only advantageous in terms of further reducing the BER in specific scenarios, where the number of simultaneous users L approaches the number of reception antennas P. This is because in this specific scenario the effective channel transfer function experienced by the different users is 'sufficiently non-flat' across the different subcarriers, with the result of exhibiting sufficient difference in terms of the associated channel quality for AOFDM to excel.

However, there are two aspects of adaptive modulation, which render its employment less convenient. First of all, it is necessary to provide an estimate of the subcarrier channel quality for the next transmission timeslot, which could be generated on the basis of the channel estimates available for the current transmission timeslot, upon assuming time-invariance of the channel. However, under time-variant channel conditions, the more elaborate, potentially decision-directed channel prediction techniques as seen in Figure 17.28 have to be invoked, in order to obtain accurate estimates of the channel transfer function for the next transmission timeslot. Secondly, the employment of adaptive modulation requires the signalling of the requested modulation mode assignment to be used during the next transmission time-slot to the remote users, which requires the existence of a reverse-link and hence its applicability is mainly confined to Time-Division Duplexing (TDD) systems, where every uplink transmission time-slot is followed by a down-link time-slot and vice-versa. Furthermore, the transmission of channel-quality related side-information reduces the AOFDM modem's effective throughput, which has to be compensated for by appropriately increasing the target throughput of the AOFDM modem.

17.5.3.5.2 Walsh-Hadamard Transform Spreading Assisted SDMA-OFDM   The above-mentioned deficiencies of AOFDM constituted the motivation for the alternative technique of employing spreading with the aid of orthogonal spreading codes across the various subcarriers, which was the topic of Section 17.4.2. We argued that as a result of the spreading codes' orthogonality the operations to be carried out at the receiver - also in the multi-user SDMA-WHTS-OFDM scenario - can be separated into that of channel transfer function equalization and WHT despreading, which substantially simplifies the receiver's design. This was illustrated in Figures 17.30 and 17.31 for the single- and multi-user OFDM scenarios, respectively.

The initial BER performance results portrayed in Figure 17.32 in the context of the single user WHTS-OFDM scenario demonstrated that with the aid of spreading almost the same BER performance can be achieved, as in conjunction with employing adaptive modulation capitalizing on perfect channel transfer function predictions used for estimating the subcarrier channel quality during the modulation mode assignment. Furthermore, in contrast

to AOFDM, there is no need for transmitting side-information to the remote transmitters. Hence, the employment of WHTS-OFDM is amenable to a wider range of transmission scenarios. As shown in [484] the WHT spreading employed at the transmitter can be efficiently combined with the OFDM-related IFFT. As for the receiver, we can argue that the additional complexity imposed by performing the despreading operation is marginal, compared to that owing to multi-user detection.

However, the main essence of our investigations was that as portrayed in Figure 17.34, with the aid of spreading the performance of the MMSE- or PIC detection assisted SDMA-OFDM systems can be significantly improved, again, provided that effective transmission channel is strongly frequency selective. As outlined in the previous section, this is the case in almost fully-loaded SDMA-OFDM scenarios, where the number of simultaneous users L approaches the number of reception antennas P. For sufficiently high SNRs the MMSE- or PIC detection-assisted WHTS-OFDM systems of Section 17.4.2.2 were capable of outperforming standard SIC detection-assisted SDMA-OFDM of Section 17.3.1.1.

Conclusions of the Book and Further Research Problems

19.1 Summary and Conclusions of Part I

19.1.1 Summary of Part I

In Chapters 2 - 7 we have discussed the basic implementational, algorithmic and performance aspects of orthogonal frequency division multiplexing in predominantly duplex mobile communications environments. Specifically, following a rudimentary introduction to OFDM in Chapter 2 in Chapter 3 we have further studied the structure of an OFDM modem and we have investigated the problem of the high peak-to-mean power ratio observed for OFDM signals, and that of clipping amplification caused by insufficient amplifier back-off. We have investigated the BER performance and the spectrum of the OFDM signal in the presence of clipping, and we have seen that for an amplifier back-off of 6 dB the BER performance was indistinguishable from the perfectly amplified case. We have investigated the effects of quantisation of the time-domain OFDM signal. The effects of phase noise on the OFDM transmission was studied, and two phase noise models were suggested. One model was based on white phase noise, only relying on the integrated phase jitter, while a second model used coloured noise, which was generated from the phase noise mask.

In Chapter 4 we have studied OFDM transmissions over time dispersive channels. The spectrum of the transmitted frequency-domain symbols is multiplied with the channel's frequency domain channel transfer function, hence the amplitude and phase of the received subcarriers is distorted. If the channel is varying significantly during each OFDM symbol's duration, then additional inter-subcarrier interference occurs, affecting the modem's performance. We have seen the importance of channel estimation on the performance of coherently detected OFDM, and we have studied two simple pilot-based channel estimation schemes. Differentially detected modulation can operate without channel estimation, but exhibits lower BER performance than coherent detection. We have seen that the signal-to-noise ratio is not constant across the OFDM symbol's subcarriers, and that this translates into a varying bit

869

error probability across the different subcarriers.

The effects of timing- and frequency errors between transmitter and receiver have been studied in Chapter 5. We have seen that a timing error results in a phase rotation of the frequency domain symbols, and possibly inter-OFDM-symbol interference, while a carrier frequency error leads to inter-subcarrier-interference. We have suggested a cyclic postamble, in order to suppress inter-OFDM-symbol interference for small timing errors, but we have seen that frequency errors of more than 5% of the subcarrier distance lead to severe performance losses. In order to combat this, we have investigated a set of frequency- and timing-error estimation algorithms. We have suggested a time-domain based joint time- and frequency-error acquisition algorithm, and studied the performance of the resulting system over fading time dispersive channels.

Based on the findings of Chapter 4 we have investigated adaptive modulation techniques to exploit the frequency diversity of the channel. Specifically, in Chapter 6, three adaptive modulation algorithms were proposed and their performance was investigated. The issue of signalling was discussed, and we have seen that adaptive OFDM systems require a significantly higher amount of signalling information than adaptive serial systems. In order to limit the amount if signalling overhead, a sub-band adaptive scheme was suggested, and the performance trade-offs against a subcarrier-by-subcarrier adaptive scheme were discussed. Blind modulation mode detection schemes were investigated, and combined with an error correction decoder. We have seen that by combining adaptive modulation techniques with a strong convolutional turbo channel codec significant system throughput improvements were achieved for low SNR values. Finally, frequency-domain pre-distortion techniques were investigated in order to pre-equalise the time-dispersive channel's transfer function. We have seen that by incorporating pre-distortion in adaptive modulation significant throughput performance gains were achieved compared to adaptive modems without pre-equalisation.

We have seen in Chapter 6 that although channel coding significantly improves the achievable throughput for low SNR values in adaptive modems, with increasing average channel quality the coding overhead limits the system's throughput. In order to combat this problem, in Chapter 7 we have investigated coding schemes which offer readily adjustable code rates. RRNS [203] and turbo BCH codes [203] were employed for implementing an adaptive coding scheme allowing us to adjust the code rate across the subcarriers of an OFDM symbol. Combinations of adaptive coding and the adaptive modulation techniques introduced in Chapter 7 were studied, and we have seen that a good compromise between the coded and uncoded transmission characteristics can be found.

19.1.2   Conclusions of Part I

(1) Based on the implementation-oriented characterisation of OFDM modems, leading to a real-time testbed implementation and demonstration at 34 Mbps we concluded that OFDM is amenable to the implementation of high bit rate wireless ATM networks, which is underlined by the recent ratification of the HIPERLAN II standard.

(2) The range of proposed joint time- and frequency synchronisation algorithms efficiently supported the operation of OFDM modems in a variety of propagation environments, resulting in virtually no BER degradation in comparison to the perfectly synchronised modems. For implementation in the above-mentioned 34 Mbps real-time testbed simplified versions of these algorithms were invoked.

(3) Symbol-by-symbol adaptive OFDM substantially increases the BPS throughput of the system at the cost of moderately increased complexity. It was demonstrated in the context of an adaptive real-time audio system that this increased modem throughput can be translated in improved audio quality at a given channel quality.

(4) The proposed blind symbol-by-symbol adaptive OFDM modem mode detection algorithms were shown to be robust against channel impairments in conjunction with twin-mode AOFDM. However, it was necessary to combine it with higher-complexity channel coding based mode detection techniques, in order to maintain sufficient robustness, when using quadruple-mode AOFDM.

(5) The combination of frequency-domain pre-equalisation with AOFDM resulted in further performance benefits at the cost of a moderate increase in the peak-to-mean envelope flluctuation and system complexity.

(6) The combination of adaptive RRNS and turbo BCH FEC coding with AOFDM provided further flexibility for the system, in order to cope with hostile channel conditions, in particular in the low SNR region.

19.2 Summary and Conclusions of Part II

19.2.1 Summary of Part II

Since their initial introduction in 1993 [52, 55, 284, 285], multi-carrier spread-spectrum systems have attracted significant research interest. Existing advanced techniques originally developed for DS-CDMA and OFDM have also been applied to MC-CDMA, while a range of new unique techniques have been proposed for solving various problems specific to multicarrier CDMA systems. The first two chapters of Part II of the book, namely Chapters 8 and 9, reviewed the basic concepts of MC-CDMA and the various spreading sequences applicable to MC-CDMA transmissions. Chapter 10 characterised the achievable performance of MC-CDMA schemes employing various detectors. Then, three further topics closely related to MC-CDMA based communications were investigated in depth.

Specifically, the peak factor reduction techniques were presented in Chapter 11. While analysing the signal envelope of MC-CDMA in Section 11.5.1, it was found that the aperiodic correlations of the spreading sequences play an important role in determining the associated peak factor. By investigating several orthogonal sequences, in Section 11.5.2.2 it was shown that a set of orthogonal complementary sequences applied to MC-CDMA has the advantageous property of limiting the peak factor of the MC-CDMA signal to 2 or 3dB, when the number of simultaneously transmitting users is less than or equal to four, regardless of the spreading factor. When the MC-CDMA system was 'fully-loaded', *i.e.* supported the highest possible number of users, Walsh codes exhibited the lowest worst-case peak-factor as well as the lowest median peak-factor. The latter property was exploited in terms of limiting the peak factor of 'fully-loaded' MC-CDMA systems having a spreading factor of 15 to a maximum peak factor of 2.5, which is comparable to the peak factor of filtered single carrier signals. This was achieved by employing a peak-factor limiting block code, as it was detailed in Section 11.5.2.3. However, our simulation study of MC-CDMA systems employing realistic

power amplifier models revealed in Section 11.5.3 that Zadoff-Chu spreading based MC-CDMA outperforms Walsh spreading based MC-CDMA, when transmitting over a Rayleigh fading channel. Investigating this unexpected result further, it was found that Zadoff-Chu spreading based MC-CDMA better exploits the frequency diversity in comparison to Walsh spreading assisted MC-CDMA, since the combined symbol after Zadoff-Chu spreading over each sub-carrier is less likely to have a low value compared to Walsh spread and combined symbols. This suggests that the effects of the frequency-domain peak-factor, in other words the dynamic range of the frequency domain symbols on the achievable diversity gain has to be further investigated. A preliminary idea related to this idea was presented in Section 11.5.4.

Chapter 12 was devoted to adaptive modulation techniques. After the introduction of a general model of various adaptive modulation schemes in Section 12.3.1, the existing techniques proposed for determining the transceiver mode-switching levels were reviewed in Section 12.4.1, 12.4.2 and 12.4.3, since the performance of adaptive schemes is predetermined by the switching levels employed as well as by the average SNR per symbol. In search of the globally optimum switching levels, the Lagrangian optimisation technique was invoked in Section 12.4.4 and the relationship amongst the different mode-switching levels was found to be independent of the underlying channel scenarios such the Multi Path Intensity (MIP) profile or the fading magnitude distribution. Having established the technique of determining the optimum switching levels, a comprehensive set of performance results was presented for adaptive PSK schemes, adaptive Star QAM schemes as well as for adaptive Square QAM schemes, when they were communicating over a flat Nakagami m fading channel. Since adaptive Square QAM exhibited the highest BPS throughput among the three adaptive schemes investigated, the performance of adaptive Square QAM schemes was further studied, employing two-dimensional Rake receivers in Section 12.5.2 and applying concatenated space-time coding in conjunction with turbo convolution coding in Section 12.5.5. As expected, in Section 12.5.1, 12.5.2 and 12.5.5, it was found that the SNR gain of the adaptive schemes over fixed-mode schemes decreased, as the fading became less severe. Hence, the adaptive schemes exhibited only a modest performance gain, when (a) the Nakagami fading parameter m was higher than four, (b) the number of diversity antennas was higher than four when MRC diversity combining was used over independent Rayleigh fading channels, or (c) the total number of transmit antennas plus receive antennas was higher than four when space-time coding was used. Specifically, in Section 12.5.5 it was found that ST block coding reduces the relative performance advantage of adaptive modulation as summarised in Figure 12.49(b), since it increases the diversity order and eventually reduces the channel quality variations. When the adaptive modulation schemes were operating over wide-band channels, their SNR gain eroded even in conjunction with a low number of antennas, since the fading depth of wideband channels is typically less deep, than that of narrow-band channels. For transmission over correlated fading channels it is expected that the SNR gain of adaptive schemes over their fixed-mode counterparts erodes less, as the number of antenna increased. However, further investigations are required for quantifying the effects of correlated fading. Even though some channel-coding based results were presented in Section 12.5.5, the investigation of coded adaptive modulation schemes is far from complete. Since our AQAM mode switching levels were optimised for uncoded systems, the performance results presented for the coded adaptive schemes are not optimum. The technique similar to that developed in Section 12.4.4 may be applied, provided that a closed-form mode-specific average BER expression becomes available for channel coded fixed modulation schemes. available. In addition,

the 'spread of BER' has to be quantified by some measure, such as its PDF. This concept arises, since the quality of service experienced by a user may differ for fixed-mode schemes and for adaptive modulation schemes, even if their average BERs are identical. The variance or in other words fluctuation of the instantaneous BER distribution may serve as a useful quality measure. The PDF of this instantaneous BER may be obtained by applying Jacobian transformation [448] to the PDF of the instantaneous SNR per symbol. It is expected that there may be a direct relationship between this measure of 'spread of BER' and the required interleaver length of the channel codec associated. More explicitly, it is expected that the distribution of the bit errors becomes less bursty in conjunction with AQAM schemes, since they are capable of near-instantaneously involving a more robust but reduced-throughput AQAM mode, when the channel quality degrades. Hence AQAM schemes may require shorter channel interleavers for randomising the position of channel errors.

In Chapter 13, a Successive Partial Detection (SPD) scheme was introduced. We analysed the BEP performance and the implementational complexity of three proposed SPD detectors, when communicating over the AWGN contaminated by an impulse noise in the time domain or a narrow band interference / a tone jamming signal in the frequency domain, assuming that one transform-domain symbol was obliterated due to a severe corruption. We found that the Type II SPD detector exhibits a lower BEP and requires a lower complexity than those of the conventional full-despreading based detector. This work has to be expanded for transmission over wideband channels. The application of the SPD scheme in the context of a joint-detector is also an interesting future research issue, since it will reduce the complexity of the joint detector.

Part II of the book concentrated on investigating the MC-CDMA [52, 53, 55] scheme, which is one of the family of three different multi-carrier CDMA techniques [333]. This technique was advocated, because MC-CDMA results in the lowest BER among the three schemes investigated in a similar scenario [333]. Our investigations concentrated on the downlink, because in the uplink stringent synchronisation of the mobile terminals has to be met. Future research should extend the results of Chapter 11 and 12 to both multi-carrier DS-CDMA [284] and to multi-tone (MT) CDMA [285], as well as to the family of more sophisticated adaptive MC-CDMA schemes [321].

19.2.2 Conclusions of Part II

The main contributions and conclusions of Part II of the book are in three specific areas closely related to Multi-Carrier Code Division Multiple Access (MC-CDMA), which are summarised in this subsection.

Crest Factor of Multi-Code MC-CDMA Signal

One of the main drawbacks of Orthogonal Frequency Division Multiplexing (OFDM) [2] is that the envelope power of the transmitted signal fluctuates widely, requiring a highly linear RF power amplifier. Finding a solution to this problem has stimulated intensive research. The accrueing advances were critically reviewed in Sections 11.3 and 11.4. Since MC-CDMA [52, 55] schemes spread a message symbol across the frequency domain and employ an OFDM transmitter for conveying each spread bit, their transmitted signal also exhibits a high crest factor (CF), which is defined as the ratio of the peak amplitude of the

modulated time-domain signal to its root mean square (RMS) value. Hence, the characteristics of the crest factor of the MC-CDMA signal were studied in Section 11.5, with a view to reduce the associated power envelope variations.
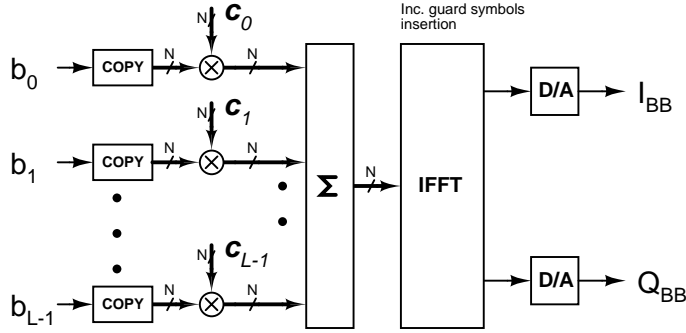
Figure 19.1: MC-CDMA transmitter model: b_l and $\mathbf{C_1}$ are the l-th message symbol and spreading sequence, respectively.

The simplified transmitter structure of a multi-code MC-CDMA system is portrayed in Figure 19.1, where L M-ary Phase Shift Keying (MPSK) modulated symbols $\{b_l \mid 0 \leq l < L\}$ are transmitted simultaneously using L orthogonal spreading sequences $\{\mathbf{C}_l \mid 0 \leq l < L\}$. Each of the spreading sequences is constituted by N chips according to $\mathbf{C}_l = \{c_l[n] \mid 0 \leq n < N\}$, where the complex spreading sequence c_l has a unit magnitude of $|c_l[n]| = 1$. Then, the normalised complex envelope $s(t)$ of an MPSK modulated multi-code MC-CDMA signal is represented for the duration of a symbol period T as:

$$s(t) = \frac{1}{\sqrt{N}} \sum_{l=0}^{L-1} \sum_{n=0}^{N-1} b_l \, c_l[n] \, e^{j2\pi F n \frac{t}{T}} \ .$$

The power envelope $|s(t)|^2$ of this MPSK modulated multi-code MC-CDMA signal was analysed in Section 11.5.1 and it was expressed as [57]:

$$|s(t)|^2 = \frac{2}{N} \mathrm{Re} \left[\sum_{n=0}^{N-1} (A[n] + X[n]) \, e^{j2\pi n \frac{t}{T}} \right] \ ,$$

where $A[n]$ is the collective aperiodic autocorrelation of the spreading sequences $\{\mathbf{C}_l\}$ defined in the context of Equation (11.38), while $X[n]$ is the collective aperiodic crosscorrelation defined in (11.39).

Having observed that the power envelope of the MPSK modulated multi-code MC-CDMA signal is completely characterised by the collective autocorrelations and crosscorrelations of the spreading sequence employed, a set of various spreading sequences was investigated in quest of the sequences yielding low CF or Peak Factor (PF), where the PF was defined as the square of the CF, namely $\mathrm{PF} \triangleq \mathrm{CF}^2$. **It was shown by Theorem 11.5 in Section 11.5.2.2 that a specific version of Sivaswamy's complementary set [384] results in a low CF, bounded by 3dB, in the context of BPSK modulated four-code MC-CDMA**

systems, regardless of the spreading factor employed, as seen in Figure 19.2.
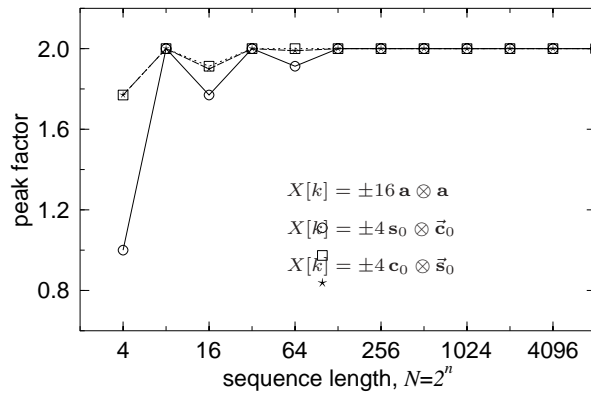
Figure 19.2: The peak-factors of Sivaswamy's complementary set of sequences. The number of simultaneously used sequences is $L = 4$ and the sequence length of $N = 2^n$ is between $2^2 = 4$ and $2^{13} = 8192$.

Since a similar family of spreading sequences yielding such a low CF could not be found for code sets having more than four codes, *i.e.* for $L > 4$, in Section 11.5.2.3 a crest factor reduction coding scheme [31] was applied instead. We found in Section 11.5.2.3 that the peak factors of BPSK modulated MC-CDMA employing an appropriate family of spreading codes could be reduced below 2.5, when using the crest factor reduction code proposed in [57], as seen in Figure 19.3(a). In order to investigate the effects of the modulated signal peak clipping

(a) Median Peak Factor
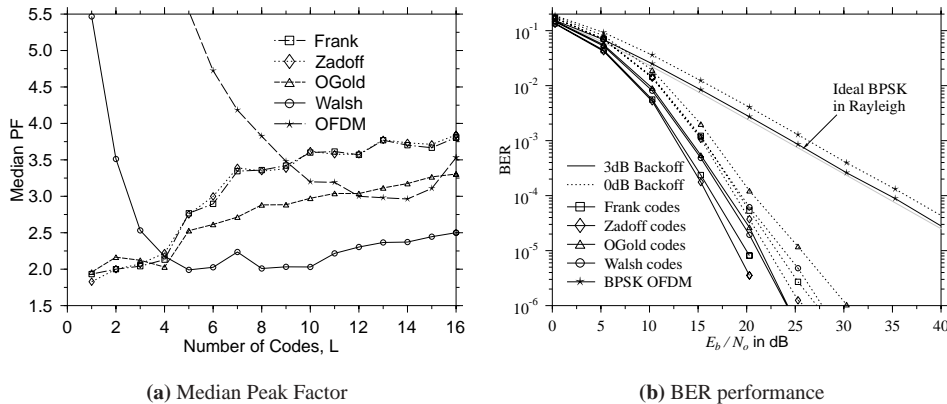
(b) BER performance

Figure 19.3: Effects of the $(L - 1)/L$-rate crest factor reduction coding for the spreading factor of $N = 16$. (a) The worst-case peak factor when using various spreading codes for BPSK modulated MC-CDMA. (b) BER versus E_b/N_o performance of BPSK modulated MMSE-JD MC-CDMA and that of BPSK modulated OFDM, when transmitting over independent Rayleigh channels for each subcarriers.

(a) Average BER

(b) Throughput at the BER of $P_{th} = 10^{-2}$
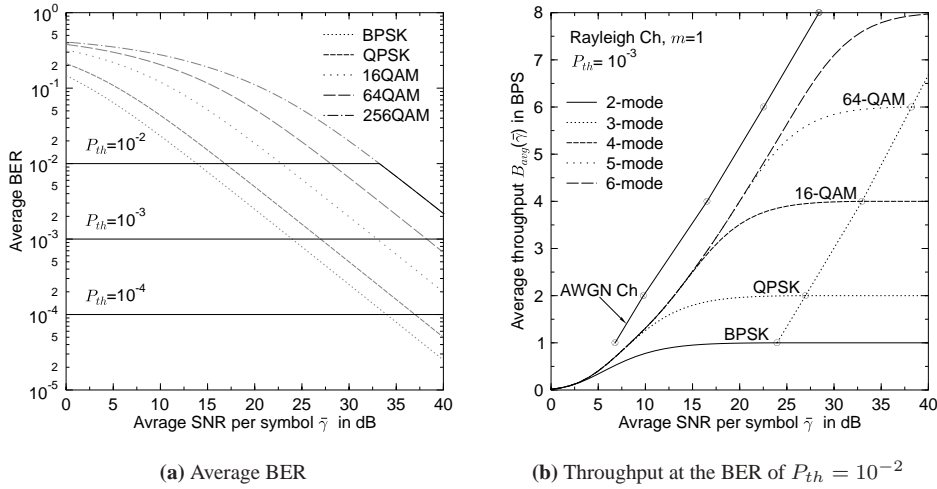
Figure 19.4: The average BER and average throughput performance of a six-mode adaptive Square QAM scheme for communicating over a flat Rayleigh channel ($m = 1$). (a) The constant target average BER is maintained over the entire range of the average SNR values up the avalanche SNR. (b) The markers '$\otimes$' and '$\odot$' represent the required SNR of the corresponding fixed-mode Square QAM schemes achieving the same target BER as the adaptive schemes, operating over an AWGN channel and a Rayleigh channel, respectively.

by the non-linear power amplifier, the Bit Error Ratio (BER) performance was studied in Section 11.5.3.3. It was expected that the Walsh spreading based scheme would result in the lowest BER, since it resulted in the lowest worst-case peak factor for 'fully-loaded $(L = N)$' BPSK modulated MC-CDMA employing a Minimum Mean Square Error (MMSE) Block-Decision Feedback Equaliser (BDFE) based Joint Detector (JD) [330], when experiencing independent Rayleigh fading for each subcarriers. However, the Zadoff-Chu based scheme performed better than Walsh based scheme [57]. We found that the Zadoff-Chu spreading based MC-CDMA scheme inflicted less Multiple User Interference (MUI), than the Walsh-spreading based scheme and it utilised the available diversity more efficiently, than the Walsh-spreading based scheme.

Adaptive Modulation

The second field, where novel contributions were made, was in realms of adaptive modulation schemes. Adaptive modulation [2, 193, 390, 392] attempts to provide the highest possible throughput given the current near-instantaneous channel quality, while maintaining the required data transmission integrity. We analysed in Section 12.3.3.1 the performance of adaptive modulation schemes and derived a closed form expression for the average BER and for the average Bits Per Symbol (BPS) throughput [492]. Since the modulation mode switching levels predetermine the average BER as well as the average BPS, it is important to optimise these switching levels for achieving the maximum possible average throughput. Having reviewed the existing techniques of determining the switching levels [209, 392], a per-SNR op-

(a) BPS throughput

(b) The SNR required versus the number of antenna D
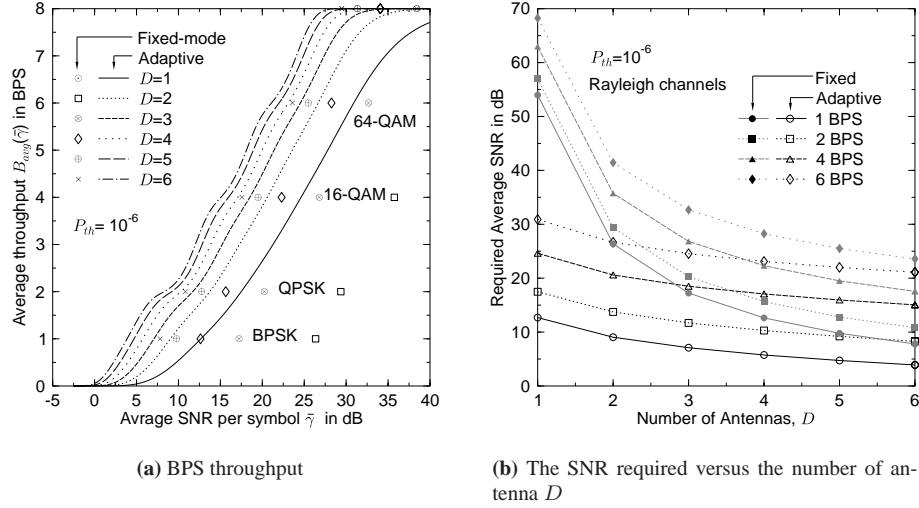
Figure 19.5: The performance of the MRC-aided antenna-diversity assisted AQAM scheme operating over independent Rayleigh fading channels at the target average BEP of $P_{th} = 10^{-6}$. (a) The markers represent the corresponding fixed-mode QAM performance. (b) The required SNR achieving the various throughput for the AQAM and fixed-mode QAM schemes.

timisation technique was proposed in [410], which was based on Powell's multi-dimensional optimisation [341], yielding a constant target BER and the maximum BPS throughput. Since this optimisation procedure was often trapped in local optima, rather than reaching the global optimum, the Lagrangian-based optimisation technique was developed [493] and was subsequently used in Section 12.5 in order to investigate the performance of adaptive modulation schemes employing various modulation modes, namely PSK, Star QAM and Square QAM phasor constellations.

Since our modulation mode switching levels were optimised in order to achieve the highest throughput, while maintaining the target BER, the average BER of our six-mode AQAM scheme remained constant over the entire range of the average SNR values up the avalanche SNR, beyond which it followed the BER of the highest throughput mode, namely that of 256-QAM, as seen in Figure 19.4(a). On the other hand, the BPS throughput increased steadily, as the average SNR increased, as seen in Figure 19.4(b). Our optimised AQAM operating over a Rayleigh fading channel required 4dB more SNR, in comparison to fixed-mode QAM operating over an AWGN channel.

Since in Section 12.5.2 receiver antenna diversity has been used for combating the effects of fading, we investigated the performance of Maximal Ratio Combining (MRC) antenna diversity assisted AQAM schemes [492]. As it is seen in Figure 19.5, the average SNRs required for achieving the target BEP of $P_{th} = 10^{-6}$ for the fixed-mode schemes and that for the adaptive schemes decrease, as the antenna diversity order increases. However, the differences between the required SNRs of the adaptive schemes and their fixed-mode counterparts also decrease, as the antenna diversity order increases.

In Section 12.5.5, the performance of Space-Time (ST) block coded constant-power adap-

(a) With ST coding   **(b)** With ST and turbo coding
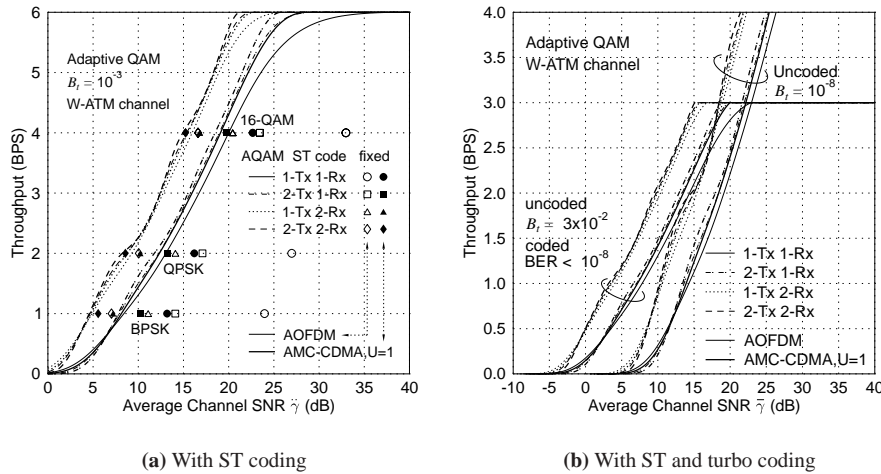
Figure 19.6: The BPS throughput performance of five-mode AOFDM and AMC-CDMA for commu-
nicating over the W-ATM channel [2, pp.474]. (a) The SNR gain of the adaptive modems
decreases, as the diversity of the ST coding increases. The BPS curves appear in pairs,
corresponding to AOFDM and AMC-CDMA - indicated by the thin and thick lines, re-
spectively - for each of the four different ST code configurations. The markers represent
the SNRs required by the fixed-mode OFDM and MC-CDMA schemes for maintaining
the target BER of 10^{-3} in conjunction with the four ST-coded schemes considered. (b)
The turbo convolutional coding assisted adaptive modems have SNR gains up to 7dB
compared to their uncoded counterparts achieving a comparable average BER.

tive multi-carrier modems employing optimum SNR-dependent modem mode switching lev-
els were investigated [418, 494]. As expected, it was found that ST block coding reduces
the relative performance advantage of adaptive modulation, since it increases the diversity
order and eventually reduces the channel quality variations, as it can be observed in Fig-
ure 19.6(a). **Having observed that 1-Tx aided AOFDM and 2-Tx ST coding aided fixed-
mode MC-CDMA resulted in a similar BPS throughput performance, we concluded
that fixed-mode MC-CDMA in conjunction with 2-Tx ST coding could be employed,
provided that we could afford the associated complexity. By contrast, AOFDM could
be a low complexity alternative of counteracting the near-instantaneous channel qual-
ity variations.** When turbo convolutional coding was concatenated to the ST block codes,
near-error-free transmission was achieved at the expense of halving the average throughput,
as seen in Figure 19.6(b) . Compared to the uncoded system, the turbo coded system was
capable of achieving a higher throughput in the low SNR region at the cost of a higher com-
plexity. Our study of the relationship between the uncoded BER and the corresponding coded
BER showed that adaptive modems obtain higher coding gains, than that of fixed modems.
This was due to the fact that the adaptive modem avoids burst errors even in deep channel
fades by reducing the number of bits per modulated symbol eventually to zero.

(a) BER   (b) Complexity
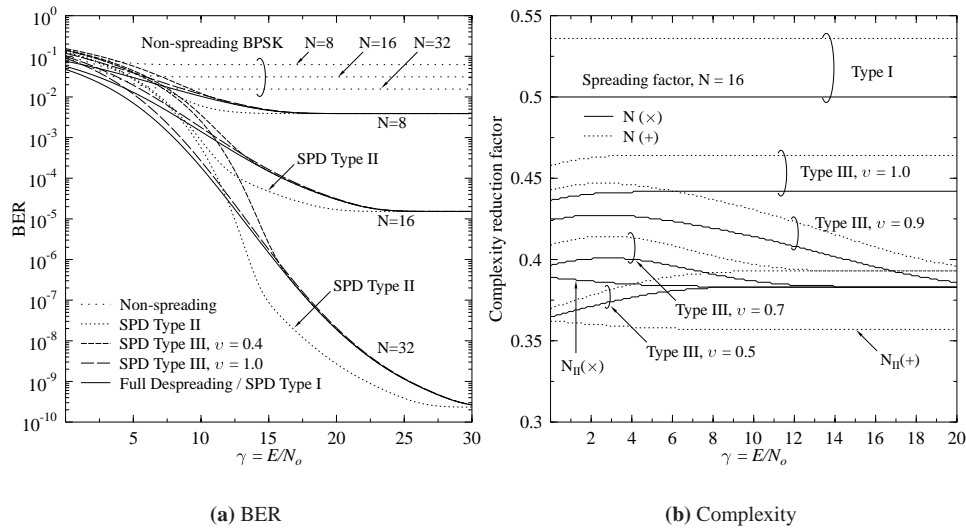
Figure 19.7: The bit error rates and complexities of the various SPD detectors and the conventional despreading scheme, where N is the spreading factor. (a) The non-spread BPSK scheme has a high irreducible BER of $0.5/N$, while the spread systems have a significantly lower error floor of $1/2^N$. The Type II SPD Detector shows a superior performance in the high SNR region in comparison to the other schemes. (b) The complexity of three types of SPD detectors quantified in terms of the required number of multiplications and additions, normalised to those of the conventional full-despreading based detector associated with the spreading factor of $N = 16$. The Type II SPD detector requires less than 40% of the operations necessitated by the conventional scheme.

Successive Partial Despreading

In Chapter 13, a Successive Partial Detection (SPD) scheme was introduced in an effort to reduce the computational efforts involved in despreading in the context of a 'fully loaded' CDMA downlink scenario. We analysed the bit error rate performance and the implementational complexity of three different types of SPD detectors, when communicating over the AWGN channel, contaminated by time-domain impulse noise or frequency-domain tone-jamming. It was found that the Type II SPD scheme resulted in a lower BER, than the conventional despreading scheme in the SNR range of $\gamma > 13dB$, while requiring significantly reduced computational efforts, namely less than 40% in comparison to the conventional scheme, when quantified in terms of the required number of multiplications and additions, as it can be observed in Figure 19.7.

19.3   Summary and Conclusions of Part III

19.3.1   Pilot-Assisted Channel Estimation for Single-User OFDM

In the context of our portrayal of single-user OFDM in Chapter 14 we highlighted that a prerequisite for performing coherent detection of the different subcarriers' symbols at the receiver is the availability of an estimate of the subcarriers' channel transfer factors.

An initial *a posteriori* estimate of the channel transfer factor associated with a specific subcarrier can be generated upon dividing the received subcarrier signal by the remodulated symbol decision obtained for this subcarrier. The initial *a posteriori* channel transfer factor estimates can then be further enhanced with the aid of generating smoothed estimates using filtering between neighbouring estimates based on exploiting the channel transfer factors' correlation in both the frequency- and the time-direction.

Depending on the origin of the sliced and remodulated symbol employed as a reference for deriving the initial *a posteriori* channel transfer factor estimates, the channel estimators can be divided into two categories, namely pilot-assisted and decision-directed approaches.

More specifically, in the context of pilot-assisted channel estimation the initial *a posteriori* channel transfer factor estimates are calculated only for a number of so-called pilot subcarriers, for which the complex transmitted symbol is known *a priori* at the receiver. This is followed by an interpolation between the different pilot subcarriers' *a posteriori* channel transfer factor estimates, in order to obtain channel transfer factor estimates for all subcarriers. While early publications on pilot-assisted channel estimation considered periodic one-dimensional (1D) pilot patterns, more recent publications considered the employment of two-dimensional (2D) pilot patterns, based on exploiting the channel transfer factors' correlation not only in the frequency-direction, but also in the time-direction. The most often-used pilot patterns are of rectangular shape, but other geometries have also been investigated in the literature. As a result of employing 2D pilot patterns, the pilot overhead imposed can be reduced, while potentially maintaining the same channel transfer factor estimation MSE as in case of a 1D pattern. A disadvantage of using 2D pilot patterns is however that a block-based processing has to be used at the receiver, where each channel estimation block typically contains several OFDM symbols. This increases the entire system's delay, which may become prohibitively high in voice-based communications. Furthermore, extra storage requirements are imposed due to the necessity of retaining a number of past OFDM symbols. However, the block-based processing could be avoided by rendering the channel transfer function interpolation filter causal, namely by employing only the *a posteriori* channel transfer factor estimates of the current- and the past OFDM symbols in the filtering process but no 'future' OFDM symbols. A consequence would be the associated degradation of the channel estimation MSE.

Two of the most prominent methods reported in the literature for performing the interpolation between the pilot subcarriers' *a posteriori* channel transfer factor estimates, are polynomial- and Wiener filter based approaches. Polynomial interpolation attempts to approximate the channel transfer function's evolution based on minimizing the squared error between the curve or surface spanned by the polynomial and the *a posteriori* channel transfer factor estimates at the pilot positions. In contrast, Wiener filtering is based on minimizing the expected squared error between the desired channel transfer factor of a *specific subcarrier* and a linear combination of the *a posteriori* channel transfer factor estimates associated with the

pilot positions. In contrast to the polynomial approach the Wiener filter requires knowledge of the channel's statistics in form of the spaced-time spaced-frequency correlation function or the related scattering function.

Due to the fundamental importance of Wiener filtering both in the context of channel transfer factor predicton as well as in multi-user detection, we concentrated in our review of pilot-assisted channel estimation techniques originally proposed in Chapter 14 on the 2D-FIR- and cascaded 1D-FIR Wiener filter based channel estimation as proposed by Höher *et al.* [58, 66, 67, 457]. Although 2D-FIR Wiener filtering provides the optimum solution for an unlimited number of filter taps, for a given moderate complexity the cascaded 1D-FIR Wiener filtering becomes more attractive in terms of achieving a lower estimation MSE. In terms of the pilot grid's dimensions a two-times oversampling in both the time- and frequency-direction was found to be sufficient for almost completely eliminating the residual estimation MSE observed at higher SNRs. Our further investigations were cast in the context of maintaining "robustness" for the channel estimator. This was achieved by assuming a uniform, ideally support-limited scattering function and its associated 2D-sinc-shaped spaced-time spaced-frequency correlation function in the calculation of the estimator's coefficients. As long as the support region of the channel's actual scattering function - potentially shifted along the multipath delay axis as a result of synchronization errors - was contained in the support region of the 'robust' estimator's associated uniform scattering function, no significant MSE degradation was observed compared to the case, when the channel's encountered scattering function was uniform as well.

For a given pilot grid the MSE performance of pilot-assisted Wiener filter aided channel estimation can be potentially improved upon increasing the number of filter taps. However, a fundamental performance limitation is imposed, because the *a posteriori* channel transfer factor estimates, which are associated with pilot subcarriers spaced further apart from the specific position, for which the channel transfer factor is to be estimated, are less correlated. This effect can be addressed upon increasing the pilot grid density. In the limit, every subcarrier could potentially be employed for pilot transmissions. This strategy is exploited in the context of decision-directed channel estimation based on the premise that the demodulated symbols are error-free or exhibit a low detection-error probability.

19.3.2   Decision-Directed Channel Estimation for Single-User OFDM

Similarly to the scenario addressed in Chapter 14 dealing with pilot-assisted chaannel estimation, in Chapter 15 we also argued that a prerequisite for performing coherent detection of the different subcarriers' symbols at the receiver is the availability of a reliable estimate of the subcarriers' channel transfer factors.

An initial *a posteriori* estimate of the channel transfer factor associated with a specific subcarrier can be generated upon dividing the received subcarrier signal by the remodulated symbol decision obtained for this subcarrier. The initial *a posteriori* channel transfer factor estimates can then be further enhanced with the aid of generating smoothed estimates using filtering between neighbouring estimates based on exploiting the channel transfer factors' correlation in both the frequency- and the time-direction.

Depending on the origin of the sliced and remodulated symbol employed as a reference for deriving the initial *a posteriori* channel transfer factor estimates, the channel estimators can be divided into two categories, namely pilot-assisted and decision-directed approaches.

More specifically, in the context of pilot-assisted channel estimation the initial *a posteriori* channel transfer factor estimates are calculated only for a number of so-called pilot subcarriers, for which the complex transmitted symbol is known *a priori* at the receiver. This is followed by an interpolation between the different pilot subcarriers' *a posteriori* channel transfer factor estimates, in order to obtain channel transfer factor estimates for all subcarriers.

By contrast, the philosophy of the decision-directed channel estimation discussed in Chapter 15 was based on the idea of employing the remodulated subcarrier symbol decisions as "pilots", or in other words as a reference signal for generating the set of K initial *a posteriori* channel transfer factor estimates for the current OFDM symbol. These initial estimates could then be further enhanced by MMSE-based 1D-FIR Wiener filtering across the K subcarriers exploiting also the channel transfer factors' correlation in the frequency-direction, as suggested by Edfors *et al.* [62, 69, 157]. An even further MSE enhancement was achieved by Li *et al.* [68] with the aid of MMSE-based 2D-FIR Wiener filtering upon also exploiting the channel's correlation in the time-direction, namely with the aid of employing also a number of previous OFDM symbols' initial *a posteriori* channel transfer factor estimates in the filtering process. These enhanced *a posteriori* channel transfer factor estimates derived for the current OFDM symbol would then be employed as *a priori* channel transfer factor estimates for frequency-domain equalization conducted during the next OFDM symbol period upon neglecting the channel's decorrelation between the two OFDM symbol periods.

19.3.2.1   Complexity Reduction by CIR-Related Domain Filtering

However, the complexity imposed upon performing the filtering across all the K different subcarriers in the frequency-domain may potentially become excessive. To be more specific, a computational complexity of K^2 number of complex multiplications and the same number of complex additions would be inflicted. In order to reduce the associated computational complexity, it was suggested by Edfors *et al.* [62, 69, 157] to transform the initial *a posteriori* channel transfer factor estimates to the CIR-related domain with the aid of the Karhunen Loeve Transform (KLT), followed by CIR-related one-tap filtering of only the first K_0 number of uncorrelated CIR-related taps, which are assumed to be the most significant taps in terms of their variance. Finally, the remaining filtered CIR-related taps are transformed back to the frequency-domain. In this case the computational complexity would be quantified in terms of $2K_0K$ complex multiplications and additions. While the KLT achieves a perfect decorrelation and hence the best possible energy compaction in the CIR-related domain, a disadvantage is that for its calculation explicit knowledge of the channel's statistics, namely the spaced-frequency correlation matrix is required, which is not known *a priori*. Hence, as suggested by van de Beek *et al.* [61], Edfors *et al.* [69] and Li *et al.* [68], the channel-independent DFT matrix could be employed instead of the optimum KLT matrix for transforming the initial *a posteriori* channel transfer factor estimates to the CIR-related domain. In the context of a sample-spaced CIR the DFT matrix is identical to the KLT matrix and hence the CIR-related taps are uncorrelated. By contrast, in the context of a non-sample-spaced CIR the DFT matrix is sub-optimum in the sense that the CIR-related taps are not perfectly decorrelated and hence the energy compaction becomes sub-optimum. As a result of windowing, the CIR-related taps generated upon retaining only a limited number of $K_0 \ll K$ taps with the aim of reducing the estimator's complexity, the DFT based estimator's MSE is significantly

degraded compared to that of the KLT-based estimator. This is because significant signal components are removed. Note that windowing is particularly effective in terms of complexity reduction, when the CIR-related taps are also filtered in the time-direction, as in case of the 2D-MMSE based estimator proposed by Li *et al.* [68]. A attractive compromise between the optimum KLT and the channel-independent DFT was found by Li and Sollenberger [80] upon employing the unitary matrix, which is related to the KLT of the uniform multipath intensity profile's spaced-frequency correlation matrix as the transform matrix required for transforming the initial *a posteriori* channel transfer factor estimates to the CIR-related domain. Thus attractive energy compaction properties, similar to those of the optimum KLT, are achieved without having exact knowledge of the channel's statistics. As a result, only a slight MSE degradation compared to that of the optimum KLT-based estimator is incurred.

19.3.2.2 Compensation of the Channel's Time-Variance by CIR-Related Tap Prediction Filtering

Our more detailed investigations of Chapter 15 concentrated on the effects of the channel's decorrelation incurred between consecutive OFDM symbols. Li *et al.* [68] proposed to employ 2D-MMSE based estimation filtering for deriving improved *a posteriori* channel transfer factor estimates for the current OFDM symbol based on the current- and a number of previous OFDM symbols' initial *a posteriori* channel transfer factor estimates. These channel estimates could then been employed as *a priori* channel transfer factor estimates for demodulation during the next OFDM symbol period. However, in the context of rapidly time-variant channels, associated with a potentially high OFDM symbol normalized Doppler frequency, it is more effective to directly predict the channel transfer factor for the next OFDM symbol period. This can be achieved by substituting the Wiener filter based CIR-related tap estimation filters of Li's 2D-MMSE based channel estimator design [68] by Wiener filter-based CIR-related tap prediction filters. Our investigations demonstrated that with the aid of CIR-related tap prediction filtering even channel scenarios having OFDM symbol normalized Doppler frequency as high as $F_D = 0.1$ can be supported, while capitalizing on relatively short prediction filters. Employing four predictor taps seemed to be sufficient for compensating most of the channel's variation, while further increasing the predictor's length resulted in additional modest MSE reduction due to averaging over a higher number of noisy samples. However, our experiments demonstrated that at lower SNRs and for higher-order modulation schemes the channel estimation MSE is potentially high, which is the result of employing erroneous subcarrier symbol decisions in the DDCE process. As a consequence, error propagation effects occur, which have to be curtailed by regularly transmitting training OFDM symbols. In order to further reduce the system's BER, the employment of turbo-coding was considered as a viable option. However, generating the DDCE's reference signal by slicing, reencoding, interleaving and remodulating the turbo-decoder's 'source'-related soft-output bits only exhibited no significant advantage compared to slicing and remodulating the turbo-decoder's soft-input bits. By contrast, generating the DDCE's reference from the turbo-decoder's 'source- plus parity'-related soft-output bits proved to be more effective.

19.3.2.3   Subject for Future Research: Successive Adaptivity of KLT and CIR-Related Tap Prediction Filtering

In the context of the 2D-MMSE based channel prediction the concepts of "robustness" with respect to the channel's true scattering function can be applied, as it was originally proposed by Li *et al.* [68] for the 2D-MMSE based channel estimator. However, in order to further improve the 2D-MMSE based channel predictor's MSE performance, the channel predictor could be rendered adaptive with respect to two components, namely the transform, which conveys the initial *a posteriori* channel transfer factor estimates to the CIR-related domain and secondly, with respect to the CIR-related tap predictors.

Recall that the optimum transform is known to be the Karhunen-Loeve transform with respect to the channel's spaced-frequency correlation matrix. An estimate of the channel's spaced-frequency correlation matrix is given by the auto-correlation matrix of the initial *a posteriori* channel transfer factor estimates. Although this matrix differs from the channel's spaced-frequency correlation matrix by an additive weighted identity matrix, which is associated with the noise contributions, the eigenvectors of both matrices are identical [90, 157]. Also recall that these eigenvectors constitute the optimum transform in terms of achieving a perfect decorrelation of the frequency-domain channel transfer factors. The auto-correlation matrix of the initial *a posteriori* channel transfer factor estimates can be estimated with the aid of the sample-correlation method [90]. Based on the current OFDM symbol's *a posteriori* channel transfer factor estimates the sample-correlation matrix can be regularly updated. Instead of entirely recomputing the KLT matrix in every OFDM symbol period, an iterative update- or tracking method proposed by Davila [495] as well as Rezayee and Gazor [496] in the context of speech coding is expected to be computationally more effective.

Apart from the above-mentioned adaptive transform, the second component of the 2D-MMSE based channel predictor, which can be rendered adaptive, are the CIR-related tap predictors. In the context of our investigations we compared the block-based Burg algorithm assisted CIR-related tap prediction approach proposed by Al-Susa and Ormondroyd [72] against the non-adaptive robust approach proposed by Li *et al.* [68]. Although these investigations demonstrated that an adaptive predictor is capable of outperforming the robust predictor, a disadvantage of the block-based adaptation was constituted by the extra storage requirements imposed. In order to avoid these disadvantages, an OFDM symbol-by-symbol adaptation technique relying on the LMS- or RLS algorithms is expected to be more attractive. We have further illustrated the concepts of the fully adaptive 2D-MMSE based channel predictor in Figure 19.8. Besides the potentially reduced estimation MSE, an additional advantage of the adaptive predictor compared to a robust predictor is its ability to better compensate for the effects of erroneous subcarrier symbol decisions, which manifest themselves similarly to the effects of impulsive noise in the DDCE process. However, the advantages of the adaptive predictor have to be viewed in the light of the disadvantage of a higher complexity compared to the robust predictor.

Our further investigations in Chapter 15 were cast in the context of employing 2D-MMSE based channel prediction in an OFDM system, which employs adaptive modulation. This was motivated by the observation that as a result of the channel's variation versus time, the modulation mode assignment computed during the current OFDM symbol period - based on the current OFDM symbol's channel transfer factor estimates - for application during the next OFDM symbol period becomes inaccurate. Hence the AOFDM modem's performance is
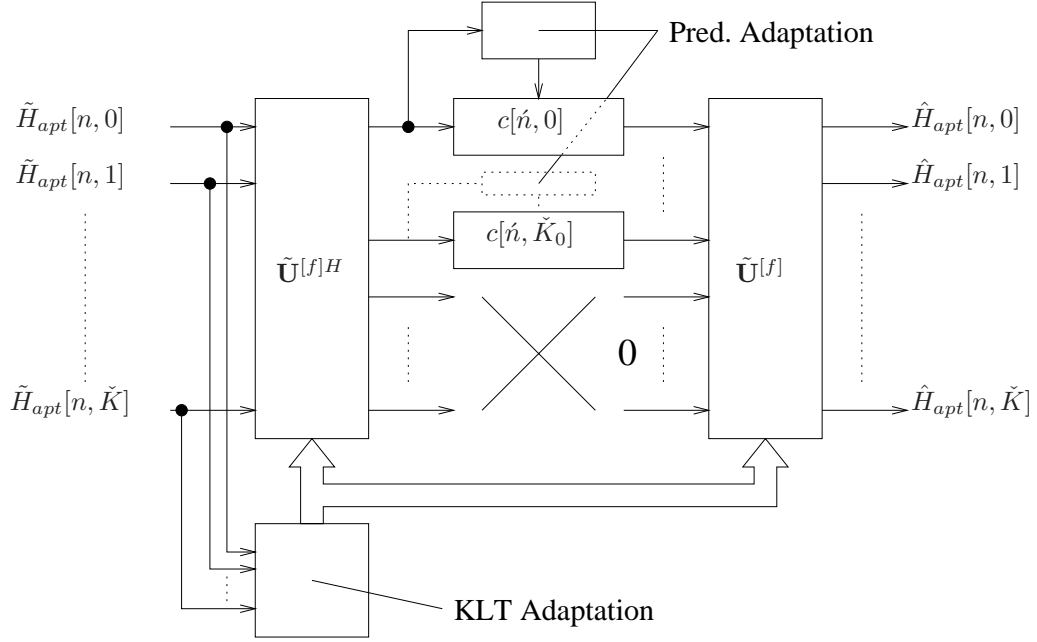
Figure 19.8: Stylized illustration of a fully adaptive 2D-MMSE based channel predictor. The KLT co-
efficients are adapted for the sake of transforming the initial *a posteriori* channel transfer
factor estimates to the CIR-related domain and for transforming the filtered CIR-related
tap predictions back to the frequency-domain. Furthermore, also the CIR-related tap pre-
dictor coefficients are subjected to adaptation, potentially invoking the RLS algorithm.
Note that we have defined $\check{K} = K - 1$.

limited. A significant performance improvement was hence achieved by computing the mod-
ulation mode assignment based on the *a priori* channel transfer factor estimates generated
for the following OFDM symbol period with the aid of the 2D-MMSE based channel pre-
dictor. Note that the benefits of combining decision-directed channel prediction and adaptive
modulation are twofold. On the one hand, the modulation mode assignment profits from
the accurate channel predictions and on the other hand the channel predictions benefit from
the more reliable remodulated reference signal invoked in the DDCE process in the light of
employing adaptive modulation.

19.3.3 Channel Estimation for Multi-User SDMA-OFDM

In the context of a single-user, single-transmit antenna assisted scenario the task of acquiring
a set of K initial *a posteriori* channel transfer factor estimates was accomplished by sim-
ply dividing the signal received in each subcarrier by the subcarrier's complex transmitted
symbol. These initial *a posteriori* channel transfer factor estimates were then employed for
deriving improved *a posteriori* channel transfer factor estimates for the current OFDM sym-
bol period or for generating *a priori* channel transfer factor estimates for employment during

the next OFDM symbol period upon invoking CIR-related tap estimation- or prediction filtering, respectively.

By contrast, in the context of a multi-user SDMA-OFDM scenario, the signal received by each antenna element at the basestation is constituted by the superposition of the L different users' transmitted and independently faded signals.

19.3.3.1   LS-Assisted DDCE

Based on the observation that the channel's multipath spread T_m - normalized to the OFDM sampling period duration T_s - is typically only a fraction of the number of subcarriers K, a subspace-based approach was proposed by Li *et al.* [91] for recovering the L sets of K-subcarrier channel transfer factors associated with a specific BS receiver antenna. Based on the Least-Squares (LS) error criterion the vector of received subcarrier signals is projected onto the sub-space spanned by the first K_0 number of column vectors associated with the K-th order DFT matrix upon taking into account the different users' unique transmitted subcarrier symbol sequences. As a result, for each of the L users a set of K_0 CIR-related tap estimates is obtained, which are then subjected to the DFT in order to obtain the desired L number of sets of channel transfer factor estimates.

Our mathematical portrayal of this estimation problem capitalized on a more compact matrix notation than that of [91], which further motivated the employment of the LS error criterion as proposed by Li *et al.* [91]. Based on this notation a necessary condition was provided for the identification of the different users' CIR-related taps. More explicitly, the product of the L number of users and the K_0 number of CIR-related taps to be estimated was required to be lower than or equal to the K number of OFDM subcarriers, namely we required that the condition of $LK_0 \leq K$ was satisfied. While this constitutes a necessary condition, it was observed that if the L number of users was close to the tolerable limit, the estimation MSE was potentially degraded depending on the specific subcarrier symbol sequences transmitted by the different users. This provided an additional motivation for devising alternative multiuser channel estimation approaches.

Furthermore, the computational complexity of the LS-assisted DDCE was found to be substantial, because a system of equations associated with a left-hand matrix of dimension $LK_0 \times LK_0$ and a right-hand matrix of dimension $LK_0 \times P$ had to be solved for estimating the CIR-related taps of the MIMO system's channels between the L users' single transmit antennas and the base-station's P receiver antennas. However, an advantage of the LS-assisted DDCE is that its MSE can be further improved by invoking pure transversal CIR-related tap filtering.

19.3.3.2   PIC-Assisted DDCE

In order to address the LS-assisted DDCE's deficiency of supporting only a limited number of users and imposing a potentially excessive computational complexity, the idea of Parallel Interference Cancellation (PIC)-assisted DDCE was further developed, which was originally suggested for the CIR-related domain by Li [93] and for the frequency-domain by Jeon *et al.* [92] was significantly further developed. We argued above that since in a multi-user SDMA-OFDM scenario the signal received by a specific antenna element is given by the superposition of the different users' transmitted signals, the low-complexity single-user tech-

niques for deriving initial *a posteriori* channel transfer factor estimates cannot be directly applied. However, a viable approach for the estimation of a specific user's channel transfer factors is constituted by first removing the remaining users' interference from the received composite multi-user signal, and then performing the channel estimation with the aid of the same techniques as in the single transmit-antenna assisted scenario. This involves generating the initial *a posteriori* channel transfer factor estimates, followed by CIR-related based domain filtering. We found that from a mathematical point of view, performing the PIC in the frequency-domain- or in the time-domain are identical. However, performing the PIC in the frequency-domain, while the filtering in the CIR-related domain seems to be the least complex solution. Note that in the context of the PIC process the remaining users' interfering signal components are reconstructed based on the sliced symbols generated at the multi-user detector's output, and upon invoking furthermore the associated *a priori* channel transfer factor estimates generated during the previous OFDM symbol period for the current OFDM symbol period.

However, compared to the single-user single-transmit antenna assisted scenario, the prediction filters to be potentially employed in the CIR-related domain for further enhancing the estimator's MSE were shown not to be transversal, but recursive. In the context of our discussions, mathematical expressions were derived for the current OFDM symbol's *a posteriori* channel transfer factor estimates' MSE and for the next OFDM symbol's predicted *a priori* channel transfer factor estimates' MSE. Furthermore, conditions for the estimator's stability were provided. Based on the system equations' contractive properties [90] an iterative algorithm was devised for the off-line optimization of the CIR-related tap predictor's coefficients with the aim of minimizing the *a priori* estimator's average MSE. Our simulation results demonstrated that the number of users each having a single transmit antenna is not limited by K/K_0, as it is the case for the LS-assisted DDCE. Furthermore we found that also the principles of "robustness" with respect to the channel's actual scattering function as invoked in the single-user scenario were also applicable for the multi-user scenario, which renders the off-line optimization of the CIR-related tap predictor coefficients an attractive option. In the context of our investigations we also illustrated the effects of a non-sampled spaced CIR on the estimator's MSE, based on using the DFT matrix as the unitary transform matrix for conveying the inital *a posteriori* channel transfer factor estimates to the CIR-related domain. We found that as a result of retaining only the K_0 most significant CIR-related taps with the aim of reducing the estimator's complexity, in the frequency-domain the channel transfer factors' estimation MSE significantly increased towards the edges of the OFDM symbol. This problem can be addressed by using the "robust" transform basis' as proposed by Li and Sollenberger [80] instead of the unitary DFT matrix.

In order to potentially further improve the estimator's MSE and for rendering the estimator capable of appropriately reacting to impulsive noise as caused for example by erroneous subcarrier symbol decisions, we demonstrated that the adaptation of the CIR-related tap predictor coefficients could also be performed with the aid of the RLS algorithm. It is interesting to note that although the different predictors associated with the CIR-related taps of a specific channel- or with different channels perform their coefficient adaptation independently, the estimators' average MSE is minimized.

19.3.4 Uplink Detection Techniques for SDMA-OFDM

Finally, in Chapter 16 we discussed a range of uplink multi-user detection techniques, which - in addition to multi-user channel estimation - constitute one of the pivotal components of the SDMA-OFDM receiver. The detection techniques investigated were separated into the sub-classes of linear- and non-linear detection. Specifically, in the context of linear detection techniques, such as the Least-Squares (LS)- and Minimum Mean-Square Error (MMSE) approaches no *a priori* knowledge about any of the other users' transmitted symbols is required for the detection of a specific user's transmitted symbol. This in contrast to the family of non-linear detectors, namely to the Successive Interference Cancellation (SIC), Parallel Interference Cancellation (PIC) and Maximum Likelihood (ML) detection based approaches. Explicitly, in the context of these schemes *a priori* knowledge about one or more of the remaining users' transmitted symbols is required for the detection of a specific user's transmitted symbol. An exception is the first cancellation stage of the SIC detector.

For the different multi-user detectors investigated a mathematical analysis as well as a performance- and complexity analysis was conducted. We found that the linear detectors, which perform the operations of linear combining and classification sequentially, constitute the lowest-complexity, but also the least powerful solutions in terms of the achievable BER. By contrast, the ML detector is associated with the highest computational complexity due to evaluating M_c^L number of L-dimensional trial-vectors in each subcarrier in terms of their Euclidean distance from the vector of received signals upon taking into account the effects of the channel. As a benefit, the ML detector's BER performance is optimum. Recall in this context that L denotes the number of simultaneous SDMA users and M_c is the number of constellation points associated with the specific modulation scheme employed. A compromise between the achievable performance and complexity imposed is given by the SIC- and PIC detectors.

19.3.4.1 SIC Detection

The philosophy of the SIC scheme is based on linearly detecting and cancelling successively in each stage of the detection process the strongest remaining user in terms of an objective measure, which could either be the SNR, SIR or SINR at the linear combiner's output of each detection stage. Thus, the minimum occuring value of the objective function is maximized. The potential of various schemes was assessed for further enhancing the SIC detector's performance, namely that of the M-SIC, partial M-SIC and SDI-M-SIC schemes, which were contrived based on the idea of tracking multiple tentative symbol decisions from each detection stage, while performing a decision as regards to which symbols were transmitted, after the cancellation of the last user. Our analysis of SIC also considered the effects of error propagation potentially occuring between the different detection stages. Based on these observations an improved metric was developed for soft-bit generation to be employed in the context of a system using turbo-decoding at the receiver. While the SIC and M-SIC schemes potentially perform close to ML detection, this is achieved at the cost of a significantly increased computational complexity compared to the MMSE detection.

19.3.4.2   PIC Detection

We found that a further enhancement of the performance versus complexity tradeoffs is constituted by the PIC detector. Recall that the signal received by the different BS antenna elements is constituted by the superposition of the different users' transmitted signals. Hence, a linear estimate of a specific user's transmitted signal can be generated upon removing the remaining users' transmitted signals, followed by single-user diversity combining. In the context of PIC detection, initial symbol decisions are generated for reconstructing the channel-impaired transmitted signals to be used in the actual cancellation process are generated with the aid of an MMSE detector. While in the context of an uncoded scenario the PIC detector was found to perform only marginally better, than the MMSE detector, in the turbo-coded scenario a significant performance improvement was observed when using the sliced, interleaved and remodulated "source- plus parity"-related soft-output bits of the turbo-decoder obtained during the first detection stage as a reference for the PIC process of the second stage. A further performance improvement can potentially be achieved with the aid of a soft-bit based PIC process instead of a hard-decision based PIC.

19.3.4.3   Improvement of MMSE- and PIC-Detection by Adaptive Modulation or WHT Spreading

In order to render the employment of MMSE- and PIC detection more attractive also in an uncoded scenario, investigations were conducted with respect to additional employing either adaptive modulation or Walsh-Hadamard Transform (WHT) based spreading in the multi-user SDMA-OFDM scenario. We found that these techniques are most effective in the context of a fully-loaded system, namely where the number of simultaneous users - and hence the number of transmit antennas - equals the number of BS receiver antenna elements. Given the restriction of employing AOFDM only in Time-Division Duplexing (TDD) scenarios and the requirement of employing prediction filtering for compensating for the channel's variations with time, a more straightforward solution is constituted by WHT spreading across the different subcarriers. While at the transmitters the Walsh Hadamard Transform can be combined with the OFDM-related IFFT, as proposed in [], at the receiver the computational complexity is increased, since the despreading has to be performed separately for each user. In the context of our investigations we highlighted that both in the single-user- and in the multi-user SDMA-OFDM system, the equalization- or linear combining at the receiver and the despreading can be performed sequentially as a result of the WHT matrix's unitar nature. Our simulation results demonstrated that with the aid of adaptive modulation or WHT spreading the performance of the MMSE- or PIC detection assisted systems can be significantly improved. Hence these schemes constitute an attractive compromise in comparison to the significantly more complex SIC-assisted SDMA-OFDM schemes. For further reading on related topics we refer to [497–505].

19.3.5   OFDM Based Wireless Video System Design

Finally, in Chapter 18 we considered a few application examples in the context of OFDM-based wireless video telephony. Specifically, in Section 18.1 a range of AOFDM video transceivers has been proposed for robust, flexible and low-delay interactive videotelephony. In order to minimize the amount of signaling required, we divided the OFDM subcarriers into

subbands and controlled the modulation modes on a subband-by-subband basis. The proposed constant target bit-rate AOFDM modems provided a lower BER than the corresponding conventional OFDM modems. The slightly more complex switched TVTBR-AOFDM modems can provide a balanced video-quality performance, across a wider range of channel SNRs than the other schemes investigated.

In Section 18.2 multiuser detection assisted, multiple transmit antenna based OFDM schemes were studied in the context of HIPRLAN 2-like systems. It was demonstrated that the system's user capacity can be improved with the aid of unique spatial user signatures. The MLSE detection algorithm outperformed the MMSE scheme by about 5dB in terms of the required SNR and this performance gain manifested itself also in terms of the system's video performance.

19.4   Closing Remarks

This monograph considered a range of OFDM and MC-CDMA-related topics applicable to both single-user and multi-user communications. However, a whole host of further recent advances in the field of communications reserach are applicable also to OFDM. Specifically, the family of classification and learning based neural network assisted receivers investigated in the context of conventional single-carrier systems provides a rich set of further research topics. Partial response modulation techniques also have the promise of performance advantages in OFDM schemes. The joint optimization of adaptive subcarrier bit-allocation and crest-factor reduction techniques constitutes a further research challange in the context of multiuser OFDM and MC-CDMA systems. All the above-mentioned techniques have the potential of improving the complexity versus performance balance of the system. The design of joint coding and modulation schemes is particularly promising in the context of OFDM and MC-CDMA. Finally, the employment of OFDM in ultra-wide band systems invoking various frequency-hopping and multiple access techniques is likely to grow in popularity as an exciting reserach area.

These enabling techniques along with those detailed in the book are expected to find their way into future standards, such as the successors of the 802.11, the High Performance Local Area Network standard known as HiPerLAN, the European Digital Audio Broadcast (DAB) and Digital Video Broadcast (DVB) arrangements and their descendents. They are also likely to be adopted by the standardisation bodies in future generations of personal communications systems.

It is expected that wireless systems of the near future are likely to witness the co-existence of space-time-coded transmit diversity arrangements and near-instantaneously adaptive OFDM as well as MC-CDMA schemes for years to come. Intelligent learning algorithms will configure the transceivers in the appropriate mode that ultimately provides the best trade-off in terms of satisfying the user's preference in the context of the service requested [7, 202, 204].

A further advantage of the near-instantaneously adaptive OFDM and MC-CDMA transceivers is that they allow the system to instantaneously drop its transmission rate, when the channel quality is reduced for example as a consequence of the instantaneously peaking co-channel interference. By contrast, a conventional fixed-mode transceiver would drop the call and hence degrade both the quality of service and the network's teletraffic capacity. The

achievable teletraffic performance of adaptive CDMA systems was documented in depth in conjunction with adaptive antenna-assisted dynamic channel allocation schemes in [204].[1]

∗   ∗

Throughout this monograph we have endeavoured to picture the range of contradictory system design trade-offs associated with the conception of OFDM and MC-CDMA systems. We intended to present the material in an unbiased fashion and sufficiently richly illustrated in terms of the associated design trade-offs so that readers will be able to find recipes and examples for solving their own particular wireless communications problems. In this rapidly evolving field it is a challenge to complete a timely, yet self-contained treatise, since new advances are discovered at an accelerating pace, which the authors would like to report on. Our sincere hope is that you, the readers, have found the book a useful source of information, but above all a catalyst of further research.

---

[1] A range of related research papers and book chapters can be found at http://www-mobile.ecs.soton.ac.uk.

Glossary

ACF	Auto-correlation Function
ACTS	Advanced Communications Technologies and Services - a European research programme
ADSL	Asynchronous Digital Subscriber Loop
AOFDM	Adaptive Orthogonal Frequency Division Multiplexing
APR	A Priori
APT	A Posteriori
AWGN	Additive White Gaussian Noise
BER	Bit-Error Ratio
BLAST	Bell Labs Space-Time architecture
BPOS	Bit per OFDM Symbol
BPSK	Binary Phase-Shift Keying
BS	Basestation
CDF	Cumulative Distribution Function
CDMA	Code-Division Multiple Access
CE	Channel Estimation
CIR	Channel Impulse Response
DAB	Digital Audio Broadcasting
DDCE	Decision-Directed Channel Estimation

893

DDCP	Decision-Directed Channel Prediction
DFT	Discrete Fourier Transform
DMUX	Demultiplexer
DTTB	Digital Terrestrial Television Broadcast
D-BLAST	Diagonal BLAST
EM	Expectation Maximization
EVD	EigenValue Decomposition
FDM	Frequency Division Multiplexing
FDMA	Frequency Division Multiple Access
FEC	Forward Error Correction
FFT	Fast Fourier Transform
FIR	Finite Impulse Response
HF	High-Frequency
ICI	Inter-subCarrier Interference
IDFT	Inverse Discrete Fourier Transform
IFFT	Inverse Fast Fourier Transform
IIR	Infinite Impulse Response
ISI	Inter-Symbol Interference
IWHT	Inverse Walsh Hadamard Transform
KLT	Karhunen-Loeve Transform
LLR	Log-Likelihood Ratio
LS	Least-Squares
LSE	Least-Squares Error
MA	Multiple Access
MC	Multi-Carrier
MIMO	Multiple-Input Multiple-Output
ML	Maximum Likelihood

MLSE	Maximum Likelihood Sequence Estimation
MMSE	Minimum Mean-Square Error
MSE	Mean-Square Error
MU	Multi-User
MUD	Multi-User Detection
MUI	Multi-User Interference
MUX	Multiplexer
MV	Minimum Variance
MVDR	Minimum Variance Distortionless Response
OFDM	Orthogonal Frequency Division Multiplexing
PAPR	Peak-to-Average Power Ratio
PDF	Probability Density Function
PIC	Parallel Interference Cancellation
PSAM	Pilot Symbol Aided Modulation
PSD	Power Spectral Density
PSK	Phase-Shift Keying
QAM	Quadrature Amplitude Modulation
QPSK	Quadrature Phase-Shift Keying
RLS	Recursive Least-Squares
RNS	Residue Number System
SB	Subband
SDM	Space-Division Multiplexing
SDMA	Space-Division Multiple Access
SDI	Selective Decision Insertion
SER	Symbol Error Ratio
SIC	Successive Interference Cancellation
SINR	Signal-to-Interference-plus-Noise Ratio

SIR	Signal-to-Interference Ratio
SMI	Sample Matrix Inversion
SNR	Signal-to-Noise Ratio
STC	Space-Time Coding
SVD	Singular-Value Decomposition
TCM	Trellis-Coded Modulation
TDD	Time-Division Duplexing
TDMA	Time-Division Multiple Access
TTCM	Turbo-Trellis Coded Modulation
V-BLAST	Vertical BLAST
WATM	Wireless Asynchronous Transfer Mode
WHT	Walsh-Hadamard Transform
WHTS	Walsh-Hadamard Transform Spreading
ZF	Zero-Forcing
1D	One-Dimensional
2D	Two-Dimensional

Bibliography

[1] R. W. Chang, "Synthesis of band-limited orthogonal signals for multichannel data transmission," *Bell Systems Technical Journal*, vol. 46, pp. 1775–1796, December 1966.

[2] L. Hanzo, W. Webb, and T. Keller, *Single- and Multi-carrier Quadrature Amplitude Modulation*. New York, USA: IEEE Press-John Wiley, April 2000.

[3] W. Webb and R. Steele, "Variable rate QAM for mobile radio," *IEEE Transactions on Communications*, vol. 43, pp. 2223–2230, July 1995.

[4] L. Hanzo, "Bandwidth-efficient wireless multimedia communications," *Proceedings of the IEEE*, vol. 86, pp. 1342–1382, July 1998.

[5] S. Nanda, K. Balachandran, and S. Kumar, "Adaptation techniques in wireless packet data services," *IEEE Communications Magazine*, vol. 38, pp. 54–64, January 2000.

[6] L. Hanzo, F. Somerville, and J. Woodard, *Voice Compression and Communications: Principles and Applications for Fixed and Wireless Channels*. IEEE Press and John Wiley, 2001. (For detailed contents and sample chapters please refer to http://www-mobile.ecs.soton.ac.uk.).

[7] L. Hanzo, P. Cherriman, and J. Streit, *Wireless Video Communications: From Second to Third Generation Systems, WLANs and Beyond*. IEEE Press and John Wiley, 2001. (For detailed contents please refer to http://www-mobile.ecs.soton.ac.uk.).

[8] M. Zimmermann and A. Kirsch, "The AN/GSC-10/KATHRYN/variable rate data modem for HF radio," *IEEE Transactions on Communication Technology*, vol. CCM–15, pp. 197–205, April 1967.

[9] S. B. Weinstein and P. M. Ebert, "Data transmission by frequency division multiplexing using the discrete fourier transform," *IEEE Transactions on Communication Technology*, vol. COM–19, pp. 628–634, October 1971.

[10] L. Cimini, "Analysis and simulation of a digital mobile channel using orthogonal frequency division multiplexing," *IEEE Transactions on Communications*, vol. 33, pp. 665–675, July 1985.

[11] M. Alard and R. Lassalle, "Principles of modulation and channel coding for digital broadcasting for mobile receivers," *EBU Review, Technical No. 224*, pp. 47–69, August 1987.

[12] *Proceedings of 1st International Symposium,DAB*, (Montreux, Switzerland), June 1992.

[13] A. Peled and A. Ruiz, "Frequency domain data transmission using reduced computational complexity algorithms," in *Proceedings of International Conference on Acoustics, Speech, and Signal Processing, ICASSP'80*, vol. 3, (Denver, CO, USA), pp. 964–967, IEEE, 9–11 April 1980.

[14] B. Hirosaki, "An orthogonally multiplexed QAM system using the discrete fourier transform," *IEEE Transactions on Communications*, vol. COM-29, pp. 983–989, July 1981.

[15] H. Kolb, "Untersuchungen über ein digitales mehrfrequenzverfahren zur datenübertragung," in *Ausgewählte Arbeiten über Nachrichtensysteme*, no. 50, Universität Erlangen-Nürnberg, 1982.

[16] H. Schüssler, "Ein digitales Mehrfrequenzverfahren zur Datenübertragung," in *Professoren-Konferenz, Stand und Entwicklungsaussichten der Daten und Telekommunikation*, (Darmstadt, Germany), pp. 179–196, 1983.

[17] K. Preuss, "Ein Parallelverfahren zur schnellen Datenübertragung Im Ortsnetz," in *Ausgewählte Arbeiten über Nachrichtensysteme*, no. 56, Universität Erlangen-Nürnberg, 1984.

[18] R. Rückriem, "Realisierung und messtechnische Untersuchung an einem digitalen Parallelverfahren zur Datenübertragung im Fernsprechkanal," in *Ausgewählte Arbeiten über Nachrichtensysteme*, no. 59, Universität Erlangen-Nürnberg, 1985.

[19] I. Kalet, "The multitone channel," *IEEE Transactions on Communications*, vol. 37, pp. 119–124, February 1989.

[20] B. Hirosaki, "An analysis of automatic equalizers for orthogonally multiplexed QAM systems," *IEEE Transactions on Communications*, vol. COM-28, pp. 73–83, January 1980.

[21] P. Bello, "Selective fading limitations of the KATHRYN modem and some system design considerations," *IEEE Trabsactions on Communications Technology*, vol. COM–13, pp. 320–333, September 1965.

[22] E. Powers and M. Zimmermann, "A digital implementation of a multichannel data modem," in *Proceedings of the IEEE International Conference on Communications*, (Philadelphia, USA), 1968.

[23] R. Chang and R. Gibby, "A theoretical study of performance of an orthogonal multiplexing data transmission scheme," *IEEE Transactions on Communication Technology*, vol. COM–16, pp. 529–540, August 1968.

[24] B. R. Saltzberg, "Performance of an efficient parallel data transmission system," *IEEE Transactions on Communication Technology*, pp. 805–813, December 1967.

[25] K. Fazel and G. Fettweis, eds., *Multi-Carrier Spread-Spectrum*. Dordrecht: Kluwer, 1997. ISBN 0-7923-9973-0.

[26] F. Classen and H. Meyr, "Synchronisation algorithms for an OFDM system for mobile communications," in *Codierung für Quelle, Kanal und Übertragung*, no. 130 in ITG Fachbericht, (Berlin), pp. 105–113, VDE–Verlag, 1994.

[27] F. Classen and H. Meyr, "Frequency synchronisation algorithms for OFDM systems suitable for communication over frequency selective fading channels," in *Proceedings of IEEE VTC '94*, (Stockholm, Sweden), pp. 1655–1659, IEEE, 8–10 June 1994.

[28] R. van Nee and R. Prasad, *OFDM for wireless multimedia communications*. London: Artech House Publishers, 2000.

[29] P. Vandenameele, L. van der Perre, and M. Engels, *Space division multiple access for wireless local area networks*. Kluwer, 2001.

[30] S. Shepherd, P. van Eetvelt, C. Wyatt-Millington, and S. Barton, "Simple coding scheme to reduce peak factor in QPSK multicarrier modulation," *Electronics Letters*, vol. 31, pp. 1131–1132, July 1995.

[31] A. E. Jones, T. A. Wilkinson, and S. K. Barton, "Block coding scheme for reduction of peak to mean envelope power ratio of multicarrier transmission schemes," *Electronics Letters*, vol. 30, pp. 2098–2099, December 1994.

[32] D. Wulich, "Reduction of peak to mean ratio of multicarrier modulation by cyclic coding," *Electronics Letters*, vol. 32, pp. 432–433, 1996.

[33] S. Müller and J. Huber, "Vergleich von OFDM–Verfahren mit reduzierter Spitzenleistung," in *2. OFDM–Fachgespräch in Braunschweig*, 1997.

[34] M. Pauli and H.-P. Kuchenbecker, "Neue Aspekte zur Reduzierung der durch Nichtlinearitäten hervorgerufenen Außerbandstrahlung eines OFDM–Signals," in *2. OFDM–Fachgespräch in Braunschweig*, 1997.

[35] T. May and H. Rohling, "Reduktion von Nachbarkanalstörungen in OFDM–Funkübertragungssystemen," in *2. OFDM–Fachgespräch in Braunschweig*, 1997.

[36] D. Wulich, "Peak factor in orthogonal multicarrier modulation with variable levels," *Electronics Letters*, vol. 32, no. 20, pp. 1859–1861, 1996.

[37] H. Schmidt and K. Kammeyer, "Adaptive Subträgerselektion zur Reduktion des Crest faktors bei OFDM," in *3. OFDM Fachgespräch in Braunschweig*, 1998.

[38] R. Dinis and A. G. ao, "Performance evaluation of OFDM transmission with conventional and 2-branch combining power amplification schemes," in *Proceeding of IEEE Global Telecommunications Conference, Globecom 96*, (London, UK), pp. 734–739, IEEE, 18–22 November 1996.

[39] R. Dinis, P. Montezuma, and A. G. ao, "Performance trade-offs with quasi-linearly amplified OFDM through a 2-branch combining technique," in *Proceedings of IEEE VTC'96*, (Atlanta, GA, USA), pp. 899–903, IEEE, 28 April–1 May 1996.

[40] R. Dinis, A. G. ao, and J. Fernandes, "Adaptive transmission techniques for the mobile broadband system," in *Proceeding of ACTS Mobile Communication Summit '97*, (Aalborg, Denmark), pp. 757–762, ACTS, 7–10 October 1997.

[41] B. Daneshrad, L. Cimini Jr., and M. Carloni, "Clustered-OFDM transmitter implementation," in *Proceedings of IEEE International Symposium on Personal, Indoor, and Mobile Radio Communications (PIMRC'96)*, (Taipei, Taiwan), pp. 1064–1068, IEEE, 15–18 October 1996.

[42] M. Okada, H. Nishijima, and S. Komaki, "A maximum likelihood decision based nonlinear distortion compensator for multi-carrier modulated signals," *IEICE Transactions on Communications*, vol. E81B, no. 4, pp. 737–744, 1998.

[43] R. Dinis and A. G. ao, "Performance evaluation of a multicarrier modulation technique allowing strongly nonlinear amplification," in *Proceedings of ICC 1998*, pp. 791–796, IEEE, 1998.

[44] T. Pollet, M. van Bladel, and M. Moeneclaey, "BER sensitivity of OFDM systems to carrier frequency offset and wiener phase noise," *IEEE Transactions on Communications*, vol. 43, pp. 191–193, February/March/April 1995.

[45] H. Nikookar and R. Prasad, "On the sensitivity of multicarrier transmission over multipath channels to phase noise and frequency offset," in *Proceedings of IEEE International Symposium on Personal, Indoor, and Mobile Radio Communications (PIMRC'96)*, (Taipei, Taiwan), pp. 68–72, IEEE, 15–18 October 1996.

[46] W. Warner and C. Leung, "OFDM/FM frame synchronization for mobile radio data communication," *IEEE Transactions on Vehicular Technology*, vol. 42, pp. 302–313, August 1993.

[47] H. Sari, G. Karam, and I. Jeanclaude, "Transmission techniques for digital terrestrial TV broadcasting," *IEEE Communications Magazine*, pp. 100–109, February 1995.

[48] P. Moose, "A technique for orthogonal frequency division multiplexing frequency offset correction," *IEEE Transactions on Communications*, vol. 42, pp. 2908–2914, October 1994.

[49] K. Brüninghaus and H. Rohling, "Verfahren zur Rahmensynchronisation in einem OFDM-System," in *3. OFDM Fachgespräch in Braunschweig*, 1998.

[50] F. Daffara and O. Adami, "A new frequency detector for orthogonal multicarrier transmission techniques," in *Proceedings of IEEE Vehicular Technology Conference (VTC'95)*, (Chicago, USA), pp. 804–809, IEEE, 15–28 July 1995.

[51] M. Sandell, J.-J. van de Beek, and P. Börjesson, "Timing and frequency synchronisation in OFDM systems using the cyclic prefix," in *Proceedings of International Symposium on Synchronisation*, (Essen, Germany), pp. 16–19, 14–15 December 1995.

[52] N. Yee, J.-P. Linnartz, and G. Fettweis, "Multicarrier CDMA in indoor wireless radio networks," in *PIMRC'93*, pp. 109–113, 1993.

[53] A. Chouly, A. Brajal, and S. Jourdan, "Orthogonal multicarrier techniques applied to direct sequence spread spectrum CDMA systems," in *Proceedings of the IEEE Global Telecommunications Conference 1993*, (Houston, TX, USA), pp. 1723–1728, 29 November – 2 December 1993.

[54] G. Fettweis, A. Bahai, and K. Anvari, "On multi-carrier code division multiple access (MC-CDMA) modem design," in *Proceedings of IEEE VTC '94*, (Stockholm, Sweden), pp. 1670–1674, IEEE, 8–10 June 1994.

[55] K. Fazel and L. Papke, "On the performance of convolutionally-coded CDMA/OFDM for mobile communication system," in *PIMRC'93*, pp. 468–472, 1993.

[56] R. Prasad and S. Hara, "Overview of multicarrier CDMA," *IEEE Communications Magazine*, pp. 126–133, December 1997.

[57] B.-J. Choi, E.-L. Kuan, and L. Hanzo, "Crest–factor study of MC-CDMA and OFDM," in *Proceeding of VTC'99 (Fall)*, vol. 1, (Amsterdam, Netherlands), pp. 233–237, IEEE, 19–22 September 1999.

[58] P. Höher, "TCM on frequency-selective land-mobile fading channels," in *International Workshop on Digital Communications*, (Tirrenia, Italy), pp. 317–328, September 1991.

[59] J. S. Chow, J. M. Cioffi, and J. A. C. Bingham, "Equalizer training algorithms for multicarrier modulation systems.," in *International Conference on Communications*, (Geneva, Switzerland), pp. 761–765, IEEE, May 1993.

[60] S. K. Wilson, R. E. Khayata, and J. M. Cioffi, "16QAM Modulation with Orthogonal Frequency Division Multiplexing in a Rayleigh-Fading Environment," in *Vehicular Technology Conference*, vol. 3, (Stockholm, Sweden), pp. 1660–1664, IEEE, June 1994.

[61] J.-J. van de Beek, O. Edfors, M. Sandell, S. K. Wilson, and P. O. Börjesson, "On channel estimation in OFDM systems," in *Proceedings of Vehicular Technology Conference*, vol. 2, (Chicago, IL USA), pp. 815–819, IEEE, July 1995.

[62] O. Edfors, M. Sandell, J. J. v. .d. Beek, S. K. Wilson, and P. O. Börjesson, "OFDM Channel Estimation by Singular Value Decomposition," in *Proceedings of Vehicular Technology Conference*, vol. 2, (Atlanta, GA USA), pp. 923–927, IEEE, April 28 - May 1 1996.

[63] P. Frenger and A. Svensson, "A Decision Directed Coherent Detector for OFDM," in *Proceedings of Vehicular Technology Conference*, vol. 3, (Atlanta, GA USA), pp. 1584–1588, IEEE, Apr 28 - May 1 1996.

[64] V. Mignone and A. Morello, "CD3-OFDM: A Novel Demodulation Scheme for Fixed and Mobile Receivers," *IEEE Transactions on Communications*, vol. 44, pp. 1144–1151, September 1996.

[65] F. Tufvesson and T. Maseng, "Pilot Assisted Channel Estimation for OFDM in Mobile Cellular Systems," in *Proceedings of Vehicular Technology Conference*, vol. 3, (Phoenix, Arizona), pp. 1639–1643, IEEE, May 4-7 1997.

[66] P. Höher, S. Kaiser, and P. Robertson, "Two-dimensional pilot-symbol-aided channel estimation by Wiener filtering," in *International Conference on Acoustics, Speech and Signal Processing*, (Munich, Germany), pp. 1845–1848, IEEE, April 1997.

[67] P. Höher, S. Kaiser, and P. Robertson, "Pilot–symbol–aided channel estimation in time and frequency," in *Proceedings of Global Telecommunications Conference: The Mini–Conf.*, (Phoenix, AZ), pp. 90–96, IEEE, November 1997.

[68] Y. Li, L. J. Cimini, and N. R. Sollenberger, "Robust Channel Estimation for OFDM Systems with Rapid Dispersive Fading Channels," *IEEE Transactions on Communications*, vol. 46, pp. 902–915, April 1998.

[69] O. Edfors, M. Sandell, J.-J. v. d. Beek, S. K. Wilson, and P. O. Börjesson, "OFDM Channel Estimation by Singular Value Decomposition," *IEEE Transactions on Communications*, vol. 46, pp. 931–939, April 1998.

[70] F. Tufvesson, M. Faulkner, and T. Maseng, "Pre-Compensation for Rayleigh Fading Channels in Time Division Duplex OFDM Systems," in *Proceedings of 6th International Workshop on Intelligent Signal Processing and Communications Systems*, (Melbourne, Australia), pp. 57–33, IEEE, November 5-6 1998.

[71] M. Itami, M. Kuwabara, M. Yamashita, H. Ohta, and K. Itoh, "Equalization of Orthogonal Frequency Division Multiplexed Signal by Pilot Symbol Assisted Multipath Estimation," in *Proceedings of Global Telecommunications Conference*, vol. 1, (Sydney, Australia), pp. 225–230, IEEE, November 8-12 1998.

[72] E. Al-Susa and R. F. Ormondroyd, "A Predictor-Based Decision Feedback Channel Estimation Method for COFDM with High Resilience to Rapid Time-Variations," in *Proceedings of Vehicular Technology Conference*, vol. 1, (Amsterdam, Netherlands), pp. 273–278, IEEE, September 19-22 1999.

[73] B. Yang, K. B. Letaief, R. S. Cheng, and Z. Cao, "Robust and Improved Channel Estimation for OFDM Systems in Frequency Selective Fading Channels," in *Proceedings of Global Telecommunications Conference*, vol. 5, (Rio de Janeiro, Brazil), pp. 2499–2503, IEEE, December 5-9 1999.

[74] Y. Li, "Pilot-Symbol-Aided Channel Estimation for OFDM in Wireless Systems," *IEEE Transactions on Vehicular Technology*, vol. 49, pp. 1207–1215, July 2000.

[75] B. Yang, K. B. Letaief, R. S. Cheng, and Z. Cao, "Channel Estimation for OFDM Transmission in Multipath Fading Channels Based on Parametric Channel Modeling," *IEEE Transactions on Communications*, vol. 49, pp. 467–479, March 2001.

[76] S. Zhou and G. B. Giannakis, "Finite-Alphabet Based Channel Estimation for OFDM and Related Multicarrier Systems," *IEEE Transactions on Communications*, vol. 49, pp. 1402–1414, August 2001.

[77] X. Wang and K. J. R. Liu, "OFDM Channel Estimation Based on Time-Frequency Polynomial Model of Fading Multipath Channel," in *Proceedings of Vehicular Technology Conference*, vol. 1, (Atlantic City, NJ USA), pp. 460–464, IEEE, October 7-11 2001.

[78] B. Yang, Z. Cao, and K. B. Letaief, "Analysis of Low-Complexity Windowed DFT-Based MMSE Channel Estimator for OFDM Systems," *IEEE Transactions on Communications*, vol. 49, pp. 1977–1987, November 2001.

[79] B. Lu and X. Wang, "Bayesian Blind Turbo Receiver for Coded OFDM Systems with Frequency Offset and Frequency-Selective Fading," *IEEE Journal on Selected Areas in Communications*, vol. 19, pp. 2516–2527, December 2001.

[80] Y. Li and N. R. Sollenberger, "Clustered OFDM with Channel Estimation for High Rate Wireless Data," *IEEE Transactions on Communications*, vol. 49, pp. 2071–2076, December 2001.

[81] M. Morelli and U. Mengali, "A Comparison of Pilot-Aided Channel Estimation Methods for OFDM Systems," *IEEE Transactions on Signal Processing*, vol. 49, pp. 3065–3073, December 2001.

[82] M.-X. Chang and Y. T. Su, "Model-Based Channel Estimation for OFDM Signals in Rayleigh Fading," *IEEE Transactions on Communications*, vol. 50, pp. 540–544, April 2002.

[83] M. C. Necker and G. L. Stüber, "Totally Blind Channel Estimation for OFDM over Fast Varying Mobile Channels," in *Proceedings of International Conference on Communications*, (New York, NY USA), IEEE, April 28 - May 2 2002.

[84] B. Yang, Z. Cao, and K. B. Letaief, "Low Complexity Channel Estimator Based on Windowed DFT and Scalar Wiener Filter for OFDM Systems," in *Proceedings of International Conference on Communications*, vol. 6, (Helsinki, Finnland), pp. 1643–1647, IEEE, June 11-14 2001.

[85] J. R. Deller, J. G. Proakis, and J. H. L. Hansen, *Discrete-Time Processing of Speech Signals*. Macmillan Publishing Company, 1993.

[86] L. Hanzo, F. C. A. Somerville, and J. P. Woodard, *Voice Compression and Communications*. IEEE Press Wiley Inter-Science, 2001.

[87] A. Duel-Hallen, S. Hu, and H. Hallen, "Long Range Prediction of Fading Signals," *IEEE Signal Processing Magazine*, vol. 17, pp. 62–75, May 2000.

[88] F. Tufvesson, *Design of Wireless Communication Systems - Issues on Synchronization, Channel Estimation and Multi-Carrier Systems*. Department of Applied Electronics, Lund University, Sweden, 2000.

[89] W. H. Press, S. A. Teukolshy, W. T. Vetterling, and B. P. Flannery, *Numerical Recipes in C*. Cambridge University Press, 1992.

[90] T. K. Moon and W. C. Stirling, *Mathematical Methods and Algorithms for Signal Processing*. Prentice Hall, 2000.

[91] Y. Li, N. Seshadri, and S. Ariyavisitakul, "Channel Estimation for OFDM Systems with Transmitter Diversity in Mobile Wireless Channels," *IEEE Journal on Selected Areas in Communications*, vol. 17, pp. 461–471, March 1999.

[92] W. G. Jeon, K. H. Paik, and Y. S. Cho, "An Efficient Channel Estimation Technique for OFDM Systems with Transmitter Diversity," in *Proceedings of International Symposium on Personal, Indoor and Mobile Radio Communications*, vol. 2, (Hilton London Metropole Hotel, London, UK), pp. 1246–1250, IEEE, September 18-21 2000.

[93] Y. Li, "Optimum Training Sequences for OFDM Systems with Multiple Transmit Antennas," in *Proc. of Global Telecommunications Conference*, vol. 3, (San Francisco, United States), pp. 1478–1482, IEEE, November 27 - December 1 2000.

[94] A. N. Mody and G. L. Stüber, "Parameter Estimation for OFDM with Transmit Receive Diversity," in *Proceedings of Vehicular Technology Conference*, vol. 2, (Rhodes, Greece), pp. 820–824, IEEE, May 6-9 2001.

[95] Y. Gong and K. B. Letaief, "Low Rank Channel Estimation for Space-Time Coded Wideband OFDM Systems," in *Proceedings of Vehicular Technology Conference*, vol. 2, (Atlantic City Convention Center, Atlantic City, NJ USA), pp. 772–776, IEEE, October 7-11 2001.

[96] W. Jeon, K. H. Paik, and Y. S. Cho, "Two-Dimensional MMSE Channel Estimation for OFDM Systems with Transmitter Diversity," in *Proceedings of Vehicular Technology Conference*, vol. 3, (Atlantic City Convention Center, Atlantic City, NJ USA), pp. 1682–1685, IEEE, October 7-11 2001.

[97] F. W. Vook and T. A. Thomas, "MMSE Multi-User Channel Estimation for Broadband Wireless Communications," in *Proceedings of Global Telecommunications Conference*, vol. 1, (San Antonio, Texas, USA), pp. 470–474, IEEE, November 25-29 2001.

[98] Y. Xie and C. N. Georghiades, "An EM-based Channel Estimation Algorithm for OFDM with Transmitter Diversity," in *Proceedings of Global Telecommunications Conference*, vol. 2, (San Antonio, Texas, USA), pp. 871–875, IEEE, November 25-29 2001.

[99] Y. Li, "Simplified Channel Estimation for OFDM Systems with Multiple Transmit Antennas," *IEEE Transactions on Wireless Communications*, vol. 1, pp. 67–75, January 2002.

[100] Bölcskei, J. R. W. Heath, and A. J. Paulray, "Blind Channel Identification and Equalization in OFDM-Based Multi-Antenna Systems," *IEEE Transactions on Signal Processing*, vol. 50, pp. 96–109, January 2002.

[101] H. Minn, D. I. Kim, and V. K. Bhargava, "A Reduced Complexity Channel Estimation for OFDM Systems with Transmit Diversity in Mobile Wireless Channels," *IEEE Transactions on Wireless Communications*, vol. 50, pp. 799–807, May 2002.

[102] S. B. Slimane, "Channel Estimation for HIPERLAN/2 with Transmitter Diversity," in *International Conference on Communications*, (New York, NY USA), IEEE, April 28 - May 2 2002.

[103] C. Komninakis, C. Fragouli, A. H. Sayed, and R. D. Wesel, "Multi-Input Multi-Output Fading Channel Tracking and Equalization Using Kalman Estimation," *IEEE Transactions on Signal Processing*, vol. 50, pp. 1065–1076, May 2002.

[104] G. J. Foschini, "Layered Space-Time Architecture for Wireless Communication in a Fading Environment when using Multi-Element Antennas"," *Bell Labs Technical Journal*, vol. Autumn, pp. 41–59, 1996.

[105] F. Vook and K. Baum, "Adaptive antennas for OFDM," in *Proceedings of IEEE Vehicular Technology Conference (VTC'98)*, vol. 2, (Ottawa, Canada), pp. 608–610, IEEE, 18–21 May 1998.

[106] X. Wang and H. V. Poor, "Robust Adaptive Array for Wireless Communications," *IEEE Transactions on Communications*, vol. 16, pp. 1352–1366, October 1998.

[107] K.-K. Wong, R. S.-K. Cheng, K. B. Letaief, and R. D. Murch, "Adaptive Antennas at the Mobile and Base Station in an OFDM/TDMA System," in *Proceedings of Global Telecommunications Conference*, vol. 1, (Sydney, Australia), pp. 183–190, IEEE, November 8-12 1998.

[108] Y. Li and N. R. Sollenberger, "Interference Suppression in OFDM Systems using Adaptive Antenna Arrays," in *Proceedings of Global Telecommunications Conference*, vol. 1, (Sydney, Australia), pp. 213–218, IEEE, November 8-12 1998.

[109] G. D. Golden, G. J. Foschini, R. A. Valenzuela, and P. W. Wolniansky, "Detection Algorithms and Initial Laboratory Results using V-BLAST Space-Time Communication Architecture," *IEE Electronics Letters*, vol. 35, pp. 14–16, January 1999.

[110] Y. Li and N. R. Sollenberger, "Adaptive Antenna Arrays for OFDM Systems with Cochannel Interference," *IEEE Transactions on Communications*, vol. 47, pp. 217–229, February 1999.

[111] P. Vandenameele, L. Van der Perre, M. Engels, and H. Man, "A novel class of uplink OFDM/SDMA algorithms for WLAN," in *Proceedings of Global Telecommunications*

Conference — Globecom'99, vol. 1, (Rio de Janeiro, Brazil), pp. 6–10, IEEE, 5–9 December 1999.

[112] M. Speth, A. Senst, and H. Meyr, "Low complexity space-frequency MLSE for multi-user COFDM," in *Proceedings of Global Telecommunications Conference — Globecom'99*, vol. 1, (Rio de Janeiro, Brazil), pp. 2395–2399, IEEE, 5–9 December 1999.

[113] C. Z. W. H. Sweatman, J. S. Thompson, B. Mulgrew, and P. M. Grant, "A Comparison of Detection Algorithms including BLAST for Wireless Communication using Multiple Antennas," in *Proceedings of International Symposium on Personal, Indoor and Mobile Radio Communications*, vol. 1, (Hilton London Metropole Hotel, London, UK), pp. 698–703, IEEE, September 18-21 2000.

[114] R. van Nee, A. van Zelst, and G. Awater, "Maximum Likelihood Decoding in a Space-Division Multiplexing System," in *Proceedings of Vehicular Technology Conference*, vol. 1, (Tokyo, Japan), pp. 6–10, IEEE, May 15-18 2000.

[115] G. Awater, A. van Zelst, and R. van Nee, "Reduced Complexity Space Division Multiplexing Receivers," in *Proceedings of Vehicular Technology Conference*, vol. 1, (Tokyo, Japan), pp. 11–15, IEEE, May 15-18 2000.

[116] A. van Zelst, R. van Nee, and G. A. Awater, "Space Division Multiplexing (SDM) for OFDM systems," in *Proceedings of Vehicular Technology Conference*, vol. 2, (Tokyo, Japan), pp. 1070–1074, IEEE, May 15-18 2000.

[117] P. Vandenameele, L. V. D. Perre, M. G. E. Engels, B. Gyselinckx, and H. J. D. Man, "A Combined OFDM/SDMA Approach," *IEEE Journal on Selected Areas in Communications*, vol. 18, pp. 2312–2321, November 2000.

[118] X. Li, H. C. Huang, A. Lozano, and G. J. Foschini, "Reduced-Complexity Detection Algorithms for Systems Using Multi-Element Arrays," in *Proc. of Global Telecommunications Conference*, vol. 2, (San Francisco, United States), pp. 1072–1076, IEEE, November 27 - December 1 2000.

[119] C. M. Degen, C. M. Walke, A. Lecomte, and B. Rembold, "Adaptive MIMO Techniques for the UTRA-TDD Mode," in *Proceedings of Vehicular Technology Conference*, vol. 1, (Rhodes, Greece), pp. 108–112, IEEE, May 6-9 2001.

[120] X. Zhu and R. D. Murch, "Multi-Input Multi-Output Maximum Likelihood Detection for a Wireless System," in *Proceedings of Vehicular Technology Conference*, vol. 1, (Rhodes, Greece), pp. 137–141, IEEE, May 6-9 2001.

[121] J. Li, K. B. Letaief, R. S. Cheng, and Z. Cao, "Joint Adaptive Power Control and Detection in OFDM/SDMA Wireless LANs," in *Proceedings of Vehicular Technology Conference*, vol. 1, (Rhodes, Greece), pp. 746–750, IEEE, May 6-9 2001.

[122] F. Rashid-Farrokhi, K. J. R. Liu, and L. Tassiulas, "Transmit Beamforming and Power Control for Cellular Wireless Systems," *IEEE Journal on Selected Areas in Communications*, vol. 16, pp. 1437–1450, October 1998.

[123] A. van Zelst, R. van Nee, and G. A. Awater, "Turbo-BLAST and its Performance," in *Proceedings of Vehicular Technology Conference*, vol. 2, (Rhodes, Greece), pp. 1282–1286, IEEE, May 6-9 2001.

[124] A. Benjebbour, H. Murata, and S. Yoshida, "Performance of Iterative Successive Detection Algorithm with Space-Time Transmission," in *Proceedings of Vehicular Technology Conference*, vol. 2, (Rhodes, Greece), pp. 1287–1291, IEEE, May 6-9 2001.

[125] M. Sellathurai and S. Haykin, "A Simplified Diagonal BLAST Architecture with Iterative Parallel-Interference Cancellation Receivers," in *Proceedings of International Conference on Communications*, vol. 10, (Helsinki, Finnland), pp. 3067–3071, IEEE, June 11-14 2001.

[126] A. Bhargave, R. J. P. Figueiredo, and T. Eltoft, "A Detection Algorithm for the V-BLAST System," in *Proceedings of Global Telecommunications Conference*, vol. 1, (San Antonio, Texas, USA), pp. 494–498, IEEE, November 25-29 2001.

[127] S. Thoen, L. Deneire, L. V. D. Perre, and M. Engels, "Constrained Least Squares Detector for OFDM/SDMA-based Wireless Networks," in *Proceedings of Global Telecommunications Conference*, vol. 2, (San Antonio, Texas, USA), pp. 866–870, IEEE, November 25-29 2001.

[128] Y. Li and Z.-Q. Luo, "Parallel Detection for V-BLAST System," in *Proceedings of International Conference on Communications*, (New York, NY USA), IEEE, April 28 - May 2 2002.

[129] Y. Li and N. Sollenberger, "Interference suppression in OFDM systems using adaptive antenna arrays," in *Proceeding of Globecom'98*, (Sydney, Australia), pp. 213–218, IEEE, 8–12 November 1998.

[130] Y. Li and N. Sollenberger, "Adaptive antenna arrays for OFDM systems with cochannel interference," *IEEE Transactions on Communications*, vol. 47, pp. 217–229, February 1999.

[131] Y. Li, L. Cimini, and N. Sollenberger, "Robust channel estimation for OFDM systems with rapid dispersive fading channels," *IEEE Transactions on Communications*, vol. 46, pp. 902–915, April 1998.

[132] C. Kim, S. Choi, and Y. Cho, "Adaptive beamforming for an OFDM sytem," in *Proceeding of VTC'99 (Spring)*, (Houston, TX, USA), IEEE, 16–20 May 1999.

[133] L. Lin, L. Cimini Jr., and J.-I. Chuang, "Turbo codes for OFDM with antenna diversity," in *Proceeding of VTC'99 (Spring)*, (Houston, TX, USA), IEEE, 16–20 May 1999.

[134] M. Münster, T. Keller, and L. Hanzo, "Co–channel interference suppression assisted adaptive OFDM in interference limited environments," in *Proceeding of VTC'99 (Fall)*, vol. 1, (Amsterdam, Netherlands), pp. 284–288, IEEE, 19–22 September 1999.

[135] S. Verdu, *Multiuser Detection*. Cambridge University Press, 1998.

[136] J. Litva and T.-Y. Lo, *Digital Beamforming in Wireless Communications*. London: Artech House Publishers, 1996.

[137] P. Vandenameele, L. Van der Perre, M. Engels, B. Gyselinckx, and H. Man, "A novel class of uplink OFDM/SDMA algorithms: A statistical performance analysis," in *Proceedings of Vehicular Technology Conference*, vol. 1, (Amsterdam, Netherlands), pp. 324–328, IEEE, 19–22 September 1999.

[138] F. Mueller-Roemer, "Directions in audio broadcasting," *Journal Audio Engineering Society*, vol. 41, pp. 158–173, March 1993.

[139] G. Plenge, "DAB — a new radio broadcasting system — state of development and ways for its introduction," *Rundfunktech. Mitt.*, vol. 35, no. 2, 1991.

[140] ETSI, *Digital Audio Broadcasting (DAB)*, 2nd ed., May 1997. ETS 300 401.

[141] ETSI, *Digital Video Broadcasting (DVB); Framing structure, channel coding and modulation for digital terrestrial television*, August 1997. EN 300 744 V1.1.2.

[142] P. Chow, J. Tu, and J. Cioffi, "A discrete multitone transceiver system for HDSL applications," *IEEE journal on selected areas in communications*, vol. 9, pp. 895–908, August 1991.

[143] P. Chow, J. Tu, and J. Cioffi, "Performance evaluation of a multichannel transceiver system for ADSL and VHDSL services," *IEEE journal on selected areas in communications*, vol. 9, pp. 909–919, August 1991.

[144] K. Sistanizadeh, P. Chow, and J. Cioffi, "Multi-tone transmission for asymmetric digital subscriber lines (ADSL)," in *Proceedings of ICC'93*, pp. 756–760, IEEE, 1993.

[145] ANSI, *ANSI/T1E1.4/94-007, Asymmetric Digital Subscriber Line (ADSL) Metallic Interface.*, August 1997.

[146] A. Burr and P. Brown, "Application of OFDM to powerline telecommunications," in *3rd International Symposium On Power-Line Communications*, (Lancaster, UK), 30 March – 1 April 1999.

[147] M. Deinzer and M. Stoger, "Integrated PLC-modem based on OFDM," in *3rd International Symposium On Power-Line Communications*, (Lancaster, UK), 30 March – 1 April 1999.

[148] R. Prasad and H. Harada, "A novel OFDM based wireless ATM system for future broadband multimedia communications," in *Proceeding of ACTS Mobile Communication Summit '97*, (Aalborg, Denmark), pp. 757–762, ACTS, 7–10 October 1997.

[149] C. Ciotti and J. Borowski, "The AC006 MEDIAN project — overview and state–of–the–art," in *Proc. ACTS Summit '96*, (Granada, Spain), pp. 362–367, 27–29 November 1996.

[150] J. Borowski, S. Zeisberg, J. Hübner, K. Koora, E. Bogenfeld, and B. Kull, "Performance of OFDM and comparable single carrier system in MEDIAN demonstrator 60GHz channel," in *Proceeding of ACTS Mobile Communication Summit '97*, (Aalborg, Denmark), pp. 653–658, ACTS, 7–10 October 1997.

[151] M. D. Benedetto, P. Mandarini, and L. Piazzo, "Effects of a mismatch in the in–phase and in–quadrature paths, and of phase noise, in QDCPSK-OFDM modems," in *Proceeding of ACTS Mobile Communication Summit '97*, (Aalborg, Denmark), pp. 769–774, ACTS, 7–10 October 1997.

[152] T. Rautio, M. Pietikainen, J. Niemi, J. Rautio, K. Rautiola, and A. Mammela, "Architecture and implementation of the 150 Mbit/s OFDM modem (invited paper)," in *IEEE Benelux Joint Chapter on Communications and Vehicular Technology, 6th Symposium on Vehicular Technology and Communications*, (Helsinki, Finland), p. 11, 12–13 October 1998.

[153] J. Ala-Laurila and G. Awater, "The magic WAND — wireless ATM network demondtrator system," in *Proceeding of ACTS Mobile Communication Summit '97*, (Aalborg, Denmark), pp. 356–362, ACTS, 7–10 October 1997.

[154] J. Aldis, E. Busking, T. Kleijne, R. Kopmeiners, R. van Nee, R. Mann-Pelz, and T. Mark, "Magic into reality, building the WAND modem," in *Proceeding of ACTS Mobile Communication Summit '97*, (Aalborg, Denmark), pp. 775–780, ACTS, 7–10 October 1997.

[155] E. Hallmann and H. Rohling, "OFDM-Vorschläge für UMTS," in *3. OFDM Fachgespräch in Braunschweig*, 1998.

[156] "Universal mobile telecommunications system (UMTS); UMTS terrestrial radio access (UTRA); concept evaluation," tech. rep., ETSI, 1997. TR 101 146.

[157] O. Edfors, *Low-Complexity Algorithms in Digital Receivers*. Lulea University of Technology, 1996.

[158] M. Sandell, *Design and analysis of estimators for multicarrier modulation and ultrasonic imaging*. Lulea University of Technology, 1996.

[159] M. Münster and L. Hanzo, "MMSE Channel Prediction For Symbol-by-symbol Adaptive OFDM Systems," in 5th *International OFDM-Workshop 2000*, pp. 35/1–35/6, Technische Universität Hamburg-Harburg, September 2000.

[160] M. Münster and L. Hanzo, "MMSE Channel Prediction Assisted Symbol-by-Symbol Adaptive OFDM," in *Proceedings of International Conference on Communications*, (Birmingham, Alabama), IEEE, April 28 - May 2 2002.

[161] M. Münster and L. Hanzo, "Parallel Interference Cancellation Assisted Decision-Directed Channel Estimation for Multi-User OFDM," in 6th *International OFDM-Workshop 2000*, (Hotel Hafen Hamburg, Germany), pp. 35/1–35/5, Technische Universität Hamburg-Harburg, September 18-19 2001.

[162] M. Münster and L. Hanzo, "PIC-Assisted Decision-Directed Channel Estimation for Multi-User OFDM Environments," in *accepted for publication in Proceedings of Vehicular Technology Conference*, IEEE, September 2002.

[163] M. Münster and L. Hanzo, "Co-Channel Interference Cancellation Techniques for Antenna Array Assisted Multiuser OFDM Systems," in *Proceedings of 3G-'2000 Conference*, vol. 1, (London, Great Britain), pp. 256–260, IEE, IEE, March 27-29 2000.

[164] L. Hanzo, W. Webb, and T. Keller, *Single- and Multi-Carrier Quadrature Amplitude Modulation: Principles and Applications for Personal Communications, WLANs and Broadcasting*. IEEE Press, 2000.

[165] H. Kolb Private Communications.

[166] J. Lindner Private Communications.

[167] D. Schnidman, "A generalized nyquist criterion and an optimum linear receiver for a pulse modulation system," *Bell Systems Technical Journal*, pp. 2163–2177, November 1967.

[168] W. V. Etten, "An optimum linear receiver for multiple channel digital transmission systems," *IEEE Transactions on Communications*, vol. COM-23, pp. 828–834, August 1975.

[169] A. Kaye and D. George, "Transmission of multiplexed PAM signals over multiple channel and diversity systems," *IEEE Tranactions on Communications Technology*, vol. COM-18, pp. 520–525, October 1970.

[170] M. Aaron and D. Tufts, "Intersymbol interference and error probability," *IEEE Transactions on Information Theory*, vol. IT-12, pp. 26–34, January 1966.

[171] D. Tufts, "Nyquist's problem: The joint optimization of transmitter and receiver in pulse amplitude modulation," *Proceedings of IEEE*, vol. 53, pp. 248–259, March 1965.

[172] H. Schüler, *Digitale Systeme zur Signalverarbeitung*. Berlin, Heidelberg, and New York: Springer Verlag, 1974.

[173] J. K. Cavers, "An Analysis of Pilot Symbol Assisted Modulation for Rayleigh Fading Channels," *IEEE Transactions on Vehicular Technology*, vol. 40, pp. 686–693, November 1991.

[174] H. Harmuth, *Transmission of Information by Orthogonal Time Functions*. Berlin: Springer Verlag, 1969.

[175] H. Harmuth, "On the transmission of information by orthogonal time functions," *AIEE*, July 1960.

[176] J. Proakis, *Digital communications*. McGraw-Hill, 1995.

[177] R. O'Neill and L. Lopes, "Performance of amplitude limited multitone signals," in *Proceedings of IEEE VTC '94*, (Stockholm, Sweden), IEEE, 8–10 June 1994.

[178] X. Li and L. Cimini, "Effects of clipping and filtering on the performance of OFDM," in *Proceedings of IEEE VTC'97*, (Phoenix, AZ, USA), pp. 1634–1638, IEEE, 4–7 May 1997.

[179] A. Garcia and M. Calvo, "Phase noise and sub–carrier spacing effects on the performance of an OFDM communications system," *IEEE Communications Letters*, vol. 2, pp. 11–13, January 1998.

[180] W. Robins, *Phase Noise in signal sources*, vol. 9 of *IEE Telecommunication series*. Peter Peregrinus Ltd., 1982.

[181] C. Tellambura, Y. Guo, and S. Barton, "Equaliser performance for HIPERLAN in indoor channels," *Wireless Personal Communications*, vol. 3, no. 4, pp. 397–410, 1996.

[182] T. Ojanperä, M. Gudmundson, P. Jung, J. Sköld, R. Pirhonen, G. Kramer, and A. Toskala, "FRAMES: - hybrid multiple access technology," in *Proceedings of IEEE ISSSTA'96*, (Mainz, Germany), pp. 334–338, IEEE, September 1996.

[183] M. Failli, "Digital land mobile radio communications COST 207," tech. rep., European Commission, 1989.

[184] J. Torrance and L. Hanzo, "Comparative study of pilot symbol assisted modem schemes," in *Proceedings of IEE Conference on Radio Receivers and Associated Systems (RRAS'95)*, (Bath, UK), pp. 36–41, IEE, 26–28 September 1995.

[185] K. Fazel, S. Kaiser, P. Robertson, and M. Ruf, "A concept of digital terrestrial television broadcasting," *Wireless Personal Communications*, vol. 2, pp. 9–27, 1995.

[186] J. Kuronen, V.-P. Kaasila, and A. Mammela, "An all-digital symbol tracking algorithm in an OFDM system by using the cyclic prefix," in *Proc. ACTS Summit '96*, (Granada, Spain), pp. 340–345, 27–29 November 1996.

[187] M. Kiviranta and A. Mammela, "Coarse frame synchronization structures in OFDM," in *Proc. ACTS Summit '96*, (Granada, Spain), pp. 464–470, 27–29 November 1996.

[188] Z. Li and A. Mammela, "An all digital frequency synchronization scheme for OFDM systems," in *Proceedings of the IEEE International Symposium on Personal, Indoor and Mobile Radio Communications (PIMRC)*, (Helsinki, Finland), pp. 327–331, 1–4 September 1997.

[189] J. Bingham, "Method and apparatus for correcting for clock and carrier frequency offset, and phase jitter in multicarrier modems." U.S. Patent No. 5206886, 27 April 1993.

[190] T. de Couasnon, R. Monnier, and J. Rault, "OFDM for digital TV broadcasting," *Signal Processing*, vol. 39, pp. 1–32, 1994.

[191] P. Mandarini and A. Falaschi, "SYNC proposals." MEDIAN Design Note, January 1996.

[192] T. Keller and L. Hanzo, "Orthogonal frequency division multiplex synchronisation techniques for wireless local area networks," in *Proceedings of IEEE International Symposium on Personal, Indoor, and Mobile Radio Communications (PIMRC'96)*, vol. 3, (Taipei, Taiwan), pp. 963–967, IEEE, 15–18 October 1996.

[193] R. Steele and W. Webb, "Variable rate QAM for data transmission over Rayleigh fading channels," in *Proceeedings of Wireless '91*, (Calgary, Alberta), pp. 1–14, IEEE, 1991.

[194] H. Matsuoka, S. Sampei, N. Morinaga, and Y. Kamio, "Adaptive modulation system with variable coding rate concatenated code for high quality multi-media communications systems," in *Proceedings of IEEE VTC'96*, vol. 1, (Atlanta, GA, USA), pp. 487–491, IEEE, 28 April–1 May 1996.

[195] S.-G. Chua and A. Goldsmith, "Variable-rate variable-power mQAM for fading channels," in *Proceedings of IEEE VTC'96*, (Atlanta, GA, USA), pp. 815–819, IEEE, 28 April–1 May 1996.

[196] D. Pearce, A. Burr, and T. Tozer, "Comparison of counter-measures against slow Rayleigh fading for TDMA systems," in *IEE Colloquium on Advanced TDMA Techniques and Applications*, (London, UK), pp. 9/1–9/6, IEE, 28 October 1996. digest 1996/234.

[197] V. Lau and M. Macleod, "Variable rate adaptive trellis coded QAM for high bandwidth efficiency applications in Rayleigh fading channels," in *Proceedings of IEEE Vehicular Technology Conference (VTC'98)*, (Ottawa, Canada), pp. 348–352, IEEE, 18–21 May 1998.

[198] J. Torrance and L. Hanzo, "Latency and networking aspects of adaptive modems over slow indoors Rayleigh fading channels," *IEEE Transactions on Vehicular Technology*, vol. 48, no. 4, pp. 1237–1251, 1998.

[199] J. Torrance, L. Hanzo, and T. Keller, "Interference aspects of adaptive modems over slow Rayleigh fading channels," *IEEE Transactions on Vehicular Technology*, vol. 48, pp. 1527–1545, September 1999.

[200] A. Czylwik, "Adaptive OFDM for wideband radio channels," in *Proceeding of IEEE Global Telecommunications Conference, Globecom 96*, (London, UK), pp. 713–718, IEEE, 18–22 November 1996.

[201] P. Chow, J. Cioffi, and J. Bingham, "A practical discrete multitone transceiver loading algorithm for data transmission over spectrally shaped channels," *IEEE Transactions on Communications*, vol. 48, pp. 772–775, 1995.

[202] L. Hanzo, C. Wong, and M. Yee, *Adaptive Wireless Transceivers*. John Wiley, IEEE Press, 2002. (For detailed contents, please refer to http://www-mobile.ecs.soton.ac.uk.).

[203] L. Hanzo, T. Liew, and B. Yeap, *Turbo Coding, Turbo Equalisation and Space-Time Coding*. John Wiley, IEEE Press, 2002. (For detailed contents, please refer to http://www-mobile.ecs.soton.ac.uk.).

[204] J. Blogh and L. Hanzo, *3G Systems and Intelligent Networking*. John Wiley and IEEE Press, 2002. (For detailed contents, please refer to http://www-mobile.ecs.soton.ac.uk.).

[205] J. Torrance, *Adaptive Full Response Digital Modulation for Wireless Communications Systems*. PhD thesis, Department of Electronics and Computer Science, University of Southampton, UK, 1997.

[206] K. Miya, O. Kato, K. Homma, T. Kitade, M. Hayashi, and T. Ue, "Wideband CDMA systems in TDD-mode operation for IMT-2000," *IEICE Transactions on Communications*, vol. E81-B, pp. 1317–1326, July 1998.

[207] O. Kato, K. Miya, K. Homma, T. Kitade, M. Hayashi, and M. Watanabe, "Experimental performance results of coherent wideband DS-CDMA with TDD scheme," *IEICE Transactions on Communications.*, vol. E81-B, pp. 1337–1344, July 1998.

[208] T. Keller and L. Hanzo, "Blind-detection assisted sub-band adaptive turbo-coded OFDM schemes," in *Proceeding of VTC'99 (Spring)*, (Houston, TX, USA), pp. 489–493, IEEE, 16–20 May 1999.

[209] J. Torrance and L. Hanzo, "Optimisation of switching levels for adaptive modulation in a slow Rayleigh fading channel," *Electronics Letters*, vol. 32, pp. 1167–1169, 20 June 1996.

[210] C. Berrou, A. Glavieux, and P. Thitimajshima, "Near shannon limit error-correcting coding and decoding: Turbo codes," in *Proceedings of the International Conference on Communications*, (Geneva, Switzerland), pp. 1064–1070, May 1993.

[211] L. Bahl, J. Cocke, F. Jelinek, and J. Raviv, "Optimal decoding of linear codes for minimising symbol error rate," *IEEE Transactions on Information Theory*, vol. 20, pp. 284–287, March 1974.

[212] T. Keller, M. Muenster, and L. Hanzo, "A burst–by–burst adaptive OFDM wideband speech transceiver." submitted to IEEE JSAC, 1999.

[213] T. Keller, J. Woodard, and L. Hanzo, "Turbo-coded parallel modem techniques for personal communications," in *Proceedings of IEEE VTC'97*, (Phoenix, AZ, USA), pp. 2158–2162, IEEE, 4–7 May 1997.

[214] T. Keller and L. Hanzo, "Adaptive orthogonal frequency division multiplexing schemes," in *Proceeding of ACTS Mobile Communication Summit '98*, (Rhodes, Greece), pp. 794–799, ACTS, 8–11 June 1998.

[215] C. E. Shannon, "Communication in the presence of noise," *Proceedings of the I.R.E.*, vol. 37, pp. 10–22, January 1949.

[216] L. Piazzo, "A fast algorithm for near-optimum power and bit allocation in OFDM systems." to appear in Electronics Letters, December 1999.

[217] T. Willink and P. Wittke, "Optimization and performance evaluation of multicarrier transmission," *IEEE Transactions on Information Theory*, vol. 43, pp. 426–440, March 1997.

[218] R. Fischer and J. Huber, "A new loading algorithm for discrete multitone transmission," in *Proceeding of IEEE Global Telecommunications Conference, Globecom 96*, (London, UK), pp. 713–718, IEEE, 18–22 November 1996.

[219] S. Lai, R. Cheng, K. Letaief, and R. Murch, "Adaptive trellis coded mqam and power optimization for ofdm transmission," in *Proceedings of VTC'99 (Spring)*, (Houston, TX, USA), IEEE, 16–20 May 1999.

[220] D. Hughes-Hartogs, "Ensemble modem structure for imperfect transmission media." U.S Patents Nos. 4,679,227 (July 1988) 4,731,816 (March 1988) and 4,833,796 (May 1989).

[221] J. Bingham, "Multicarrier modulation for data transmission: an idea whose time has come," *IEEE Communications Magazine*, pp. 5–14, May 1990.

[222] L. Godara, "Applications of antenna arrays to mobile communications, part II: Beamforming and direction-of-arrival considerations," *Proceedings of the IEEE*, vol. 85, pp. 1193–1245, August 1997.

[223] Y. Li, "Pilot-symbol-aided channel estimation for OFDM in wireless systems," in *Proceedings of VTC'99 (Spring)*, (Houston, TX, USA), IEEE, 16–20 May 1999.

[224] N. Szabo and R. Tanaka, *Residue Arithmetic and Its Applications to Computer Technology*. New York, USA: McGraw-Hill, 1967.

[225] R. Watson and C. Hastings, "Self-checked computation using residue arithmetic," *Proceedings of the IEEE*, vol. 54, pp. 1920–1931, December 1966.

[226] R. Pyndiah, "Iterative decoding of product codes: Block turbo codes," in *Proceedings of the International Symposium on Turbo Codes & Related Topics*, (Brest, France), pp. 71–79, 3–5 September 1997.

[227] P. Adde, R. Pyndiah, O. Raoul, and J.-R. Inisan, "Block turbo decoder design," in *Proceedings of the International Symposium on Turbo Codes & Related Topics*, (Brest, France), pp. 166–169, 3–5 September 1997.

[228] W. Jenkins and B. Leon, "The use of residue number system in the design of finite impulse response filters," *IEEE Transactions on Circuits Systems*, vol. CAS-24, pp. 191–201, April 1977.

[229] M. Soderstrand, "A high-speed, low-cost, recursive digital filter using residue number arithmetic," *Proceedings of IEEE*, vol. 65, pp. 1065–1067, July 1977.

[230] M. Soderstrand and E. Fields, "Multipliers for residue number arithmetic digital filters," *Electronics Letters*, vol. 13, pp. 164–166, March 1977.

[231] M. Soderstrand, W. Jenkins, and G. Jullien, *Residue Number System Arithmetic: Modern Applications in Digital Signal Processing*. New York, USA: IEEE Press, 1986.

[232] E. Claudio, G. Orlandi, and F. Piazza, "A Systolic Redundant Residue Arithmetic Error Correction Circuit," *IEEE Transactions on Computers*, vol. 42, pp. 427–432, April 1993.

[233] H. Krishna, K.-Y. Lin, and J.-D. Sun, "A coding theory approach to error control in redundant residue number systems - part I: theory and single error correction," *IEEE Transactions on Circuits Systems*, vol. 39, pp. 8–17, January 1992.

[234] J.-D. Sun and H. Krishna, "A coding theory approach to error control in redundant residue number systems — part II: multiple error detection and correction," *IEEE Transactions on Circuits Systems*, vol. 39, pp. 18–34, January 1992.

[235] T. Liew, L.-L. Yang, and L. Hanzo, "Soft-decision redundant residue number system based error correction coding," in *Proceeding of VTC'99 (Fall)*, (Amsterdam, Netherlands), pp. 2974–2978, IEEE, 19–22 September 1999.

[236] L.-L. Yang and L. Hanzo, "Residue number system arithmetic assisted m-ary modulation," *IEEE Communications Letters*, vol. 3, pp. 28–30, February 1999.

[237] L.-L. Yang and L. Hanzo, "Performance of residue number system based DS-CDMA over multipath fading channels using orthogonal sequences," *ETT*, vol. 9, pp. 525–536, November–December 1998.

[238] H. Krishna and J.-D. Sun, "On theory and fast algorithms for error correction in residue number system product codes," *IEEE Transactions on Comput.*, vol. 42, pp. 840–852, July 1993.

[239] D. Chase, "A class of algorithms for decoding block codes with channel measurement information," *IEEE Transactions on Information Theory*, vol. IT-18, pp. 170–182, January 1972.

[240] J. Hagenauer, E. Offer, and L. Papke, "Iterative decoding of binary block and convolutional codes," *IEEE Transactions on Information Theory*, vol. 42, pp. 429–445, March 1996.

[241] H. Nickl, J. Hagenauer, and F. Burkett, "Approaching shannon's capacity limit by 0.27 dB using simple hamming codes," *IEEE Communications Letters*, vol. 1, pp. 130–132, September 1997.

[242] T. Liew, C. Wong, and L. Hanzo, "Block turbo coded burst-by-burst adaptive modems," in *Proceedings of Microcoll'99, Budapest, Hungary*, pp. 59–62, 21–24 March 1999.

[243] B. Yeap, T. Liew, J. Hamorsky, and L. Hanzo, "Comparative study of turbo equalisers using convolutional codes and block-based turbo-codes for GMSK modulation," in *Proceedings of VTC 1999 Fall*, (Amsterdam, Holland), pp. 2974–2978, 19-22 September 1999.

[244] M. Yee, T. Liew, and L. Hanzo, "Radial basis function decision feedback equalisation assisted block turbo burst-by-burst adaptive modems," in *Proceedings of VTC '99 Fall*, (Amsterdam, Holland), pp. 1600–1604, 19-22 September 1999.

[245] C. Wong, T. Liew, and L. Hanzo, "Turbo coded burst by burst adaptive wideband modulation with blind modem mode detection," in *Proceeding of ACTS Mobile Communication Summit '99*, (Sorrento, Italy), pp. 303–308, ACTS, 8–11 June 1999.

[246] A. Viterbi, *CDMA: Principles of Spread Spectrum Communication*. Reading MA, USA: Addison-Wesley, June 1995. ISBN 0201633744.

[247] L. Miller and J. Lee, *CDMA Systems Engineering Handbook*. London, UK: Artech House, 1998.

[248] R. A. Scholtz, "The origins of spread spectrum communications," *IEEE Transactions on Communications*, vol. 30, no. 5, pp. 822–854, 1982.

[249] G. R. Cooper and R. W. Nettleton, "A spread-spectrum technique for high-capacity mobile communications," *IEEE Transactions on Vehicular Technology*, vol. 27, pp. 264–275, November 1978.

[250] O. C. Yue, "Spread spectrum mobile radio, 1977-1982," *IEEE Transactions on Vehicular Technology*, vol. 32, pp. 98–105, February 1983.

[251] M. Simon, J. Omura, R. Scholtz, and B. Levitt, *Spread Spectrum Communications Handbook*. New York, USA: McGraw-Hill, 1994.

[252] Y. Yoon, R. Kohno, and H. Imai, "A SSMA system with cochannel interference cancellation with multipath fading channels," *IEEE Journal on Selected Areas in Communications*, vol. 11, pp. 1067–1075, September 1993.

[253] K. Gilhousen, I. Jacobs, R. Padovani, A. Viterbi, L. Weaver Jr., and C. Wheatley III, "On the capacity of a cellular CDMA system," *IEEE Transactions on Vehicular Technology*, vol. 40, pp. 303–312, May 1991.

[254] P. Patel and J. Holtzman, "Analysis of a simple successive interference cancellation scheme in a DS/CDMA system," *IEEE Journal on Selected Areas in Communications*, vol. 12, pp. 796–807, June 1994.

[255] R. Lupas and S. Verdú, "Linear multiuser detectors for synchronous code divison multiple access channels," *IEEE Transactions on Information Theory*, vol. 35, pp. 123–136, January 1989.

[256] P. Jung and J. Blanz, "Joint detection with coherent receiver antenna diversity in CDMA mobile radio systems," *IEEE Transactions on Vehicular Technology*, vol. 44, pp. 76–88, February 1995.

[257] J. Thompson, P. Grant, and B. Mulgrew, "Smart antenna arrays for CDMA systems," *IEEE Personal Communications Magazine*, vol. 3, pp. 16–25, October 1996.

[258] R. Steele and L. Hanzo, eds., *Mobile Radio Communications*. New York, USA: IEEE Press - John Wiley & Sons, 2nd ed., 1999.

[259] K. Feher, *Wireless digital communications: Modulation and spread spectrum*. Englewood Cliffs, NJ: Prentice-Hall, 1995.

[260] R. Kohno, R. Meidan, and L. Milstein, "Spread spectrum access methods for wireless communication," *IEEE Communications Magazine*, vol. 33, pp. 58–67, January 1995.

[261] R. Price and E. Green Jr., "A communication technique for multipath channels," *Proceedings of the IRE*, vol. 46, pp. 555–570, March 1958.

[262] U. Grob, A. L. Welti, E. Zollinger, R. Kung, and H. Kaufmann, "Microcellular direct-sequence spread-spectrum radio system using n-path rake receiver," *IEEE Journal on Selected Areas in Communications*, vol. 8, no. 5, pp. 772–780, 1990.

[263] P. W. Baier, "A critical review of CDMA," in *Proceedings of the IEEE Vehicular Technology Conference (VTC)*, (Atlanta, GA, USA), pp. 6–10, 28 April–1 May 1996.

[264] Telcomm. Industry Association (TIA), Washington, DC, USA, *Mobile station — Base station compatibility standard for dual-mode wideband spread spectrum cellular system, EIA/TIA Interim Standard IS-95*, July 1993.

[265] S. Verdú, *Multiuser Detection*. Cambridge, UK: Cambridge University Press, 1998.

[266] E. Kuan and L. Hanzo, "Burst-by-burst adaptive multiuser detection cdma: A framework for existing and future wireless standards," *Proceedings of the IEEE*, December 2002.

[267] R. Prasad, *Universal Wireless Personal Communications*. London, UK: Artech House Publishers, 1998.

[268] S. Glisic and B. Vucetic, *Spread Spectrum CDMA Systems for Wireless Communications*. London, UK: Artech House, April 1997. ISBN 0890068585.

[269] G. Woodward and B. Vucetic, "Adaptive detection for DS-CDMA," *Proceedings of the IEEE*, vol. 86, pp. 1413–1434, July 1998.

[270] S. Moshavi, "Multi-user detection for DS-CDMA communications," *IEEE Communications Magazine*, vol. 34, pp. 124–136, October 1996.

[271] A. Duel-Hallen, J. Holtzman, and Z. Zvonar, "Multiuser detection for cdma systems," *IEEE Personal Communications*, vol. 2, pp. 46–58, April 1995.

[272] J. Laster and J. Reed, "Interference rejection in digital wireless communications," *IEEE Signal Processing Magazine*, vol. 14, pp. 37–62, May 1997.

[273] J. Thompson, P. Grant, and B. Mulgrew, "Performance of antenna array receiver algorithms for CDMA," in *Proceedings of the IEEE Global Telecommunications Conference (GLOBECOM)*, (London, UK), pp. 570–574, 18–22 November 1996.

[274] A. Naguib and A. Paulraj, "Performance of wireless CDMA with m-ary orthogonal modulation and cell site antenna arrays," *IEEE Journal on Selected Areas in Communications*, vol. 14, pp. 1770–1783, December 1996.

[275] L. Godara, "Applications of antenna arrays to mobile communications, part I: Performance improvement, feasibility, and system considerations," *Proceedings of the IEEE*, vol. 85, pp. 1029–1060, July 1997.

[276] R. Kohno, H. Imai, M. Hatori, and S. Pasupathy, "Combination of adaptive array antenna and a canceller of interference for direct-sequence spread-specturn multiple-access system," *IEEE Journal on Selected Areas in Communications*, vol. 8, pp. 675–681, May 1998.

[277] A. J. Viterbi, A. M. Viterbi, and E. Zehavi, "Performance of power-controlled wideband terrestrial digital communication," *IEEE Transactions on Communications*, vol. 41, no. 4, pp. 559–569, 1993.

[278] F. Simpson and J. Holtzman, "Direct sequence CDMA power control, interleaving, and coding," *IEEE Journal on Selected Areas in Communications*, vol. 11, pp. 1085–1095, September 1993.

[279] S. Ariyavisitakul and L. Chang, "Signal and interference statistics of a CDMA system with feedback power control," *IEEE Transactions on Communications*, vol. 41, pp. 1626–1634, November 1993.

[280] S. Ariyavisitakul, "Signal and interference statistics of a CDMA system with feedback power control - Part II," *IEEE Transactions on Communications*, vol. 42, no. 2/3/4, pp. 597–605, 1994.

[281] J. G. Proakis, *Digital Communications*. Mc-Graw Hill International Editions, 3rd ed., 1995.

[282] R. W. Chang and R. A. Gibby, "A theoretical study of performance of an orthogonal multiplexing data transmission scheme," *IEEE Transactions on Communication Technology*, vol. 16, no. 4, pp. 529–540, 1968.

[283] P. V. Eetvelt, S. J. Shepherd, and S. K. Barton, "The distribution of peak factor in QPSK multi-carrier modulation," *Wireless Personal Communications*, vol. 2, pp. 87–96, 1995.

[284] V. M. DaSilva and E. S. Sousa, "Performance of orthogonal CDMA codes for quasi-synchronous communication systems," in *Proceedings of IEEE ICUPC 1993*, (Ottawa, Canada), pp. 995–999, October 1993.

[285] L. Vandendorpe, "Multitone direct sequence CDMA system in an indoor wireless environment," in *Proceedings of IEEE SCVT 1993*, (Delft, The Netherlands), pp. 4.1:1–8, October 1993.

[286] R. Prasad and S. Hara, "Overview of multi-carrier CDMA," in *Proceedings of the IEEE International Symposium on Spread Spectrum Techniques and Applications (ISSSTA)*, (Mainz, Germany), pp. 107–114, 22–25 September 1996.

[287] D. Scott, P. Grant, S. McLaughlin, G. Povey, and D. Cruickshank, "Research in reconfigurable terminal design for mobile and personal communications," tech. rep., Department of Electrical Engineering, The University of Edinburgh, March 1997.

[288] N. Yee and J. P. Linnartz, "MICRO 93-101: Multi-carrier CDMA in an indoor wireless radio channel," tech. rep., University of California at Berkeley, 1994.

[289] L.-L. Yang and L. Hanzo, "Performance of generalized multicarrier DS-CDMA over Nakagami-m fading channels," *IEEE Transactions on Communications, (http://www-mobile.ecs.soton.ac.uk/lly)*, vol. 50, pp. 956–966, June 2002.

[290] L.-L. Yang and L. Hanzo, "Slow frequency-hopping multicarrier DS-CDMAfor transmission over Nakagami multipath fading channels," *IEEE Journal on Selected Areas in Communications*, vol. 19, no. 7, pp. 1211–1221, 2001.

[291] E. A. Sourour and M. Nakagawa, "Performance of orthogonal multicarrier CDMA in a multipath fading channel," *IEEE Transactions on Communications*, vol. 44, pp. 356–367, March 1996.

[292] L.-L. Yang and L. Hanzo, "Slow frequency-hopping multicarrier DS-CDMA," in *International Symposium on Wireless Personal Multimedia Communications (WPMC'99)*, (Amsterdam, The Netherlands), pp. 224–229, September:21–23 1999.

[293] L.-L. Yang and L. Hanzo, "Blind soft-detection assisted frequency-hopping multicarrier DS-CDMA systems," in *Proceedings of IEEE GLOBECOM'99*, (Rio de Janeiro, Brazil), pp. 842–846, December:5-9 1999.

[294] S. Slimane, "MC-CDMA with quadrature spreading for wireless communication systems," *European Transactions on Telecommunications*, vol. 9, pp. 371–378, July–August 1998.

[295] I. Kalet, "The multitone channel," *IEEE Transactions on Communications*, vol. 37, pp. 119–124, February 1989.

[296] R.-Y. Li and G. Stette, "Time-limited orthogonal multicarrier modulation schemes," *IEEE Transactions on Communications*, vol. 43, pp. 1269–1272, February/March/April 1995.

[297] L. Goldfeld and D. Wulich, "Multicarrier modulation system with erasures-correcting decoding for nakagami fading channels," *European Trans. on Telecommunications*, vol. 8, pp. 591–595, November–December 1997.

[298] E. Sousa, "Performance of a direct sequence spread spectrum multiple access system utilizing unequal carrier frequencies," *IEICE Transactions on Communications*, vol. E76-B, pp. 906–912, August 1993.

[299] B. Saltzberg, "Performance of an efficient parallel data transmission system," *IEEE Transactions on Communication Technology*, vol. 15, pp. 805–811, December 1967.

[300] C. Baum and K. Conner, "A multicarrier transmission scheme for wireless local communications," *IEEE Journal on Selected Areas in Communications*, vol. 14, pp. 512–529, April 1996.

[301] V. Dasilva and E. Sousa, "Multicarrier orthogonal CDMA signals for quasi-synchronous communication systems," *IEEE Journal on Selected Areas in Communications*, vol. 12, pp. 842–852, June 1994.

[302] L. Vandendorpe and O. V. de Wiel, "MIMO DEF equalization for multitone DS/SS systems over multipath channels," *IEEE Journal on Selected Areas in Communications*, vol. 14, pp. 502–511, April 1996.

[303] N. Al-Dhahir and J. Cioffi, "A bandwidth-optimized reduced-complexity equalized multicarrier transceiver," *IEEE Transactions on Communications*, vol. 45, pp. 948–956, August 1997.

[304] P. Jung, F. Berens, and J. Plechinger, "A generalized view on multicarrier CDMA mobile radio systems with joint detection (Part i)," *FREQUENZ*, vol. 51, pp. 174–184, July–August 1997.

[305] S. Hara and R. Prasad, "Design and performance of multicarrier CDMA system in frequency-selective Rayleigh fading channels," *IEEE Transactions on Vehicular Technology*, vol. 48, pp. 1584–1595, September 1999.

[306] V. Tarokh and H. Jafarkhani, "On the computation and reduction of the peak-to-average power ratio in multicarrier communications," *IEEE Transactions on Communications*, vol. 48, pp. 37–44, January 2000.

[307] D. Wulich and L. Goldfied, "Reduction of peak factor in orthogonal multicarrier modulation by amplitude limiting and coding," *IEEE Transactions on Communications*, vol. 47, pp. 18–21, January 1999.

[308] H.-W. Kang, Y.-S. Cho, and D.-H. Youn, "On compensating nonlinear distortions of an OFDM system using an efficient adaptive predistorter," *IEEE Transactions on Communications*, vol. 47, pp. 522–526, April 1999.

[309] Y.-H. Kim, I. Song, Seokho, and S.-R. Park, "A multicarrier CDMA system with adaptive subchannel allocation for forward links," *IEEE Transactions on Vehicular Technology*, vol. 48, pp. 1428–1436, September 1999.

[310] X. Gui and T.-S. Ng, "Performance of asynchronous orthogonal multicarrier CDMA system in frequency selective fading channel," *IEEE Transactions on Communications*, vol. 47, pp. 1084–1091, July 1999.

[311] T.-M. Lok, T.-F. Wong, and J. Lehnert, "Blind adaptive signal reception for MC-CDMA systems in Rayleigh fading channels," *IEEE Transactions on Communications*, vol. 47, pp. 464–471, March 1999.

[312] B. Rainbolt and S. Miller, "Multicarrier CDMA for cellular overlay systems," *IEEE Journal on Selected Areas in Communications*, vol. 17, pp. 1807–1814, October 1999.

[313] S.-M. Tseng and M. Bell, "Asynchronous multicarrier DS-CDMA using mutually orthogonal complementary sets of sequences," *IEEE Transactions on Communications*, vol. 48, pp. 53–59, January 2000.

[314] D. Rowitch and L. Milstein, "Convolutionally coded multicarrier DS-CDMA systems in a multipath fading channel – Part I: Performance analysis," *IEEE Transactions on Communications*, vol. 47, pp. 1570–1582, October 1999.

[315] D. Rowitch and L. Milstein, "Convolutionally coded multicarrier DS-CDMA systems in a multipath fading channel – Part II: Narrow-band interference suppression," *IEEE Transactions on Communications*, vol. 47, pp. 1729–1736, November 1999.

[316] D.-W. Lee and L. Milstein, "Comparison of multicarrier DS-CDMA broadcast systems in a multipath fading channel," *IEEE Transactions on Communications*, vol. 47, pp. 1897–1904, December 1999.

[317] N. Yee, J.-P. Linnartz, and G. Fettweis, "Multi-carrier CDMA in indoor wireless radio network," *IEICE Transactions on Communications*, vol. E77-B, pp. 900–904, July 1994.

[318] S. Kondo and L. Milstein, "On the use of multicarrier direct sequence spread spectrum systems," in *Proceedings of IEEE MILCOM'93*, (Boston, MA), pp. 52–56, Oct. 1993.

[319] V. M. DaSilva and E. S. Sousa, "Performance of orthogonal CDMA codes for quasi-synchronous communication systems," in *Proceedings of IEEE ICUPC'93*, (Ottawa, Canada), pp. 995–999, Oct. 1993.

[320] L. Vandendorpe, "Multitone direct sequence CDMA system in an indoor wireless environment," in *Proceedings of IEEE First Symposium of Communications and Vehicular Technology in the Benelux, Delft, The Netherlands*, pp. 4.1–1–4.1–8, Oct. 1993.

[321] L. L. Yang and L. Hanzo, "Blind joint soft-detection assisted slow frequency-hopping multi-carrier DS-CDMA," *IEEE Transactions on Communication*, vol. 48, no. 9, pp. 1520–1529, 2000.

[322] D.-W. Lee and L. Milstein, "Analysis of a multicarrier DS-CDMA code-acquisition system," *IEEE Transactions on Communications*, vol. 47, pp. 1233–1244, August 1999.

[323] B. Steiner, "Time domain uplink channel estimation in multicarrier-CDMA mobile radio system concepts," in *Multi-Carrier Spread-Spectrum* (K. Fazel and G. Fettweis, eds.), pp. 153–160, Kluwer Academic Publishers, 1997.

[324] K. W. Yip and T. S. Ng, "Tight error bounds for asynchronous multicarrier cdma and their application," *IEEE Communications Letters*, vol. 2, pp. 295–297, November 1998.

[325] S. Kondo and L. Milstein, "Performance of multicarrier DS CDMA systems," *IEEE Transactions on Communications*, vol. 44, pp. 238–246, February 1996.

[326] B. M. Popovic, "Spreading sequences for multicarrier CDMA systems," *IEEE Transactions on Comminications*, vol. 47, no. 6, pp. 918–926, 1999.

[327] P. Jung, P. Berens, and J. Plechinger, "Uplink spectral efficiency of multicarrier joint detection code division multiple access based cellular radio systems," *Electronics Letters*, vol. 33, no. 8, pp. 664–665, 1997.

[328] D.-W. Lee, H. Lee, and J.-S. Kim, "Performance of a modified multicarrier direct sequence CDMA system," *Electronics and Telecommunications Research Institute Journal*, vol. 19, pp. 1–11, April 1997.

[329] L. Rasmussen and T. Lim, "Detection techniques for direct sequence and multicarrier variable rate for broadband CDMA," in *Proceedings of the ICCS/ISPACS '96*, pp. 1526–1530, 1996.

[330] P. Jung, F. Berens, and J. Plechinger, "Joint detection for multicarrier CDMA mobile radio systems - Part II: Detection techniques," in *Proceedings of IEEE ISSSTA 1996*, vol. 3, (Mainz, Germany), pp. 996–1000, September 1996.

[331] Y. Sanada and M. Nakagawa, "A multiuser interference cancellation technique utilizing convolutional codes and multicarrier modulation for wireless indoor communications," *IEEE Journal on Selected Areas in Communications*, vol. 14, pp. 1500–1509, October 1996.

[332] Q. Chen, E. S. Sousa, and S. Pasupathy, "Multicarrier CDMA with adaptive frequency hopping for mobile radio systems," *IEEE Journal on Selected Areas in Communications*, vol. 14, pp. 1852–1857, December 1996.

[333] T. Ojanperä and R. Prasad, "An overview of air interface multiple access for IMT-2000/UMTS," *IEEE Communications Magazine*, vol. 36, pp. 82–95, September 1998.

[334] R. L. Peterson, R. E. Ziemer, and D. E. Borth, *Introduction to Spread Spectrum Communications*. Prentice Hall International Editions, 1995.

[335] S. W. Golomb, *Shift Register Sequences*. Holden-Day, 1967.

[336] F. Adachi, K. Ohno, A. Higashi, T. Dohi, and Y. Okumura, "Coherent multicode DS-CDMA mobile Radio Access," *IEICE Transactions on Communications*, vol. E79-B, pp. 1316–1324, September 1996.

[337] S. C. Bang, "ETRI wideband CDMA system for IMT-2000," in *Presentation material in 1st IMT-2000 Workshop*, (Seoul, Korea), pp. II–1–1 – II–1–21, KIET, August 1997.

[338] H. Rohling, K. Brüninghaus, and R. Grünheid, "Comparison of multiple access schemes for an OFDM downlink system," in *Multi-Carrier Spread-Spectrum* (K. Fazel and G. P. Fettweis, eds.), pp. 23–30, Kluwer Academic Publishers, 1997.

[339] R. Prasad, *CDMA for Wireless Personal Communications*. London: Artech House, May 1996. ISBN 0890065713.

[340] M. Schnell and S. Kaiser, "Diversity considerations forMC-CDMA systems in mobile communications," in *Proceedings of IEEE ISSSTA 1996*, pp. 131–135, 1996.

[341] W. H. Press, S. A. Teukolsky, W. T. Vetterling, and B. P. Flannery, *Numerical Recipies in C*. Cambridge University Press, 1992.

[342] M. R. Schroeder, "Synthesis of low-peak-factor signals and binary sequences with low autocorrelation," *IEEE Transactions on Information Theory*, pp. 85–89, 1970.

[343] E. V. der Ouderaa, J. Schoukens, and J. Renneboog, "Peak factor minimization using a time-frequency domain swapping algorithm," *IEEE Transactions on Instrumentation and Measurement*, vol. 37, pp. 145–147, March 1988.

[344] L. J. Greenstein and P. J. Fitzgerald, "Phasing multitone signals to minimize peak factors," *IEEE Transactions on Communications*, vol. 29, no. 7, pp. 1072–1074, 1981.

[345] R. W. Bäuml, R. F. H. Fischer, and J. B. Huber, "Reducing the peak-to-average power ratio of multicarrier modulation by selected mapping," *Electronics Letters*, vol. 32, pp. 2056–2057, October 1996.

[346] X. Li and J. A. Ritcey, "M-sequences for OFDM peak-to-average power ratio reduction and error correction," *Electronics Letters*, vol. 33, pp. 554–555, March 1997.

[347] J. Jedwab, "Comment : M-sequences for OFDM peak-to-average power ratio reduction and error correction," *Electronics Letters*, vol. 33, pp. 1293–1294, July 1997.

[348] C. Tellambura, "Use of m-sequences for OFDM peak-to-average power ratio reduction," *Electronics Letters*, vol. 33, pp. 1300–1301, July 1997.

[349] S. Narahashi and T. Nojima, "New phasing scheme of N-multiple carriers for reducing peak-to-average power ratio," *Electronics Letters*, vol. 30, pp. 1382–1383, August 1994.

[350] M. Friese, "Multicarrier modulation with low peak-to-average power ratio," *Electronics Letters*, vol. 32, pp. 713–714, April 1996.

[351] P. V. Eetvelt, G. Wade, and M. Tomlinson, "Peak to average power reduction for OFDM schemes by selective scrambling," *Electronics Letters*, vol. 32, pp. 1963–1964, October 1996.

[352] J. A. Davis and J. Jedwab, "Peak-to-mean power control and error correction for OFDM transmission using Golay sequences and Reed-Muller codes," *Electronics Letters*, vol. 33, no. 4, pp. 267–268, 1997.

[353] S. Boyd, "Multitone signals with low crest factor," *IEEE Transactions on Circuits and Systems*, vol. 33, pp. 1018–1022, October 1986.

[354] W. Rudin, "Some theorems on Fourier coefficients," *Proceedings of American Mathematics Society*, vol. 10, pp. 855–859, December 1959.

[355] D. J. Newman, "An L^1 extrimal problem for polynomials," *Proceedings of American Mathematics Society*, vol. 16, pp. 1287–1290, December 1965.

[356] B. M. Popovic, "Synthesis of power efficient multitone signals with flat amplitude spectrum," *IEEE Transactions on Communications*, vol. 39, no. 7, pp. 1031–1033, 1991.

[357] H. S. Shapiro, "Extremal problems for polynomials and power series," Master's thesis, Massachusetts Institute of Technology, 1951.

[358] M. Golay, "Complementary series,," *IRE Transactions on Information Theory*, vol. IT-7, pp. 82–87, 1961.

[359] C. Tellambura, "Upper bound on peak factor of n-multiple carriers," *Electronics Letters*, vol. 33, pp. 1608–1609, September 1997.

[360] C.-C. Tseng and C. L. Liu, "Complementary sets of sequences," *IEEE Transactions on Information Theory*, vol. 18, pp. 644–652, September 1972.

[361] R. Sivaswamy, "Multiphase complementarty codes," *IEEE Transactions on Information Theory*, vol. 24, pp. 546–552, September 1978.

[362] R. L. Frank, "Polyphase complementary codes," *IEEE Transactions on Information Theory*, vol. 26, pp. 641–647, November 1980.

[363] D. Wulich and L. Goldfeld, "Reduction of peak factor in orthogonal multcarrier modulation by amplitude limiting and coding," *IEEE Transactions on Communications*, vol. 47, no. 1, pp. 18–21, 1999.

[364] R. H. Barker, "Group synchronizing of binary digital systems," *in Communication Theory*, pp. 273–287, 1953.

[365] R. H. Pettit, "Pulse sequences with good autocorrelation properties," *The Microwave Journal*, pp. 63–67, February 1967.

[366] R. Turyn and J. Storer, "On binary sequences," *Proceedings of American Mathematics Society*, vol. 12, pp. 394–399, June 1961.

[367] S. W. Golomb and R. A. Scholtz, "Generalized Barker sequences," *IEEE Transactions on Information Theory*, vol. 4, pp. 533–537, October 1965.

[368] D. J. G. Mestdagh and P. M. P. Spruyt, "A method to reduce the probability of clipping in DMT-based transceivers," *IEEE Transactions on Communications*, vol. 44, no. 10, pp. 1234–1238, 1996.

[369] D. J. G. Mestdagh, P. M. P. Spruyt, and B. Biran, "Effect of amplitude clipping in DMT-ADSL transceivers," *Electronics Letters*, vol. 29, pp. 1354–1355, July 1993.

[370] S. J. Shepherd, J. Oriss, and S. K. Barton, "Asymptotic limits in peak envelope power reduction by redundant coding in orthogonal frequency-division multiplex modulation," *IEEE Transactions on Communications*, vol. 46, no. 1, pp. 5–10, 1998.

[371] M. Breiling, S. H. Müller-Weinfurtner, and J. B. Huber, "Peak-power reduction in OFDM without explicit side information," in *Proceedings of International OFDM Workshop 2000*, (Hamburg, Germany), September 2000.

[372] S. H. Müller and J. B. Huber, "OFDM with reduced peak-to-mean power ratio by optimum combination of partial transmit sequences," *Electronics Letters*, vol. 33, pp. 368–369, February 1997.

[373] C. Tellambura, "Phase optimisation criterion for reducing peak-to-average power ratio in OFDM," *Electronics Letters*, vol. 34, pp. 169–170, January 1998.

[374] J. Kreyszig, *Advanced engineering mathematics*. Wiley, 7th edition ed., 1993.

[375] R. C. Heimiller, "Phase shift pulse codes with good periodic correlation properties," *IRE Transactions on Information Theory*, vol. 7, pp. 254–257, October 1961.

[376] R. L. Frank, "Phase shift pulse codes with good periodic correlation properties," *IRE Transactions on Information Theory*, vol. 8, pp. 381–382, October 1962.

[377] R. L. Frank, "Polyphase codes with good nonperiodic correlation properties," *IEEE Transactions on Information Theory*, vol. 9, pp. 43–45, 1963.

[378] D. C. Chu, "Polyphase codes with good periodic correlation properties," *IEEE Transactions on Information Theory*, vol. 18, pp. 531–532, July 1972.

[379] R. L. Frank, "Comments on polyphase codes with good correlation properties," *IEEE Transactions on Information Theory*, vol. 19, p. 244, March 1973.

[380] B. M. Popović, "Comment: Merit factor of Chu and Frank sequences," *Electronics Letters*, vol. 27, pp. 776–777, April 1991.

[381] M. Antweiler and L. Bömer, "Reply: Merit factor of Chu and Frank sequences," *Electronics Letters*, vol. 27, pp. 777–778, April 1991.

[382] M. Antweiler and L. Bömer, "Merit factor of Chu and Frank sequences," *Electronics Letters*, vol. 26, pp. 2068–2070, December 1990.

[383] R. Gold, "Optimal binary sequences for spread spectrum multiplexing," *IEEE Transactions on Information Theory*, vol. 13, pp. 619–621, October 1967.

[384] R. Sivaswamy, "Digital and analog subcomplementary sequences for pulse compression," *IEEE Transactions on Aerospace and Electronic Systems*, vol. 14, pp. 343–350, March 1978.

[385] E. Costa, M. Midrio, and S. Pupolin, "Impact of amplifier nonlinearities on OFDM transmission system performance," *IEEE Communications Letters*, vol. 3, pp. 37–39, February 1999.

[386] G. Santella and F. Mazzanga, "A model for performance evaluation in M-QAM-OFDM schemes in presence of non-linear distortions," in *Proceedings of IEEE VTC 1995*, pp. 830–834, July 1995.

[387] C. Rapp, "Effects of HPA-nonlinearity on 4-DPSK-OFDM-signal for digital sound broadcasting system," in *Proceedings of 2nd European Conference on Satellite Communications*, (Liege, Belgium), ESA-SP-332, October 1991.

[388] P802.11a/D6.0, *Draft supplement to standard for tellecommunications and information exchange between systems - LAN/MAN specific requirements - Part 11: Wireless MAC and PHY specifications: High Speed Physical Layer in the 5 GHz Band*, May 1999.

[389] D. V. Sarwate, "Bounds on crosscorrelation and autocorrelation of sequences," *IEEE Transactions on Information Theory*, vol. 25, pp. 720–724, November 1979.

[390] J. F. Hayes, "Adaptive feedback communications," *IEEE Transactions on Communication Technology*, vol. 16, no. 1, pp. 29–34, 1968.

[391] J. K. Cavers, "Variable rate transmission for rayleigh fading channels," *IEEE Transactions on Communications Technology*, vol. COM-20, pp. 15–22, February 1972.

[392] W. T. Webb and R. Steele, "Variable rate QAM for mobile radio," *IEEE Transactions on Communications*, vol. 43, no. 7, pp. 2223–2230, 1995.

[393] M. Moher and J. Lodge, "TCMP—a modulation and coding strategy for rician fading channels," *IEEE Journal on Selected Areas in Communications*, vol. 7, pp. 1347–1355, December 1989.

[394] S. Sampei and T. Sunaga, "Rayleigh fading compensation for QAM in land mobile radio communications," *IEEE Transactions on Vehicular Technology*, vol. 42, pp. 137–147, May 1993.

[395] S. Otsuki, S. Sampei, and N. Morinaga, "Square QAM adaptive modulation/TDMA/TDD systems using modulation level estimation with Walsh function," *Electronics Letters*, vol. 31, pp. 169–171, February 1995.

[396] W. Lee, "Estimate of channel capacity in Rayleigh fading environment," *IEEE Transactions on Vehicular Technology*, vol. 39, pp. 187–189, August 1990.

[397] A. Goldsmith and P. Varaiya, "Capacity of fading channels with channel side information," *IEEE Transactions on Information Theory*, vol. 43, pp. 1986–1992, November 1997.

[398] M. S. Alouini and A. J. Goldsmith, "Capacity of Rayleigh fading channels under different adaptive transmission and diversity-combining technique," *IEEE Transactions on Vehicular Technology*, vol. 48, pp. 1165–1181, July 1999.

[399] A. Goldsmith and S. Chua, "Variable rate variable power MQAM for fading channels," *IEEE Transactions on Communications*, vol. 45, pp. 1218–1230, October 1997.

[400] M. S. Alouini, X. Tand, and A. J. Goldsmith, "An adaptive modulation scheme for simultaneous voice and data transmission over fading channels," *IEEE Journal on Selected Areas in Communications*, vol. 17, pp. 837–850, May 1999.

[401] D. Yoon, K. Cho, and J. Lee, "Bit error probability of M-ary Quadrature Amplitude Modulation," in *Proc. IEEE VTC 2000-Fall*, vol. 5, pp. 2422–2427, IEEE, September 2000.

[402] C. Wong and L. Hanzo, "Upper-bound performance of a wideband burst-by-burst adaptive modem," *IEEE Transactions on Communications*, vol. 48, pp. 367–369, March 2000.

[403] E. L. Kuan, C. H. Wong, and L. Hanzo, "Burst-by-burst adaptive joint-detection CDMA," in *Proc. of IEEE VTC'99 Fall*, vol. 2, (Amsterdam, Netherland), pp. 1628–1632, September 1999.

[404] K. J. Hole, H. Holm, and G. E. Oien, "Adaptive multidimensional coded modulation over flat fading channels," *IEEE Journal on Selected Areas in Communications*, vol. 18, pp. 1153–1158, July 2000.

[405] J. Torrance and L. Hanzo, "Upper bound performance of adaptive modulation in a slow Rayleigh fading channel," *Electronics Letters*, vol. 32, pp. 718–719, 11 April 1996.

[406] M. Nakagami, "The m-distribution - A general formula of intensity distribution of rapid fading," in *Statistical Methods in Radio Wave Propagation* (W. C. Hoffman, ed.), pp. 3–36, Pergamon Press, 1960.

[407] I. S. Gradshteyn and I. M. Ryzhik, *Table of Integrals, Series and Products*. New York, USA: Academic Press, 1980.

[408] J. Lu, K. B. Letaief, C. I. J. Chuang, and M. L. Lio, "M-PSK and M-QAM BER computation using signal-space concepts," *IEEE Transactions on Communications*, vol. 47, no. 2, pp. 181–184, 1999.

[409] T. Keller and L. Hanzo, "Adaptive modulation technique for duplex OFDM transmission," *IEEE Transactions on Vehicular Technology*, vol. 49, pp. 1893–1906, September 2000.

[410] B. J. Choi, M. Münster, L. L. Yang, and L. Hanzo, "Performance of Rake receiver assisted adaptive-modulation based CDMA over frequency selective slow Rayleigh fading channel," *Electronics Letters*, vol. 37, pp. 247–249, February 2001.

[411] G. S. G. Beveridge and R. S. Schechter, *Optimization: Theory and Practice*. McGraw-Hill, 1970.

[412] W. Jakes Jr., ed., *Microwave Mobile Communications*. New York, USA: John Wiley & Sons, 1974.

[413] "COST 207 : Digital land mobile radio communications, final report," tech. rep., Luxembourg, 1989.

[414] M. K. Simon and M. S. Alouini, *Digital Communication over Fading Channels: A Unified Approach to Performance Analysis*. John Wiley & Sons, Inc., 2000. ISBN 0471317799.

[415] C. Y. Wong, R. S. Cheng, K. B. Letaief, and R. D. Murch, "Multiuser OFDM with adaptive subcarrier, bit, and power allocation," *IEEE Journal on Selected Areas in Communications*, vol. 17, pp. 1747–1758, October 1999.

[416] T. Keller and L. Hanzo, "Adaptive multicarrier modulation: A convenient framework for time-frequency processing in wireless communications," *Proceedings of the IEEE*, vol. 88, pp. 611–642, May 2000.

[417] A. Klein, G. Kaleh, and P. Baier, "Zero forcing and minimum mean square error equalization for multiuser detection in code division multiple access channels," *IEEE Transactions on Vehicular Technology*, vol. 45, pp. 276–287, May 1996.

[418] B. J. Choi, T. H. Liew, and L. Hanzo, "Concatenated space-time block coded and turbo coded symbol-by-symbol adaptive OFDM and multi-carrier CDMA systems," in *Proceedings of IEEE VTC 2001-Spring*, p. P.528, IEEE, May 2001.

[419] B. Vucetic, "An adaptive coding scheme for time-varying channels," *IEEE Transactions on Communications*, vol. 39, no. 5, pp. 653–663, 1991.

[420] H. Imai and S. Hirakawa, "A new multi-level coding method using error correcting codes," *IEEE Transactions on Information Theory*, vol. 23, pp. 371–377, May 1977.

[421] G. Ungerboeck, "Channel coding with multilevel/phase signals," *IEEE Transactions on Information Theory*, vol. IT-28, pp. 55–67, January 1982.

[422] S. M. Alamouti and S. Kallel, "Adaptive trellis-coded multiple-phased-shift keying Rayleigh fading channels," *IEEE Transactions on Communications*, vol. 42, pp. 2305–2341, June 1994.

[423] S. Chua and A. Goldsmith, "Adaptive coded modulation for fading channels," *IEEE Transactions on Communications*, vol. 46, pp. 595–602, May 1998.

[424] T. Keller, T. Liew, and L. Hanzo, "Adaptive rate RRNS coded OFDM transmission for mobile communication channels," in *Proceedings of VTC 2000 Spring*, (Tokyo, Japan), pp. 230–234, 15-18 May 2000.

[425] T. Keller, T. H. Liew, and L. Hanzo, "Adaptive redundant residue number system coded multicarrier modulation," *IEEE Journal on Selected Areas in Communications*, vol. 18, pp. 1292–2301, November 2000.

[426] T. Liew, C. Wong, and L. Hanzo, "Block turbo coded burst-by-burst adaptive modems," in *Proceedings of Microcoll'99*, (Budapest, Hungary), pp. 59–62, 21-24 March 1999.

[427] C. Wong, T. Liew, and L. Hanzo, "Turbo coded burst by burst adaptive wideband modulation with blind modem mode detection," in *ACTS Mobile Communications Summit*, (Sorrento, Italy), pp. 303–308, 8-11 June 1999.

[428] V. Tarokh, N. Seshadri, and A. R. Calderbank, "Space-Time Codes for High Data Rate Wireless Communication: Performance Criterion and Code Construction," *IEEE Transactions on Information Theory*, vol. 44, pp. 744–765, March 1998.

[429] S. M. Alamouti, "A simple transmit diversity technique for wireless communications," *IEEE Journal on Selected Areas in Communications*, vol. 16, pp. 1451–1458, October 1998.

[430] V. Tarokh, H. Jafarkhani, and A. R. Calderbank, "Space-time block coding for wireless communications: Performance results," *IEEE Journal on Selected Areas in Communications*, vol. 17, pp. 451–460, March 1999.

[431] C. Berrou and A. Glavieux, "Near optimum error correcting coding and decoding: Turbo codes," *IEEE Transactions on Communications*, vol. 44, pp. 1261–1271, October 1996.

[432] W. T. Webb and L. Hanzo, *Modern Quadrature Amplitude Modulation : Principles and Applications for Fixed and Wireless Channels*. London: IEEE Press, and John Wiley & Sons, 1994.

[433] Y. Chow, A. Nix, and J. McGeehan, "Analysis of 16-APSK modulation in AWGN and rayleigh fading channel," *Electronics Letters*, vol. 28, pp. 1608–1610, November 1992.

[434] F. Adachi and M. Sawahashi, "Performance analysis of various 16 level modulation schemes under Rrayleigh fading," *Electronics Letters*, vol. 28, pp. 1579–1581, November 1992.

[435] F. Adachi, "Error rate analysis of differentially encoded and detected 16APSK under rician fading," *IEEE Transactions on Vehicular Technology*, vol. 45, pp. 1–12, February 1996.

[436] Y. C. Chow, A. R. Nix, and J. P. McGeehan, "Diversity improvement for 16-DAPSK in Rayleigh fading channel," *Electronics Letters*, vol. 29, pp. 387–389, February 1993.

[437] Y. C. Chow, A. R. Nix, and J. P. McGeehan, "Error analysis for circular 16-DAPSK in frquency-selective Rayleigh fading channels with diversity reception," *Electronics Letters*, vol. 30, pp. 2006–2007, November 1994.

[438] C. M. Lo and W. H. Lam, "Performance analysis of bandwidth efficient coherent modulation schems with L-fold MRC and SC in Nakagami-m fading channels," in *Proceedings of IEEE PIMRC 2000*, vol. 1, pp. 572–576, September 2000.

[439] S. Benedetto, E. Biglierri, and V. Castellani, *Digital Transmission Theory*. Prentice-Hall, 1987.

[440] Z. Dlugaszewski and K. Wesolowski, "WHT/OFDM - an imporved OFDM transmission method for selective fading channels," in *Proceedings of IEEE SCVT 2000*, (Leuven, Belgium), pp. 71–74, 19 October 2000.

[441] Z. Dlugaszewski and K. Wesolowski, "Performance of several OFDM transceivers in the indoor radio channels in 17 ghz band," in *Proceedings of IEEE VTC 2001 Spring*, p. P.644, IEEE, May 2001.

[442] S. Verdú, "Minimum probability of error for asynchronous Gaussian multiple-access channel," *IEEE Transactions on Communications*, vol. 32, pp. 85–96, January 1986.

[443] K. M. Wong, J. Wu, T. N. Davidson, Q. Jin, and P. C. Ching, "Performance of wavelet packet-division multiplexing in impulsive and Gaussian noise," *IEEE Transactions on Communication*, vol. 48, no. 7, pp. 1083–1086, 2000.

[444] M. Ghosh, "Analysis of the effect of impulse noise on multicarrier and single carrier QAM systems," *IEEE Transactions on Communications*, vol. 44, no. 2, pp. 145–147, 1996.

[445] Q. Wang, T. A. Gulliver, L. J. Mason, and V. K. Bhargava, "Performance of SFH/MDPSK in tone interference and Gaussian noise," *IEEE Transactions on Communications*, vol. 42, no. 2/3/4, pp. 1450–1454, 1994.

[446] G. E. Atkin and I. F. Blake, "Performance of multitone FFH/MFSK systems in the presence of jamming," *IEEE Transactions on Communications*, vol. 35, no. 2, pp. 428–435, 1989.

[447] L. B. Milstein and P. K. Das, "An analysis of a real-time transform domain filtering digital communication system - Part i: Narrow-band interference rejection," *IEEE Transactions on Communications*, vol. 28, no. 6, pp. 816–824, 1980.

[448] A. Papoulis, *Probability, Random Variables, and Stochastic Processes*. McGraw-Hill, 3 ed., 1991.

[449] M. R. Spiegel, *Mathematical Handbook of Formulas and Tables*. McGraw-Hill Book Company, 1968.

[450] W. X. Zheng, "Design of adaptive envelope-constrained filters in the presence of impulsive noise," *IEEE Transactions on Circuits and Systems II*, vol. 48, pp. 188–192, February 2001.

[451] Y. Zhang and R. S. Blum, "Iterative multiuser detection for turbo-coded synchronous cdma in gaussian and non-gaussian impulsive noise," *IEEE Transactions on Communication Technology*, vol. 49, no. 3, pp. 397–400, 2001.

[452] M. Moeneclaey, M. V. Bladel, and H. Sari, "Sensitivity of multiple-access techniques to narrow-band interference," *IEEE Transactions on Communication Technology*, vol. 49, no. 3, pp. 497–505, 2001.

[453] K. Cheun and T. Jung, "Performance of asynchronous fhss-ma networks under rayleigh fading and tone jamming," *IEEE Transactions on Communications*, vol. 49, no. 3, pp. 405–408, 2001.

[454] Y. Li, "Pilot-symbol-aided channel estimation for OFDM in wireless systems," in *Proc. of Vehicular Technology Conference*, (Houston, Texas), p. 1999, IEEE, May 1999.

[455] R. M. Mersereau and T. C. Speake, "The Processing of Periodically Sampled Multidimensional Signals," *IEEE Transactions on Acoustics, Speech and Signal Processing*, vol. ASSP-31, pp. 188–194, February 1983.

[456] D. E. Dudgeon and R. M. Mersereau, *Multidimensional Digital Signal Processing*. Prentice Hall, Inc., 1984.

[457] P. Höher, S. Kaiser, and P. Robertson, "Pilot-symbol-aided Channel Estimation in Time and Frequency," in *Proceedings of International Workshop on Multi-Carrier Spread-Spectrum*, pp. 169–178, K.Fazel and G. P. Fettweis (Eds.), Kluver Academic Publishers, April 1997.

[458] H. D. Lüke, *Signalübertragung*. Springer-Verlag Berlin Heidelberg New York, 1995.

[459] R. Steele and L. Hanzo, *Mobile Radio Communications*. John Wiley & Sons, LTD, Chichester, 1999.

[460] P. A. Bello, "Time-frequency duality," *IEEE Transactions on Information Theory*, vol. 10, pp. 18–33, January 1964.

[461] T. Keller, *Adaptive OFDM techniques for personal communications systems and local area networks*. PhD Thesis, Department of Electronics and Computer Science, University of Southampton, United Kingdom, 1999.

[462] T. Chen and P. P. Vaidyanathan, "The Role of Integer Matrices in Multidimensional Multirate Systems," *IEEE Transactions on Signal Processing*, vol. 41, pp. 1035–1047, March 1993.

[463] C. C. M. Duffee, *The Theory of Matrices*. Verlag Julius Springer, 1933.

[464] M. Newman, *Integral Matrices*. Academic Press, Inc., 1972.

[465] S. Kaiser, *Multi-Carrier CDMA Mobile Radio Systems - Analysis and Optimization of Detection, Decoding and Channel Estimation*. VDI Verlag GmbH, 1998.

[466] S. Weiss and R. W. Stewart, *On Adaptive Filtering in Oversampled Subbands*. Shaker Verlag GmbH, Aachen, Germany, 1998.

[467] S. Haykin, *Adaptive Filter Theory*. Prentice Hall, Inc., 1996.

[468] G. Grosche, V. Ziegler, and D. Ziegler, *Taschenbuch der Mathematik*. BSB B. G. Teubner Verlagsgesellschaft, Leipzig, 1989.

[469] J. W. C. Jakes, *Mobile Microwave Communications*. John Wiley & Sons, New York, 1974.

[470] M. Münster and L. Hanzo, "First-Order Channel Parameter Estimation Assisted Cancellation of Channel Variation-Induced Inter-Subcarrier Interference in OFDM Systems," in *Proceedings of EUROCON '2001*, vol. 1, (Bratislava, Czech), pp. 1–5, IEEE, July 2001.

[471] A. Chini, Y. Wu, M. El-Tanany, and S. Mahmoud, "Filtered Decision Feedback Channel Estimation for OFDM Based DTV Terrestrial Broadcasting System," *IEEE Transactions on Broadcasting*, vol. 44, pp. 2–11, Mar 1998.

[472] G. Strang, *Linear Algebra and Its Applications, 2nd edition*. Academic Press, 1980.

[473] "EN 300 744, V1.1.2, Digital Video Broadcasting (DVB); Framing structure, channel coding and modulation for digital terrestrial television," in *European Standard (Telecommunications Series)*, pp. 26–28, ETSI, ETSI, 1997.

[474] C. Berrou, A. Glavieux, and P. Thitimajshima, "Near shannon limit error-correcting coding and decoding: Turbo codes," in *Proc. of International Conference on Communications*, (Geneva, Switzerland), pp. 1064–1070, IEEE, May 1993.

[475] C. Berrou and A. Glavieux, "Near optimum error correcting coding and decoding: turbo codes," *IEEE Transactions on Communications*, vol. 44, pp. 1261–1271, October 1996.

[476] H. Rohling and R. Gruenheid, "Adaptive Coding and Modulation in an OFDM-TDMA Communication System," in *Proceedings of Vehicular Technology Conference*, vol. 2, (Ottawa, Canada), pp. 773–776, IEEE, May 18-21 1998.

[477] D. Hughes-Hartogs, "Ensemble modem structure for imperfect transmission media," *U.S. Patents Nos. 4,679,222 (July 1987), 4,731,816 (March 1988) and 4,833,796 (May 1989)*.

[478] T. Keller and L. Hanzo, " Blind-detection Assisted Sub-band Adaptive Turbo-Coded OFDM Schemes," in *Proc. of Vehicular Technology Conference*, (Houston, USA), pp. 489–493, IEEE, May 1999.

[479] F. Rashid-Farrokhi, L. Tassiulas, and K. J. R. Liu, "Joint Optimal Power Control and Beamforming in Wireless Networks Using Antenna Arrays," *IEEE Transactions on Communications*, vol. 46, pp. 1313–1324, October 1998.

[480] F. R. Gantmacher, *The Theory of Matrices*, vol. 2. New York: Chelsea, 1990.

[481] W. Fischer and I. Lieb, *Funktionentheorie*. Vieweg Verlag, Braunschweig, Germany, 1983.

[482] S. M. Kay, *Fundamentals of Statistical Signal Processing, Estimation Theory*. Prentice Hall, New Jersey, 1993.

[483] K. Fazel and G. Fettweis, *Multi-carrier Spread Spectrum & Related Topics, ISBN 0-7923-7740-0*. Kluwer, 2000.

[484] H. Bogucka, "Application of the New Joint Complex Hadamard Transform - Inverse Fourier Transform in a OFDM/CDMA Wireless Communication System," in *Proceedings of Vehicular Technology Conference*, vol. 5, (Amsterdam, Netherlands), pp. 2929–2933, IEEE, September 19-22 1999.

[485] A. Goldsmith and S. Chua, "Variable-rate variable-power MQAM for fading channels," *IEEE Transactions on Communications*, vol. 45, pp. 1218–1230, October 1997.

[486] M. Yee and L. Hanzo, "Upper-bound performance of radial basis function decision feedback equalised burst-by-burst adaptive modulation," in *Proceedings of ECMCS'99, CD-ROM*, (Krakow, Poland), 24–26 June 1999.

[487] E. Kuan, C. Wong, and L. Hanzo, "Burst-by-burst adaptive joint detection CDMA," in *Proceeding of VTC'99 (Spring)*, (Houston, TX, USA), IEEE, 16–20 May 1999.

[488] H. Rohling and R. Grünheid, "Peformance of an OFDM-TDMA mobile communication system," in *Proceeding of IEEE Global Telecommunications Conference, Globecom 96*, (London, UK), pp. 1589–1593, IEEE, 18–22 November 1996.

[489] P. Cherriman, T. Keller, and L. Hanzo, "Constant-rate turbo-coded and block-coded orthogonal frequency division multiplex videophony over UMTS," in *Proceeding of Globecom'98*, vol. 5, (Sydney, Australia), pp. 2848–2852, IEEE, 8–12 November 1998.

[490] J. Woodard, T. Keller, and L. Hanzo, "Turbo-coded orthogonal frequency division multiplex transmission of 8 kbps encoded speech," in *Proceeding of ACTS Mobile Communication Summit '97*, (Aalborg, Denmark), pp. 894–899, ACTS, 7–10 October 1997.

[491] P. Cherriman and L. Hanzo, "Programmable H.263-based wireless video transceivers for interference-limited environments," *IEEE Transactions on Circuits and Systems for Video Technology*, vol. 8, pp. 275–286, June 1998.

[492] B. J. Choi and L. Hanzo, "Performance analysis of Rake receiver assisted adaptive QAM using antenna diversity over frequency selective Rayleigh channels," *Submitted to IEEE Journal on Selected Areas in Communications*, January 2001.

[493] B. J. Choi and L. Hanzo, "Optimum mode-switching levels for adaptive modulation systems," in *Submitted to IEEE GLOBECOM 2001*, 2001.

[494] T. H. Liew, B. J. Choi, and L. Hanzo, "Space-time block coded and space-time trellis coded OFDM," in *Proceedings of IEEE VTC 2001-Spring*, p. P.533, IEEE, May 2001.

[495] C. E. Davila, "Blind Adaptive Estimation of KLT Basis Vectors," *IEEE Transactions on Signal Processing*, vol. 49, pp. 1364–1369, July 2001.

[496] A. Rezayee and S. Gazor, "An Adaptive KLT Approach for Speech Enhancement," *IEEE Transactions on Speech and Audio Processing*, vol. 9, pp. 87–95, February 2001.

[497] Y. Li, J. C. Chuang, and N. R. Sollenberger, "Transmitter Diversity for OFDM Systems and Its Impact on High-Rate Data Wireless Networks," *IEEE Journal on Selected Areas in Communications*, vol. 17, pp. 1233–1243, July 1999.

[498] B. Lu and X. Wang, "Iterative Receivers for Multi-User Space-Time Coding Systems," *IEEE Journal on Selected Areas in Communications*, vol. 18, pp. 2322–2335, November 2000.

[499] M. L. Honig and W. X. Xiao, "Performance of Reduced-Rank Linear Interference Cancellation," *IEEE Transactions on Information Theory*, vol. 47, pp. 1928–1946, July 2001.

[500] D. R. Brown, M. Motani, V. V. Veeravalli, H. V. Poor, and J. C. R. Johnson, "On the Performance of Linear Parallel Interference Cancellation," *IEEE Transactions on Information Theory*, vol. 47, pp. 1957–1970, July 2001.

[501] A. Grant and C. Schlegel, "Convergence of Linear Interference Cancellation Multiuser Receivers," *IEEE Transactions on Communications*, vol. 49, pp. 1824–1834, October 2001.

[502] H. Dai and H. V. Poor, "Turbo Multiuser Detection for Coded DMT VDSL Systems," *IEEE Journal on Selected Areas in Communications*, vol. 20, pp. 351–362, February 2002.

[503] K.-W. Cheong, W.-J. Choi, and J. M. Cioffi, "Multiuser Soft Interference Canceler via Iterative Decoding for DSL Applications," *IEEE Journal on Selected Areas in Communications*, vol. 20, pp. 363–371, February 2002.

[504] A. Lampe, R. Schober, W. Gerstacker, and J. Huber, "A Novel Iterative Multiuser Detector for Complex Modulation Schemes," *IEEE Journal on Selected Areas in Communications*, vol. 20, pp. 339–350, February 2002.

[505] B. Lu, X. Wang, and Y. Li, "Iterative Receivers for Space-Time Block-Coded OFDM Systems in Dispersive Fading Channels," *IEEE Transactions on Wireless Communications*, vol. 1, pp. 213–225, April 2002.